Numerical Modelling of Local Climate inside Electronics Enclosures

PhD Thesis

$$(EIv'')'' = q - \rho A\ddot{v}$$

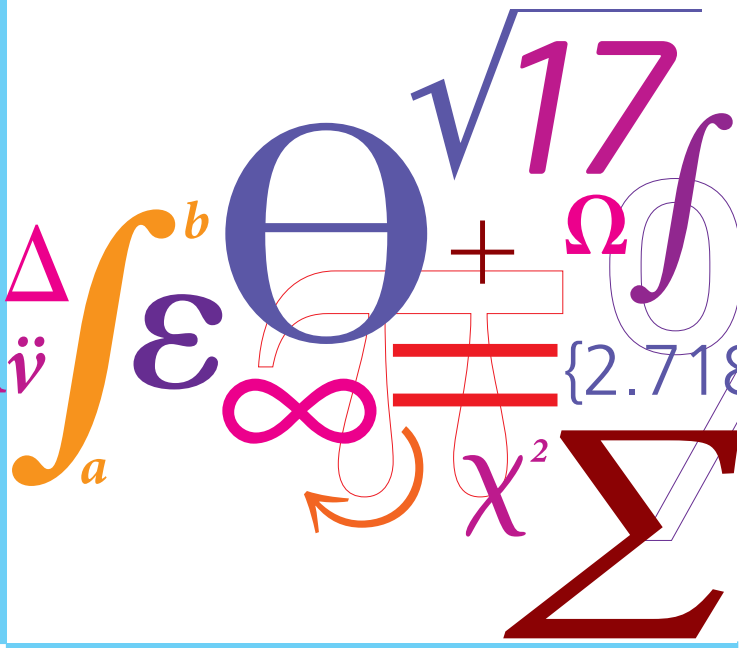

Parizad Shojaee Nasirabadi
October 2017

DTU Mechanical Engineering
Department of Mechanical Engineering

Numerical Modelling of Local Climate inside Electronics Enclosures

Parizad Shojaee Nasirabadi
Department of Mechanical Engineering
Technical University of Denmark

A thesis submitted for the degree of
Doctor of Philosophy
October 2017

To my beloved family

Preface

The present work, carried out at the Department of Mechanical Engineering (MEK) at the Technical University of Denmark (DTU), in the period 2014–2017, is submitted in partial fulfillment of the requirement for the Doctor of Philosophy degree.

The current research has been conducted as part of the "Improved Climate Control inside Electronic Equipment Enclosures Based on a Modelling Approach (ICCI)" project from the Danish Council for Independent Research, Technology and Production (FTP) and the "Innovationskonsortium for Pålidelig Elektronik (IN SPE)" project from the Danish Innovations Fonden, which are highly acknowledged. The consortium members were researchers at DTU Mechanical Engineering and Danfoss, Vestas, Grundfos, Eltek, Velux, DELTA and IPU.

I would like to express my sincere gratitude to Professor Jesper H. Hattel for his patience, motivation, enthusiasm, continuous support and immense knowledge. I have been extremely lucky to have a supervisor who cared so much about my work, and who responded to my questions and queries so promptly. I would also like to thank all the colleagues, current and former PhD students and Post-Doc researchers of the Process Modelling Group (PMG) for the amazing working environment. I am especially grateful to Masoud Jabbari and Sankhya Mohanty for their help and guidance through my PhD studies.

I would like to thank Professor S. Mostafa Ghiaasiaan, most sincerely, for the opportunity he gave me to be part of his group at the George W. Woodruff School of Mechanical Engineering, Georgia Institute of Technology. I have benefited greatly from his comments and suggestions during my research stay. Further thanks to Ardalan Lotfi and Mahmoud Parto for their scientific assistance. That was an unforgettable experience to work at the Georgia Institute of Technology.

Finally, I wish to express my deepest appreciation to my family for the love, support, and constant encouragement I have gotten over the years.

Parizad Shojaee Nasirabadi
Kgs. Lyngby,
October 2017

Abstract

Condensation and moisture related problems are the cause of failures in many cases and consequently serious concerns for reliability in electronics industry. Therefore, it is important to control the moisture content and the relative humidity inside electronics enclosures. In many applications electronics enclosures are exposed to uncontrolled environmental conditions. Understanding the effects of harsh ambient conditions on the relative humidity management and local climate inside the enclosures and applying this knowledge during the design phase is crucial for reducing the chance of failure and controlling maintenance costs. For decades thermal management has been extensively studied; however, the RH (relative humidity) of the operating environment is commonly disregarded during the design of electronics enclosures.

Considering the fact that experiments for monitoring the local climate inside enclosures are often tedious, and are typically lasting for a couple of days, there is a need for a reliable predictive model which is computationally fast enough and therefore capable of long term predictions.

In this work, the effect of ambient conditions on local climate inside electronics enclosure is numerically investigated. First, a finite element based CFD (computational fluid dynamic) model is developed to estimate the time constant of the moisture transfer into a typical enclosure exposed to constant ambient conditions. Comparing the CFD simulation results with experimental data from the literature, a good agreement is found. In order to study the effects of initial moisture content, temperature and size of the opening in the enclosure, an analysis of variance is applied on both experiments and CFD simulation results in factorial designed set of points. Thereafter, several cyclic ambient conditions are applied on a typical enclosure and the relative humidity evolution on the PCB is monitored. Since the CFD simulations are time consuming and CPU-intensive, a Cauer ladder RC circuit model is developed for the long term prediction of the local climate inside the enclosure. The conventional RC (resistance-capacitor) modelling is not very clear in describing the resistance and capacity values for natural convection. In this work, using the CFD simulation data, a correlation is developed for estimating these values.

The presence of the components inside the enclosure especially the heatsink causes a delay to the ambient thermal cycles and also shortens the amplitude of the cyclic changes. Thus, it helps to reduce RH on the PCB (printed circuit board). Considering this effect, unlike the conventional configuration of heatsinks, where they are attached to the walls of the enclosure in order to facilitate the transfer of the generated heat to the ambient, a new configuration where the heatsink is placed inside the enclosure with no contacts with the walls is studied in this work. With this arrangement the heat sink can store the heat generated by the electronics to be used for lowering the RH later when the electronics are not working. In this part of the study, the electronics enclosure is exposed to Copenhagen outdoor conditions. According to the results, a well-designed thermal mass can maintain RH low enough to avoid condensation. Due to the dynamic nature of the heat transfer in an electronics enclosure, an excessively large thermal mass does not necessarily provide the most

desirable conditions for the PCB. The size of the thermal mass should be optimized based on the enclosure's boundary and operational conditions, including the working cycle of the electronics, the amount of the generated heat, and the ambient conditions.
The buoyant flow inside the enclosure reduces the mass transfer resistance inside the enclosure. The cyclic internal heat load also helps this effect. The simulation results demonstrate that the temperature profile and consequently the RH profile are mainly controlled by the buoyant air flow (natural convection) rather than heat conduction inside the enclosure. On the other hand, the moisture transfer into the enclosure happens through the bottom hole. Despite the fact that a temperature increase accelerates the diffusion, the mass transfer resistance which is affected by the geometrical sizes beside the diffusion coefficient is not significantly affected. Thus, the moisture transfer is mostly controlled by the opening size rather than the temperature.
According to the simulations for the Cauer ladder RC model, it is demonstrated that in an enclosure with fixed geometry the dependence of Nu (representing natural convection heat transfer coefficient) on Ra and ΔT inside the enclosure follows a simple power function. Furthermore, a linear relation is observed between Ra and ΔT. A comparison between the magnitudes of the thermal energy and kinetic energy that are stored in the trapped air inside the enclosure reveals that the kinetic energy can be neglected. Although, the Cauer ladder RC model slightly underestimates the temperature, it predicts the trends of temperature and RH changes inside the enclosure successfully. The technique is useful for long-term predictions.

Resumé

Kondensation og fugt relaterede problemer er årsagen til fejl i mange tilfælde og dermed en alvorlig problemstilling for pålidelighed i elektronik industrien. Derfor er det vigtigt at styre fugt indholdet og den relative luftfugtighed inden i elektronik kabinetter. I mange anvendelser er elektronik kabinetter udsat for ukontrollerede miljøtilstande. At forstå effekten af barske miljøtilstande på den relative fugtstyring og lokale klima indeni kabinetter og at bruge denne viden under design fasen, er afgørende for at reducere sandsynligheden for fejl og styring af vedligeholdelsesomkostninger. Termisk styring har været grundigt undersøgt i årtier, men RH i drift tilstand er oftest set bort fra under design af elektronik kabinetter.
Taget i betragtning af at eksperimenter for at monitorere lokal klima i kabinetter ofte er tidskrævende og typisk varer et par dage, er der behov for en pålidelig model, som er beregningsmæssigt hurtig nok og dermed i stand til at lave langsigtede forudsigelser.
I dette arbejde er indflydelsen af miljøtilstande på lokal klima i elektronik kabinetter undersøgt på numerisk vis. Først er en finite element baseret CFD model udviklet til at estimere tidskonstanten af fugt transmission ind i et typisk kabinet udsat for konstante omgivende forhold. En sammenligning af resultaterne for CFD simulationerne med eksperimental data fra litteraturen, giver en god overensstemmelse. For at undersøge effekten af initial fugtindholdet, temperatur og størrelse af kabinettets åbning, bruges variansanalyse på både eksperimenter og resultaterne for CFD simulationerne med et sæt af punkter bestemt af faktorforsøg. Efterfølgende udsættes kabinettet for forskellige omgivelsesforhold og evolutionen af den relative fugtighed på PCB'en monitoreres. Da CFD simulationerne er tidskrævende og CPU-intensive, er en Cauer ladder RC kredsløb model udviklet for at forudsige den langsigtede lokale klima indeni kabinettet. Den konventionelle RC model er ikke i stand til tydeligt at beskrive modstande og kapacitetsværdier for naturlig konvektion. I dette arbejde er der udviklet en korrelation til at estimere disse værdier, ved at bruge CFD simulationsdata.
Tilstedeværelsen af komponenter i kabinettet, særligt kølepladen, forårsager en forsinkelse af de omgivende temperatursvingninger og dertil forkorter amplituden af de cykliske ændringer. Dermed hjælper den med at reducere RH på overfladen af PCB. Taget denne effekt i betragtning, i modsætning til konventionel konfiguration af køleplader, hvor de er monteret på væggene af kabinettet for at facilitere transmissionen af den genererede varme til omgivelserne, undersøges der i dette arbejde en ny konfiguration hvor kølepladen er placeret indeni kabinettet uden kontakt med væggene. Med denne konfiguration kan kølepladen lagre varmen genereret af elektronikken, for at efterfølgende sænke RH, når elektronikken ikke er aktiv. I denne del af undersøgelsen, er elektronik kabinettet udsat for udendørs forhold i København. Ifølge resultaterne, kan en vel designet termisk masse opretholde en lav nok RH værdi for at undgå kondensering. På grund af den dynamiske karakter af varmetransmission indeni en elektronik kabinet, leverer en unødvendigt stor termiske masse ikke nødvendigvis de mest ønskelige forhold for PCB'en. Størrelsen af den

termiske masse bør være optimeret baseret på kabinettets rand- og funktionsbetingelser, inklusiv arbejdscyklen af elektronikkomponenterne, mængden af genereret varme og miljøforhold.
Den oppebærende gennemstrømning indeni kabinettet reducerer massetransmissionens modstand. Den cykliske interne varmeproduktion hjælper også til denne effekt. Simulationsresultaterne demonstrerer at temperaturprofilen og dermed RH profilen er primært styret af den oppebærende luft gennemstrømning (naturlig konvektion) frem for varmledningen indeni kabinettet. På den anden side, foregår fugt transmissionen ind i kabinettet igennem hullet i bunden. Selvom det faktum at temperaturen øgning accelererer diffusionen, er modstanden mod massetransmission, som er påvirket af geometriske størrelser udover diffusionskoefficienten, ikke væsentligt påvirket. Dermed er fugt transmissionen mest styret af størrelsen af åbningen frem for temperaturen.
Ifølge simulationerne for Cauer ladder RC modellen, er det demonstreret at indeni et kabinet med fast geometri, afhængigheden af Nu (som repræsenterer varmeovergangstallet for naturlig konvektion) af Ra og ΔT indeni kabinettet følger en simpel potensfunktion. Ydermere, er et lineært forhold mellem Ra og ΔT observeret. En sammenligning mellem størrelsesforholdene af det termiske energi og den kinetiske energi, som er lagret i den indelukkede luft i kabinettet, afslører at den kinetiske energi kan negligeres. Selvom Cauer ladder RC modellen underestimerer temperaturen en anelse, forudsiger den tendensen af temperaturen og RH ændringer indeni kabinettet korrekt. Metoden er nyttigt for langsigtede forudsigelser.

List of publications

Appended publications

Journal papers:

I. Parizad Shojaee Nasirabadi, Masoud Jabbari, Jesper H. Hattel, "CFD Simulation and Statistical Analysis of Moisture Transfer into an Electronic Enclosure", Applied Mathematical Modelling, Vol. 44 (2017) p 246-260, DOI: 10.1016/j.apm.2016.09.004.

II. Parizad Shojaee Nasirabadi, Jesper H. Hattel, "A 3D Numerical study of humidity evolution and condensation risk on a Printed Circuit Board (PCB) exposed to harsh ambient conditions", Microelectronics Reliability, Vol. 83 (2018) p39-49, DOI: 10.1016/j.microrel.2018.02.008.

III. Parizad Shojaee Nasirabadi, S. Mostafa Ghiaasiaan, Jesper H. Hattel, "Long Term Prediction of Local Climate inside an Electronics Enclosure", *submitted to the "Applied Thermal Engineering", Elsevier.*

Conference proceedings:

IV. Parizad Shojaee Nasirabadi, Helene Conseil-Gudla, Sankhya Mohanty, Masoud Jabbari, Rajan Ambat, J.H. Hattel, "Semi-empirical prediction of moisture build-up in an electronic enclosure using analysis of variance (ANOVA)", Electronics Packaging Technology Conference (EPTC), IEEE, 2016, 785-790.

V. Parizad Shojaee Nasirabadi, Masoud Jabbari, Jesper H. Hattel, "Numerical simulation of transient moisture transfer into an electronic enclosure", International Conference of Numerical Analysis and Applied Mathematics (ICNAAM), 2015.

VI. Parizad Shojaee Nasirabadi, Jesper H. Hattel, "A Numerical Investigation of the Effect of Ambient Conditions on Natural Convection Cooling of Electronics", International Workshop on Thermal Investigations of ICs and Systems (Therminic), IEEE, 2017.

VII. Parizad Shojaee Nasirabadi, Masoud Jabbari, J.H. Hattel, "Numerical simulation of transient moisture and temperature distribution in polycarbonate and aluminum electronic enclosures", Thermal, Mechanical and Multi-Physics Simulation and Experiments in Microelectronics and Microsystems (EuroSimE), IEEE, 2016.

Non-Appended publications

Journal paper:

I. Masoud Jabbari, Parizad Shojaee Nasirabadi, V.A. Jambhekar, Jesper H. Hattel, R. Helmig, "Drying of a tape-cast layer: Numerical investigation of influencing parameters", International Journal of Heat and Mass Transfer, Vol. 108, Part B, (2017), p 2229-2238, DOI: 10.1016/j.ijheatmasstransfer.2017.01.074.

Conference proceedings:

II. Parizad Shojaee Nasirabadi, Masoud Jabbari, Jesper H. Hattel, "Estimation of water diffusion coefficient into polycarbonate at different temperatures using numerical simulation", International Conference of Numerical Analysis and Applied Mathematics (ICNAAM), 2015.

III. S. Mohanty, Z. Staliulionis, Parizad Shojaee Nasirabadi, R. Ambat, J.H. Hattel, "Optimization of electronic enclosure design for thermal and moisture management using calibrated models of progressive complexity", Electronics Packaging Technology Conference (EPTC), 2016 IEEE 18th, 483-487.

NOMENCLATURE

A	cross sectional area [m^2]
c	concentration of the species [$mole/m^3$]
C_p	specific heat of the fluid at constant pressure [J/kg.K]
D	moisture diffusion coefficient [m/s]
E	energy [j]
F	volume force vector [N]
g	acceleration due to gravity [m/s^2]
h	heat transfer coefficient [$W/(m^2.K)$]
I	unit tensor
k	thermal conductivity [W/(m.K)]
L	length [m]
M	molecular weight [gr/mole]
n	normal vector
n	number of data points
p	pressure [pa]
q”	heat flux [W/m^2]
r	residual
R	universal gas constant [j/(mole.K)]
R^2	coefficient of determination
S	summed square of residuals
T	temperature [K]
t	time [s]
u	velocity vector [m/s]
V	volume [m^3]
x	molar fraction
y	response value
$\hat{y}$	fitted value
Z	compressibility factor

Greek symbols

α	thermal diffusivity [m^2/s]
β	volumetric thermal expansion coefficient [1/K]
λ	transformation power
μ	dynamic viscosity [Pa.s]
υ	kinematic viscosity [m^2/s]

ρ	mass density [kg/m^3]
ϕ	interaction parameter
τ	time constant [s], [day]

Subscripts

a	dry air
i	counter
k	kinetic
m	mixture
r	ratio
sub	substrate
v	vapour
x, y, z	direction coordinates

Content

PREFACE I
ABSTRACT II
RESUMÉ IV
LIST OF PUBLICATIONS VI
CONTENT X
CHAPTER 1 1
INTRODUCTION 1

1.1 Local climate inside electronics enclosures 1
1.2 Mathematical models 12
1.3 Objectives of the thesis 14
1.4 Structure of the thesis 14

CHAPTER 2 16
TRANSPORT PHENOMENA 16

2.1 Momentum transfer 16
2.2 Heat transfer 16
2.2 Mass transfer 19
2.3 Thermo-physical properties of humid air 19
2.4 Multiphysics modelling 24

CHAPTER 3 28
THE RESPONSE OF A TYPICAL ELECTRONICS ENCLOSURE EXPOSED TO CONSTANT AMBIENT CONDITIONS 28

3.1 Isothermal moisture transfer into a typical enclosure 28
3.2 Factorial design based on CFD results 33
3.3 Factorial design based on Experiments 38
3.4 Cyclic internal Conditions 47

CHAPTER 4 52
THE RESPONSE OF A TYPICAL ELECTRONICS ENCLOSURE EXPOSED TO CYCLIC AMBIENT CONDITIONS 52

4.1 Rectangular sharp temperature cycles and constant RH of 100 [%] 52
4.2 STANAG 2895 conditions 61
4.3 Copenhagen outdoor conditions 63

CHAPTER 5 69
DERIVING A CAUER LADDER RC MODEL 69

5.1 Equivalent RC circuit for natural convection 69
5.2 Comparison of RC results with CFD calculations 74

CHAPTER 6 81
SUMMARY OF THE APPENDED PAPERS 81

6.1 Paper I 81
6.2 Paper II 81
6.3 Paper III 81
6.4 Paper IV 82
6.5 Paper V 82
6.6 Paper VI 82
6.7 Paper VII 82

CHAPTER 7 83
CONCLUSION AND OUTLOOK 83

7.1 Summary of the results 83
7.2 Future work 84

REFERENCES 86
APPENDIX 91

Chapter 1
Introduction

This chapter presents an introduction to the present thesis, which is the result of the project entitled "Modelling Climatic Reliability of Electronic Devices", carried out at the Process Modelling Group, Department of Mechanical Engineering, Technical University of Denmark. A brief introduction to the electronics enclosures and the local climate inside is given in section 1.1. Then the numerical models used for design of the enclosure and prediction of the local climate are presented in section 1.2. The objectives and the structure of the thesis come in section 1.3 and 1.4, respectively.

1.1 Local climate inside electronics enclosures

Temperature and relative humidity (RH) management inside electronics enclosures exposed to uncontrolled environmental conditions are critically important for the reliability and durability of electronic components housed in enclosures [1]–[3]. Exposure to high RH and the consequent condensation is a severe concern because it accelerates corrosion and migration mechanisms [3]. Thus, understanding the effects of environmental conditions, both at component and system levels, and applying this knowledge during the design phase are crucial for reducing the chance of failure and controlling maintenance costs [2].

1.1.1 Electronics enclosures

There are several factor affecting the reliability and lifetime of electronics. Figure 1-1 demonstrates the share of the different factors causing failure of electronics during operation. Considering this, electronics enclosures are of great importance as they serve several protection functions, such as cooling, touch protection and input-output (of any unwanted mass e.g. moisture) [4]. The significance of any of the mentioned issues can vary with application, ambient conditions, operating conditions, etc. Thus, the criteria of selection and design of a reliable enclosure requires a lot of attention.

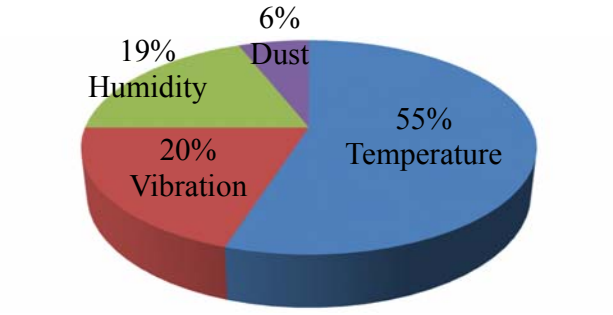

Figure 1-1 The responsible factors in failure of electronics during operation [5].

1.1.1.1Global standards of the electronics enclosures

Industry standards for electrical enclosures have been defined to promote safety, encourage design efficiency and define minimum levels of product performance. In the European and North American electrical industries, several standards are enforced for these reasons. Globally, IEC, NEMA and UL are the three most commonly recognized standards organizations.

International electrotechnical commission (IEC) standard 60529

The IEC is the world's leading organization that prepares and publishes International Standards for all electrical, electronic and related technologies— collectively known as electro-technology. IEC 60529 includes a list of codes, called Characteristic Numerals, which are used to identify ingress protection levels. Commonly referred to as the IP rating, these codes reflect an electrical enclosure's ability to protect against access to electrified parts by people, tools, moisture, dust or dirt.

National electrical manufacturer's association (NEMA) standard 250

Similar to IEC 60529, NEMA 250 covers enclosures for electrical equipment. Like IEC 60529, NEMA 250 addresses ingress protection, but it differs in that it also addresses specifications detailing minimum construction, performance and test criteria, corrosion resistance and more. Although its beginnings are based in the United States, NEMA is a global organization that is working to promote electrical standards worldwide. NEMA promotes the competitiveness of the US electrical product industry through the development of standards, advocacy in federal and state legislatures and executive agencies, and the collection and analysis of economic data.

Underwriter laboratories® (UL) 50, 50E

Underwriters Laboratories® is an independent product safety certification organization that has been testing products and writing safety standards for more than a century. UL 50, 50E is based on

NEMA 250 standards. While they address many of the same points, NEMA simply indicates the design intent but does not mandate compliance via third party testing and on-site compliance visits. A product can be built to NEMA standards but actual performance compliance is at the discretion of the manufacturer. UL certification, however, is formal confirmation that required construction and performance are met after analyses and testing is completed. In summary, both NEMA and UL define standards, but only UL enforces compliance to their standards with third-party testing and inspection [6].Table 1-1 describes the enclosure type ratings as defined by UL 50, 50E and NEMA 250.

Table 1-1 Enclosure type ratings as defined by UL and NEMA [6].

	NEMA		Enclosure Rating	UL	
	Solids	Liquids		Paint Options	Holes and Cutouts
Indoor	Provides a degree of protection against access to hazardous parts and ingress of solid foreign objects (falling dirt)	No protection	Type 1	Provides a degree of protection against incidental contact and falling dirt	No protection
	Provides a degree of protection against access to hazardous parts and ingress of solid foreign objects (falling dirt)	Provides a degree of protection against ingress of water (dripping and light splashing)	Type 2	Provides a degree of protection against incidental contact and falling dirt	Provides a degree of protection against dripping and light splashing of non-corrosive liquids
	Provides a degree of protection against access to hazardous parts and ingress of solid foreign objects (falling dirt and settling airborne dust, lint, fibers and flyings)	Provides a degree of protection against ingress of water (dripping and light splashing)	Type 5	Provides a degree of protection against incidental contact and falling dirt, settling airborne dust, lint, fibers and flyings	Provides a degree of protection against dripping and light splashing of non-corrosive liquids
	Provides a degree of protection against access to hazardous parts and ingress of solid foreign objects (falling dirt and circulating dust, lint, fibers and flyings)	Provides a degree of protection against ingress of water (dripping and light splashing) and light splashing and seepage of oil and noncorrosive coolants	Type 12	Provides a degree of protection against incidental contact and falling dirt, circulating dust, lint, fibers and flyings	Provides a degree of protection against dripping and light splashing of non-corrosive liquids; and against light splashing and consequent seepage of oil and non-corrosive coolants

	Provides a degree of protection against access to hazardous parts and ingress of solid foreign objects (falling dirt and circulating dust, lint, fibers and flyings)	Provides a degree of protection against ingress of water (dripping and light splashing) and spraying, splashing, and seepage of oil and non-corrosive coolants	Type 13	Provides a degree of protection against incidental contact and falling dirt, circulating dust, lint, fibers and flyings	Provides a degree of protection against spraying, splashing, and seepage of water, oil, and non-corrosive coolants
Indoor and Outdoor	Provides a degree of protection against access to hazardous parts and ingress of solid foreign objects (falling dirt and windblown dust)	Provides a degree of protection against ingress of water (windblown rain, sleet, snow)	Type 3	Provides a degree of protection against incidental contact, falling dirt and windblown dust	Provides a degree of protection against rain, sleet and snow
	Provides a degree of protection against access to hazardous parts and ingress of solid foreign objects (falling dirt)	Provides a degree of protection against ingress of water (falling rain, sleet, snow)	Type 3R	Provides a degree of protection against incidental contact and falling dirt	Provides a degree of protection against rain, sleet and snow
	Provides a degree of protection against access to hazardous parts and ingress of solid foreign objects (falling dirt and windblown dust)	Provides a degree of protection against ingress of water (rain, sleet, snow, splashing water and hose-directed water)	Type 4	Provides a degree of protection against incidental contact, falling dirt and windblown dust	Provides a degree of protection against rain, sleet, snow, splashing water and hosedirected water
	Provides a degree of protection against access to hazardous parts and ingress of solid	Provides a degree of protection against ingress of water (rain, sleet, snow, splashing	Type 4X	Provides a degree of protection against incidental contact,	Provides a degree of protection against rain, sleet, snow, splashing water,

	foreign objects (falling dirt and windblown dust)	water and hose-directed water) and provides an increased level of protection against corrosion		falling dirt and windblown dust	hose-directed water and corrosion
	Provides a degree of protection against access to hazardous parts and ingress of solid foreign objects (falling dirt)	Provides a degree of protection against ingress of water (hose directed and occasional temporary submersion at a limited depth)	Type 6	Provides a degree of protection against incidental contact and falling dirt	Provides a degree of protection against rain, sleet, snow, hose-directed water and occasional temporary submersion at a limited depth
	Provides a degree of protection against access to hazardous parts and ingress of solid foreign objects (falling dirt)	Provides a degree of protection against ingress of water (hose directed and prolonged submersion at a limited depth)	Type 6P	Provides a degree of protection against incidental contact and falling dirt	Provides a degree of protection against rain, sleet, snow, hose-directed water and prolonged submersion at a limited depth

1.1.1.2 Materials of the electronics enclosures

Electronics enclosures are made of metals (such as aluminum, carbon steel and stainless steel) or non-metals (such as polycarbonate, ABS and fiberglass) [7]. Table 1-2 and 1-3 summarize common metallic and non-metallic enclosure materials and some of their properties.

Table 1-2 Common metallic materials for electronics enclosures [8].

Material	Cost	Strength	Corrosion resistance
Carbon Steel	Low	High	Poor
Galvannealed steel	Low to moderate	High	Good
Stainless Steel	High	High	Excellent
Aluminum	Moderate	Moderate	Good to Excellent

Table 1-3 Common non-metallic materials for electronics enclosures [8].

Material	Cost	Chemical Resistance
ABS*	Low	Low
ABS/PC* Blend	Low	Low to moderate
PC	Moderate	Moderate
PC/PBT* Blend	Moderate	Moderate
Fiberglass	High	High

*ABS (acrylonitrile butadiene styrene), PC (poly carbonate), PBT (polybutylene terephthalate).

Generally, non-metallic materials are much less thermally conductive compared to metallic materials; on the other hand, they have much higher moisture permeability relative to the non-metals. The contrast between the heat and mass transfer properties of these two materials makes the comparison of local climate inside the electronics enclosures made of these two groups of materials very interesting.

1.1.2 Cooling and thermal management

Advances in the electronics manufacturing have resulted in a significant increase in power density and also an emerging trend of miniaturization of modern electronics. These trends have promoted the need for efficient dissipation of heat flux. In order to satisfy the temperature requirements, in terms of performance and reliability, improvements in cooling technologies are required. Thus, thermal management has become important and increasingly critical to the electronics industry [5]. Generally, thermal management of electronics is categorized into active and passive cooling techniques. Active cooling refers to the mechanically assisted techniques that typically have higher cooling capacity. Some active cooling techniques make it possible to cool the electronics to temperatures below the ambient. On the other hand, passive cooling systems are not assisted by

mechanical equipment. Conventional passive cooling techniques include applying heat spreaders and heatsinks to the electronic package [9].
In another classification by Scott [10], the cooling techniques have been divided into four groups and compared according to their heat removal capacitance. Figure 1-2 shows the comparison.

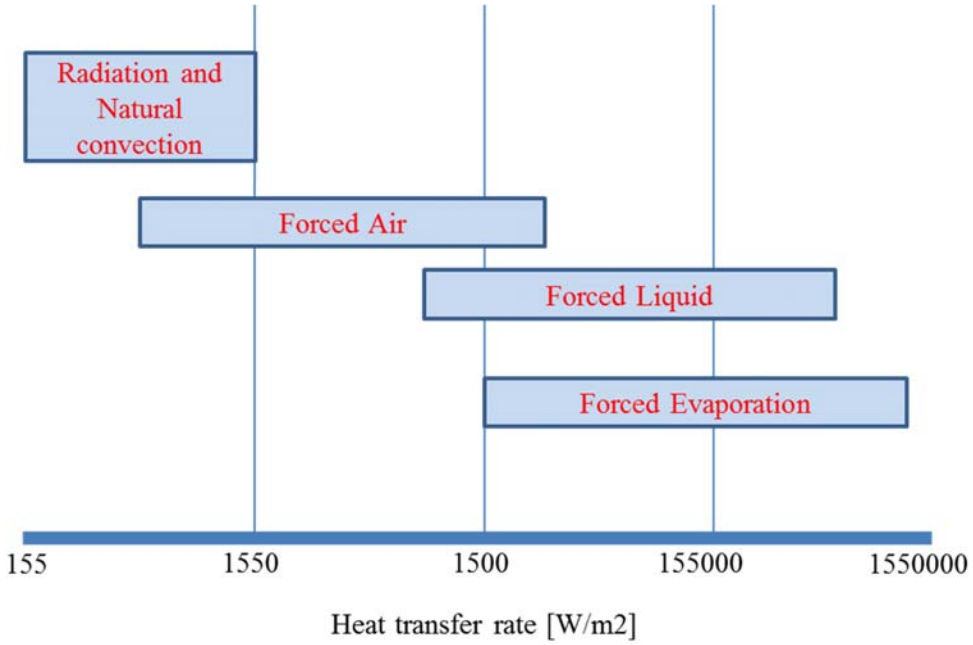

Figure 1-2 Comparison between cooling methods [5].

Anandan and Ramalingam [5] had a thorough review on the cooling techniques. In their study, the cooling techniques are categorized as:

a. air cooling

- Natural convection
- Forced convection

b. liquid cooling

- Direct liquid immersion cooling
- Indirect cooling

c. heat pipes
d. refrigeration cooling
e. thermoelectric cooling
f. phase change material based cooling

Air cooling is recognized as an important and widely used cooling technique. This is mainly because air is the most accessible coolant and the methods are simple and robust, particularly with respect to safe operation in hostile environments (contaminated air, vibrations, noise and humidity). These advantages stimulated considerable research on the development and optimization of heat

sinks for both natural and forced convection [11]. However, the poor thermal transport properties of air reduce its potential for high heat flux devices [12], [13].
A typical air-cooled heat sink is shown in Figure 1-3. The heat sink is constructed of a base region that is in contact with the module to be cooled. Fins protruding from the base aim to extend surface area for heat transfer to the air. Heat is conducted through the base, up into the fins and then transferred by convection to the air flowing in the spaces between the fins [14].

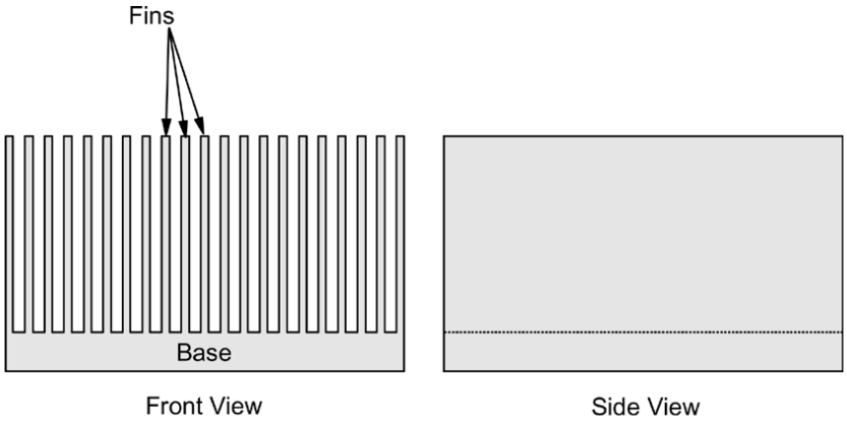

Figure 1-3 Typical air-cooled heat sink [15].

For high heat flux devices, better results are obtained by direct and indirect liquid cooling. Even better performance is possible by phase change (boiling) of the liquid coolant [15].
Heat pipe is another available technology to deal with the high density electronic cooling problems. Some of its positive features are the high effective thermal conductivity, reliability and low weight.
Another available alternative is refrigeration cooling. The term "refrigeration cooling" refers to the application of a refrigeration system capable of lowering the junction temperature (T_j) below the ambient temperature. Maintenance of low junction temperatures while dissipating high heat fluxes is another advantage of refrigeration cooling. However, these advantages must be balanced against the complexity, power consumption and cost of this cooling system as well as possible increase in cooling system volume, and uncertainties in the system reliability issues, such as moving parts in the compressor [16].
Thermoelectric cooling (TEC) technology is attractive for sub-ambient cooling of electronics. It is a solid state technology and works on the principle of Seebeck and Peltier effects where the flow of electric current through the thermoelectric material leads to heat transport against an unfavorable temperature gradient [17], [18]. TECs, has advantages of high reliability, no mechanical moving parts, compact in size and light in weight, and no working fluid. The main disadvantages are the high cost and low energy efficiency, which has restricted its application to cases where system cost and energy efficiency are less important than energy availability, system reliability and quiet operation environment [19].

A phase change material (PCM) is a substance that is capable of storing or releasing a large amount of heat at a certain temperature with phase change. The heat storage is based on the absorption/desorption of energy when a storage material undergoes a phase change from solid to liquid, liquid to gas, or vice versa. It is particularly attractive since it provides a high energy storage density and has the capacity to store energy at a constant temperature – or over a limited range of temperature variation – which is the temperature that corresponds to the phase transition temperature of the material [14], [20].
Despite the extensive studies on cooling techniques and thermal management on PCBs, there is not much research addressing the local climate inside the electronics enclosures exposed to ambient conditions.

1.1.3 Moisture ingress

Even if the enclosure is perfectly sealed and made of truly hermetic materials, moisture may enter it. There are two sources of moisture ingress into a sealed electronics enclosure. The first is the moisture that is sealed into the package during manufacture. This quantity of water is fixed at assembly time and the moisture may reside in the ambient atmosphere, be adsorbed to free surfaces or dissolved into component materials. Even for hermetically sealed enclosures, this moisture must be considered. The second source of moisture is leakage or permeation into the package from the external environment. The magnitude of this contribution can increase with storage time and depends on the details of the seal design as well as the storage conditions [21].
Exposure to high relative humidity may lead to condensation of water on metal surfaces. The thickness of the water layer eventually permits ionic conduction that accelerates the rate of corrosion. These degradation mechanisms can lead to changes in electrical resistance and eventually short circuits [22]. In order to protect the electronic devices from such failures, it is essential to keep the RH inside the electronics enclosure at a low level. The critical range of relative humidity for corrosion failure modes is 60–90% depending on the electronics design and cleanliness [21].
An electronic package may be designed to provide resistance to moisture and ionic contaminants besides removing heat that is either generated internally during device operation or due to the external environment. Figure 1-4 shows some of the design strategies to reduce water induced corrosion. Careful design of enclosure to avoid entry of external contamination and regulating the humidity inside is important, as even a highly reliable PCBA will not survive under severe condensing conditions [23].

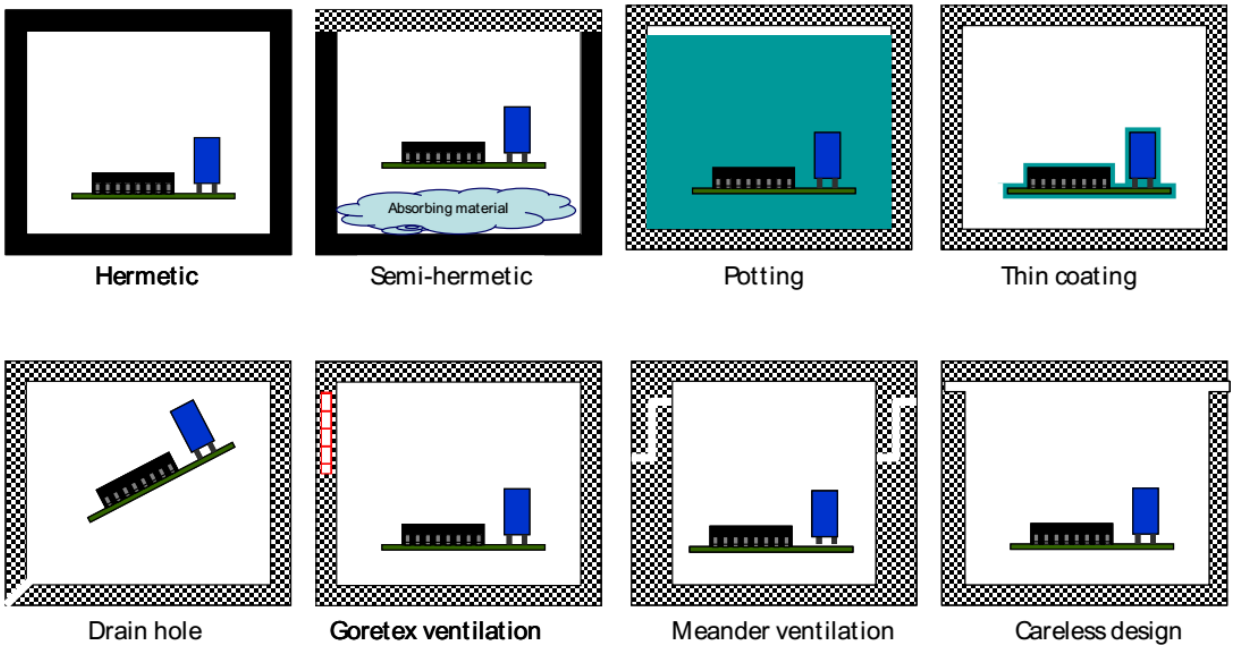

Figure 1-4 Some simple design strategies to avoid water induced corrosion [23].

In general, RH can be kept below the critical value either by maximizing the saturation limit or by minimizing of the dewpoint. These two approaches have their respective advantages and disadvantages. The former is basis of the relative humidity control module, the latter of the absolute humidity control module [24].

Yet another approach might be to use some kind of protective coating or potting; however, it should be noted that an additional plastic layer over the circuit board surface will delay the moisture ingress to the surface but it will not prevent it [25].

Many studies have investigated configuration of electronic devices inside enclosures and diffusion of moisture into the body of these devices, their coatings and mold compounds [26]–[28]. However, there are only few papers that concern local climate inside the enclosures and also how the enclosure itself or the surrounding can affect it.

Tencer [29] developed a quasi-steady state (QSS) model with the purpose of understanding the factors that govern the kinetics of moisture transfer into enclosures, in terms of the properties of the applied materials and the ambient conditions. The time constants for moisture diffusion through plastic walls and openings were estimated by the lumped model [29]. Using this model, one can estimate the average moisture content inside the enclosure. However, it is difficult to apply when the geometry is complex or when several materials are employed in the body of the enclosure [30].

In another study, Tencer and Moss [24] discussed several methods for humidity control inside an electronics enclosure such as limiting moisture ingress into the enclosure, utilizing desiccants and maintaining a dewpoint temperature difference between the critical surface and the ambient. According to the study, controlling the saturation limit is a preferred approach when heat

dissipation is adequate and relatively constant. On the other hand, the methods focusing on limiting moisture ingress into the enclosure provide the designer with more thermal flexibility. Furthermore, coating/potting is generally not recommended except for special applications, e.g., using gels for weatherproofing of outdoor connectors [24].
In another study, Conseil-Gudla [31] used experimental tests and Resistance-Capacitance (RC) circuit modeling to assess the effect of hole/vent size on moisture ingress and water permeability through polymer enclosure material. Results from the work are useful in predicting the interior humidity response in electronics enclosures [31]. Dahan et al. [32] also used an electrical circuit analogy to adapt the QSS model to the moisture ingress into a package containing walls or elements of different thicknesses or properties.
It is worth mentioning that in the electrical analogy, only the volume of the enclosure is considered in the calculation, regardless of its geometrical shape. On the other hand, computational fluid dynamics (CFD) modeling helps us to analyze complex geometries and provides detailed information on temperature and humidity distributions. With CFD, air and moisture transport in an enclosure can be simulated while taking all boundary conditions into account [30].
Belov et al. [33] presented a set of CFD simulation-based methods in combination with experiments, to prevent formation of condensation on the printed circuit assembly (PCA) housed in a non-hermetic metallic enclosure. The enclosure is exposed to a severe storage environment with considerable variation of relative humidity and temperature. They achieved a level of relative humidity of less than 60% inside the enclosure to minimize the risk of dew formation on the printed circuit boards using a heater [33]. In another study, Kremp and Schilling [34] experimentally investigated the influence of different cycling profiles on condensation risk inside an enclosure. Furthermore, they studied the condensation risk stemmimg from long term humidity build-up inside an electronics enclosure.

1.2 Mathematical models

Modeling tools are very helpful for reliable design in electronic industry. Mathematical models have been widely used for predicting and evaluating the thermal performance of PCBs, heatsinks, configuration of the system, etc.
Most of the mathematical models used for humidity and thermal management can be categorized in two groups:

I. Multiphysics modeling
II. RC ladder approach

1.2.1 Multiphysics modeling

In order to describe and control the local climate inside an electronics enclosure, it is crucially important to have an accurate and clear understanding of the interconnected transport phenomena and physics inside the enclosure.

The descriptions of laws of physics for space- and time-dependent problems are usually expressed in terms of partial differential equations (PDEs). For the vast majority of geometries and problems, these PDEs cannot be solved with analytical methods. However, using different type of numerical methods, an approximate solutions of the equations can be constructed. [35].
Nowadays, multiphysics modeling has been proven as a useful tool to develop the detailed information about fluid flow and heat and mass transfer. Thus, it can be helpful for predicting local climate inside the electronics enclosures. One major drawback of such models though, is the high computational cost [22].

1.2.2 RC ladder approach

The RC ladder models come in two types: Foster ladder models and Cauer ladder models. Figure 1-5 presents the two systems. A Cauer ladder models provide a better physical description of the heat flow path in the system, while Foster ladder models only capture the thermal behavior but have no physical equivalent [36].
The RC ladder approach is particularly attractive because it provides the possibility of the use of standard circuit simulators to perform thermal simulations. While this method is quite conventional for transient heat conduction, there are still some challenges in using it for convective heat transfer [37].

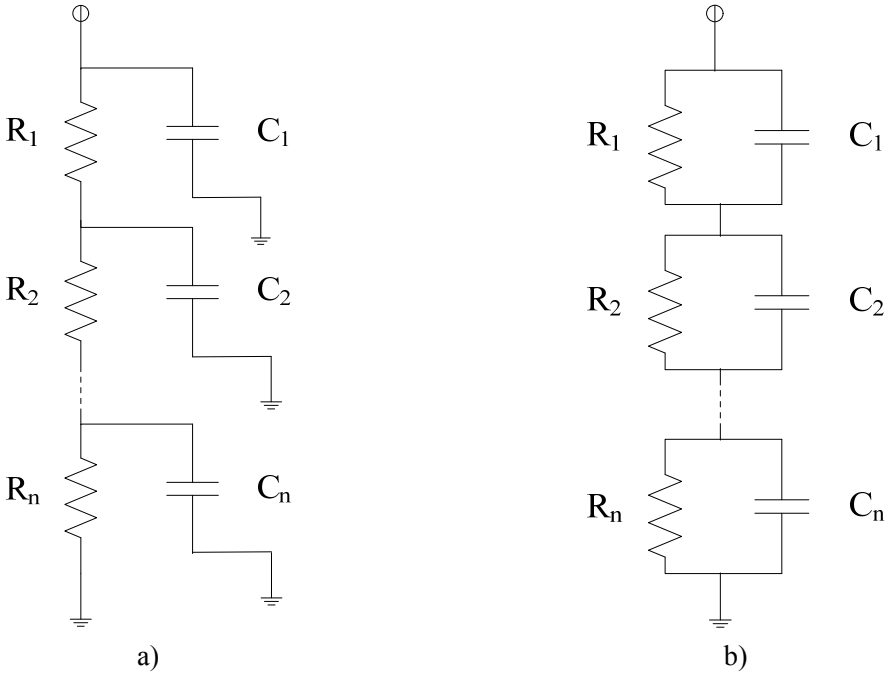

Figure 1-5 a) Cauer and b) Foster RC ladder circuits [36].

1.3 Objectives of the thesis

Since experiments for monitoring the local climate inside enclosures are often tedious, and due to operational difficulties typically last for couple of days, there is a need for a reliable predictive model that is computationally fast and therefore capable of long term predictions, such as seasonal or annual, predictions, using realistic ambient conditions. CFD simulations can provide detailed information about transient temperature and RH distributions by considering all the geometric complexities of an electronics enclosure and the components inside. For that reason CFD simulation is a widely used method in the design of electronics enclosures. However, such simulations are often time consuming and CPU-intensive, and are therefore unsuitable for true long term analyses. On the other hand, lumped models, based on the fundamental similarity of heat and mass transfer with the transfer of electric charge in an electrical circuit, are capable of fast and easy predictions [38]. Nevertheless, because of their underlying simplifying assumptions, as well as their implementation constraints, they lack accuracy. Thus, unfortunately there is a lack of reliable and fast models for long term prediction of the local climate inside electronics enclosures.
The present thesis aims at

1. Developing reliable models for estimating the transient response of the internal RH and temperature of a typical electronics enclosure to the ambient conditions. At this stage, 2D and lumped models are compared with 3D models. This step is to evaluate and compare the accuracy of the 2D, 3D and lumped models by comparing the results with experimental data.
2. Studying the effects of different parameters, namely geometrical (size and place of the opening …) and operating conditions (heat load of the electronics, ambient conditions …) on the local climate inside the enclosure.
3. Deriving semi-empirical functions using statistical analysis of experimental and simulation data.
4. Deriving fast and reliable models for long term prediction of the local climate inside a typical electronics enclosure exposed to uncontrolled ambient conditions.

1.4 Structure of the thesis

The thesis is composed of 7 chapters and 7 appended publications as follows:
This research comes into three main parts as follows:

Chapter 1: Introduction

- This chapter gives an introduction to the electronics enclosures and the local climate inside. The predictive modelling tools are also briefly discussed, following by the objectives and structure of the thesis.

Chapter 2: Transport phenomena

- The transport phenomena occurring in a typical electronics enclosure are given in this chapter. The thermophysical properties of the humid air are also numerically estimated by considering humid air as mixture of dry air and water vapor. Finally, the multiphysics modelling approach is presented.

Chapter 3: The response of a typical electronics enclosure exposed to constant ambient conditions

- This chapter discusses CFD modeling in isothermal conditions to study the moisture distribution as well as the transfer time into a typical electronics enclosure with an opening. Thereafter, an analysis of variance (ANOVA) is applied on both CFD simulation results and experimental data to study the effect of the potentially influential factors.

Chapter 4: The response of a typical electronics enclosure exposed to cyclic ambient conditions

- This chapter focuses on the response of a typical electronics enclosure to different cyclic ambient conditions. Several cases of an empty enclosure and an enclosure with components inside are extensively studied.

Chapter 5: Deriving an RC model for fast prediction of the local climate inside a typical electronics enclosure

- A CFD adapted RC Cauer ladder model for the purpose of fast calculation of temperature of the electronics and moisture content of the trapped air inside an electronics enclosure for long term predictions is presented in this chapter.

Chapter 6: Summary of the appended papers

- In this chapter a short summary of the appended publications is given.

Chapter 7: Conclusion and outlook

- The conclusion of the thesis and the perspectives for further studies are summarized in this chapter.

Chapter 2
Transport phenomena

Generally, the subject of transport phenomena includes three closely related topics: fluid dynamics (momentum transfer), heat transfer, and mass transfer. Fluid dynamics involves the transport of momentum, heat transfer deals with the transport of energy, and mass transfer is concerned with the transport of mass of various chemical species.
All these three happen in an electronics enclosure. Thus, in order to describe and control the local climate, it is crucially important to have an accurate and clear understanding of these interconnected transport phenomena inside an electronics enclosure. The thermophysical properties of the humid air are also numerically studied. Finally, the multiphysics modelling approach in this work is discussed.

2.1 Momentum transfer

Momentum can be transferred by molecular motion and/or the bulk fluid motion. The simple shear flow between parallel plates demonstrates how momentum is transferred through the fluid by viscous action. The molecules are in continuous random motion, colliding with one another and exchanging energy and momentum. This is an elementary example of molecular momentum transport and it serves to introduce "Newton's law of viscosity" along with the definition of viscosity. On the other hand, convective momentum transport is proportional to the fluid density [39]–[41].
The combined momentum flux, which is the sum of the molecular momentum flux and the convective momentum flux is:

$$\emptyset = \boldsymbol{\pi} + \rho \mathbf{u}\mathbf{u} \qquad (2.1)$$

The terms '$\boldsymbol{\pi}$' and '$\rho\mathbf{u}\mathbf{u}$' describe the viscous and convective momentum, respectively and $\emptyset$ is the combination.

2.2 Heat transfer

Heat transfer for the trapped air inside an electronics enclosures is mostly dominated by convection. Convective heat transfer is categorized in natural and forced convection. Figure 2-1 demonstrates the two categories for the air inside electronics enclosures.

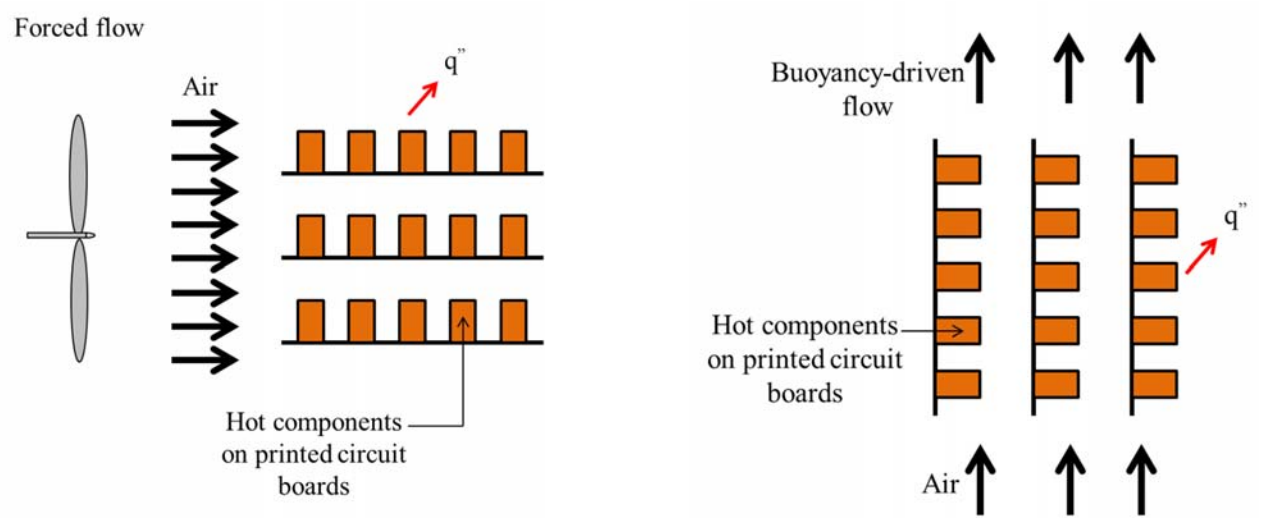

Figure 2-1 Air flow inside electronics enclosures [40].

2.2.1 Natural convection

Natural convection is due to buoyancy forces within the fluid; buoyancy is due to the combined presence of a fluid density gradient and a body (volume) force that is proportional to density. The body force is usually gravitational. There are several ways in which a mass density gradient may arise in a fluid; however, the most common situation is due to the presence of a temperature gradient. Generally, natural convection in air-filled enclosures can be described in terms of the full Navier-Stockes equation, the energy equation and the continuity equation. The energy equation and the Navier-Stokes equations are coupled because the temperature dependence of the fluid properties has to be taken into account. This makes natural convection a complex problem [7].
Over the years of research on empirical relations for describing natural convection, it has been found that average free-convection heat-transfer coefficients can be represented in the following functional form:

$$Nu = \frac{hL}{k} = c(Gr \times Pr)^m = c(Ra)^m \qquad (2.2)$$

$$Gr_L = \frac{g\beta\,(\Delta T)L^3}{\nu^2} \qquad (2.3)$$

$$Pr = \frac{C_p\mu}{k} = \frac{\nu}{\alpha} \qquad (2.4)$$

, where Nu, Gr, Pr and Ra represent Nusselt, Grashof, Prandtl and Rayleigh numbers, respectively. The values of the constants c and m depend on geometry, configuration (orientation), and whether the natural convection boundary layer is laminar or turbulent. Transition in a natural convection boundary layer depends on the relative magnitude of the buoyancy and viscous forces in the fluid. It is customary to correlate its occurrence in terms of the Ra. For vertical plates the critical Ra is

about 10^9 [40]–[42]. Ra is simply the product of the Gr and Pr numbers.

Gr number provides a measure of the ratio of buoyancy forces to viscous forces in the velocity boundary layer. The physical interpretation of the Pr follows from its definition as a ratio of the momentum diffusivity (ν) to the thermal diffusivity (α). The Pr provides a measure of the relative effectiveness of momentum and energy transport by diffusion in the velocity and thermal boundary layers, respectively.

In conduction problems that involve surface convection, the Bi (Biot) number plays a fundamental role. The Bi is defined as:

$$Bi = \frac{hL}{k} \qquad (5.4)$$

The Bi number compares the relative magnitudes of surface convection and internal conduction. In the conditions corresponding to Bi<<1, it is reasonable to assume a uniform temperature distribution within a solid at any time during a transient process. This result can be associated with interpretation of the Biot number as a ratio of thermal resistances.

A very low value of the Bi (Bi<<1) means that internal conduction resistance is negligible in comparison with surface convection resistance. This in turn implies that the temperature will be nearly uniform throughout the solid, and its behavior can be approximated by the lumped RC method [40].

2.2.2 Forced convection

Convective heat transfer between a solid surface and a fluid is proportional to the velocity of the fluid. The fluid velocities associated with natural convection heat transfer are relatively low; thus, natural convection cooling is limited to low-power electronic systems. When natural convection cooling is not sufficient, a fan is added to blow air through the enclosure that houses the electronic components. By doing so, we can increase the heat transfer coefficient, depending on the size of the fan; so that the heat is removed at much higher rates for a specified temperature difference between the components and the air, or the surface temperature of the components is reduced for specific power dissipation [43].

Essentially that since free convection relies on sufficiently large temperature gradient, is very important to consider the temperature-dependency of fluid properties [44].

In a transient study of such a non-isothermal fluid flow, it is important to investigate the variations of the thermophysical and transport properties of air such as density, viscosity, thermal conductivity, etc. versus temperature and relative humidity. Tsilingiris [45] evaluated these properties as a function of temperature with relative humidity, ranging between dry air and saturation conditions.

2.2 Mass transfer

A significant portion of environmental reliability problems are directly or indirectly related to high atmospheric humidity [21]. Possible moisture transport in an electronics enclosure is demonstrated in Figure 2-2. Moisture can enter an enclosure by diffusion and/or convection through openings.

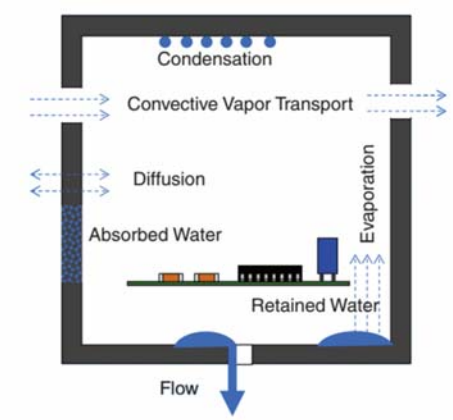

Figure 2-2 Moisture transport in an electronics enclosure [4].

2.3 Thermo-physical properties of humid air

Thermophysical properties of air are influenced by the moisture content, as well; consequently, natural convection heat transfer is also affected. Tsilingiris [45] evaluated the thermophysical properties of humid air as a function of temperature (from 0-100 [°C]) and RH, ranging from dry air to saturation conditions. Considering humid air as a mixture of dry air and water vapour, correlations were presented to derive the temperature and RH dependence of the mixture density, viscosity, specific heat capacity and thermal conductivity under the total barometric pressure of 101.3 [kPa]. In another study, Melling et al. [46] provided simple analytical correlations. The correlations were derived from theory and numerical curve fitting for a working pressure of 1 [bar] in the temperature range of 100-200 [°C]. In this work (as presented in Paper 6), the thermophysical properties of humid air as a mixture of vapour and dry air are estimated using the following equations based on Tsilingiris's work [45]:

$$\rho_m = \frac{1}{Z_m} \times \frac{p_0}{RT} \times \left(M_a \frac{p_0 - p_v}{p_0} + M_v \frac{p_v}{p_0}\right) \qquad (2.5)$$

$$\mu_m = \frac{(1 - x_v)\mu_a}{(1 - x_v) + x_v \Phi_{av}} + \frac{x_v \mu_v}{(1 - x_v)\Phi_{va} + x_v} \qquad (2.6)$$

$$\Phi_{av} = \frac{\sqrt{2}}{4}\left(1 + \frac{M_a}{M_v}\right)^{\frac{-1}{2}} \times \left[1 + \left(\frac{\mu_a}{\mu_v}\right)^{\frac{1}{2}} \left(\frac{M_a}{M_v}\right)^{\frac{-1}{4}}\right]^2 \qquad (2.7)$$

$$\Phi_{va} = \frac{\sqrt{2}}{4}(1+\frac{M_a}{M_v})^{\frac{1}{2}} \times \left[1+(\frac{\mu_a}{\mu_v})^{\frac{-1}{2}}(\frac{M_a}{M_v})^{\frac{1}{4}}\right]^2 \quad (2.8)$$

$$k_m = \frac{(1-x_v)k_a}{(1-x_v)+x_v\Phi_{av}} + \frac{x_v k_v}{(1-x_v)\Phi_{va}+x_v} \quad (2.9)$$

$$Cp_m = \frac{\mathrm{C}_{pa}(1-x_v)M_a + \mathrm{C}_{pv}x_v M_v}{(1-x_v)M_a + x_v \mathrm{M}_v} \quad (2.10)$$

Where,

- ρ is mass density [kg/m^3]
- Z is compressibility factor
- p is pressure [pa]
- R is universal gas constant [J/(mol.K)]
- T is temperature [K]
- M is molecular weight [gr/mole]
- μ is dynamic viscosity [Pa.s]
- x is molar fraction
- ϕ is interaction parameter
- k is thermal conductivity [W/(m.K)]
- C_p is specific heat of the fluid at constant pressure [J/kg.K]

The subscripts are “a” for air, “v” for vapor and “m” for the mixture.
In order to study the effect of RH and temperature on the material properties of humid air, a case where a vertically positioned PCB with a length of 10 [cm] is considered exposed to the ambient temperature of 20 [°C]. Density, viscosity, thermal conductivity and the specific heat capacity of humid air are shown in Figures 2-3 to 2-6, respectively, at different PCB temperatures.

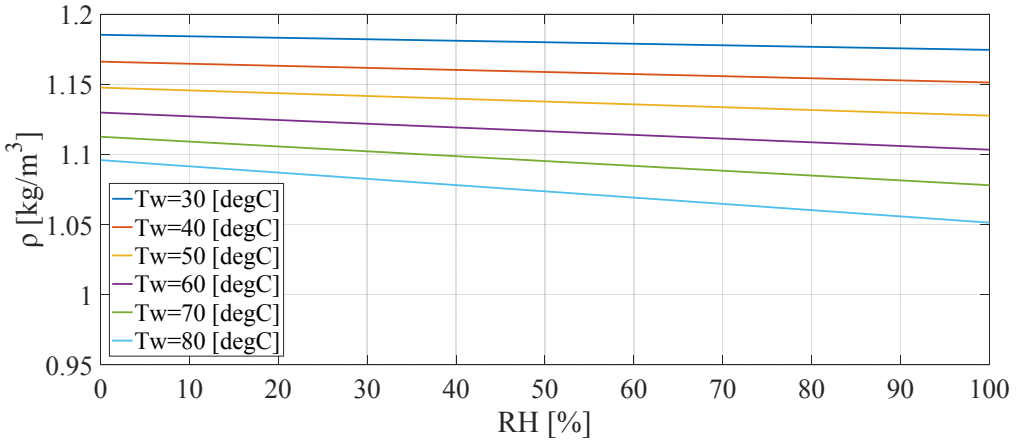

Figure 2-3 The density of humid air as a function of RH.

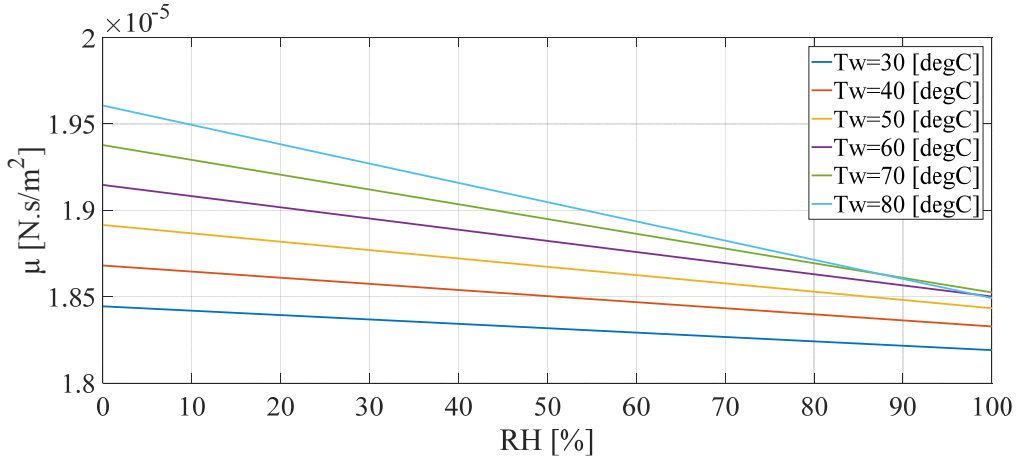

Figure 2-4 The viscosity of humid air as a function of RH.

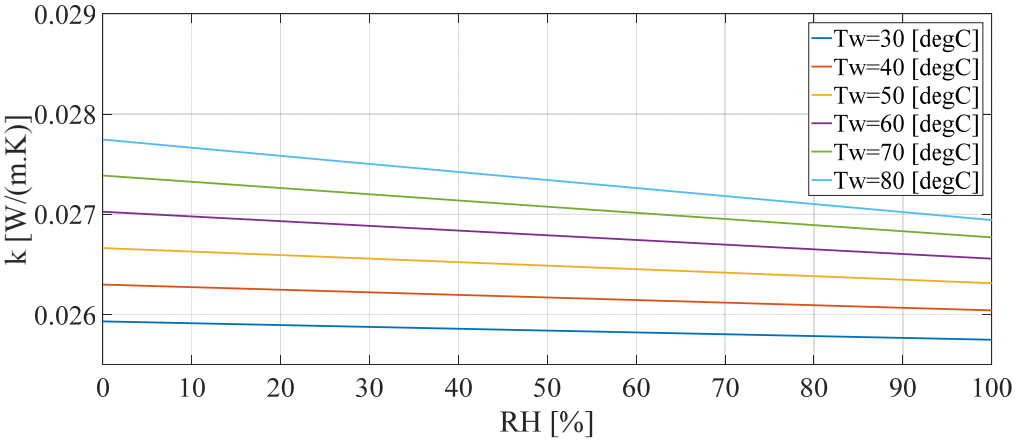

Figure 2-5 The thermal conductivity of humid air as a function of RH.

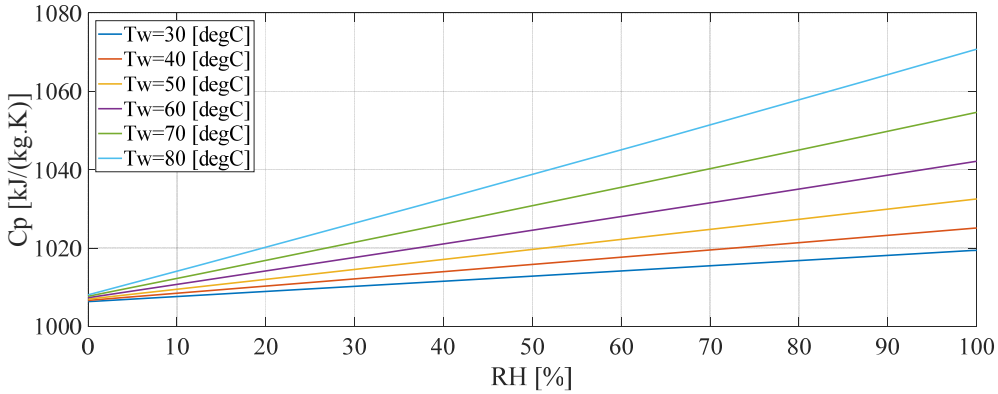

Figure 2-6 The specific heat capacity of humid air as a function of RH.

The effect of RH is more noticeable at higher temperatures; however, the four properties do not drastically change with RH changes. Figure 2-7 demonstrates the average velocity next to the

vertical PCB at different temperatures. It is shown that the effect of temperature is more significant compared to the RH.
In order to study the effect of RH on the heat transfer, the Pr and Gr number are also calculated. According to Figure 2-8, the Pr is not highly affected by any of the RH and temperature changes. The Gr changes with RH are negligible (see Figure 2-9). Thus, it makes sense to only consider the effect of temperature on the above mentioned material properties while the temperature is below 80 [°C].

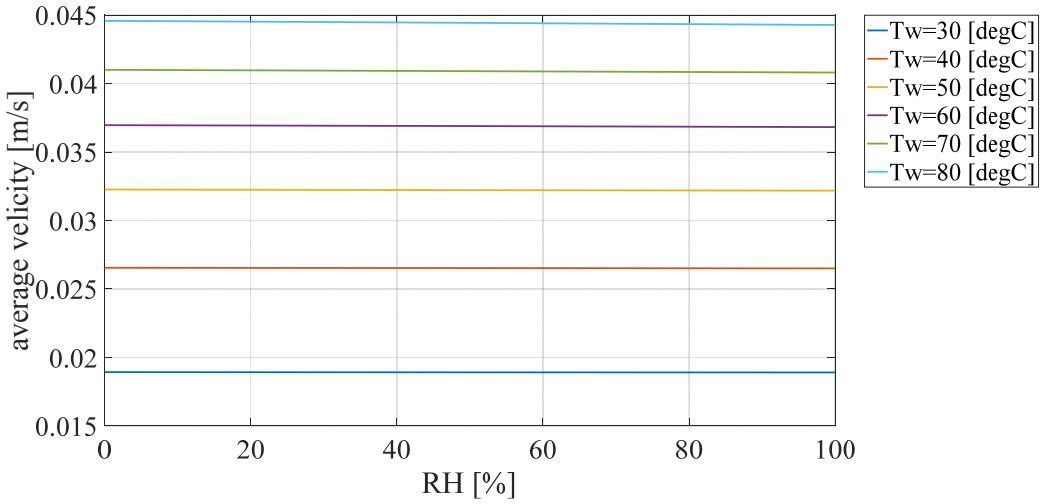

Figure 2-7 The average velocity of humid air as a function of RH.

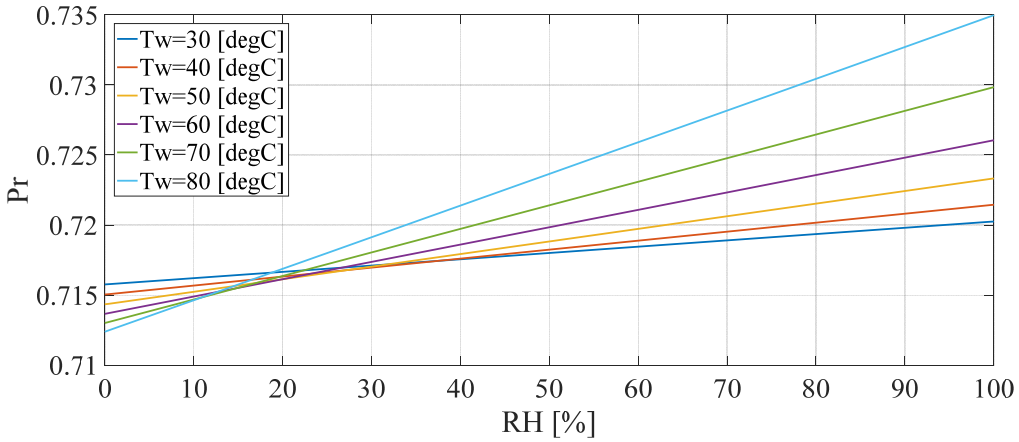

Figure 2-8 The Pr of humid air as a function of RH.

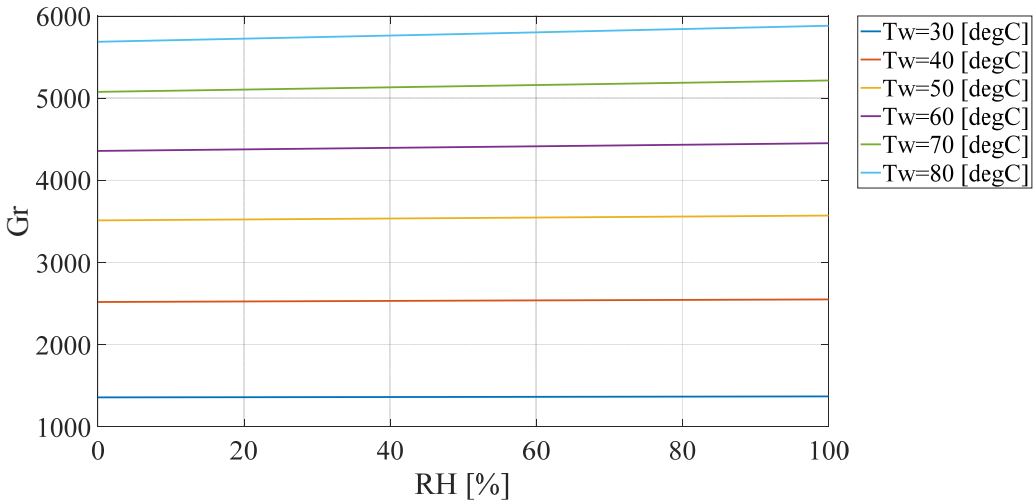

Figure 2-9 The Gr of humid air as a function of RH.

Air cooling by natural convection through a heatsink is investigated in different ambient conditions of several cities, namely Copenhagen, Mashhad, Singapore, Las Vegas and Jakarta for one day (Paper 6). The thermophysical properties of humid air are estimated using the correlations from Tsilingiris' [45] work because of the operating temperatures. The ambient data (moisture concentration and temperature) are taken from the *COMSOl Multiphysics*^{TM} database. The calculations are done in *MATLAB R2016b*. The Grashof (Gr) and Prandtl (Pr) numbers are calculated transiently with the dynamic ambient changes and finally the Rayleigh numbers (Ra) of the five cases are compared.

The moisture diffusion coefficient into the air is also a function of temperature. Marrero and Mason suggested the following equation for estimation the diffusion coefficient [47]:

$$D_{air} = 1.87 \times 10^{-10} \times T^{2.072} \qquad (2.11)$$

The moisture diffusion coefficient into air can also be obtained by a regression curve fit to data from Bolz and Tuve [48]–[51]:

$$D_{air} = -2.775 \times 10^{-6} + (4.479 \times 10^{-8}) \times T + (1.656 \times 10^{-10})T^2 \qquad (2.12)$$

Figure 2-10 compares the two correlations. It is seen that the estimated values are very close within the temperature range of 0 to 100 [°C]. In this work, the correlation developed by Boltz and Tuve is used.

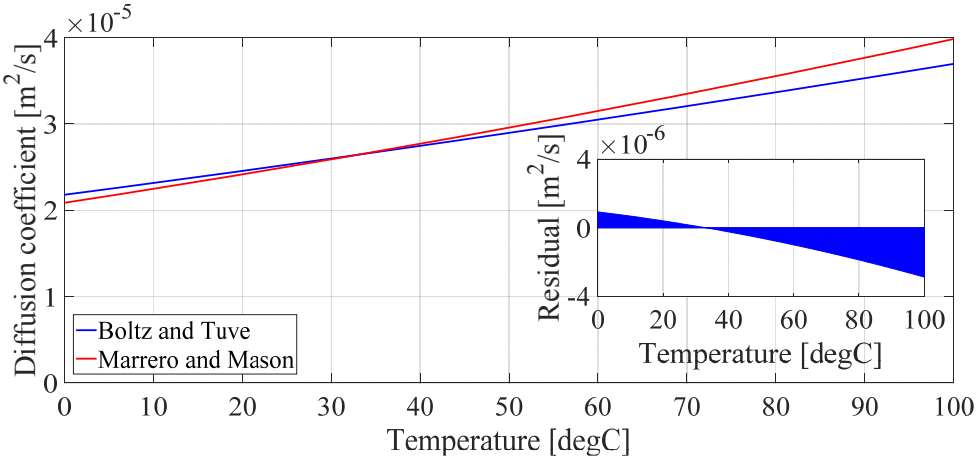

Figure 2-10 Moisture diffusion coefficients into air

2.4 Multiphysics modelling

In this study, the air flow is assumed to remain laminar due to relatively low transient temperature gradients that will lead to low free convection-induced flow rates. The working fluid is modeled as a binary mixture (air + water vapor), and is therefore assumed to be Newtonian and compressible. As explained above, the thermophysical properties (density, specific heat capacity, conductivity and viscosity) of the fluid depend on temperature and RH. However, in the temperature range of interest in this study, the effects of RH on the thermophysical properties of air are small and are therefore neglected [45].

For a laminar compressible fluid flow (air, in this study), the mass, momentum and energy conservation equations are:

$$\frac{\partial \rho}{\partial t} + \nabla.(\rho \mathbf{u}) = 0 \qquad (\mathbf{1})$$

$$\rho\left(\frac{\partial \mathbf{u}}{\partial t} + \mathbf{u}.\nabla\mathbf{u}\right) = -\nabla p + \nabla.\left[(\mu(\nabla\mathbf{u} + (\nabla\mathbf{u})^T) - \frac{2}{3}\mu(\nabla.\mathbf{u})\mathbf{I}\right] + \mathbf{F} \qquad (2.13)$$

$$\rho c_p \frac{\partial T}{\partial t} + \rho c_p \mathbf{u}.\nabla T = \nabla.k(\nabla T) + Q \qquad (2.14)$$

, where

$$F_z = -\rho g;\ F_x = F_y = 0 \qquad (2.15)$$

The species mass conservation equation is:

$$\frac{\partial c}{\partial t} + \mathbf{u}.\nabla c = D\nabla^2 \mathrm{c} \qquad (2.16)$$

In this work, the differential equations are coupled in two different ways. In the first method, the transient temperature and velocity profile are calculated by solving the coupled continuity, momentum and energy conservation equations. The calculated transient velocity and temperature distributions are then used for solving the mass species equation in order to derive the moisture distributions (see Figure 2-11). As demonstrated in Figure 2-12, in the other way, all the differential

equations are solved simultaneously for every simulation time step. Not surprisingly, the results of the simulations are not different as the moisture transfer does not significantly affect the temperature and velocity profile. On the other hand, solving the equations in the second configuration takes more than double the CPU-time.

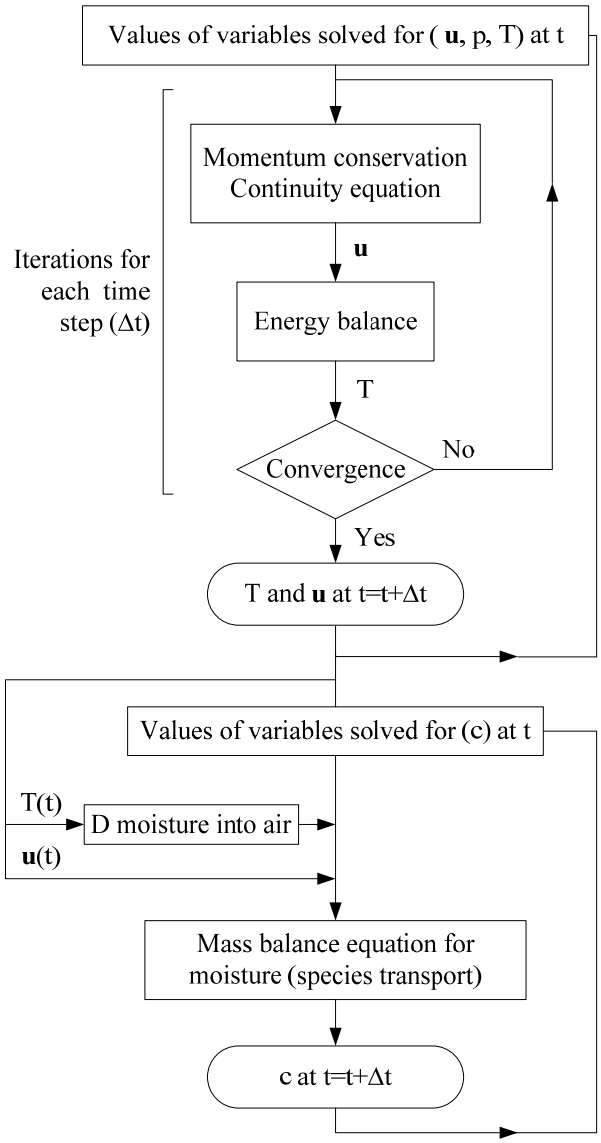

Figure 2-11 Flowchart of the solution method.

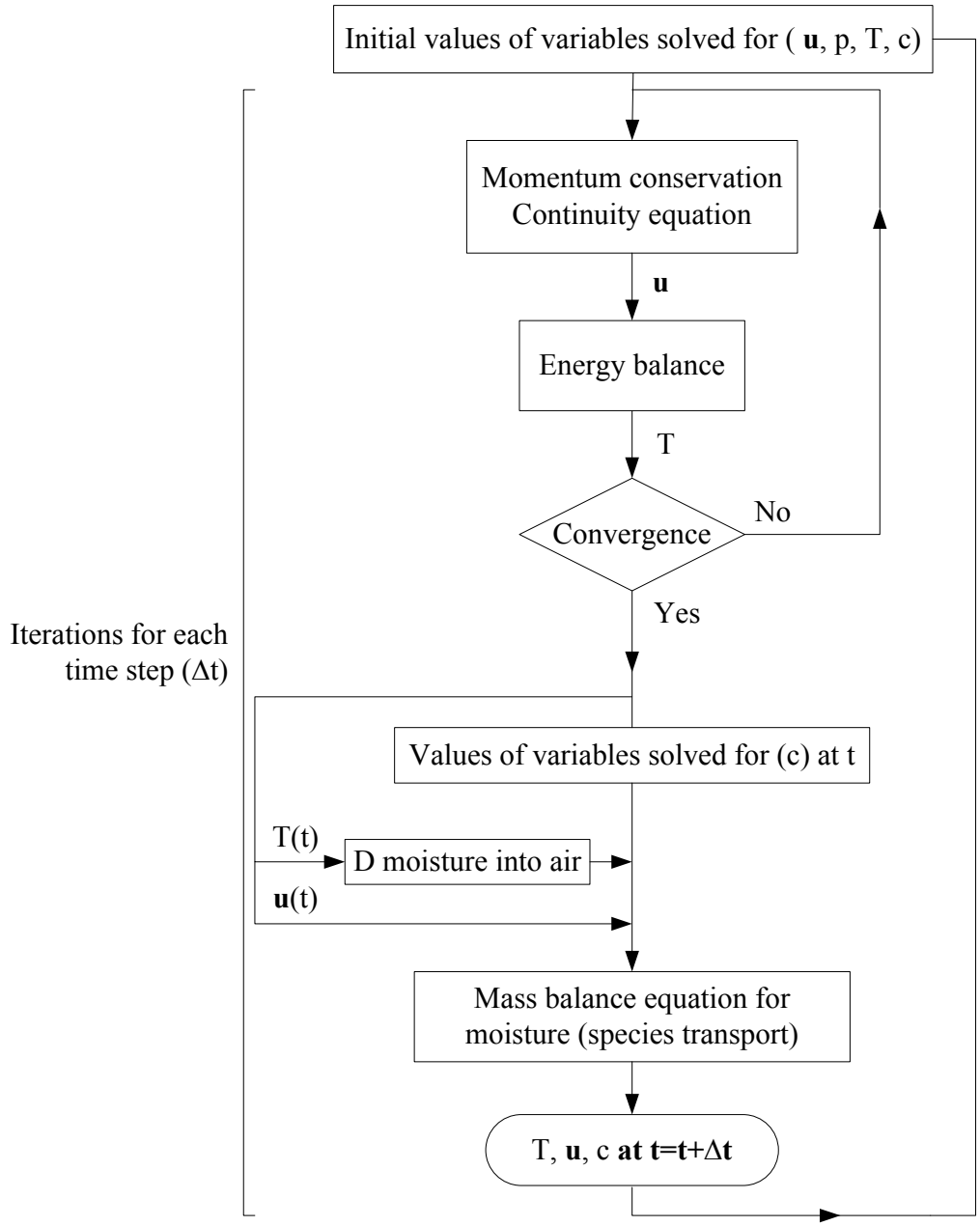

Figure 2-12 Flowchart of the solution method.

The CFD simulations are conducted using the commercial finite element code COMSOL Multiphysics^{TM} version 5.1 and 5.2. In COMSOL Multiphysics^{TM}, the solvers split each problem – whether linear or nonlinear– into one or more linear systems of equations by approximating the given problem with a linearized problem. In this work, velocity is part of the nonlinear solution of coupled energy and momentum transfer equations. The parallel direct solver (PARDISO) is utilized as the solver linear system. This memory efficient solver works on general sparse linear systems

of the form Ax = b and uses LU (lower-upper) factorization on the matrix A to compute the solution x [52]. The time-dependent solver is based on the backward differentiation formula (BDF) method, with the maximum order set to two.

Due to the complicated structure of the modeled system, an unstructured mesh composed of tetrahedral elements is applied on the computational domain in all the simulations. The adaptive mesh refinement method is used to improve the mesh quality. Mesh convergence was examined to ensure the accuracy of the numerical results.

Chapter 3
The response of a typical electronics enclosure exposed to constant ambient conditions

In this chapter, first CFD modeling with an isothermal condition is used to study the moisture distribution as well as the transfer time into a typical poly carbonate electronics enclosure with an opening. Then the results are compared with the well-known RC modeling approach. Using the CFD results, an analysis of variance (ANOVA) is performed to provide a design space of the potentially influential factors, which affect the moisture ingress into the enclosure, so that the level of significance of each factor can be clarified at the whole range. The aim of this part of the study is to replace the CFD calculations with a simple equation derived from the ANOVA of the factorial design (FD) points (Paper I). Furthermore, this study provides useful data enabling the design of a breathable enclosure that allows moisture and dust to escape or let the electronics inside the enclosure to dry out on hot, sunny days or similar occasions. An ANOVA is also applied on a set of experiments designed by a fractional factorial design (Paper IV). Thereafter, the effects of a heat producing electronic device inside the enclosure are also simulated numerically for constant ambient exposure conditions. Thereafter, the RH built-up inside the enclosure is studied in case of internal cyclic heating (Paper I, IV and V).

3.1 Isothermal moisture transfer into a typical enclosure

The electronics enclosure investigated in this chapter is shown in Figure 3-1. Table 3-1 shows the dimensions.

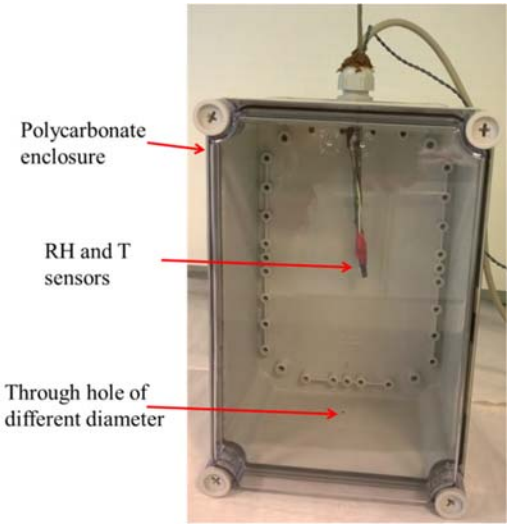

Table 3-1 Dimensions of the electronics enclosure

Inner dimensions (W × D × L) [mm]	188× 128 × 276
Outer dimensions (W × D × L) [mm]	190× 130 × 280
Opening Diameter [mm]	From 1 to 10

Figure 3-2 displays the average moisture concentration in the enclosure vs. time in the case that the ambient RH is kept at 98 [%], at the temperature of 25 [°C]. The estimated curve, using the RC approach developed by Tencer [29] for the same conditions is displayed. The initial relative humidity was 40 [%] at 25 [°C]. As it is shown in Figure 3-2, it takes about 20 days for the air inside the enclosure to reach the ambient RH of 98%. However, after about 7 days the RH is more than 90%. Not surprisingly, as the mass transfer driving force (the concentration difference between the enclosure and the ambient air) decreases with time, the moisture transfer rate also decreases. The time constant in the RC approach and the mean moisture concentration inside the enclosure are calculated using Equations (3.1) and (3.2), respectively, [29].

$$\tau = \frac{V \times L}{A \times D} \quad (3.1)$$

$$RH_{enclosure} = RH_{ambient} + (RH_{ambient} - RH_{initial}) \times exp(-time/\tau) \quad (3.2)$$

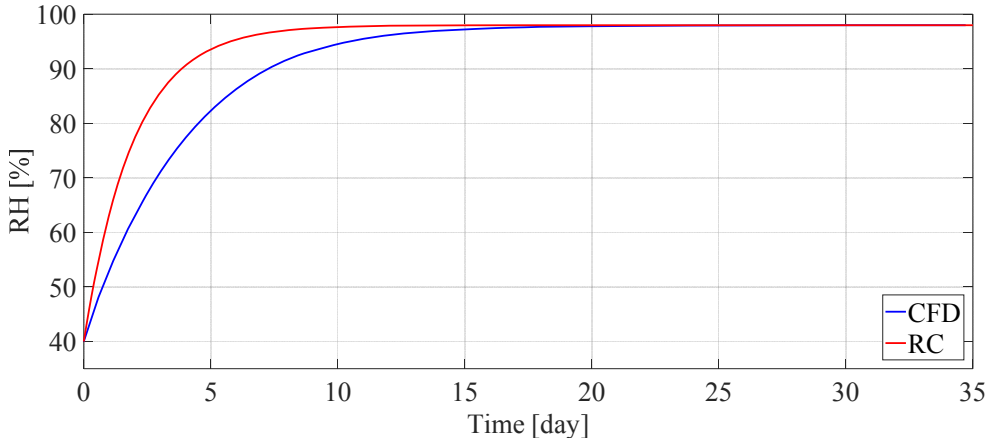

Figure 3-2 The average moisture content in the enclosure (opening diameter= 2 [mm]).

The RC approach generally shows the same behavior as the CFD simulation. However, the pace of the RH increase is faster in the RC method (the time constants for the RC and the CFD in this case are 1.95 and 3.87 days, respectively). There are some simplifying assumptions in the RC method that can explain this deviation. In the RC approach, the resistance against the mass transfer inside the volume of the enclosure is completely neglected; in other words, the concentration is assumed to be homogeneous throughout the volume inside the enclosure over time. Figure 3-3 depicts the concentration profile at the centerline, in the symmetry face of the enclosure. According to this figure, there is a concentration gradient inside the enclosure that does not seem to be negligible, especially at the initial days. The concentration gradient decreases over time, though. This gradient reveals the presence of the resistance inside the volume, which delays the mass transfer into the enclosure. This effect is less significant compared to the delay that the opening causes (as explained in Paper I).

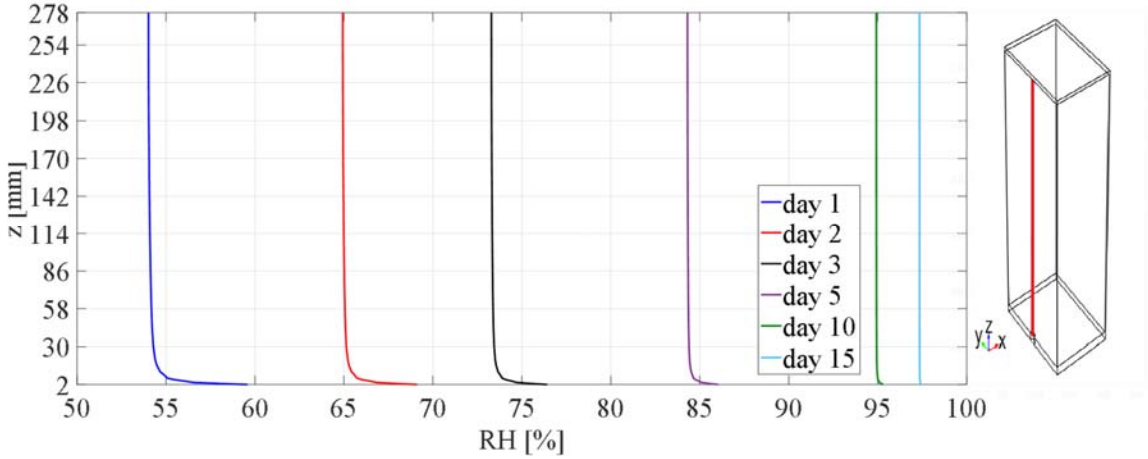

Figure 3-3 The concentration profile at the center of the symmetry face at different times (opening diameter= 2 [mm]).

Furthermore, the RC approach only considers the size of the volume, not the geometrical shape or other details such as the position of the opening. On the other hand, in the 3D CFD simulations all the details of the enclosure are taken into account. Figure 3-4 demonstrates the effect of the position of the opening in the enclosure, comparing three different cases. In position 1, the opening is located in the center of the bottom face of the enclosure (standard case); in position 2 it is located at the corner of the bottom face, and finally in position 3 it is located in the center of a side face (see sub-Figure 3-4). According to the simulation results presented in Figure 3-4, the RH inside the enclosure follows the same trend for the positions 1 and 3 (time constant = 3.8 days). Nevertheless, for position 2 the trend is slightly different; in this case, the moisture passes longer distance to reach the corners of the enclosure (time constant = 4.6 days).

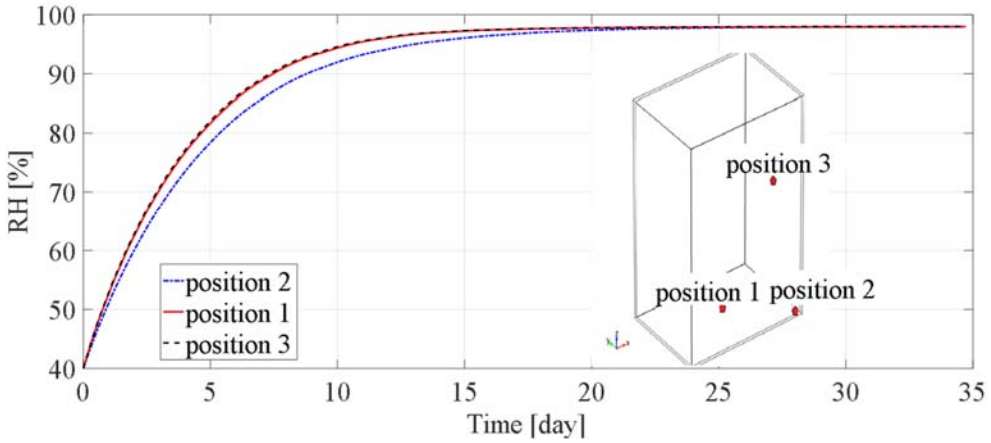

Figure 3-4 The average RH inside the enclosure for different positions of the opening at 25 [°C]. The sub-figure shows the position of the opening in the three investigated cases.

As the opening seems to be the significant resistance against the mass transfer, the moisture transfer into the enclosure with different opening sizes is compared (see Figure 3-5). It is important to maintain a RH below the threshold value of 60%; damaging could occur when the RH inside the enclosure exceeds this critical level (in the range of 60–90% depending on the electronics design and cleanliness) [4], [24], [53]. According to Figure 3-5, it takes about four times longer for the enclosure with the 1 mm diameter opening to reach the critical values of 60% relative compared to the one with the 2 mm diameter opening. On the other hand, for the enclosure with the 3 mm diameter opening it is about 9 times faster. This demonstrates the non-linear nature of the diffusion time as a function of the opening radius (Table 3-2). However, it should be noted that the diffusion time is changing linearly with the surface area of the opening.

Table 3-2 Resistance values against the mass transfer.

$R_{opening}$[s/m^3]				$R_{enclosure}$[s/m^3]
R=0.5 [mm]	R = 1[mm]	R = 1.5[mm]	R = 2.5[mm]	
1.0186×10^8	2.5465×10^7	1.1318×10^7	4.0744×10^6	4.5878×10^5

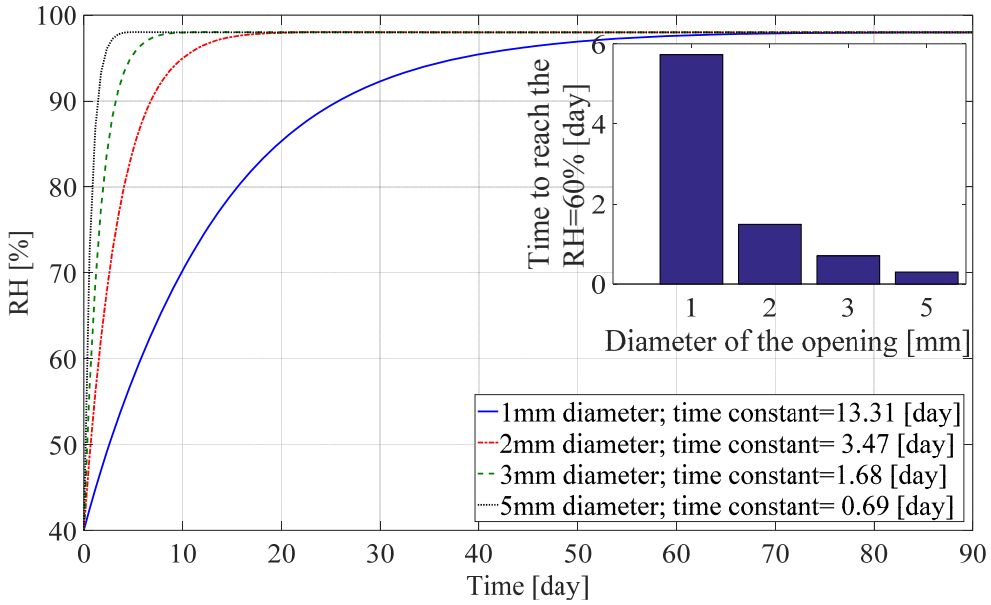

Figure 3-5 The effect of the opening radius size at 25 [°C] (The sub-figure shows the estimated diffusion time to reach RH = 60 [%] for the different opening sizes).

The CFD model is validated by comparing the simulation results with experimental data from the study carried out by Conseil et al. [54], in which a climatic chamber was used to set specific predefined values for the ambient temperature and RH in the surrounding of the enclosure. First, the enclosure was exposed to the temperature of 25 [°C] and RH of 98[%]. Then, the ambient condition was set to a RH of 33 [%]. The temperature was kept at 25 [°C]. The initial RH in the enclosure was 28 [%]. According to Figure 3-6, the CFD simulation results are visually in a good agreement with the experimental data. The time constants derived from the experimental data and the simulations for the 3.13 and 3.82 days are moisture ingress part, respectively. The values are 30.8 and 30.2 days for the second part of the graph, respectively, where the RH is decreasing inside the enclosure.

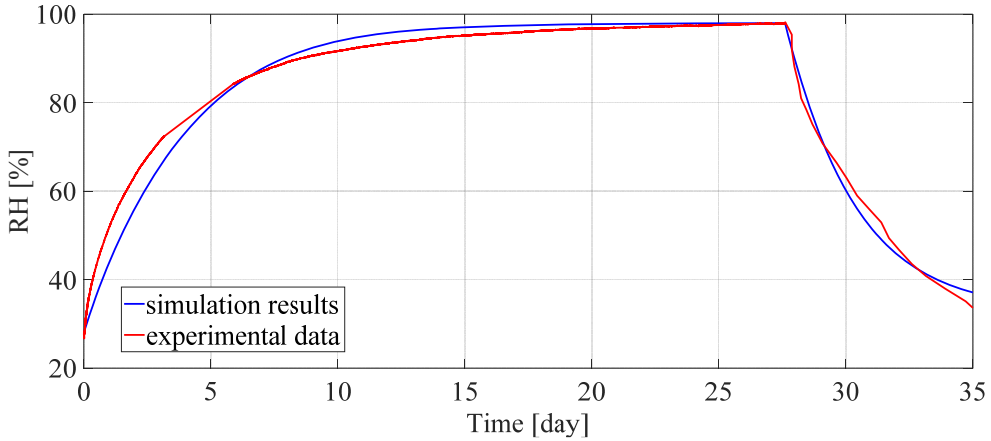

Figure 3-6 Comparison between the CFD simulation result (position 1) and the experimental data from Conseil et al. [54].

3.2 Factorial design based on CFD results

When a system is potentially affected by several factors, a screening statistical method can be used to estimate the main effects of active factors and possible interactions that involve the active factors. A two-level factorial design (FD) provides suitable designs for screening the influential factors, assuming the linear behavior model [55], [56]. In a 2^k factorial design, the model for analyzing responses (observations) is given by Montgomery [57]:

$$y = \beta_0 + \sum_{j=1}^{k} \beta_j x_j + \sum_{i<j} \sum \beta_{ij} x_i x_j + \epsilon \qquad (3.3)$$

, where y is the response, the β's are parameters whose values are to be determined, x's are variables that represent the factors and $\in$ is a random error term. In this approach, higher-order interaction effects are initially neglected. However, the presences of such effects are checked.

Here, a two level full factorial design is applied on four parameters (2^4) based on the CFD simulation results in order to check the significance of their influence on the diffusion time of moisture into the enclosure at constant ambient temperature and relative humidity. To check for the presence of probable curvatures, a center-point is also added to the design. Therefore, there are 17 cases to be investigated *($2^4 + 1 = 17$)*. These four parameters and their range of study are summarized in Table 2. It should be noticed that in order to study the effect of the size of the opening, the length of the cylindrical shape opening is in the range of 2–50 mm (see Table 3-3); as the thickness of the wall is 2 mm, higher values of the length describe the case of a tube connected to the enclosure at the opening position. The ANOVA calculation is done by the *Minitab 17* statistical software. All the calculations are based on a confidence level of 95 [%].

Table 3-3 The studied ranges of the parameters in the factorial design

Factor	Notification	Low level	High level	Unit
Length of the tube	A	2.00	50.00	mm
Radius of the hole	B	0.50	5.00	mm
Temperature	C	273.15	333.15	K
Initial RH	D	40.00	80.00	%

3.2.1 Model fitting and statistical analysis

Table 3-4 shows the factorial design matrix and the CFD simulation results (moisture diffusion time into the enclosure) for each of the 17 cases. It should be noticed that regarding the distribution of the results, a data transformation is recommended based on the Box–Cox method. Constancy of the error variance and normality of distribution are two essential assumptions in the ANOVA [58]. Based on the Box–Cox method, if a logarithmical transformation is applied on CFD simulation results of the 17 cases, the two assumptions are better satisfied. The half-normal probability plot of the effects is displayed in the Figure 3-7a, together with the rank of the effects by the Pareto chart in Figure 3-7b. According to the half-normal probability plot, radius and length of the opening as well as the initial relative humidity are the significant factors affecting the moisture transfer time into the enclosure. The rank of their significance is as below:

$$B > A \gg D$$

Table 3-4 The factorial design table for the factors and the responses.

Case #	A	B	C	D	Response-diffusion time (s)
1	2.00	0.50	273.15	40.00	8500000
2	50.00	0.50	273.15	40.00	208000000
3	2.00	5.00	273.15	40.00	143000
4	50.00	5.00	273.15	40.00	1474000
5	2.00	0.50	333.15	40.00	6210000
6	50.00	0.50	333.15	40.00	149450000
7	2.00	5.00	333.15	40.00	464000
8	50.00	5.00	333.15	40.00	1544000
9	2.00	0.50	273.15	80.00	4892000
10	50.00	0.50	273.15	80.00	166460000
11	2.00	5.00	273.15	80.00	108000
12	50.00	5.00	273.15	80.00	1095000
13	2.00	0.50	333.15	80.00	3815000
14	50.00	0.50	333.15	80.00	28500000
15	2.00	5.00	333.15	80.00	72000

16	50.00	5.00	333.15	80.00	880000
17	26.00	2.75	303.15	60.00	18318000

Thus, a regression model consisting of the significant factors is proposed:

$$\log(Time\ constant\ ) = 7.52153 + 2.022926 \times A - 0.39190 \times B - 8.03837 \times 10^{-3} \times D \qquad (3.4)$$

The statistical ANOVA of the results obtained with a confidence level of 95% (*p*-value equals to 0.05) is summarized in Table 3-5. The *p*-values provide a cut-off beyond which assert that the findings are statistically significant [59]. According to Table 5, the *F*-test yields a very low probability value (*P*-value < 0.0001) which indicates that the model is highly significant. The curvature is significant. Thus, the regression model is not suitable enough for predicting the center-point and consequently other internal points of the investigated space. In fact, it can only predict the factorial points successfully. It is worth mentioning that, this regression model can be used to find the critical parts of the design space for further investigations and it is the initial step for finding an accurate model that can describe the behavior of the response in the whole space.

Table 3-5 The factorial design table for the factors and the responses.

Source	Sum of squares	Degree of freedom	Mean square	F value	p-value	
Model	17.70	3	5.90	104.85	> 0.0001	Significant
A	4.84	1	4.84	86.09	> 0.0001	Significant
B	12.44	1	12.44	221.11	> 0.0001	Significant
D	0.41	1	0.41	7.35	0.0189	Significant
Curvature	0.53	1	0.53	9.39	0.0098	Significant
Residual	0.68	12	0.056			
Total	18.90	16				

3.2.2 Model adequacy checking

The coefficient of determination (R^2) measures the proportion of total variability explained by the model. For an acceptable fit model, R^2 should be higher than 0.80 [60]; hence, the closer R^2 is to unity, the better. The R^2 always gets closer to 1 as more terms are added to the regression model; thus, it is recommended to use an adjusted-R^2 to evaluate the model adequacy since it is adjusted for the number of terms in the model. For a well fitted regression model, the adjusted-R^2 should be higher than 0.90 [57], [60]. In this work, the R^2 and adjusted-R^2 for the regression model are 0.9363 and 0.9216, respectively. These numbers indicate that the regression model describes the process well.

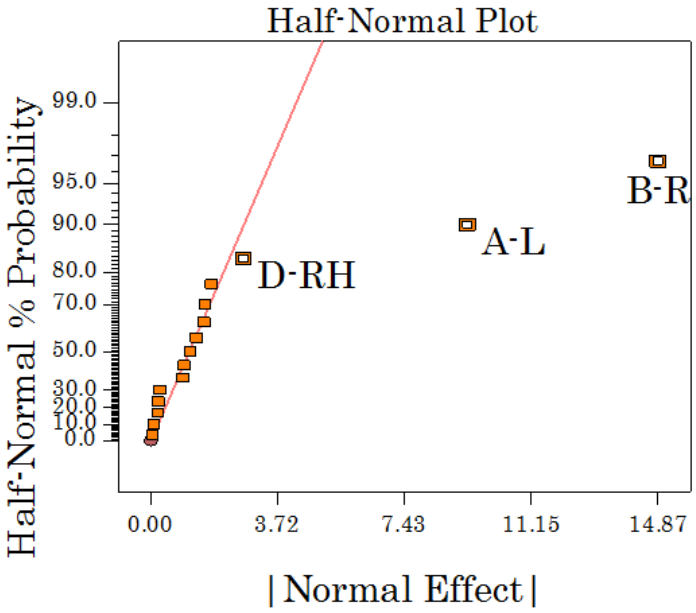

(a)

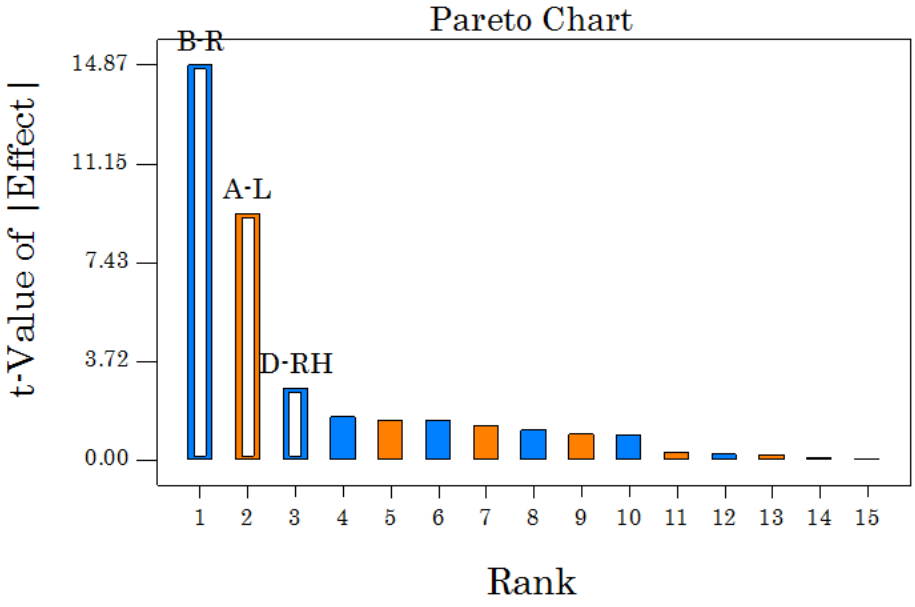

(b)

Figure 3-7 a) Half normal probability plot of the effects, and (b) the Pareto chart.

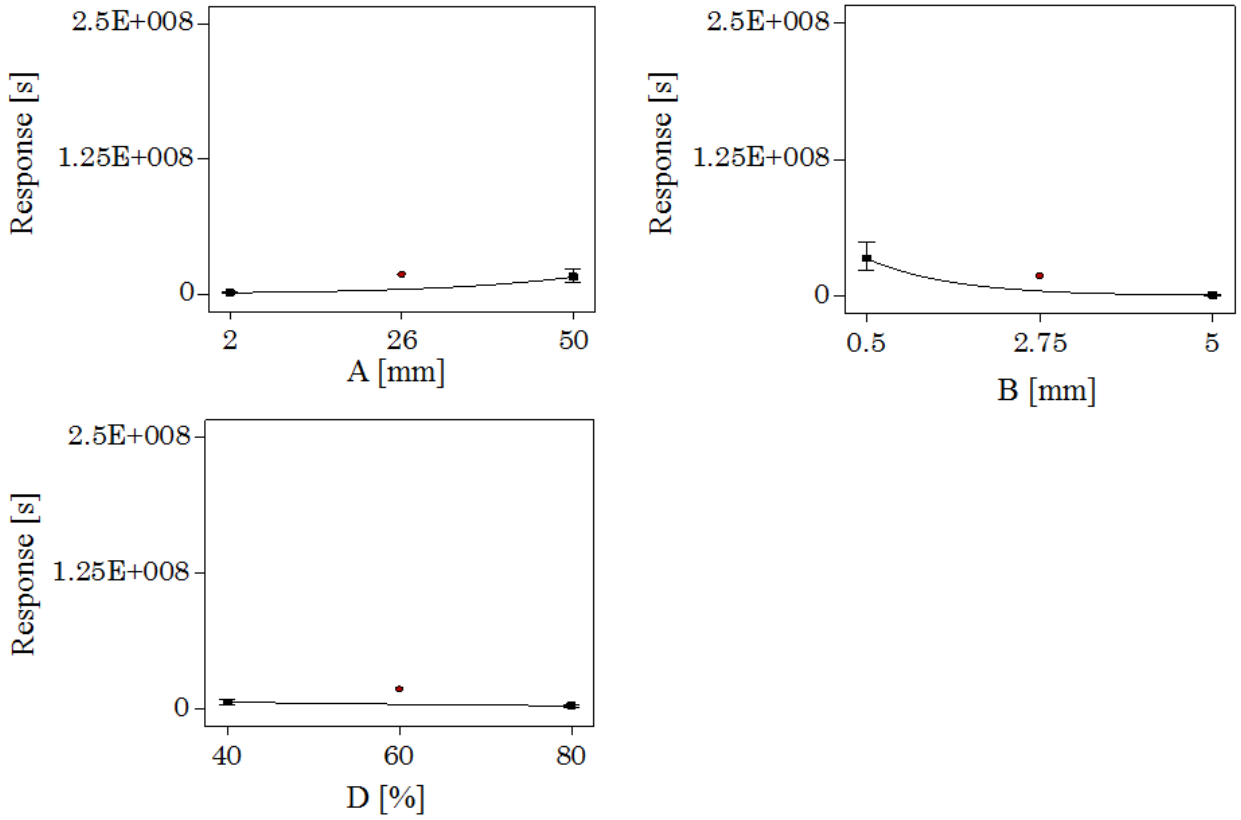

Figure 3-8 The main effect plots.

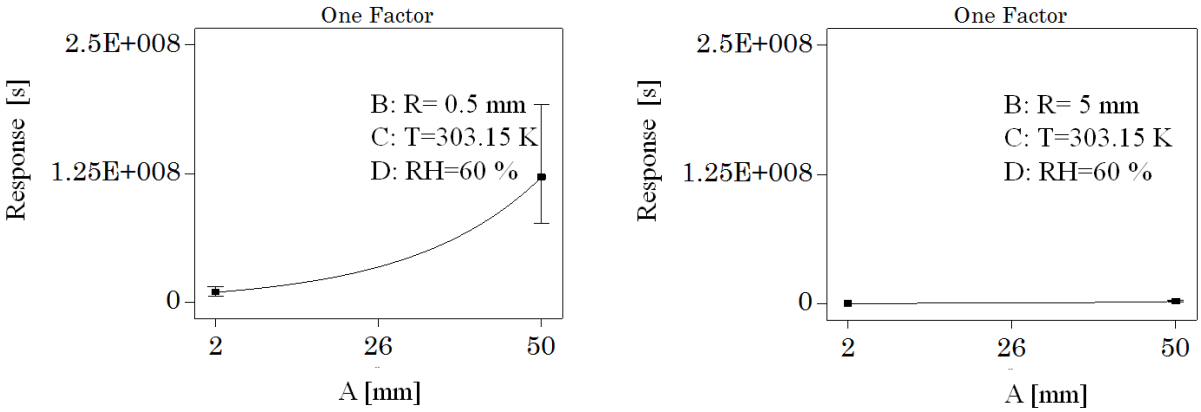

Figure 3-9 The effect of the length of the opening at (a) the low and (b) high level of the radius

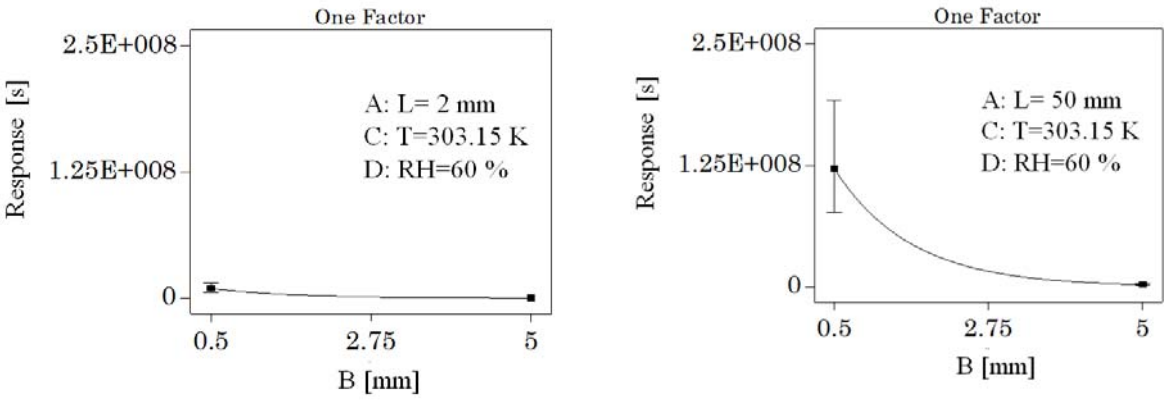

Figure 3-10 The effect of the radius of the opening at (a) the low and (b) high level of the length.

The significance of these effects is shown in Figure 3-9 and 3-10. In the case that radius is 5 mm (Figure 3-9b), the length changes do not influence the response significantly; on the other hand, in case that radius is only 0.5 mm, the length of the opening plays a key role (see Figure 3-9a). Similarly, when the length is 2 mm (see Figure 3-10a), the response changes are not that significant; however, in the case of 50 mm length, the response changes are noticeable (see Figure 3-10b)

3.3 Factorial design based on Experiments

In this part, the effects of four factors on the RH built-up time constants are investigated, namely initial RH inside the enclosure, radius of the opening, length of the opening and operating temperature. Table 3-6 shows the range of the investigated factors.

Table 3-6 The investigated parameters and their ranges.

Factor	Notation	Low level -	High level +	Unit
Initial RH	A	40	70	%
Opening radius	B	0.5	1.5	mm
Opening length	C	2	50	mm
Temperature	D	25	60	°C

A full 2^4 factorial design proposes 16 cases of experiments. However, considering the fact that such experiments are very time-consuming, it is important to limit the number of the tests to few as possible. Thus, a fractional factorial design (2^{4-1}) is used in this work. Moreover, instead of replicating all the experiments, the center point is replicated twice so that the repeatability of the

experiments is checked. The presence of center points in two-level factorial designs provides protection against curvature. Furthermore, adding center points to the design allows an independent estimate of error to be obtained [60]. The experiments proposed by the half fractional factorial design are summarized in Table 3-7.

In a full factorial design, the effects of all the factors are determined individually. On the other hand, in a fractional factorial design the effects are aliased together. In the fractional factorial design used in this study, the defining relation is taken as $I=ABCD$; so that the proposed design has the resolution of IV, which is the highest possible for a 2^{4-1} design. In such designs, no main effect is aliased with any other main effect or with any two-factor interaction, but two-factor interactions are aliased with each other [57]. The alias structure of the design in this work is as following:

[A] → A + BCD
[B] → B + ACD
[C] → C + ABD
[D] → D + ABC
[AB] → AB + CD
[AC] → AC + BD
[AD] → AD + BC

Table 3-7 The proposed experiments by the fractional factorial design.

Case #	A	B	C	D
1	40	0.5	2	25
2	70	0.5	2	60
3	40	1.5	2	60
4	70	1.5	2	25
5	40	0.5	50	60
6	70	0.5	50	25
7	40	1.5	50	25
8	70	1.5	50	60
9	55	1	26	42.5
10	55	1	26	42.5
11	55	1	26	42.5

The investigated range of parameter were based on the manufacturing feasibility and the operating conditions proposed by the industrial partners.

The experiments were conducted on electronics enclosures made of PC with dimensions of 280 [mm] ×190 [mm] ×130 [mm]. The gasket for the enclosure was made of polyurethane. The IP rating for the enclosure was 66/67, which demonstrated that the enclosures assure a total protection against dust and a protection against strong jets of water or against the effect of immersion in water at a depth of 15 [cm] to 1 [m] [61]. Either a hole with a radius of 0.5, 1 or 1.5 [mm] was drilled on

the bottom side of the enclosures, with a corresponding thickness of 2 mm, or a tube with inner radius of 0.5, 1 or 1.5 [mm] and length of 26 and 50 [mm] was mounted on the bottom side of the enclosure. Calibrated sensors placed in the enclosures monitored the temperature and RH (PT1000 and HIH4021, Honeywell), connected to a data logging system (Model 2700 Multimeter, Keithley Instruments). The enclosures were exposed to different climate environments in a climatic chamber (Espec, Escorp PL-3KPH).

The transient RH build-up was recorded for each test. Then fitting the QSS approach developed by Tencer et al. [29] (Equation (3.2)) to the experimental data in each case, the time constants (τ) were calculated using the Matlab 2016b Curve Fitting toolbox. The Curve Fitting toolbox uses the method of least squares when fitting data. Generally, fitting requires a parametric model (here, it is Equation (3.2)) that relates the response data (here, it is the RH inside the enclosure) to the predictor data (here, it is time) with one or more parameters. The result of the fitting process is an estimate of the model parameters (here, the only parameter is τ).

To obtain the parameter, the least-squares method minimizes the summed square of residuals. The residual for the *i*th data point (r_i), is defined as the difference between the observed response value (y_i) and the fitted response value ($\hat{y}_i$). The summed square of residuals is given by [62]:

$$S = \sum_{i=1}^{n} r_i^2 = \sum_{i=1}^{n} (y_i - \hat{y}_i)^2 \qquad (3.5)$$

Figure 3-11 demonstrates the experimental results for the RH build-up in the electronics enclosure for each case. Regardless of the operating conditions, it does not take more than 19 days for the internal RH to reach the ambient value of 98 [%].

As shown in Table 3-7, each case should start at a specific initial RH. However, precise control of the starting values is difficult experimentally; thus there were deviations from these values in each test. Figure 3-12 shows the initial RH for each case. This fact imposes some error to the estimations. The fitted QSS model to the experimental data for case 5 is shown in Figure 3-13, as an example. The residuals for the fitted curve are shown in the sub-figure. For all the 11 cases, the same procedure was applied to derive the time constant value.

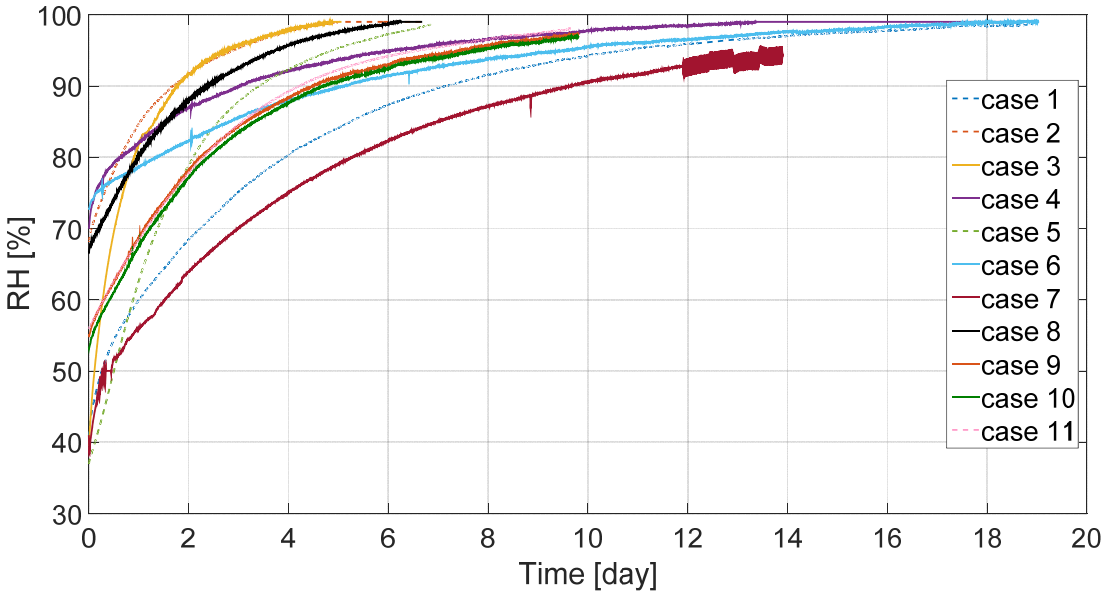

Figure 3-11 The RH build-up in the electronics enclosure for the factorial cases.

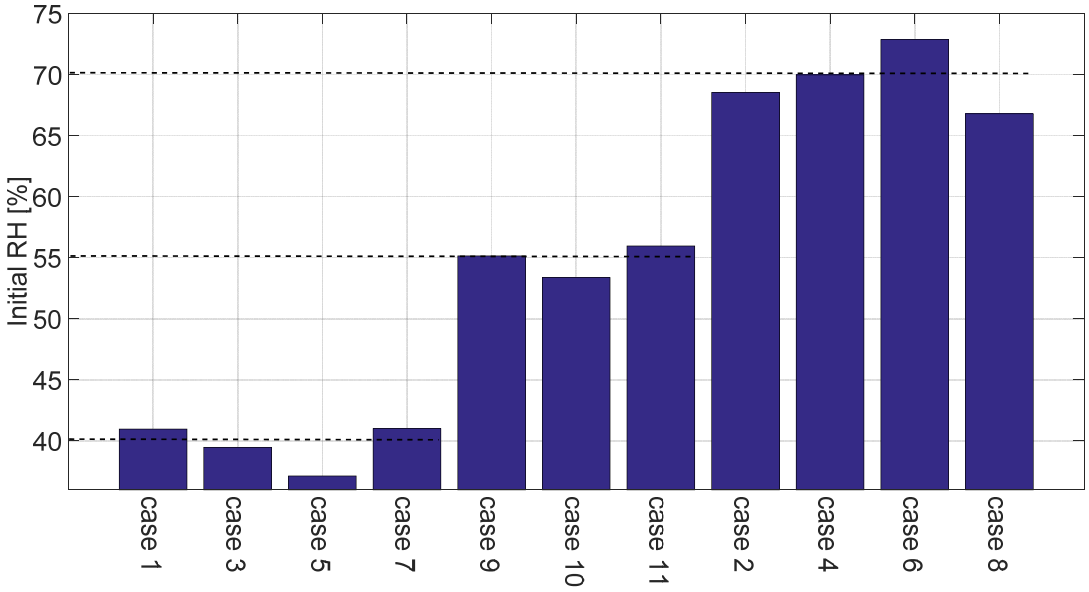

Figure 3-12 The initial RH for the factorial cases.

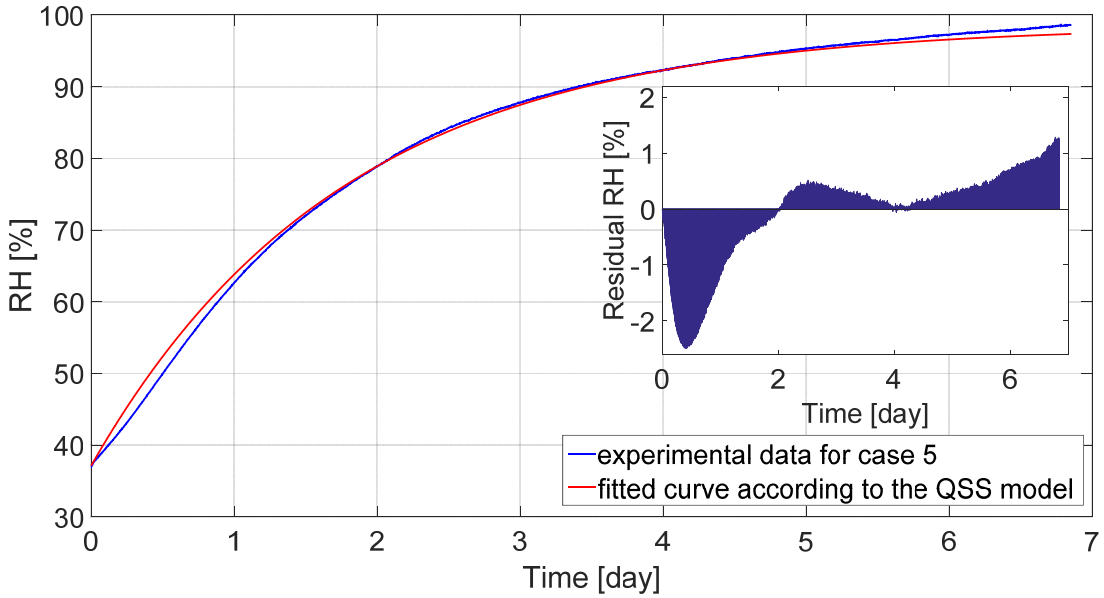

Figure 3-13 The fitted QSS model to the experimental data for case 5.

Figure 3-14 demonstrates the time constant values and the corresponding adjusted R^2 for each case. For an acceptable fit model, R^2 should be higher than 0.80 [60]; the closer R^2 is to unit, the better. The R^2 typically gets closer to 1 as more terms are added to the model. The QSS model is based on the aforementioned analytical solution to Fick's second law; thus it is not reasonable to modify the function or to add more terms for making a better fit. Instead it is recommended to use an adjusted R^2 to evaluate the fit adequacy, because it is adjusted for the number of terms in the model. For a well fitted model, the adjusted R^2 should be higher than 0.90 [57], [60]. In this work, for most of the cases (9 out of 11) the adjusted R^2 is well above 0.98; however, there are two cases with an adjusted $R^2 < 0.97$. Regarding the complex nature of such experiments and also the simplifying assumptions of the QSS model, the accuracy of the estimations seems reasonable.

Generally, in the analysis of data it is often assumed that observations are independently normally distributed with constant variance. The normality of the distribution of the data can be improved after some suitable transformation of the investigated response [58]. In this study, the normality of the distribution of the response (time constant) is checked. According to the Box-Cox plot, a power transformation (λ=0.51) on the response values is proposed for a more normal distribution (see Figure 3-15); then the ANOVA is done on the transformed data.

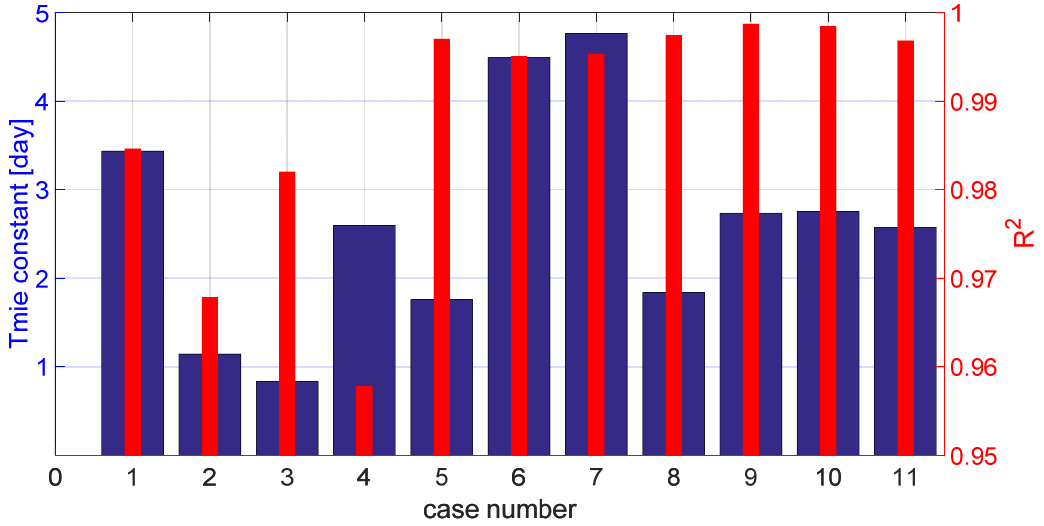

Figure 3-14 The time constant values and the adjusted R^2 for the factorial cases.

Table 3-8 summarizes the ANOVA calculation results. According to Table 3-8, the F-test yields a very low probability value (p-value = 0.005) for the regression model, which indicates that the model is highly significant. For the curvature, the p-value is only a bit higher than the considered cut-off; thus, it is not considered as a significant term. Considering a model of higher order can predict the curvature more accurately. Furthermore, the calculated p-values demonstrate that temperature and the opening length are the most significant factors. Figure 3-16a and Figure3-16b displays the normal probability distribution of the effects and rank of the investigated terms, respectively. The *[AD]* term which represents the effect of $A \times D + B \times C$ interactions is also found to be important. Since neither *A* nor *B* are among the influential factors and considering the fact that *B* and *C* are affecting the response in reverse directions, it can be concluded that the significance of *[AD]* is mostly due to the effect of $A \times D$.

Table 3-8 The ANOVA results for the 2^{4-1} design.

Source	Degree of freedom	Adjusted sum of squares	Adjusted mean square	F-value	P-value
Model	5	1.63978	0.32796	96.75	0.000
A (initial RH)	1	0.00215	0.00215	0.64	0.462
C (opening length)	1	0.31355	0.31355	92.50	0.000
D (temperature)	1	1.27625	1.27625	376.50	0.000
AD	1	0.03131	0.03131	9.24	0.029
Curvature	1	0.01652	0.01652	4.87	0.078

Error	5	0.01695	0.00339		
Lack of fit	3	0.01507	0.00502	5.34	0.162
Pure error	2	0.00188	0.00094		
Total	10	1.65673			

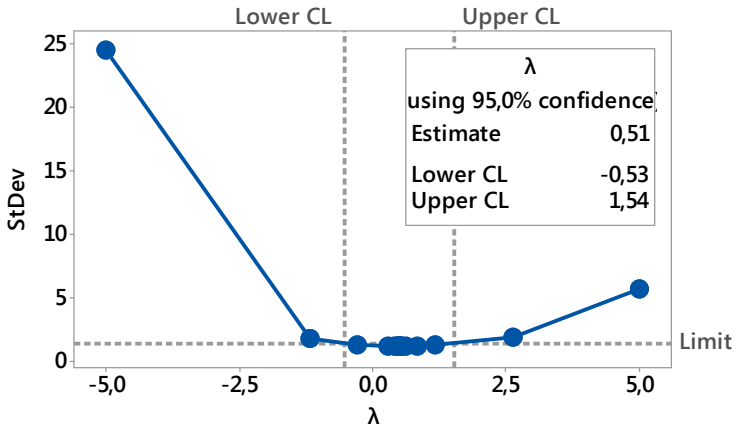

Figure 3-15 The Box-Cox plot

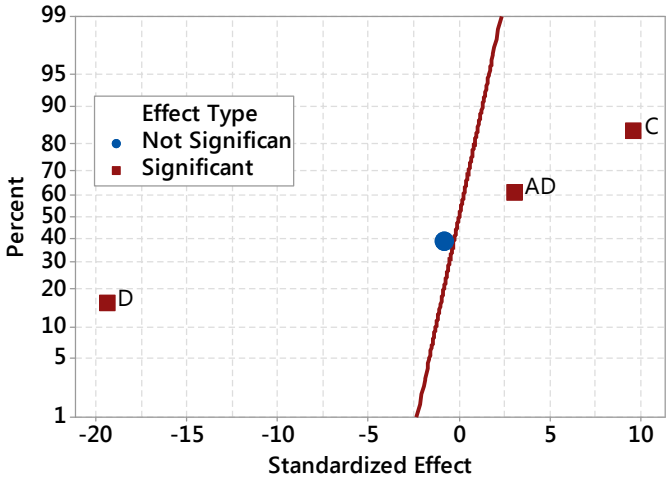

(a)

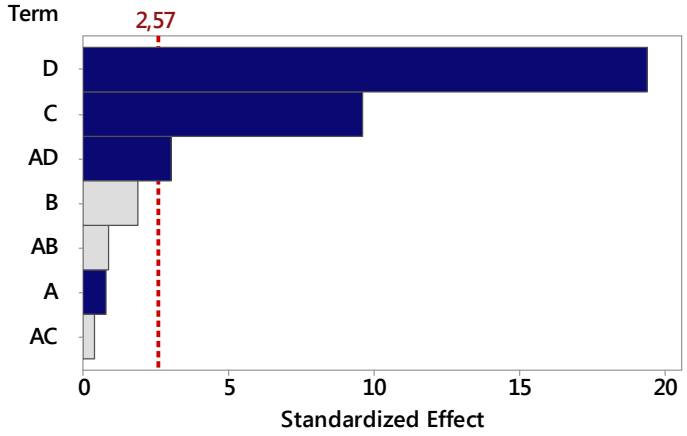

(b)

Figure 3-16 The normal probability plot of the effects (a), and the Pareto chart (b)

Based on the ANOVA calculations, a predictive model for the moisture transfer time constant is proposed which can be used in the space of the investigated ranges of the parameters (see equation (3.6)).

$$Time\ constant^{0.51} = 2.941 - 0.01122 \times A + 0.008249 \times C - 0.03593 \times D + 0.000238 \times A \times D \quad (3.6)$$

The adjusted R^2 for this regression model is 0.98, which is satisfying. Another important issue to check for the adequacy of a regression model derived from ANOVA, is the distribution of the residuals. The normal probability plot of the residuals in this study does not reveal anything troublesome (see Figure 3-17). Thus, the proposed regression model based on the experimental results is suitable for prediction over the studied design space. It is worth mentioning that this regression model can be used to find the critical parts of the design space for further investigations, too.

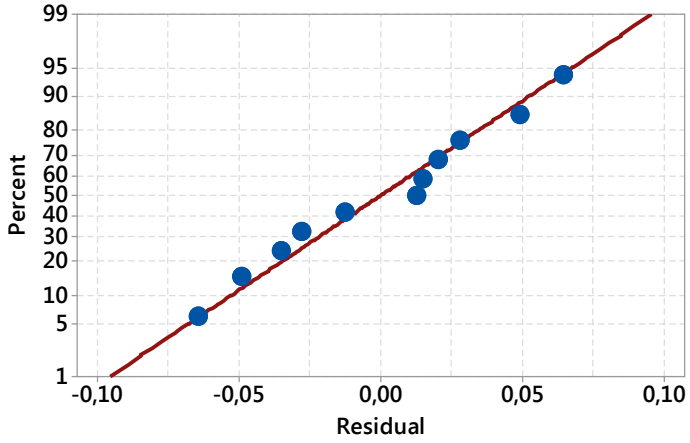

Figure 3-17 The normal probability plot of the residuals

Figure 3-18 shows the time constant changes vs. temperature at different values of opening length when the initial RH is 40 [%]. As the temperature increased, the time constants changes less over the length changes; in other words, the length of the opening plays a more effective role at lower temperatures (the time constant variation is 1.8 times bigger at 25 [^{o} C] compared to 60 [^{o} C] vs length changes). The same trend happens when the initial RH is at 70 [%].

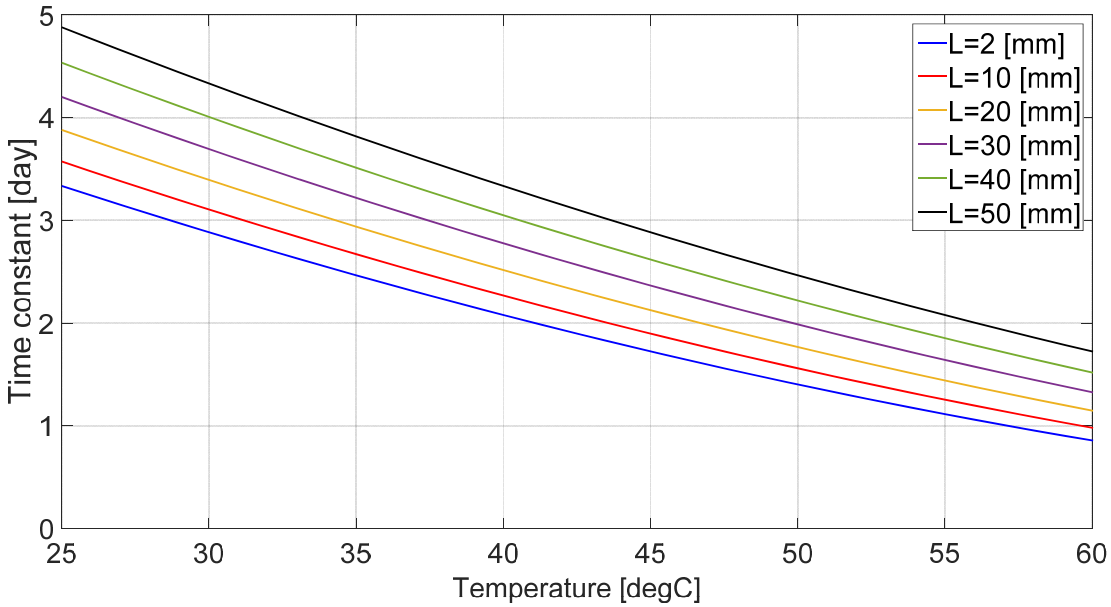

Figure 3-18 The time constant vs. temperature at initial RH=40 [%].

3.4 Cyclic internal Conditions

A heating plate with the size of 50 mm × 50 mm × 1 mm is considered at the top of the enclosure, in the center (see Figure 3-19). The plate is switched on and heats up to 42.5 °C for 12 h and then is switched off for another 12 h so that its temperature reaches and stays at 26 °C. This cycle is repeated for more than eight days. The local climate inside the enclosure is studied in two cases:
(i) Exposure to an ambient temperature and RH of 25 [°C] and 98 [%], respectively.
(ii) Exposure to an ambient temperature and RH of 25 [°C] and 40 [%], respectively.
In case (i), the initial RH and temperature are 70 [%] and 25 [°C] and in case (ii) these values are 100 [%] and 25 [°C], respectively. It should be noted that all the operation conditions are based on the experimental study conducted by Conseil et al. [54]. Figure 3-20 shows the simulation results and compares them with the experimental data for case (i). The simulation results, like the experimental data, show a gradual increase of RH inside the enclosure; however, the trend is slower in the simulations for the first couple of days. After about 4 days, the simulation results and the experimental measurements get much closer, visually. The point at the top of the heater, experiences large RH changes, consistent with the temperature changes. On the other hand, the two other investigated points do not see severe RH changes with the 12 h on/off scenario. This is due to the buoyancy effect that drives the natural convection inside the enclosure. As the warm air tends to stay at the top (because of lower density) and cold air at the bottom, the thermal energy is not much distributed in the enclosure. Figure 3-20b displays the small changes of temperature over the on/off cycles for these points; however, the point on top of the enclosure is just following the cycles. It should be noted that in the experimental measurements, some deviations from the higher set point value (42.5 [°C]) are observed; especially at the beginnings, where even values of about 46 have been recorded. In the CFD simulations these deviations have not been regarded and it is considered that the high and low temperature are exactly 42.5 and 26 [°C] every 12 [hr], respectively.

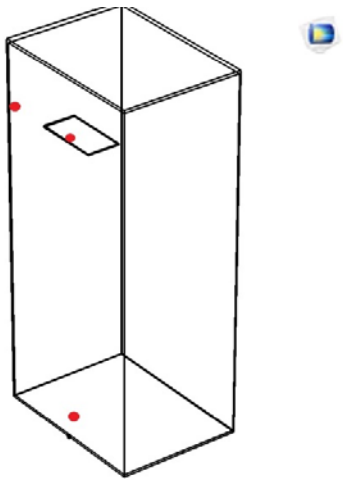

Figure 3-19 The geometry of the PC enclosure and positions of the investigated points in the non-isothermal studies.

Generally, the RH changes are more affected by temperature than the moisture concentration. As presented previously in the isothermal section, even in the case that the mass transfer is just driven by diffusion, there

is not a big diversity in the distribution of moisture concentration inside the enclosure. In the non-isothermal cases, there are some air movements driven by the volumetric forces that increase the rate of mass transfer. It is seen that when the heater is on, the RH at the top of the heater is at least 40% lower than the two other points during the 10 days. Figure 3-21 shows the local climate inside the enclosure for case (ii). Gradually the RH inside the enclosure decreases from 100% to the ambient value (40%). This takes about 8 days and a half. In the initial days the predicted mass transfer rate by the CFD simulations is lower than what the experimental measurements show. However, after three days the estimated and the measured values get much closer. The lower-estimation of the mass transfer rate could be due to the fact that in the non-isothermal studies the air flow outside the enclosure is not considered in the CFD simulations—the air flow might help the moisture ingress through the 2 mm diameter hole.

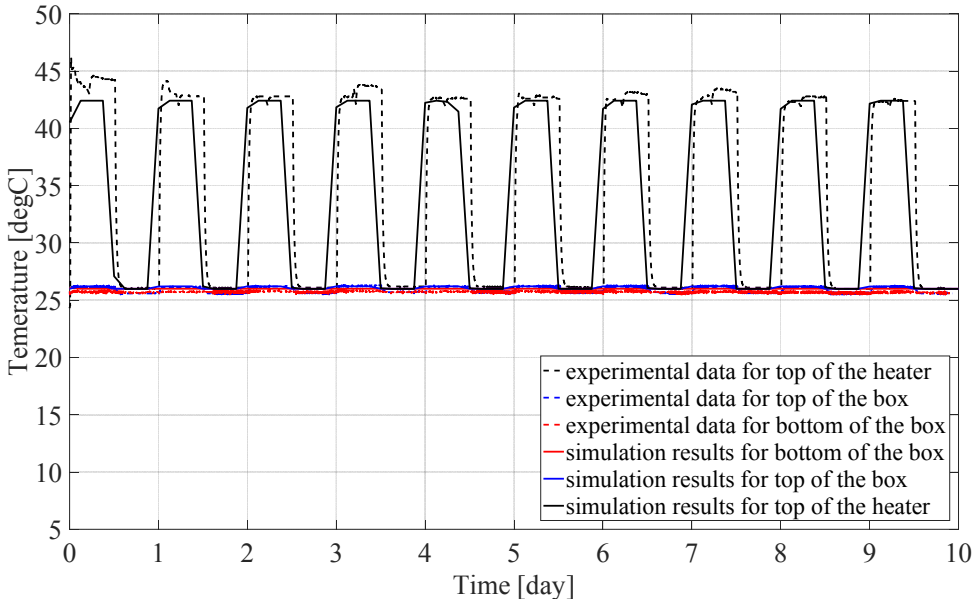

(a)

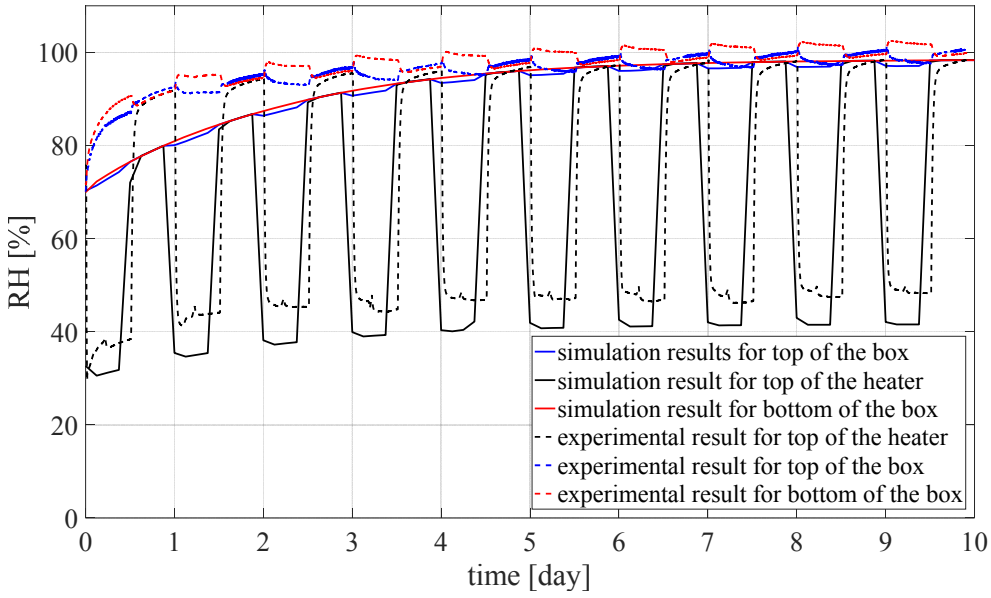

(b)

Figure 3-20 (a) The the local climate, RH, and (b) temperature inside the enclosure for case (i).

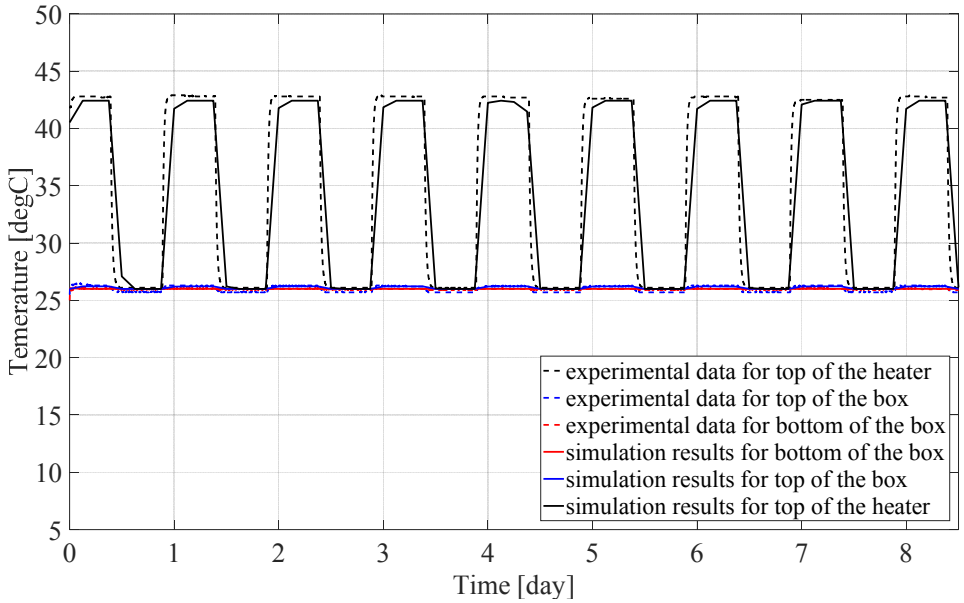

(a)

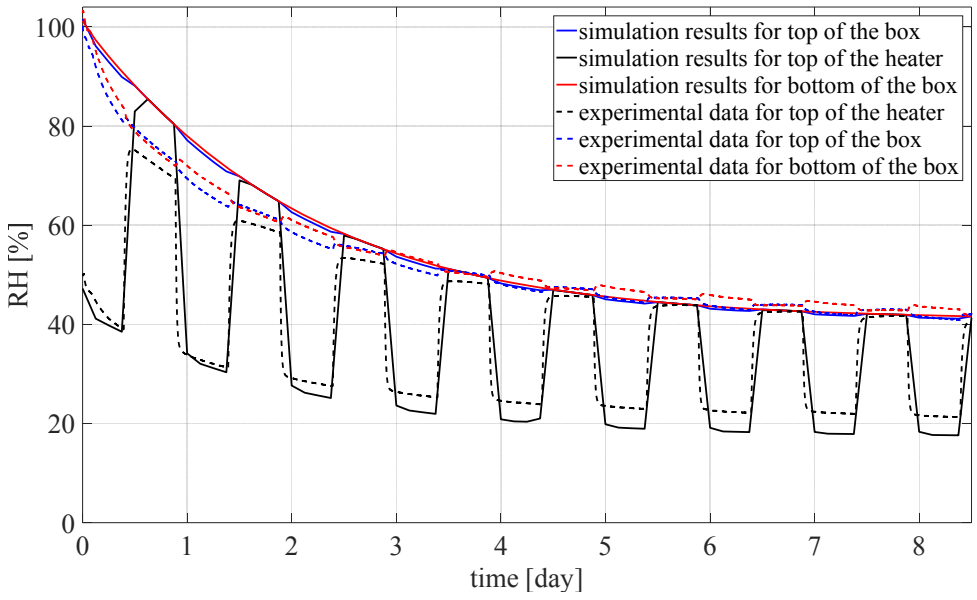

(b)

Figure 3-21 (a) The the local climate, RH, and (b) temperature inside the enclosure for case (ii).

The following concluding remarks can be made:

- For a typical electronic enclosure, the position of the opening does not make a huge change in the moisture diffusion time into the enclosure, in isothermal conditions.

- The RC method under-estimates the time constant for the moisture ingress into the enclosure.
- Fitting the experimental data to the QSS model for all the cases admits the exponential nature of the RH changes inside the electronic enclosure over time.
- A linear regression model is not suitable enough for predicting all the points in the design space; in fact, the proposed regression model can estimate the response only at the factorial points.
- As the heater is located on the top, it does not cause a sensible air flow so that the heat can be transferred to all parts of the enclosure.

Chapter 4
The response of a typical electronics enclosure exposed to cyclic ambient conditions

This chapter discusses the response of a typical electronics enclosure to different cyclic ambient conditions; in the first part, sharp rectangular shaped temperature cycles are extensively studied. The conditions are prescribed according to experimental work from the literature, so that the CFD simulation results can be compared with the results from their study. The effect of the presence of electronic components inside the enclosure is also studied (Paper II). Thereafter, the local climate inside the enclosure is studied in response to a harsh environmental conditions defined by the STANAG standard (Paper I). Finally, the enclosure is exposed to Copenhagen outdoor conditions and the response is studied. In this part a different configuration of the heatsink is considered in a way that the heat sink can store the heat generated by the electronics; the heat is to be used for lowering the RH later when the electronics are not working (Paper III).

4.1 Rectangular sharp temperature cycles and constant RH of 100 [%]

To look into the effects of both maximizing the saturation limit and minimizing the absolute humidity, four different cases are defined. In the first two cases, an empty enclosure is exposed to cyclic ambient temperature and high RH with two different opening sizes. In the other two cases, the PCB, heatsink and heater are located inside the enclosure and exposed to the same ambient conditions with two different opening sizes, as before. The effect of an internal cyclic heat load to the PCB is also studied.

It is worth mentioning that the thermal behavior of plate fin heatsinks in passive cooling conditions has been extensively studied and there are robust correlations that govern the convective heat transfer. However, most of them are focusing on the heat removal efficiency of the heat sinks [63]–[65]. The main purpose of this work is to study the local climate inside the enclosure. Thus, here, the heat sink is a just a block of aluminum or copper.

The commercial software package COMSOL Multiphysics^{TM} version 5.1 is used for running all the CFD simulations. The simulation results for temperature are compared with experimental data from a similar work in the literature.

Figure 4-1 presents the studied symmetry geometries in case of a) an empty enclosure and b) an enclosure with the components (PCB, heatsink and heater) inside. Table 4-1 shows the dimensions of each of these components.

Table 4-1 The Dimensions of the Geometries

Item	Dimensions [mm]	Material
Enclosure	Inner: 188×128×276 Outer: 190×130×280	Aluminum
Heater	50×1×50	Silicon
Heatsink	80×10×100	Aluminum
PCB	30×1.6×130	Compact FR-4 and copper layers

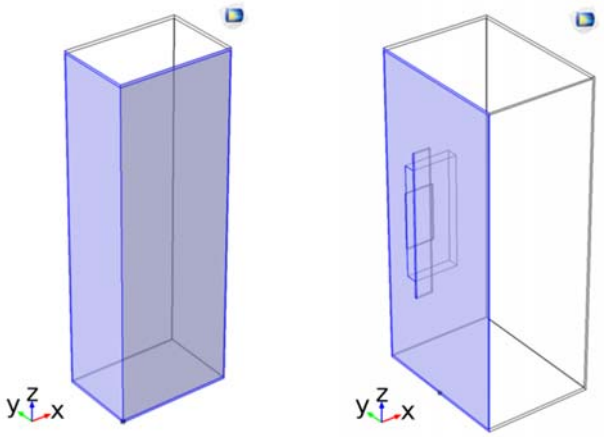

(a) (b)

Figure 4-1 Illustration of the investigated geometries; (a) empty enclosure, (b) enclosure with components inside (Symmetry faces are shown in blue).

PCB thermal conductivity

A PCB is typically a layered composite consisting of copper foils and a glass-reinforced polymer (FR-4). A cross-sectional view of such a laminated structure is illustrated in Figure 4-2. The figure displays the numbering system that will be used for indicating the different layers, numbered 1 to n. In many thermal calculations, it is convenient to treat such a layered structure as a homogeneous material with two different effective thermal conductivities: one describing heat flow within the plane ($k_{\text{in plane}}$) and another for heat flow through the thickness of the plane (k_{through}) [66]. However, it should be mentioned that local geometries in the circuit board cause local variations in the board thermal conductivity.

$$k_{in\,plane} = \frac{\sum_{i=1}^{n}(k_i \times thickness_i)}{\sum_{i=1}^{n} thickness_i} \qquad (4.1)$$

$$k_{through} = \frac{\sum_{i=1}^{n} thickness_i}{\sum_{i=1}^{n}(thickness_i / k_i)} \qquad (4.2)$$

Figure 4-2 A schematic cross-sectional view of a PCB

Now, the anisotropic heat conductivity of the PCB is taken into the calculations by the following diagonal matrix:

$$k_{PCB} = \begin{bmatrix} k_{in\,plane} & 0 & 0 \\ 0 & k_{through} & 0 \\ 0 & 0 & k_{in\,plane} \end{bmatrix} \qquad (4.3)$$

The initial relative humidity, temperature, pressure and velocity are 30 [%], 24 [°C], 0 [Pa] and 0 [m/s], respectively. The ambient RH is set at 100 [%] at the opening. The temperature of the outer walls of the enclosure is cycles as shown in Figure 4-3. The opening is considered as an open boundary with no viscous stress.

$$\left[\mu(\nabla \mathbf{u} + (\nabla \mathbf{u}^T)) - \frac{2}{3}\mu(\nabla . \mathbf{u})\mathbf{I}\right]\mathbf{n} = 0 \qquad (4.4)$$

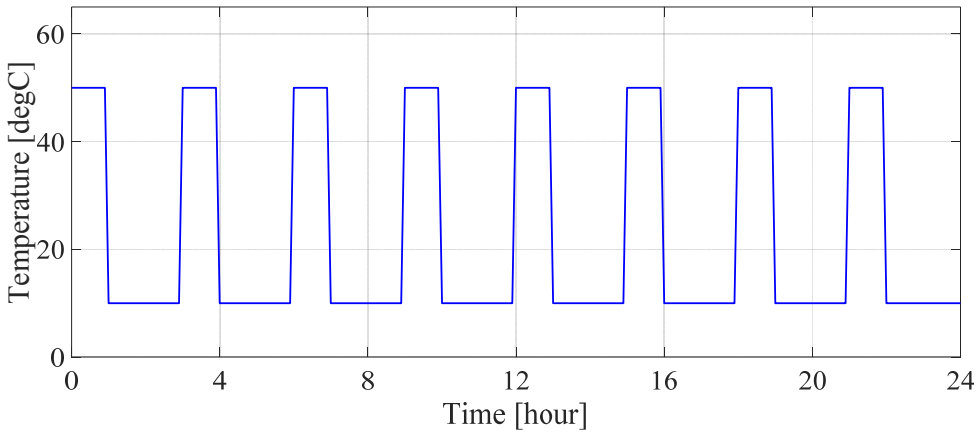

Figure 4-3 The cyclic ambient temperature boundary condition.

To study the effect of ambient condition changes, opening size, presence of electronics and internal heat load cycles of the electronics on the local climate (temperature and RH) inside the enclosure, four cases are considered as explained in Table 4-2. In all four cases, the enclosure is exposed to the same ambient conditions. In the first part of the study, the responses of empty enclosures with two different opening sizes are studied. Next the RH and temperature of the PCB are estimated in cases 3 and 4. Finally, the local climate on the PCB is studied when a cyclic heat load is imposed to the PCB by the heater, as displayed in Figure 4-4.

Table 4-2 The four investigated cases

Case #	Opening size (diameter)	Content of the enclosure
1	1 [mm]	empty
2	3 [mm]	empty
3	1 [mm]	PCB, heater, heatsink
4	3 [mm]	PCB, heater, heatsink

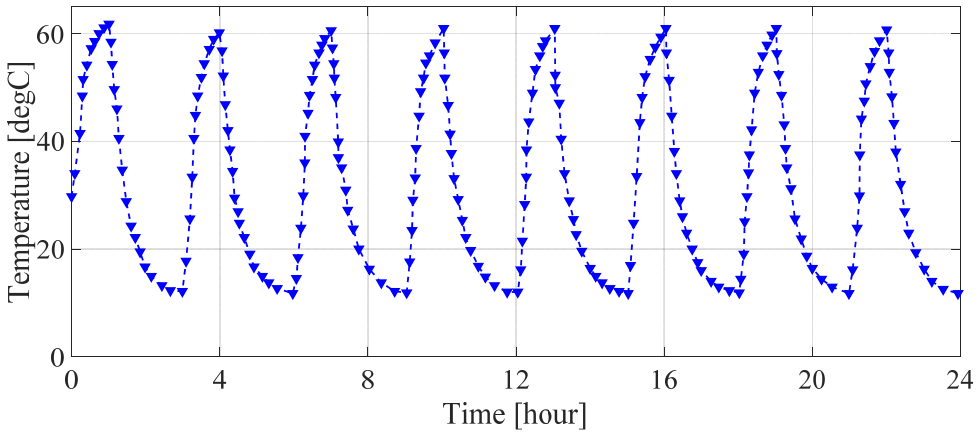

Figure 4-4 The measured transient temperature of the silicon heater [67].

The temperature of the heater is prescribed according to the experimental work conducted by Conseil et al [67], so that the CFD simulation results can be compared with the results from their study.

4.1.1 Response of the empty enclosure

Figure 4-5 shows the temperature at the center of the aluminum enclosure. The temperature has a fast response to the ambient changes in both cases of opening sizes of 1 and 3 [mm] diameter. The outer walls being exposed to the ambient changes are mainly responsible for the internal temperature and the opening size cannot make a severe change. Not surprisingly, the air flow through the opening is negligible due to its small size; thus, the air flow does not cause sensible

convection to accelerate the heat transfer and consequently does not influence the temperature response. Hence, the estimated temperatures are not noticeably different for the cases 1 and 2.

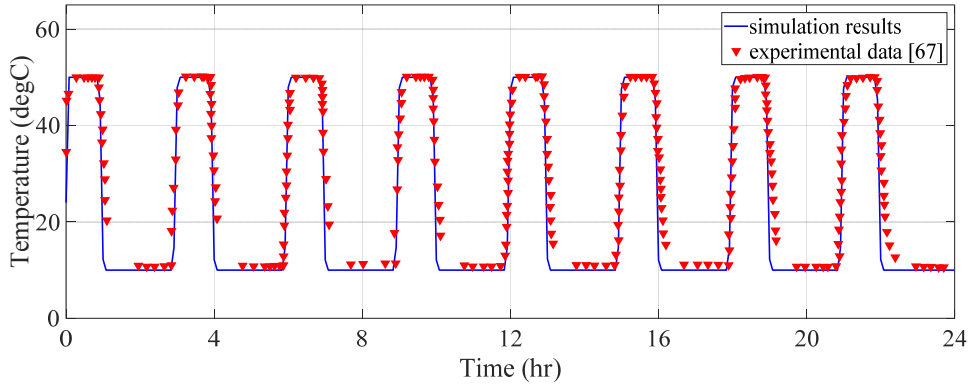

(a)

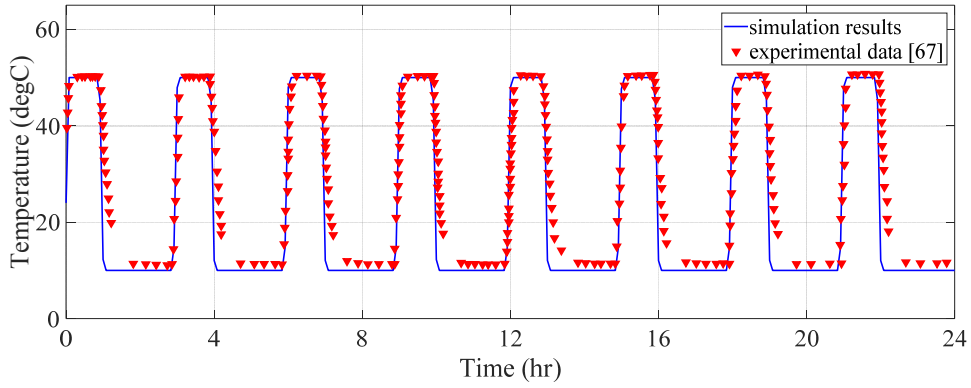

(b)

Figure 4-5 The temperature at the center of the Al enclosure for (a) case 1 and (b) case 2

Figure 4-6 shows the RH changes at the center of the enclosure versus time. In case 2, the moisture transfer through the opening is so fast that in the first cycle (about 1 hour) the internal RH has reached the maximum value (100 [%]); on the other hand, in case 1, the RH has reached the 100 [%] value after 3 temperature cycles (9 hours). Similarly, the minimum RH value for every cycle increases over time more rapidly for case 2 as compared to case 1. This is due to the fact that the moisture ingress through the 3 [mm] diameter opening is about a factor of 9 ($3^2/1^2$) faster than the 1 [mm] diameter one, i.e. proportional to the opening. Hence, in case 2 both moisture concentration and temperature changes actively affect the RH. However, in case 1, after 3 cycles when the moisture concentration in the enclosure has reached the saturation value at 10 [°C], the RH cycling behavior is not changing, demonstrating the small rate of moisture transfer through the 1 [mm] diameter opening.

According to Figure 4-6, in case of constantly high ambient RH, minimizing the absolute humidity is a more effective solution compared to maximizing the saturation limit.

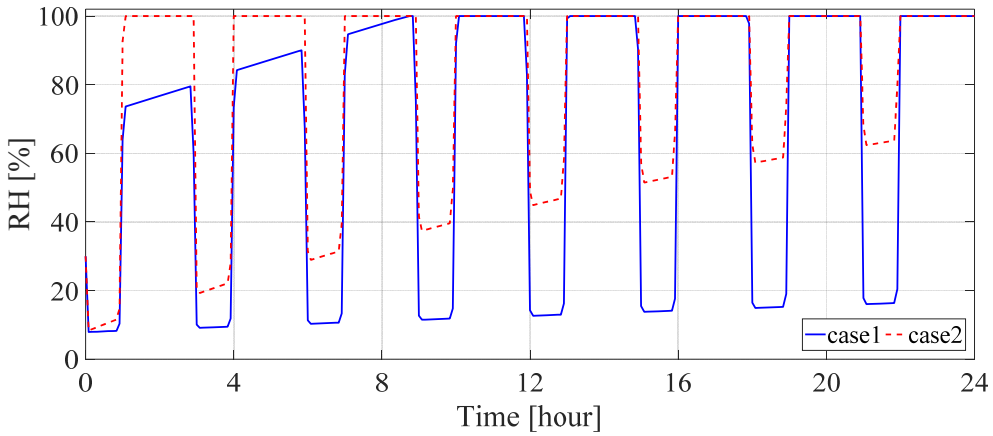

Figure 4-6 The RH at the center of the Al enclosure.

4.1.2 Response of an enclosure with a PCB, heatsink and heater with no heat load

For cases 3 and 4, the temperature and RH on top of the PCB are displayed in Figure 4-7 and Figure 4-8, respectively. The presence of the components, especially the heatsink, reduces the internal temperature changes compared to the case which the enclosure was empty. In fact, the amplitude of the temperature change is reduced in the presence of the thermal mass, which causes a delay in the temperature response. In this case, temperature cycles are not long enough to heat and cool the components to the highest and lowest ambient values (50 and 10 [°C]). Thus, if the thermal mass was small enough or the time period of the maximum and minimum temperatures were long enough, the temperature of the thermal mass could reach the ambient maximum and minimum values.

According to Figure 4-8, the presence of the components, especially the heatsink, decreases the risk of condensation in the enclosure; however, it does not prevent it. For case 3 the RH reaches the 100 [%] after 6 cycles. For case 4, the period that the RH is at 100 [%] is shorter compared with the empty enclosure.

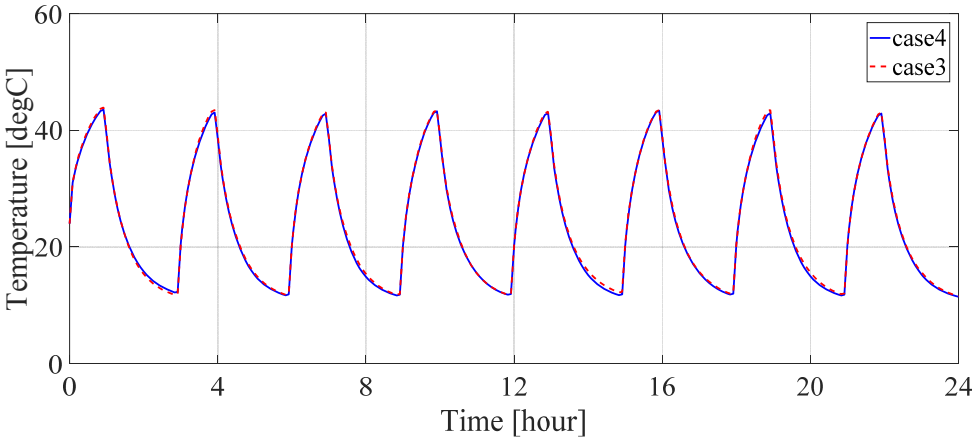

Figure 4-7 The temperature at the center of the Al enclosure.

Figure 4-9 displays the temperature and velocity profiles at different time sections of the cycling period. After 0.5 [hr], the devices inside the enclosure are heating up from the initial temperature (25 [°C]) to the ambient value (50 [°C]). It is shown that the devices are colder than the trapped air. Thus, the air close to the devices flows downwards. After 1 [hr], the ambient is getting cold; thus, the air and the electronics inside start getting influenced by the new conditions. In Figure 4-9b, it is shown that in spite of the fact that the temperature of the trapped air is influenced rapidly by the new condition, the devices inside are still about 50 [°C]. In this case, as the devices inside are warmer, the air close to them flows upwards. It should be noticed that the velocity magnitudes for Figure 4-9b are higher than Figure 4-9a. This is due to the higher temperature gradient inside the enclosure. In Figure 4-9c, the ambient temperature has heated up to 50 [°C]; however, the devices inside are much colder and it takes much more time for them to reach the ambient temperature and considering this, the air close to them flows downwards. On the other hand, the air close to the vertical walls of the enclosure moves upwards, since they are warmer. It is seen that the ambient changes have caused some considerable buoyant flow inside the enclosure with a maximum air velocity of about 0.25 [m/s].

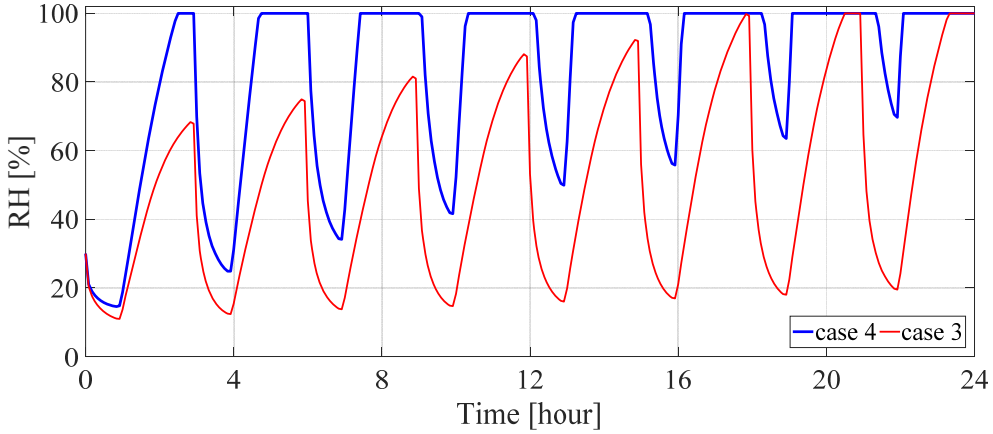

Figure 4-8 The RH on the PCB.

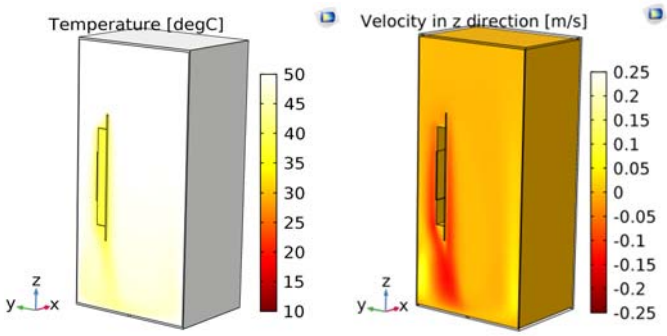

(a) t=0.5 hr

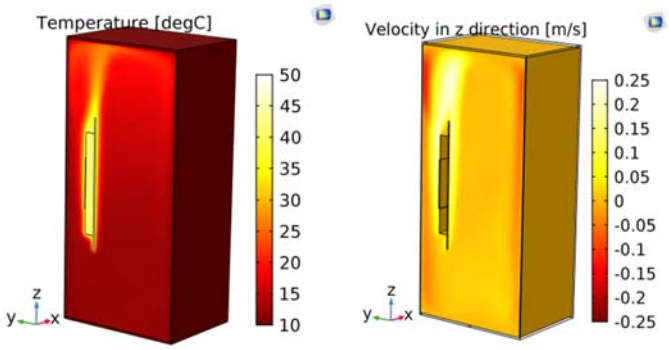

(b) t=1 hr

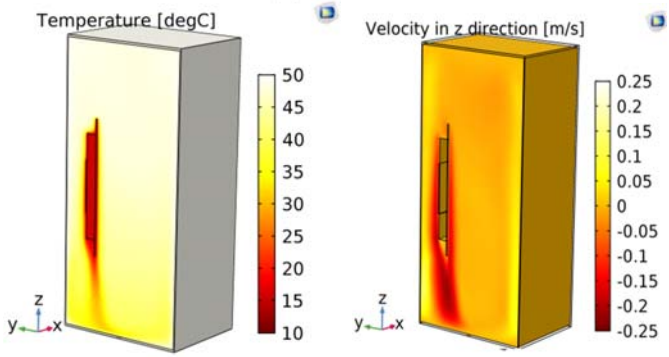

(c) t=3 hr

Figure 4-9 The temperature and velocity profile inside the enclosure at different times.

4.1.3 PCB, heatsink, Heater- heat load

Figure 4-10 compares the numerical simulation results with the experimental data from the literature, when a cyclic heat load is imposed to the PCB by the silicon heater. As demonstrated, there is an acceptable agreement between the numerical and the experimental work; however, it is noted that the maximum temperature peak is underestimated up to 3 [°C] by the CFD results. It is worth mentioning that there is an inevitable error in experimental data at the peaks where the changes are sharp and consequently the gradients are high. Besides, performing the experiments also involves errors, especially at these peaks when sudden changes happen to the both internal and external conditions.

The RH value on the PCB, during the heat loading cycles is shown in Figure 4-11. Despite the fact that the average RH value over the day for both case 3 and 4 is less than in the situation where there is no internal heating, the condensation risk is not significantly decreased.

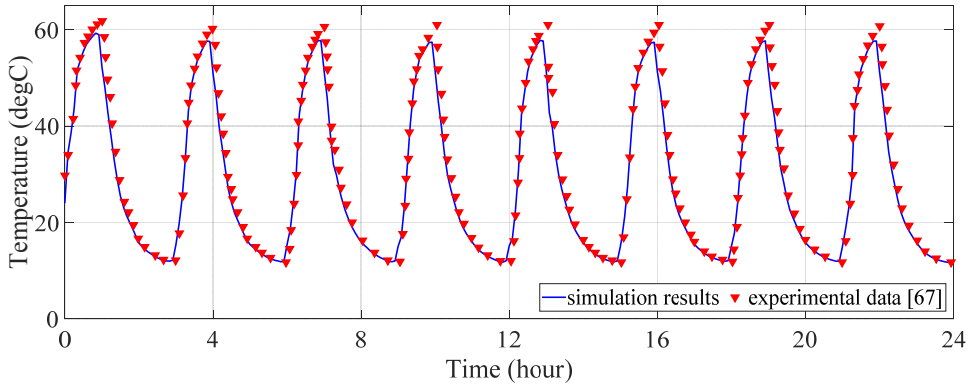

(a)

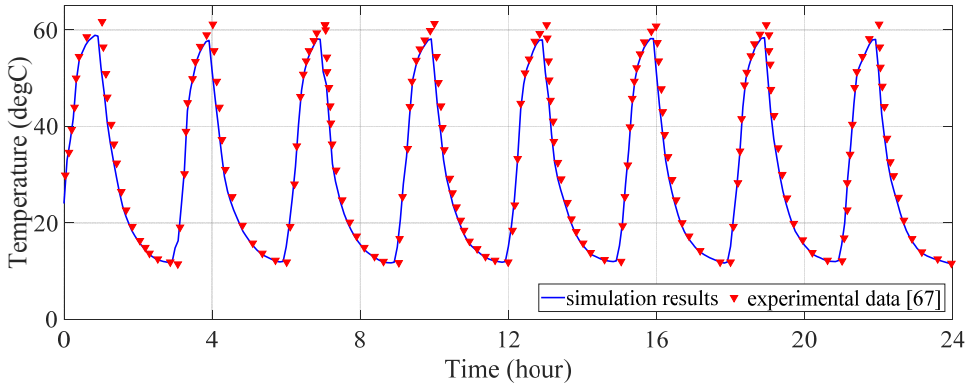

(b)

Figure 4-10 The temperature on the PCB for (a) case 3 and (b) case 4, during the heat loading cycles.

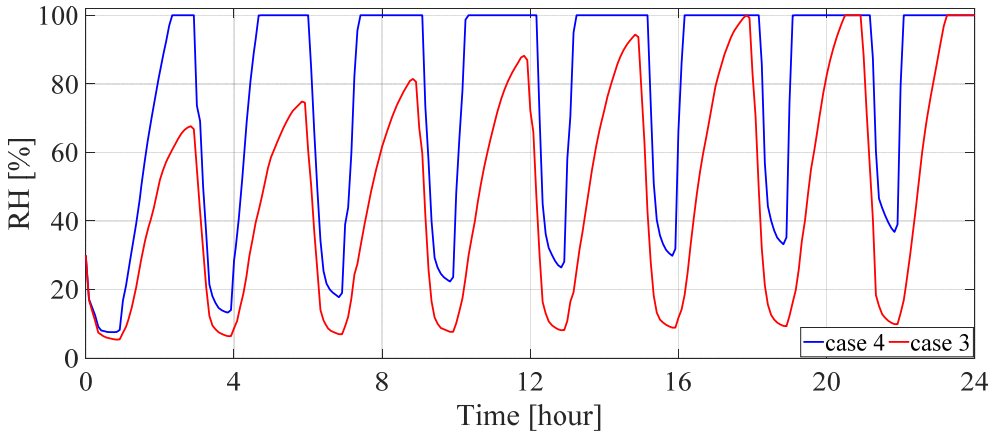

Figure 4-11 The RH on the PCB during the heat loading cycles.

The presence of the components inside the enclosure, especially the aluminum heatsink, causes a delay to the ambient thermal cycles and also shortens the amplitude of the cyclic changes. Thus, it helps to reduce RH on the PCB. On the other hand, the moisture transfer happens through the bottom hole of the enclosure. Despite the fact that a temperature increase accelerates the diffusion,

the mass transfer resistance, which is affected by the geometrical sizes in addition to the diffusion coefficient, is not significantly affected. Thus, the moisture transfer is mostly controlled by the opening size rather than the temperature. Controlling the moisture concentration inside the enclosure is more effective compared to the temperature cycles in reducing the condensation risk on the PCB.
It should be noted that the buoyant flow inside the enclosure reduces the mass transfer resistance inside the enclosure. The cyclic internal heat load also helps this effect.
The simulation results demonstrate that the temperature profile and consequently the RH profile are mainly controlled by the buoyant air flow (natural convection) rather than heat conduction inside the enclosure.

4.2 STANAG 2895 conditions

In this part, the enclosure is exposed to cyclic conditions defined in the STANAG (standard agreement) 2895, category of B2, which specifies the temperature, RH for 24 [hr] [68]. Category B2 applies to those areas that experience moderately high temperatures accompanied by high humidity [68]. Figure 4-12a–c shows the STANAG-B2 conditions as well as the estimated temperature and RH inside the enclosure. According to Figure 4-12b, the estimated temperature inside the enclosure follows the same trend as the experiments. It should be noted that the experimental measurements show values of higher than 35 [°C]. However, according to the STANAG 2895, category of B2, the highest ambient temperature is 35 [°C], and thus the temperature inside the enclosure should always be lower than this value. Figure 4-12c shows that the RH inside the enclosure is lower in the CFD simulations compared to the experimental data; however, it still shows the same trend. As the temperature prediction is close to the measured values. The gap in the RH comparison is most likely due to mass transfer calculations. As previously explained, this could be due to disregarding the air flow from outside the enclosure in the CFD simulations. Furthermore, moisture uptake by the PC might influence the local climate in the first couple of cycles, based on the initial moisture concentration in the PC walls of the enclosure, after few cycles it will also get consistent with the cyclic changes. The maximum ambient temperature seen in the STANAG 2895 is 35 [°C], which happens after 7 [hr] (0.3 [day]) for the first time. According to the CFD results, this value is recorded inside the enclosure also after 7 [hr] (0.3 [day]). In fact, in the experiments the maximum temperature happens at this time, first. This observation demonstrates the fast rate of heat transfer into the PC enclosure. In other words, the temperature inside the enclosure responds to the ambient temperature changes relatively fast (compared to RH). For RH, despite the fact that the ambient value is at 100 [%] for 8 days, the inner RH for the PC enclosure does not reach higher values than 67 and 76 [%] at the first day, according to the CFD simulations and the experimental data, respectively. This is due to the fact that heat is transferred through the outer walls and also the small opening; on the other hand, moisture can only get into the enclosure through the small opening.

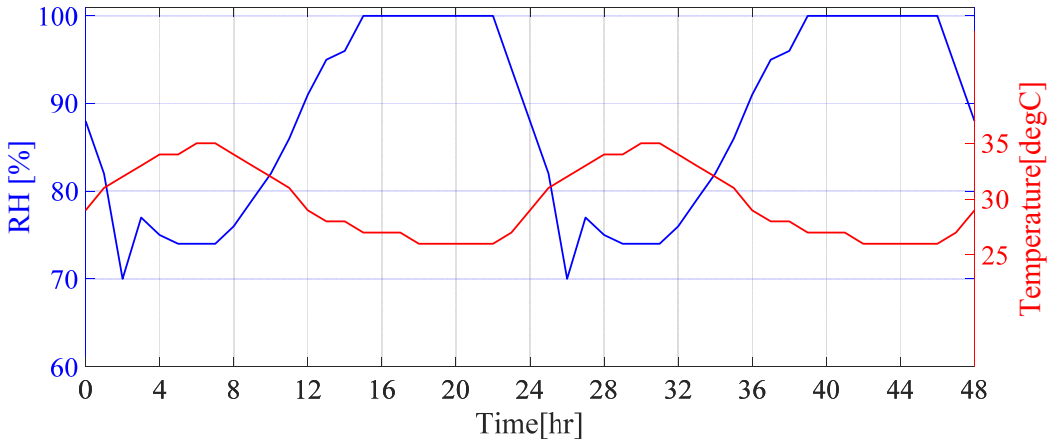

(a)

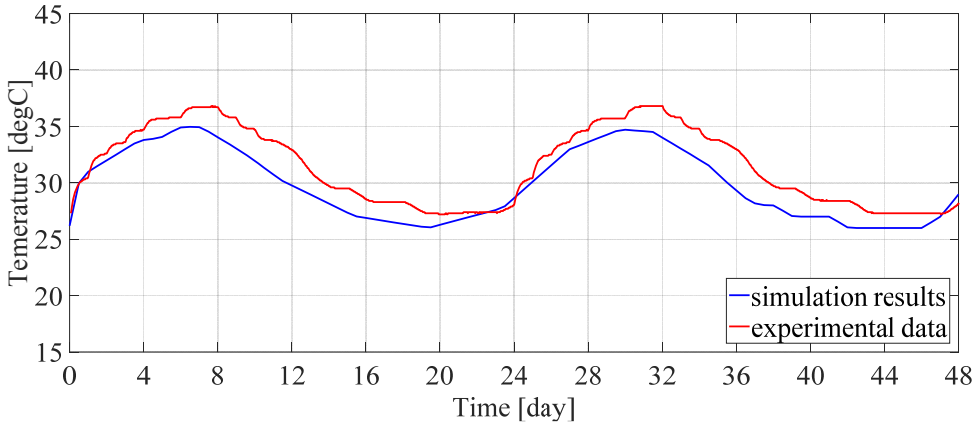

(b)

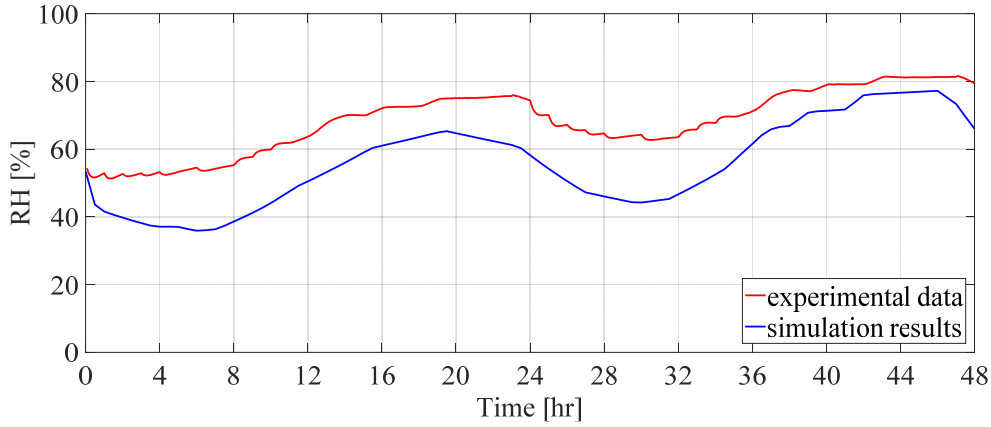

(c)

Figure 4-12 The STANAG 2895 conditions (a) and the temperature (b) and RH (c) changes inside the PC enclosure exposed to the STANAG 2895.

4.3 Copenhagen outdoor conditions

In electronics enclosure applications the heatsink is often attached to the walls of the enclosure to facilitate the transfer of the heat that is extracted from the devices to the ambient. A major problem with this arrangement is that the electronics can be directly influenced by the ambient temperature. Thus, during night or early morning when the device may not be working, its temperature falls down as the ambient temperature does. The RH in the enclosure then increases and there is a risk of condensation.

Here, we model a heatsink that is placed inside an enclosure without contacting the enclosure walls, which are exposed to Copenhagen outdoor conditions. With this arrangement, the heat sink can store the heat generated by the electronics to be used for lowering the RH later when the electronics are not working. We thus utilize the time delay that heat sinks can provide for heat transfer because of their high thermal capacity, to mitigate the adverse effects of surface-humidity interactions. Figure 4-13 presents a schematic diagram of the electronics enclosure investigated in this work. It contains a PCB, a heat producing component and a thermal mass (heatsink). Table 4-3 shows the material and dimensions of each of these components. These parameters are typical of outdoors electronics enclosures.

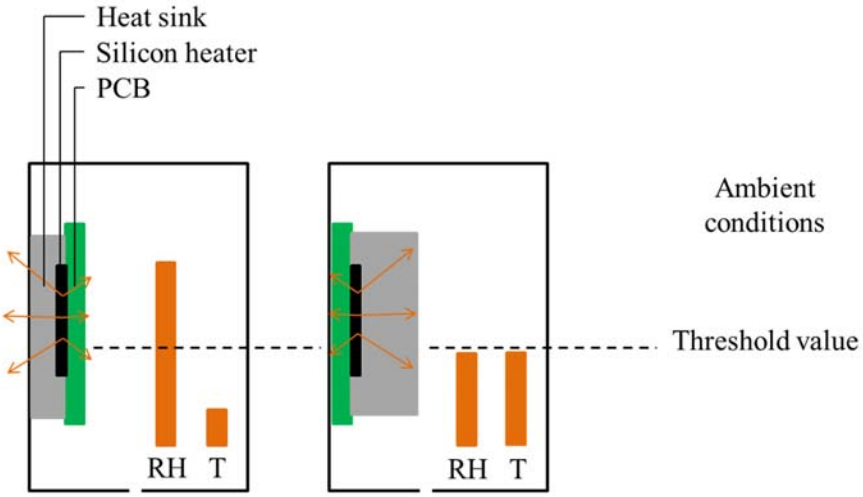

Figure 4-13 The schematic diagram of the electronics enclosure and the components inside.

Table 4-3 Material and dimensions of the electronics enclosure and the components inside

	Material	**Dimensions *[mm]***
Enclosure	Aluminum	Inner 188×128×276 Outer 190×130×280
PCB	FR4 (epoxy circuit board material)	30×1.6×130
Heat producing component	Silicon	30×1.6×50
Thermal mass	Copper	80×10-70×100

To examine parametric dependencies, four cases, representing 4 different sizes for the thermal mass, are modeled (the width and the length of the thermal mass are constant for all the cases). Table 4-4 summarizes the thermal masses for the studied cases.

Table 4-4 The four studied cases.

	Thermal mass		
Case number	size *[m^3]*	heat capacity *[j/K]*	thermal resistance *[K/W]*
1	8×10^{-5}	268	0.00313
2	2×10^{-4}	669.9	0.00781
3	4×10^{-4}	1340	0.01563
4	5.6×10^{-4}	1876	0.02188

The ambient temperatures and vapor concentrations represent Copenhagen's conditions on typical summer days (July 1st and 2nd). The data have been derived from COMSOL database. Figure 4-14 shows the ambient temperatures and moisture concentrations during the aforementioned two days.

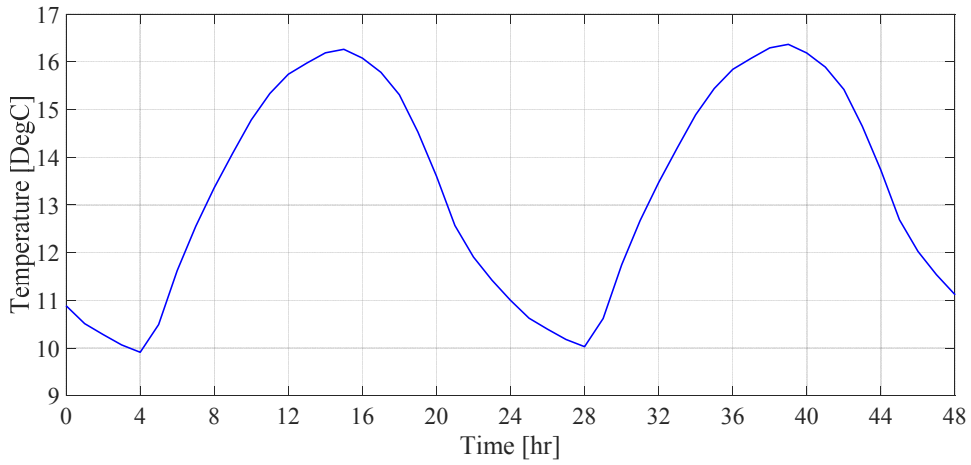

(a)

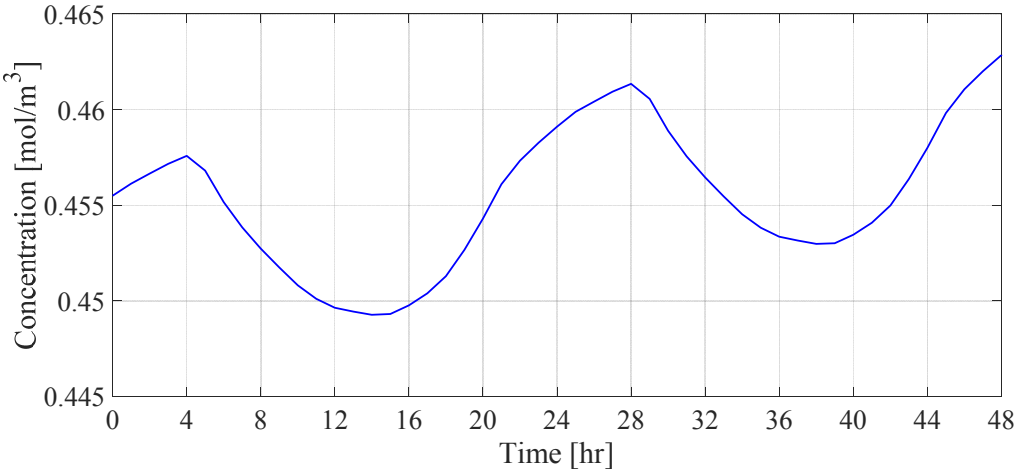

(b)

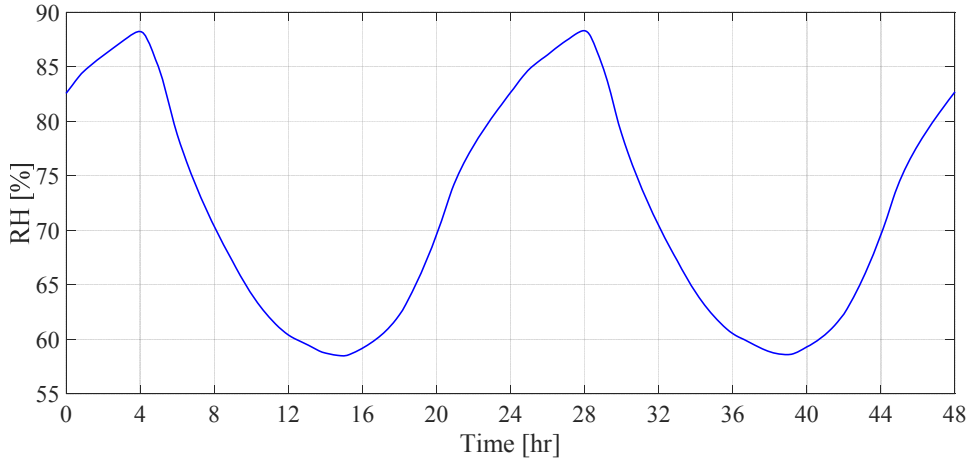

(c)

Figure 4-14 The (a) temperature, (b) moisture concentration and (c) RH transient changes on July 1st and 2nd 2016 in Copenhagen.

In the simulated electronics enclosures the heater works on ON/OFF cycles for the first 24 hours but works continuously afterwards. Figure 4-15 shows the heat flux of the heater versus time. For the CFD simulations, the dynamic boundary conditions are directly imported to and read by COMSOL Multiphysics*TM*.

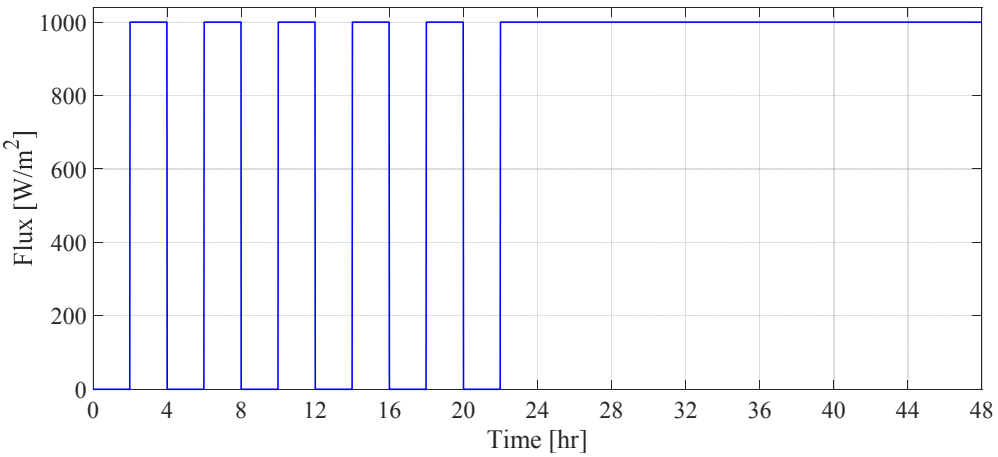

Figure 4-15 The heat flux emitted from the heater versus time.

The parametric effect of different sizes of copper thermal mass on the temperature of the PCB is shown in Figure 4-16. The temperature of the PCB is affected by the size of the thermal mass as well as natural convection in the air trapped inside the enclosure. All other parameters are kept unchanged in the depicted four cases. During the ON/OFF cycle, the amplitudes of the temperature changes are damped as the thickness of the thermal mass is increased. Furthermore, when the heater is working continuously, a larger thermal mass cools down the PCB more than a smaller one. As expected, with a bigger thermal mass, the temperature of the thermal mass will be lower during the time that the heater is on. Lower temperature difference in the trapped air leads to a lower Gr and therefore a lower Nu and a weaker natural convection heat transfer coefficient. Thus, on one hand increasing the size of the thermal mass enhances conduction, which tends to help the cooling down of the PCB. On the other hand, increasing the size of the thermal mass slows down free convection, which has an opposite effect on the cooling of the PCB. It should be emphasized, however, that this cooling process is dynamic. The thermal behavior of the system is influenced by the cycle period and the heat flux as well.

Figure 4-17 shows the variation of the average RH in the enclosure with time for the aforementioned four cases. The moisture concentration in the ambient air remained almost unchanged during the two days. As a result, the moisture concentration difference between the ambient air and the air trapped inside the enclosure (the driving force for moisture transfer) was small and consequently the vapor mass transfer through the opening was insignificant. Thus, the RH inside the enclosure was mostly affected by temperature rather than moisture concentration.

In general, there is a risk of condensations when the electronics are in OFF mode, especially during early hours of the day when the ambient temperature is low (see Figure 4-14a). Increasing the thickness of the thermal mass from 10 *mm* to any of the other three values reduces the RH at the vicinity of the PCB. However, the largest thermal mass does not necessarily provide the most desirable local climate for the PCB, and this is due to the dynamic nature of the heat transfer in this

system. For instance, in the second, third and fourth cycles the 25 mm and 50 mm thickness thermal masses provide the surface of the PCB with a lower RH than the 70 mm-thick thermal mass-one. Therefore, the size of the thermal mass should be optimized based on several parameters including the working cycle of the electronics, the rate of heat generation, and the ambient conditions.

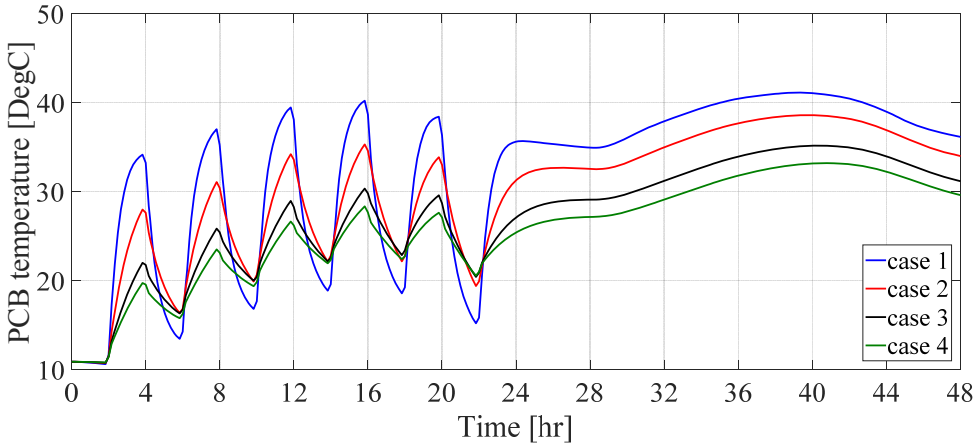

Figure 4-16 The average PCB temperature for the four case studies versus time.

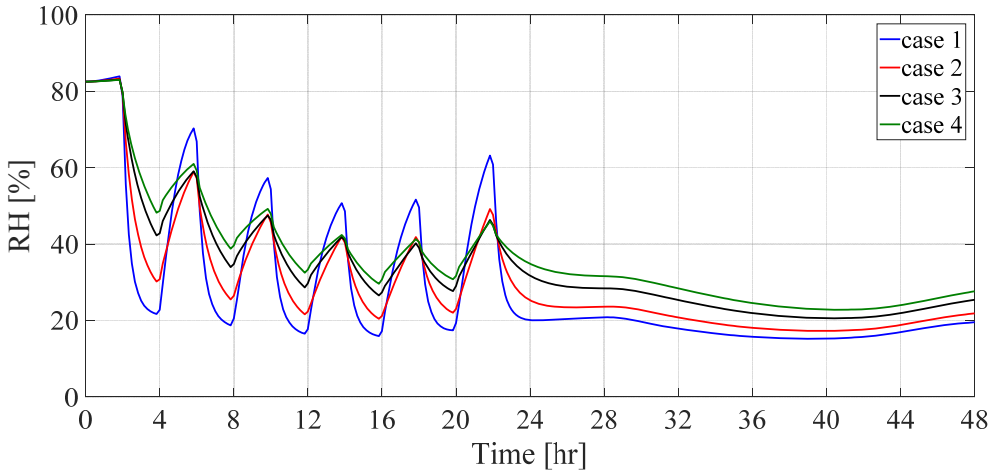

Figure 4-17 The average RH on the PCB for the four case studies versus time.

The following concluding remarks can be made:

- The presence of the components inside the enclosure especially the heatsink causes a delay to the ambient thermal cycles and also shortens the amplitude of the cyclic changes.
- Despite the fact that a temperature increase accelerates the di□usion, the mass transfer resistance which is a□ected by the geometrical sizes beside the di□usion coe□cient is not significantly a□ected.

- The moisture concentration inside the enclosure is more effective compared to the temperature cycles in reducing the condensation risk on the PCB, in case of high ambient RH.
- The buoyant flow inside the enclosure reduces the mass transfer resistance inside the enclosure. The cyclic internal heat load also helps this effect.
- The temperature profile and consequently the RH profile are mainly controlled by the buoyant air flow (natural convection) rather than heat conduction inside the enclosure.

Chapter 5
Deriving a Cauer ladder RC model

This chapter presents CFD adapted RC Cauer ladder model for the purpose of fast calculation of temperature of the electronics and moisture content of the trapped air inside an electronics enclosure (Paper III).

5.1 Equivalent RC circuit for Natural convection

Lumped models, based on the fundamental similarity between heat and mass transfer and the transfer of electric charge in an electrical circuit are capable of fast and easy predictions [38]; nevertheless, because of their underlying simplifying assumptions as well as their implementation constraints they lack accuracy. For instance, implementing natural convection in a RC model is challenging because quantification of capacitance for a convective system is not straightforward. A complicating factor with respect to implementing natural convection in a RC model is that the natural convection heat transfer coefficient is a function of the temperature difference between the fluid and the cooled surface. Since this temperature difference is part of the solution itself, an iteration loop is needed for the temperature calculations. Khane and Usman [37] attempted to estimate the capacitance of the energy stored in a fluid during natural convection. They conducted CFD simulations for a Rayleigh–Benard convection system using FLUENT commercial software. They applied a constant heat flux on the heat source side of their simulated system and monitored the sink side heat flux. By analyzing the variation of the heat flux of the heat-sink side with time, they estimated the total energy stored in the fluid. Thereafter, by comparing the conduction vs. convection system, they determined the capacitance [37].
The equivalent electrical circuit for steady state is only composed of resistances, the values of which can be obtained using well-known equations. For transient analysis, electrical capacitors are needed to represent the accumulation of energy in the materials. For conduction heat transfer the capacity can be easily calculated (see Table 5-1); however, for convection, specifically natural convection, in addition to the fluid internal energy, energy is also stored in the form of kinetic energy of the fluid [37].

Table 5-1. Resistance and capacity values for equivalent electrical circuit analogy

	Resistance	Capacitor
Conduction	$\frac{L}{k \times A}$	$\rho \times V \times C_p$
Convection	$\frac{1}{h \times A}$	$studied\ in\ this\ work$

As stated in chapter 2, for natural convection, the heat transfer coefficient (h) is found from correlations of the following form [40]–[42]:

$$Nu = \frac{[q_s^{"}/(\Delta T)]L}{k} = \frac{hL}{k} = c(Gr \times Pr)^m = c(Ra)^m \qquad (5.1)$$

$$Gr_L = \frac{g\beta\ (\Delta T)L^3}{\nu^2} \qquad (5.2)$$

$$Pr = \frac{C_p \mu}{k} \qquad (5.3)$$

, where Nu, Gr and Pr represent Nusselt, Grashof, and Prandtl numbers, respectively. The values of the constants c and m depend on geometry, configuration (orientation), and whether the natural convection boundary layer is laminar or turbulent. Disregarding the material thermophysical property changes with temperature, the heat transfer coefficient (h) is evidently a function of temperature difference (ΔT). Furthermore, the capacity of the capacitor responsible for the natural convection also depends on temperature because the temperature gradient is the sole cause of the buoyant flow in the bulk of the fluid. In this work, the ΔT dependency of the convective resistance and capacity value is derived from the CFD simulations.

Thermal resistances of the medium are not the only resistances against heat transfer. When heat leaves a heat source of finite dimensions and enters a larger region (substrate), there is a spreading resistance. Generally, expressions that can be used for the calculation of this resistance depend on dimensionless geometric and thermal parameters [69]. Here, the spreading resistance is calculated using the following equation [40]:

$$R_{spreading} = \frac{1 - 1.410A_r + 0.344{A_r}^3 + 0.043{A_r}^5 + 0.034{A_r}^7}{4k_{sub}{A_h}^{1/2}} \qquad (5.5)$$

Where, A_h is the heat source area and A_r is the ratio of the heat source area to the substrate area. It is worth mentioning that, $\sqrt{A_r}$ should be $0 \leq \sqrt{A_r} \leq 0.5$ [70].

Figure 5-1 demonstrates the Cauer ladder circuit for the investigated system (the latter case in Chapter 4).

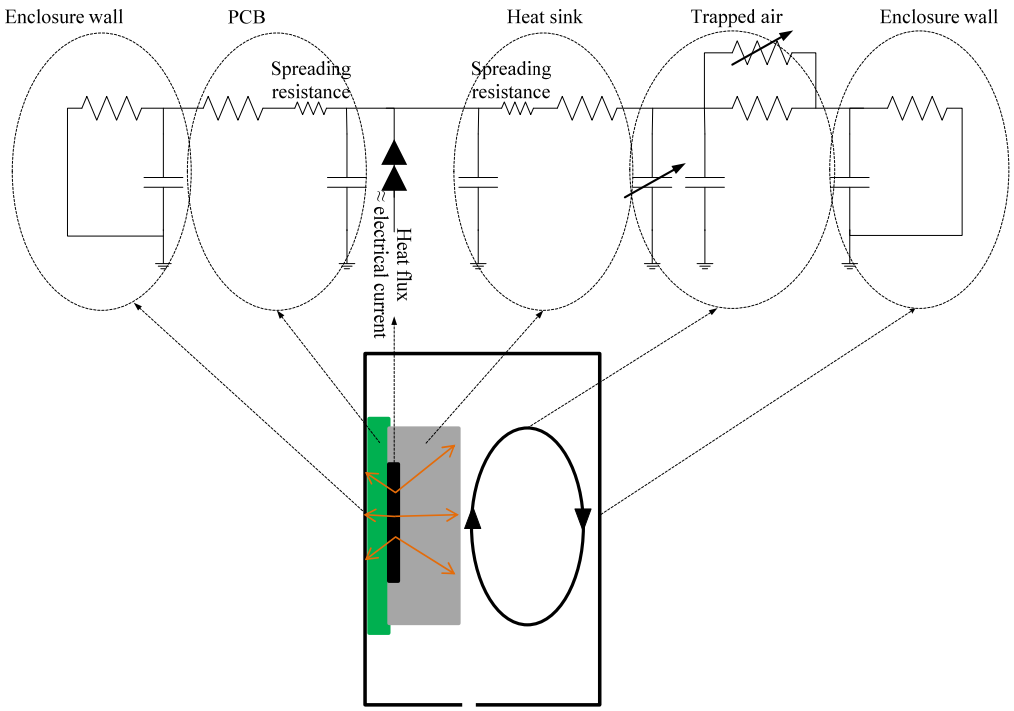

Figure 5-1 The equivalent electrical Cauer ladder circuit for heat transfer inside the enclosure.

The equivalent electrical circuit for moisture transfer is shown in Figure 5-2. For mass transfer, the only resistance considered is associated with the small opening at the bottom of the enclosure, and the capacitance represents the volume of the cavity inside the enclosure [29]. This is justified because saturated air-vapor condensations were not approached anywhere in the system in any of the simulations and therefore no condensation could have occurred in any of the simulations.

The equivalent circuits are implemented in the *Matlab/Simulink* version *2016b*. *SimRF* and *Simscape* modules are used to represent and analyze the electrical circuit. The constant and variable resistances and capacitors are obtained from the SimRF module and the voltage and current sources are obtained from the Simscape module [62].

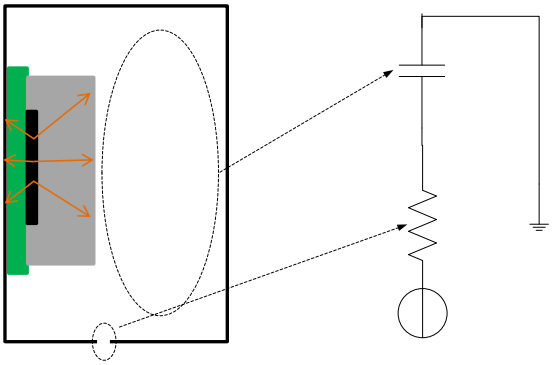

Figure 5-2 The equivalent electrical Cauer ladder circuit for the moisture transfer.

The dependence of Nu on ΔT and Ra for the natural convection is displayed in Figure 5-3 for the four cases. In comparison with the case with the largest thermal mass, the air trapped inside the enclosure with the smaller thermal mass experiences higher temperature gradients and therefore experiences a slightly larger range of variation in Ra. The profiles of Nu versus Ra and ΔT are approximately the same for all four cases, in terms of trend as well as magnitude. The variations of Nu as a function of Ra and ΔT are monotonic and appear to follow a power function, while the relation between Ra and ΔT is approximately linear. These functional dependencies are of course the result of the complex dependence of Nu and Ra on fluid properties as well as geometry. However, given that in practice the fluid properties (i.e., properties of air that is partially saturated with water vapor) vary only over small ranges, similar functional dependencies should be expected. For a specific geometry it should therefore be possible to derive simple empirical correlations for the calculation of the Nu and Ra using the ΔT . Equation (5.6) demonstrates Nu versus Ra and ΔT for the system studied here (see Figure 5-3). Equation (5.6) is only valid for $\Delta T \leq 25[K]$.

$$Nu = 9.968(\Delta T)^{0.2353} = 0.5096(Ra)^{0.2536} \qquad (5.6)$$

In this study, the highest ΔT is about 25 [K] and the Nu is less than 25 (see Figure 5-3). Considering the highest possible *Nu* and *k* in the system, the highest estimated *h* is:

$$h = \frac{Nu \times k_{air}}{L} = \frac{25 \times 0.028\ [\frac{W}{m.K}]}{0.1\ [m]} = 7\ [\frac{W}{m^2.K}] \qquad (5.7)$$

Thus, the highest *Bi* can be estimated as:

$$Bi = \frac{h \times L}{k_{copper}} = \frac{7\ [\frac{W}{m^2.K}] \times 0.1\ [m]}{385\ [\frac{W}{m.K}]} = 0.0018 \qquad (5.8)$$

Since the Bi is well below unity, the thermal behavior of the system can be approximated by the lumped RC method [40].

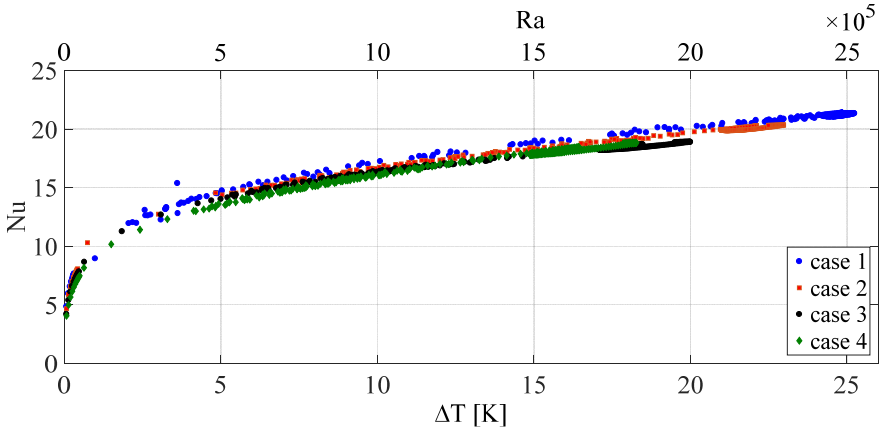

Figure 5-3 The Nu correlation with Ra and the temperature difference

In transient convection problems, the change in the kinetic energy of the fluid must be considered in the energy balance. The relative significance of stored kinetic energy in electronics enclosures

will now be discussed. The contribution of fluid kinetic energy in natural convection electronics cooling was discussed by Khane et al. [37] in 2010. Khane et al. performed a set of numerical simulations representing the Rayleigh–Bénard convection in an experimental apparatus. The portion of the kinetic energy stored in the fluid was determined by monitoring the heat flux from the heat sink while a constant flux was imposed by the heat source. The difference between the two fluxes represented the total rate of energy gain by the fluid (internal energy + the energy associated with the motion). The rate of accumulation of kinetic energy was then determined by subtracting the rate of accumulation of internal energy from the total rate of energy accumulation in the fluid [37]. In this work, the kinetic energy of the trapped air is directly estimated by the forthcoming integration over the fluid volume:

$$E_K = \frac{1}{2}\int_V \rho(\lfloor \boldsymbol{u} \rfloor) dV \qquad (5.9)$$

Where, ρ and $\boldsymbol{u}$ are calculated by the full 3D CFD simulations. Figure 5-4 shows the kinetic energy changes inside the system versus the temperature difference that the trapped air experiences. For design and analysis convenience, the correlation between the kinetic energy and the temperature of the air should be derived. We define the design energy capacity as:

$$C_{KE} = \frac{\Delta E_{KE}}{\Delta T} \qquad (5.10)$$

However, a comparison between the thermal capacity and the kinetic energy capacity of the fluid in the systems considered revealed that the stored kinetic energy is smaller than the stored thermal energy, typically by 9 orders of magnitude, and could be neglected, as expected.

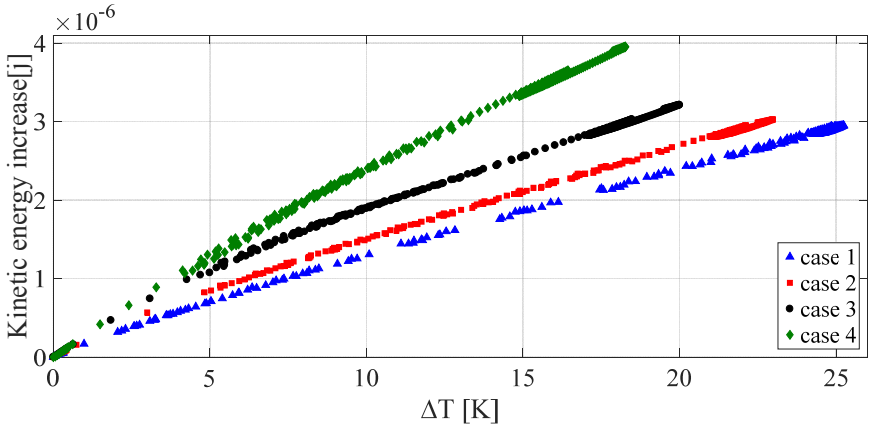

Figure 5-4 The Kinetic energy changes for the trapped air inside the enclosure.

Figure 5-5 displays the thermal resistance and thermal capacity values for the solid bodies in the simulated systems. The magnitude of the spreading resistances for the heatsink and PCB are comparable with the thermal resistances of the heatsink and the PCB. They must therefore be considered in the analysis.

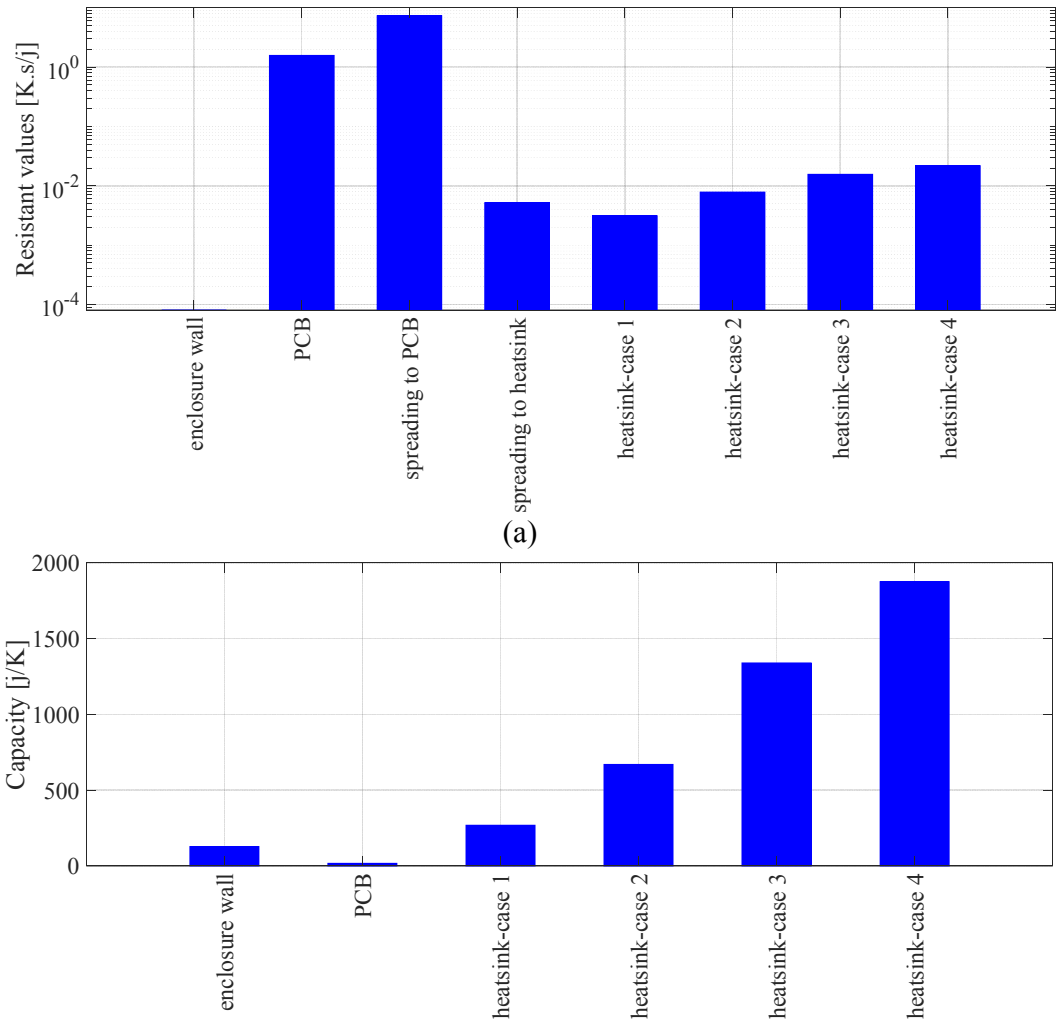

Figure 5-5 The a) thermal resistance and b) thermal capacity values for solid bodies in the simulated systems.

5.2 Comparison of RC results with CFD calculations

Using the derived resistance and capacity values from the CFD simulations for the air trapped inside the enclosure, an RC-based modeling is now conducted for the aforementioned four cases that are summarized in Table 4-4.

Figure 5-6 compares the results from the RC method with the CFD simulations. For all the four cases, the RC model underestimates the temperature during the two days, except for about 10 hours in the second day for case 4 where the difference between the RC and CFD results is less than 1°C. Despite this, the lumped analysis is presenting the same trend during both ON/OFF cycles, as well as during the time when the heating is continuously on. There are several assumptions in the RC

analysis that cause the differences with the CFD calculations, such as the 1D heat transfer assumption, uniformity of the temperature in each of the thermal bodies as well as the trapped air, and the potential inaccuracies in the correlations for the spreading resistance and Nu.

Figure 5-6 shows that for case 4, where the heatsink is the largest, the CFD result is very close to the RC estimation. On the other hand the discrepancy between the RC model and CFD simulations is the largest for case 1, where the heatsink inside the enclosure is the smallest and the system is experiencing the largest temperature change. Evidently the discrepancy between the RC model and CFD simulations diminishes as the temperature fluctuations diminish, and is large only when such temperature fluctuations are drastic.

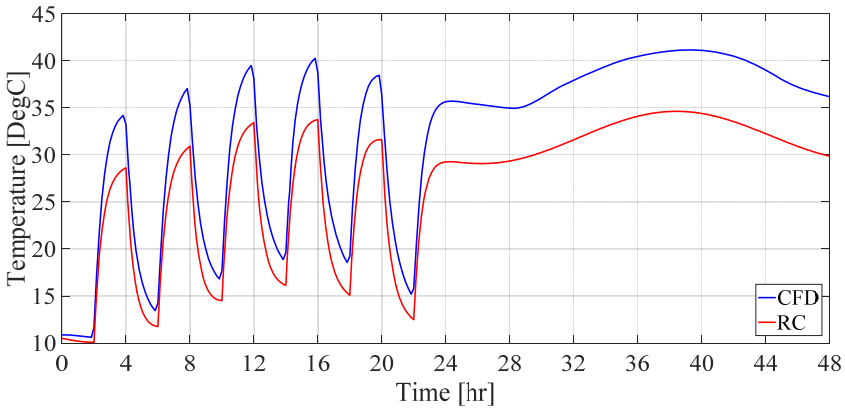

(a)

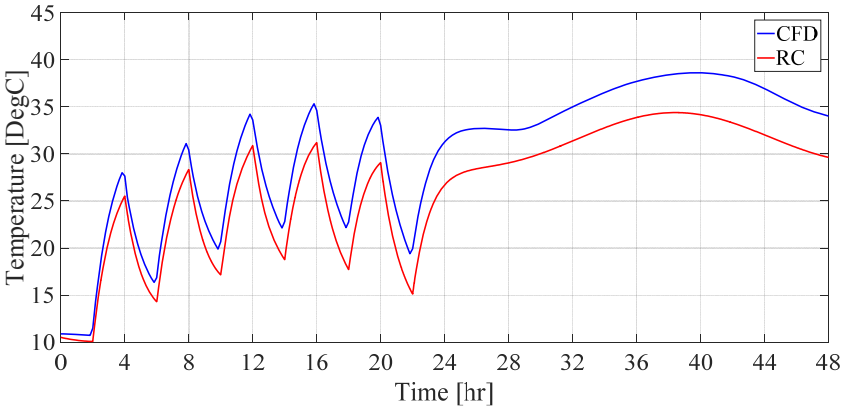

(b)

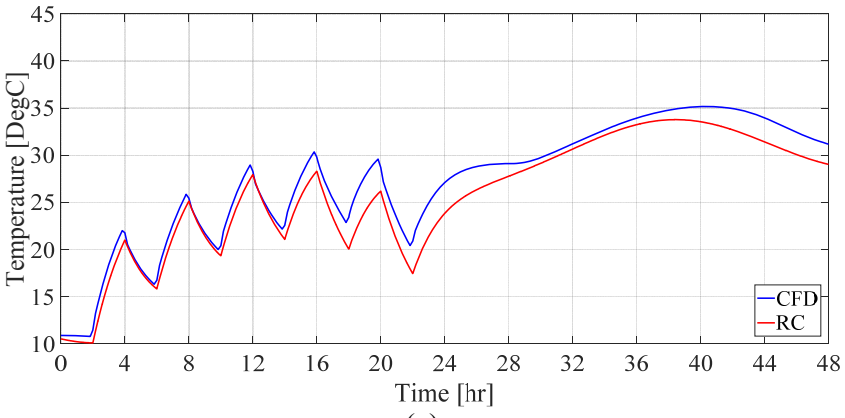

(c)

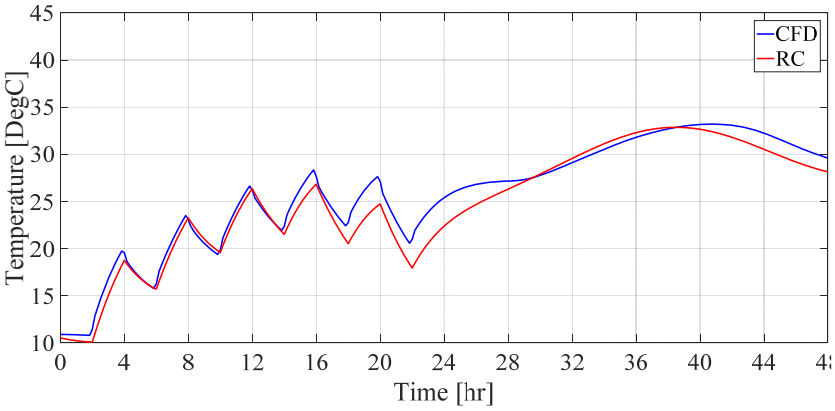

(d)

Figure 5-6 The PCB temperature for (a) case1, (b) case2, (c) case3 and (d) case4

Regarding the air that is trapped inside the enclosure, it should be noted that, even though the monotonic and simple relation between ΔT and Nu is approximately the same for all four cases (see Figure 5-6), ΔT does not remain constant over time. This variation in ΔT results in the variation in convection heat transfer resistances for air. Thus, at each specific time the convection heat transfer resistance is different from case to case. Figure 5-7 demonstrates the ΔT values for the four studied cases. After two ON/OFF cycles, the ΔT values all follow the same trend despite the ambient temperature changes. During the second day, when the heaters work non-stop, after about 10 hours the ΔTs reach steady values. The sub-figure shows the ΔT variation versus the heatsink depth, which can be represented by second order polynomial:

$$\Delta T = -0.0002514\ (depth)^{2.077} + 18.54 \qquad (5.11)$$

The ΔT values are important because the aforementioned derived Nu vs. ΔT correlation should be used only within the temperature range over which simulations that were the basis of the correlation have been performed. However, note that the correlations (see Equation (5.6)) can be used for heat fluxes, heat sink materials, or ambient conditions that are different from those

applied in these simulations, as long as the ΔTs in the systems are within the range of ΔT that constitute the basis of the aforementioned correlation.

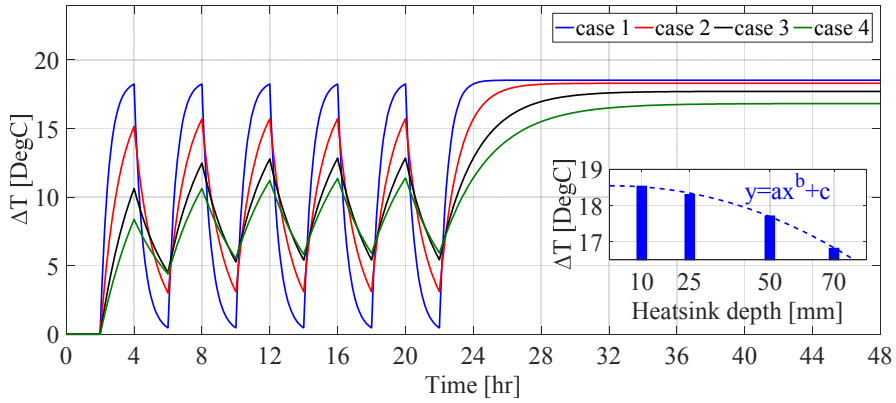

Figure 5-7 The ΔT values for the four case studied cases.

In the analysis presented here, the vapor concentration is assumed to remain uniform inside the enclosure. This assumption is reasonable, except at very close proximity to cooled surfaces when condensation takes place. The air recirculation caused by natural convection ensures the essentially uniform distribution of vapor concentration in the bulk gas, in particular when condensation does not occur. The vapor concentration varies with time, of course, primarily because of the variation of the vapor concentration in the ambient air. Figure 5-8 demonstrates the variation of vapor concentration with time over the two days. As the heatsink size increases, the volume of the air inside the system is decreased (the ratio of heat sink volume to the air volume is 0.0123, 0.0313, 0.0645 and 0.0927 for case 1, 2, 7 and 4, respectively) and consequently, the response to the ambient changes becomes faster. However, in general, the variation of the ambient moisture concentration is small and smooth. Nevertheless, the RH in the enclosure varies over a significant range, primarily due to the change in temperature.

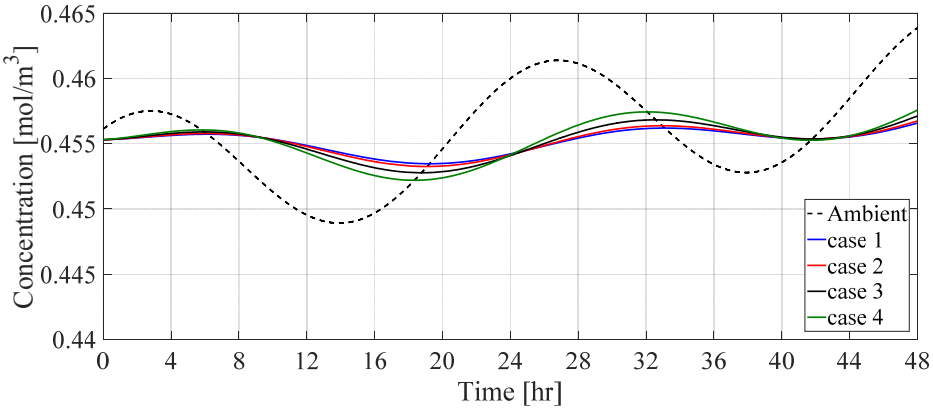

Figure 5-8 The average moisture concentration inside the enclosure versus time.

It should be emphasized that, in spite of its relatively small to moderate discrepancy with detailed multi-dimensional CFD simulations, the RC method is a useful design tool because it is faster than CFD simulations by orders of magnitude. Thus, for short-term transients a reliable RC model can be used for scoping analysis, making multiple-iteration design procedures feasible. More importantly, RC models can be used for long-term (month or even year-long) simulations. Figure 5-9, for example, shows the temperature, moisture concentration and RH histories for the enclosure represented by case 4, in response to the previously described ON/OFF cycles for the months of June, July and August in Copenhagen. For calculating RH for 92 days, these simulations took only 7 minutes on a personal computer with an Intel Core i7 (4600M / 2.9 GHz) CPU. On the other hand, a similar calculation using CFD, covering only two days, took about 1460 mins (almost 1 day) on 20 nodes of a scientific Linux 6.4 cluster; where each node was configured with Intel Xeon Processor X5550.

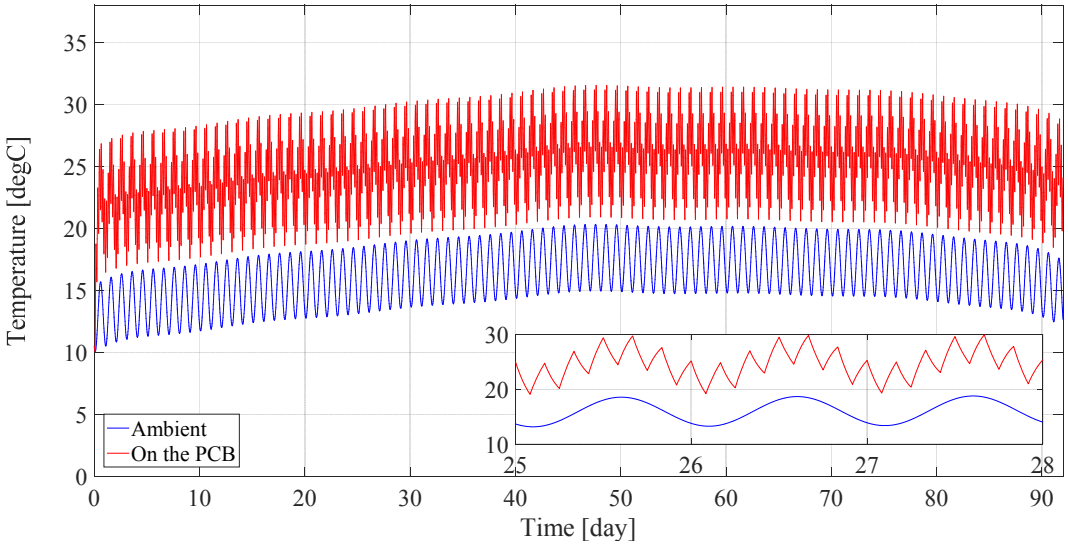

(a)

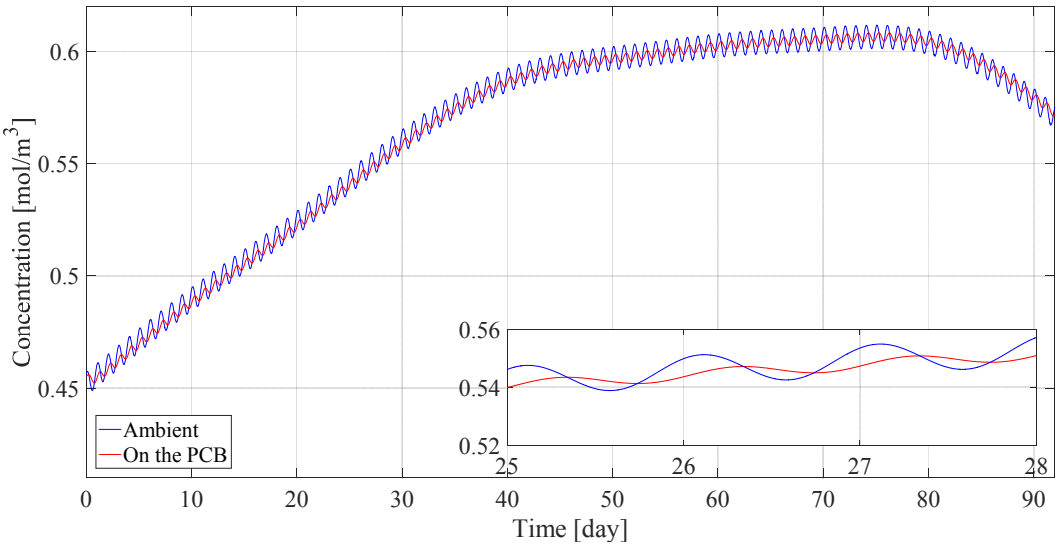

(b)

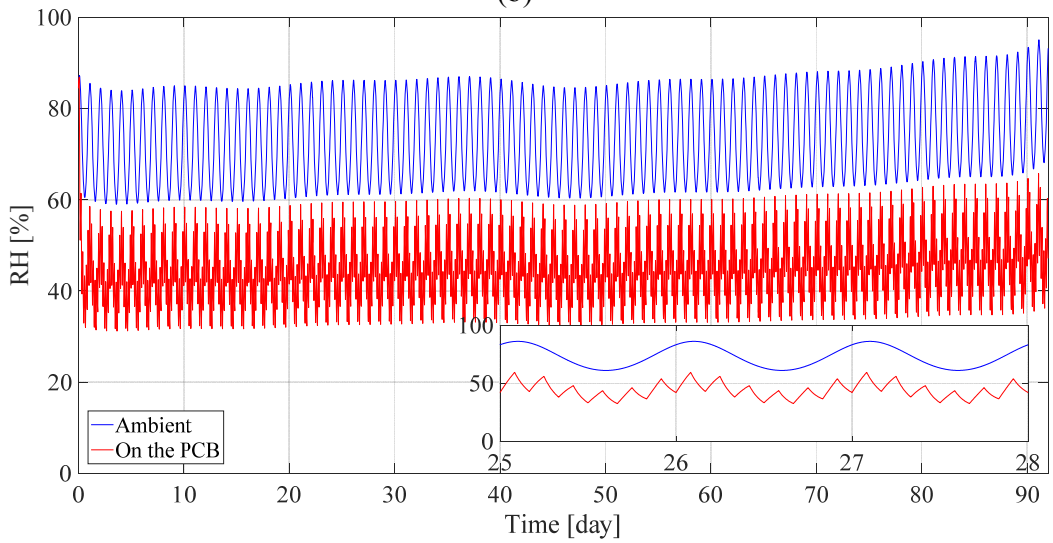

(c)

Figure 5-9 The average a) temperature, b) moisture concentration and c) RH on the PCB on June, July and August in Copenhagen.

The following concluding remarks can be made:

- In an enclosure with fixed geometry the dependence of Nu representing natural convection on Ra and ΔT inside the enclosure follows a simple power function; furthermore, a linear relation is observed between Ra and ΔT. These simple correlations can be utilized for fast scoping analyses.
- A comparison between the magnitudes of the thermal energy and kinetic energy that are stored in the air inside a typical enclosure reveals that the kinetic energy is small and can be neglected.

- The Cauer ladder RC model slightly underestimated the temperature during the two days in all the four cases. The typical discrepancy was about 1 to 7 [°C]. However, the lumped RC model successfully predicted the trends of temperature and RH changes inside the enclosure. The technique can be useful for scoping analysis for short transients, and more importantly for long-term transients.
- Spreading resistances are important for both the heatsink and PCB and should be considered in the analysis of electronics enclosures.
- Even when the daily ambient moisture concentration changes are small and smooth, the RH undergoes drastic variations primarily because of the variation of ambient temperature.

Chapter 6
Summary of the appended papers

This chapter presents a summary of the seven appended publications.

6.1 Paper I

In this paper, first moisture distribution and transfer time into a typical electronic enclosure with an opening is modelled using CFD in an isothermal condition. Then the results are compared with the well-known RC modeling approach. The discrepancy between the two approaches is investigated. Based on the CFD simulation results, a factorial design is employed to provide a design space of the investigated factors so that the level of significance of each factor can be clarified at the whole range. The effects of a heat producing electronic device inside the enclosure are also simulated numerically in a non-isothermal study.

6.2 Paper II

In this study, the RH evolution is studied in three stages: first, in an empty enclosure, then in an enclosure with a PCB, heatsink and a heater, and finally in the case of an internal cyclic heat load. In all three parts, the effect of the opening size of the enclosure is also studied. The numerical simulation results are compared with corresponding experimental results from the literature, and a good agreement is found.

6.3 Paper III

In this work, the functionality of a heatsink for partially storing the heat that is generated by the electronics and releasing the stored energy with a time lag for the purpose of enhancing the stability of the local climate inside a typical electronics enclosure is studied using transient 3D CFD simulations. In addition to CFD modeling, a Cauer ladder RC model is also developed for fast and long term predictions. A correlation for calculating the Nusselt number representing heat transfer between the trapped air inside the enclosure and the heat sink is derived based on the CFD simulation results.

6.4 Paper IV

In this paper, a semi-empirical regression model is developed using the analysis of variance of the experimental data in a factorial design frame work for prediction of time constants for humidity buildup in an electronic enclosure. The effects of four influential parameters namely, initial relative humidity inside the enclosure, radius and length of the opening and temperature are studied. The investigated range of parameter is based on the manufacturing feasibility and the operating conditions proposed by our industrial partners.

6.5 Paper V

In this work, in order to reduce the CPU-time and make a way for further analysis, a simplifying modification is applied in which the real 3D geometry is approximated by a 2D axial symmetry one. The results for 2D and 3D models were compared in order to calibrate the 2D representation. Furthermore, simulation results were compared with experimental data and good agreement was found.

6.6 Paper VI

In this work, the effects of ambient conditions on the air cooling by natural convection through a heatsink for five cities are compared. The Grashof (Gr) and Prandtl (Pr) numbers are calculated transiently with the dynamic ambient changes and finally the Rayleigh (Ra) and Nusselt (Nu) numbers of the five cases are compared.

6.7 Paper VII

In this study, the effects of material of the enclosure on the moisture, temperature and velocity distributions are investigated in idealized perfectly sealed enclosures made of aluminum (Al) and polycarbonate (PC). The effects of the wall thickness and also the convective heat transfer coefficient between the outer walls and the ambient air are discussed.

Chapter 7
Conclusion and outlook

7.1 Summary of the results

In this work, the moisture transfer into a typical electronics enclosure is extensively studied using mathematical simulations. The results are compared with corresponding experimental data from the literature at different stages of the study.

First, in an isothermal study, the effects of several parameters (initial RH inside the enclosure, temperature, radius and length of the cylindrical shaped opening, position of the opening) on the time constant of the moisture built-up into the enclosure are investigated by a full 3D CFD model. The CFD model shows a good agreement with the experimental data. Thereafter, the results are compared with a QSS approach in form of an RC circuit model. A discrepancy between the two models is observed. It is demonstrated that neglecting the resistance against the mass transfer inside the enclosure in the QSS model is a reason for that. Based on a fractional factorial design, a set of experiments was conducted. Fitting the experimental data to the QSS model for all the cases demonstrates the exponential nature of the RH changes inside the electronic enclosure over time. The analysis of variance of the results led to a semi-empirical model that can be used to find the critical parts of the design space of the investigated parameters for further investigations with a reasonable accuracy.

The CFD model is then used to study the RH evolution on a PCB inside an electronics enclosure exposed to cyclic ambient temperature. The local climate inside the enclosure is investigated in three stages: First, the response of an empty enclosure to the ambient conditions is investigated, then an enclosure with some components inside is considered and finally the effect of simultaneous internal and external temperature changes is studied. The numerical simulation results are compared with corresponding experimental results from the literature and a good agreement is found. The presence of components inside the enclosure, especially the aluminum heatsink, causes a delay to the ambient thermal cycles and also shortens the amplitude of the cyclic changes. Thus, it helps to reduce RH on the PCB. On the other hand, the moisture transfer happens through the bottom hole of the enclosure. Despite the fact that a temperature increase accelerates the diffusion, the mass transfer resistance, which is affected by the geometrical sizes beside the diffusion coefficient, is not significantly affected. Thus, the moisture transfer is mostly controlled by the opening size rather than the temperature. According to the simulation results, controlling the moisture concentration inside the enclosure is more effective compared to the temperature cycles in reducing the condensation risk on the PCB. It should be noted that the buoyant flow inside the

enclosure reduces the mass transfer resistance inside the enclosure. The cyclic internal heat load also helps this effect. The simulation results demonstrate that the temperature profile and consequently the RH profile are mainly controlled by the buoyant air flow (natural convection) rather than heat conduction inside the enclosure.

In light of these observations, unlike the conventional configuration of a heatsink, which is attached to the walls of the enclosure in order to facilitate the transfer of the generated heat to the ambient, the heatsink is placed inside the enclosure with no contacts with the walls. With this arrangement the heat sink can store the heat generated by the electronics to be used for reducing the RH later when the electronics are not operating. In this part of the study, the electronics enclosure is exposed to Copenhagen outdoor conditions. According to the results, a well-designed thermal mass can maintain RH low enough to avoid condensation. Due to the dynamic nature of the heat transfer in an electronics enclosure, an excessively large thermal mass does not necessarily provide the most desirable conditions for the PCB. The size of the thermal mass should be optimized based on the enclosure's boundary and operational conditions, including the working cycle of the electronics, the amount of the generated heat, and the ambient conditions.

A Cauer ladder RC model was also developed with the aim of long term prediction of the local climate inside the enclosure. The capacitance and resistance values for the natural convection were derived from the CFD results. It is demonstrated that, in an enclosure with fixed geometry the dependence of Nu (representing natural convection) on Ra and ΔT inside the enclosure follows a simple power function. Furthermore, a linear relation is observed between Ra and ΔT. A comparison between the magnitudes of the thermal energy and kinetic energy that are stored in the trapped air inside the enclosure reveals that the kinetic energy can be neglected. Although, the Cauer ladder RC model slightly underestimates the temperature, it predicts the trends of temperature and RH changes inside the enclosure successfully. The technique is useful for scoping analysis for short transients, and more importantly for long-term transients. Spreading resistances are very important for the transient conductive heat transfer among the components inside the enclosure and should be considered in the analysis of temperature.

The CFD model is useful for a thorough design of an electronics enclosure considering all the complexities and details and the developed lumped model capable of fast estimation of the temperature and RH for the trapped air, all the components inside the enclosure and walls of the enclosure, is very helpful for studying the local climate in a long period of time such as annual predictions.

7.2 Future work

Improving the local climate inside electronics enclosures is not yet comprehensively studied. In this work, several physics are simultaneously modelled using the commercial software package *COMSOL Multiphysics*^{TM}. The developed model is flexible for the addition of further physics such as adsorption/desorption. This makes possible to look into the effects of the presence of some commercial desiccants such as zeolite, bentonite, etc. inside the enclosure. The adsorbents,

adsorbing moisture at low temperatures (where the temperature is not in favor of RH decrease) and releasing it when the temperature is high, can behave like a buffer to damp the effect of temperature on the RH. This is similar to the effect of the heatsink studied in Chapters 4 and 5. The simultaneous effect of the thermal mass and adsorbents and optimizing the conditions according to the heat load and ambient conditions seems very interesting. Generally, polymeric potting and coating materials, display the same behavior as the adsorbents, with much less capacity to keep the moisture. Thus, further studies are essential to determine the optimum thickness of such materials on the electronics.

In this study, the effect of conventional aluminum and copper heatsinks is studied. However, it is interesting to see how different new cooling methods such as heatpipes or thermoelectric coolers affect the RH on the PCBs and critical places.

References

[1] I. Belov *et al.*, "Application of CFD modelling for energy efficient humidity management of an electronics enclosure in storage under severe climatic conditions," in *9th International Conference on Thermal, Mechanical and Multi-Physics Simulation and Experiments in Microelectronics and Micro-Systems*, 2008, pp. 1–8.

[2] R. Ciprian and B. Lehman, "Modeling effects of relative humidity, moisture, and extreme environmental conditions on power electronic performance," in *IEEE Energy Conversion Congress and Exposition*, 2009, pp. 1052–1059.

[3] J. Punch; R. Grimes; G. Heaslip ;T. Galkin;K. Viikevainen; V. Kyyhkynen and E. Elonen, "Transient hygrothermal behaviour of portable electronics," in *International Conference on Thermal Mechunical and Multiphysics Simularion and Experiments in Micro-Electronics and Micro-Sysrem*, 2005, pp. 398–405.

[4] J. B. Jacobsen, J. P. Krog, A. H. Holm, and L. Rimestad, "Climate-Protective Packaging," no. september, pp. 51–59, 2014.

[5] S. S. Anandan and V. Ramalingum, "Thermal Management of Electronics: a Review of Literature," *Therm. Sci.*, vol. 12, no. 2, pp. 5–26, 2008.

[6] "Global Enclosure Standards within the Electrical Industry." [Online]. Available: hoffmanonline.com.

[7] P. Shojaee Nasirabadi, M. Jabbari, and J. H. Hattel, "Numerical simulation of transient moisture and temperature distribution in polycarbonate and aluminum electronic enclosures," in *International Conference on Thermal, Mechanical and Multi-Physics Simulation and Experiments in Microelectronics and Microsystems, EuroSimE*, 2016, pp. 1–6.

[8] "Enclosure Design Tips Handbook." [Online]. Available: www.newark.com.

[9] M. D. Shende and A. Mahalle, "Cooling Of Electronic Equipments with Heat Sink : A Review of Literature," vol. 5, no. 2, pp. 56–61, 2013.

[10] W. A. Scott, *Cooling of Electronic Equipment*. New York: John Wiley and Sons – Interscience, 1974.

[11] A. Bejan and G. Ledezma, "Heat sinks with sloped plate fins in natural and forced convection," *Int. J. Heat Mass Transf.*, vol. 39, no. 9, pp. 1773–1783, 1996.

[12] H. E. Ahmed, "Optimization of thermal design of ribbed flat-plate fin heat sink," *Appl. Therm. Eng.*, vol. 102, pp. 1422–1432, 2016.

[13] H.-C. Chiu, R.-H. Hsieh, J.-T. Yao, and J.-H. Janl, "Numerical analysis on the liquid cooling of micro channel heatsink with phase change material," in *Semiconductor Technology International Conference*, 2015, pp. 6–8.

[14] R. C. Chu, R. E. Simons, M. J. Ellsworth, R. R. Schmidt, and V. Cozzolino, "Review of Cooling Technologies for Computer Products," vol. 4, no. 4, pp. 568–585, 2004.

[15] N. Khan, "Pool Boiling Heat transfer Enhancement by Surface modification," 2004.

[16] S. Trutassanawin, E. A. Groll, S. V Garimella, and L. Cremaschi, "Experimental

Investigation of a Miniature-Scale Refrigeration System for Electronics Cooling," vol. 29, no. 3, pp. 678–687, 2006.
[17] R. Ranjan, M. R. Pearson, and S. Krishnamurthy, "Thermoelectric Package Design for High Ambient Temperature Electronics Cooling," 2016.
[18] C. Li, D. Jiao, H. Mohan, F. Guo, and J. Wang, "Thermoelectric Cooling for Power Electronics Circuits : Modeling and Applications," pp. 3275–3282, 2013.
[19] D. Zhao and G. Tan, "A review of thermoelectric cooling: Materials, modeling and applications," *Appl. Therm. Eng.*, vol. 66, no. 1–2, pp. 15–24, 2014.
[20] D. R. Rousse, N. Ben Salah, and S. Lassue, "An Overview of Phase Change Materials and their Implication on Power Demand," pp. 1–6, 2009.
[21] P. Shojaee Nasirabadi, H. Conseil-gudla, S. Mohanty, M. Jabbari, R. Ambat, and H. Jesper, "Semi-Empirical Prediction of Moisture Build-up in an Electronic Enclosure Using Analysis of Variance (ANOVA)," in *IEEE Electronics Packaging Technology Conference, EPTC*, 2016, pp. 785–790.
[22] P. Shojaee Nasirabadi, M.Jabbari, and J. H. Hattel, "Numerical simulation of transient moisture transfer into an electronic enclosure," *AIP Conf. Proc.*, vol. 1738, pp. 1–4, 2016.
[23] H. C. R. Ambat, M.S. Jellesen, V. Verdingovas, K. Piotrowska, "Perspectives on the climatic reliability issues of electronic devices," 2014.
[24] M. Tencer and J. S. Moss, "Humidity management of outdoor electronic equipment: Methods, pitfalls, and recommendations," *IEEE Trans. Components Packag. Technol.*, vol. 25, no. 1, pp. 66–72, 2002.
[25] M. Tencer, "Conductive aqueous layer formation at the gel-substrate interface in equilibrium with 100% RH environment," *IEEE Trans. Components Packag. Technol.*, vol. 23, no. 4, pp. 693–699, 2000.
[26] S. Ogata, E. Sukegawa, and T. Kimura, "Performance Evaluation of Ultra-thin Polymer Pulsating Heat Pipes," vol. i.
[27] H. B. Fan and M. M. F. Yuen, "Multi-scale Modeling of Moisture Transfer in Electronic Packaging," pp. 758–761, 2010.
[28] M. Lindgren, I. Belov, A. Johansson, T. Danielsson, N. Gunnarsson, and P. Leisner, "Multi-disciplinary Approach to Design of a Power Electronics Module for Harsh Environments," vol. 3, pp. 1–8, 2009.
[29] M. Tencer, "Moisture ingress into nonhermetic enclosures and packages. A quasi-steady state model for diffusion and attenuation of ambient humidity variations," *Electron. Components Technol.*, pp. 196–209, 1994.
[30] P. Shojaee Nasirabadi, M. Jabbari, and J. H. Hattel, "CFD simulation and statistical analysis of moisture transfer into an electronic enclosure," *Appl. Math. Model.*, vol. 44, pp. 246–260, 2017.
[31] H. Conseil-Gudla, Z. Staliulionis, M. S. Jellesen, M. Jabbari, J. H. Hattel, and R. Ambat, "Humidity Buildup in Electronic Enclosures Exposed to Constant Conditions," vol. 7, no. 3, pp. 412–423, 2017.
[32] N. Dahan, A. Vanhoestenberghe, and N. Donaldson, "Moisture Ingress into Packages With Walls of Varying Thickness and / or Properties : A Simple Calculation Method," vol. 2, no. 11, pp. 1796–1801, 2012.
[33] I. Belov *et al.*, "Application of CFD modelling for energy efficient humidity management of an electronics enclosure in storage under severe climatic conditions," in *International*

Conference onThermal, Mechanical and Multi-Physics Simulation and Experiments in Microelectronics and Micro-Systems, EuroSimE, 2008, pp. 1–8.

[34] S. Kremp and O. Schilling, "Realistic climatic profiles and their effect on condensation in encapsulated test structures representing power modules," *Microelectron. Reliab.*, vol. in press, 2017.

[35] "COMSOL Multiphysics 5.1 User Guide," 2015.

[36] M. N. Touzelbaev, J. Miler, Y. Yang, G. Refai-Ahmed, and K. E. Goodson, "High-Efficiency Transient Temperature Calculations for Applications in Dynamic Thermal Management of Electronic Devices," *J. Electron. Packag.*, vol. 135, no. 3, p. 31001, 2013.

[37] V. Khane and S. Usman, "Further on integrator circuit analogy for natural convection," *Nucl. Eng. Des.*, vol. 240, pp. 609–615, 2010.

[38] D. Chiozzi, M. Bernardoni, N. Delmonte, and P. Cova, "A simple 1-D fi nite elements approach to model the effect of PCB in electronic assemblies," *Microelectron. Reliab.*, vol. 58, pp. 126–132, 2016.

[39] R. B. Bird, W. E. Stewart, and E. N. L. Oot, *Transport Phenomena*, 2nd ed. JOHN WILEY & SONS, 2002.

[40] T. L. Bergman, A. S. Lavine, F. P. Incropera, and D. P. Dewitt, *Fundamentals of Heat and Mass Transfer*, 7th ed. Jefferson City: John Wiley & sons, 2011.

[41] J. P. Holman, *Heat Transfer*, 10th ed. Jefferson City: McGraw-Hill, 2010.

[42] S. M. Ghiaasiaan, *Convective Heat and Mass Transfer*. New York: Cambridge University Press, 2011.

[43] Yunus A Çengel; Afshin J Ghajar, *Heat and mass transfer : fundamentals & applications*, 6th ed. New York: McGraw-Hill., 2011.

[44] D.-Y. Shang, *Free Convection Film Flows and Heat Transfer*, 2nd ed. Ottawa, ON: Springer, 2012.

[45] P. T. Tsilingiris, "Thermophysical and transport properties of humid air at temperature range between 0 and 100 °C," *Energy Convers. Manag.*, vol. 49, no. 5, pp. 1098–1110, 2008.

[46] H. V. Adrian Melling and Stefan Noppenberger and Martin Still, "Interpolation correlations for fluid properties of humid air in the temperature range of 100 °C to 200 °C," *J. Phys. Chem.*, vol. 26, no. 4, 1997.

[47] T. R. Marrero and E. A. Mason, "Gaseous Diffusion Coefficients," *J. Phys. Chem. Ref. Data*, vol. 1, no. 1, pp. 3–118, 1972.

[48] A. Fabbri and C. Cevoli, "2D water transfer finite elements model of salami drying, based on real slice image and simplified geometry," *J. Food Eng.*, vol. 158, pp. 73–79, 2015.

[49] M. Bakhshi, B. Mobasher, and C. Soranakom, "Moisture loss characteristics of cement-based materials under early-age drying and shrinkage conditions," *Constr. Build. Mater.*, vol. 30, pp. 413–425, 2012.

[50] P. Eliaers, J. Ranjan Pati, S. Dutta, and J. De Wilde, "Modeling and simulation of biomass drying in vortex chambers," *Chem. Eng. Sci.*, vol. 123, pp. 648–664, 2015.

[51] J. Songok, P. Salminen, and M. Toivakka, "Temperature effects on dynamic water absorption into paper," *J. Colloid Interface Sci.*, vol. 418, pp. 373–377, 2014.

[52] G. A. Reis, I. V. M. Tasso, L. F. Souza, and J. A. Cuminato, "A compact finite differences exact projection method for the Navier – Stokes equations on a staggered grid with fourth-order spatial precision," *Comput. FLUIDS*, vol. 118, pp. 19–31, 2015.

[53] R. Ciprian and B. Lehman, "Modeling effects of relative humidity, moisture, and extreme

environmental conditions on power electronic performance," *2009 IEEE Energy Convers. Congr. Expo. ECCE 2009*, pp. 1052–1059, 2009.

[54] H. Conseil, M. S. Jellesen, and R. Ambat, "Experimental study of water absorption of electronic components and internal local temperature and humidity into electronic enclosure," *Electron. Packag. Technol. Conf. (EPTC), 2014 IEEE 16th*, pp. 355–359, 2014.

[55] T. I. Katsaounis and M. L. Aggarwal, "Two-level screening designs derived from binary nonlinear codes," *J. Korean Stat. Soc.*, 2014.

[56] S. J. Cheng, J. M. Miao, and S. J. Wu, "Investigating the effects of operational factors on PEMFC performance based on CFD simulations using a three-level full-factorial design," *Renew. Energy*, vol. 39, no. 1, pp. 250–260, 2012.

[57] D. C. Montgomery, *Design and Analysis of Experiments Eighth Edition*. Hoboken: Wiley, 2013.

[58] G. E. P. Box and D. R. Cox, "An Analysis of Transformations Revisited, Rebutted," *J. Am. Stat. Assoc.*, vol. 77, no. 377, p. 209, 1982.

[59] W. Rukthong, W. Weerapakkaroon, U. Wongsiriwan, P. Piumsomboon, and B. Chalermsinsuwan, "Integration of computational fluid dynamics simulation and statistical factorial experimental design of thick-wall crude oil pipeline with heat loss," *Adv. Eng. Softw.*, vol. 86, pp. 49–54, 2015.

[60] S. M. Seyed Shahabadi and A. Reyhani, "Optimization of operating conditions in ultrafiltration process for produced water treatment via the full factorial design methodology," *Sep. Purif. Technol.*, vol. 132, pp. 50–61, 2014.

[61] "Degrees of protection provided by enclosures CENELEC - EN 60529." [Online]. Available: http://standards.globalspec.com/std/1638833/cenelec-en-60529. [Accessed: 09-Sep-2016].

[62] "Matlab user's guide," 2016.

[63] A. Bar-Cohen, M. Iyengar, and A. D. Kraus, "Design of Optimum Plate-Fin Natural Convective Heat Sinks," *J. Electron. Packag.*, vol. 125, no. 2, p. 208, 2003.

[64] J. R. Culham, S. Lee, and M. M. Yovanovich, "Thermal Modeling of Isothermal Cuboids and Rectangular Heat Sinks Cooled by Natural Convection," *IEEE Trans. Components Packag. Manuf. Technol. Part A*, vol. 18, no. 3, pp. 559–566, 1995.

[65] W. A. Khan, R. J. Culham, and M. M. Yovanovich, "Performance of Shrouded Pin-Fin Heat Sinks for Electronic Cooling," *J. Thermophys. Heat Transf.*, vol. 20, no. 3, pp. 408–414, 2006.

[66] J. R. Culham and M. M. Yovanovich, "Factors affecting the calculation of effective conductivity in printed circuit boards," in *InterSociety Conference on Thermal Phenomena*, 1998.

[67] H. Conseil, V. C. Gudla, M. S. Jellesen, and R. Ambat, "Humidity Build-Up in a Typical Electronic Enclosure Exposed to Cycling Conditions and Effect on Corrosion Reliability," *IEEE Trans. Components, Packag. Manuf. Technol.*, pp. 1–10, 2016.

[68] "The climatic and environmental conditions," 1986. .

[69] M. M. Yovanovich, Y. S. Muzychka, and J. R. Culham, "Spreading Resistance of Isofux Rectangles and Strips on Compound Flux Channels," *J. Thermophys. HEAT Transf.*, vol. 13, no. 4, pp. 495–500, 1999.

[70] M. M. Yovanovich, "Thermal Resistances of Circular Source on Finite Circular Cylinder With Side and End Cooling," *J. Electron. Packag.*, vol. 125, no. 2, p. 169, 2003.

Appendix A
Paper I

Applied Mathematical Modelling 44 (2017) 246–260

Contents lists available at ScienceDirect

Applied Mathematical Modelling

journal homepage: www.elsevier.com/locate/apm

CFD simulation and statistical analysis of moisture transfer into an electronic enclosure☆

P. Shojaee Nasirabadi[a,*], M. Jabbari[a,b], J.H. Hattel[a]

[a] Process Modelling Group, Department of Mechanical Engineering, Technical University of Denmark, Nils Koppels Allé, Kongens Lyngby 2800, Denmark
[b] Warwick Manufacturing Group, University of Warwick, Coventry CV4 7AL, UK

ARTICLE INFO

Article history:
Received 23 February 2016
Revised 20 August 2016
Accepted 5 September 2016
Available online 14 September 2016

Keywords:
Moisture
Diffusion
Electronic enclosure
CFD
Factorial design
Cyclic changes

ABSTRACT

Condensation and moisture related problems are the cause of failures in many cases and consequently serious concerns for reliability in electronics industry. Thus, it is important to control the moisture content and the relative humidity inside electronic enclosures. In this work, a computational fluid dynamics (CFD) model is developed to simulate moisture transfer into a typical electronic enclosure. In the first attempt, an isothermal case is developed and compared against the well-known RC circuit analogy considering the behavior of an idealized electronic enclosure. It is shown that the RC method predicts a faster trend for the moisture transfer into the enclosure compared to the CFD. The effect of several important parameters, namely, position of the opening, initial relative humidity inside the enclosure, length and radius of the opening and temperature is studied using the developed CFD model for the isothermal case. The model is then combined with a two level factorial design to identify the significant factors as well as the potential interactions using the numerical simulation results. In the second part of this study, a non-isothermal case is studied, in which the enclosure is exposed to two different conditions, i.e., internal temperature oscillation only and combined cyclic changes of ambient relative humidity and temperature. The results are compared with experimental data from literature, and show that the local climate inside the enclosure responds faster to the temperature changes compared to the RH changes. The trends predicted by the CFD simulations can be used to decide for the right time and position of a commercial adsorbent and/or thermal mass inside the enclosure to control the local climate.

1. Introduction

One of the major concerns in electronics industry when designing a new product or component is reliability [1]. Reliability issues associated with temperature, humidity and vapor pressure have become increasingly significant for electronic devices [2]. Considering this, electronic enclosures are of great importance as they serve several protection functions, such as cooling, touch protection, input-output (of any unwanted mass e.g. moisture) and appearance. Unless the enclosure is

☆ This article belongs to the Special Issue: Theoretical, Experimental, and Computational Mechanics.

* Corresponding author. Fax: +45 45251961.
E-mail addresses: parnas@mek.dtu.dk, parizad.shojaee@gmail.com (P. Shojaee Nasirabadi).

http://dx.doi.org/10.1016/j.apm.2016.09.004
0307-904X/

perfectly sealed and made from truly hermetic materials, moisture will at some point enter it [3]. On the other hand, it is not always possible or desirable to use hermetically sealed packages for reasons of manufacturability, cost or workability [4].

Analysing the presence of moisture is a truly multi-dimensional problem in electronics packaging and it can affect the performance of the devices in many ways. In fact, moisture can introduce corrosion; develop hygro-stresses and cause pop-corn failure and degradation of the polymer parts present in the assembly [5]. There are four sources of moisture in a closed package: the water vapor in the air inside the package; the water vapor adsorbed by the materials inside, the water vapor on the walls of the package; and the permeation of water vapor into the package through the walls [5]. In order to protect electronic devices from the effects of water vapor, it is essential that the relative humidity inside the enclosure does not reach a level that threatens the electronic function within the required lifetime [6].

Modeling tools describing the moisture behavior are very useful to predict and evaluate moisture related problems. Tencer [7] developed a simple quasi-steady state (QSS) model with the purpose of understanding the factors governing the kinetics of moisture transfer into enclosures in terms of the properties of the applied materials and the ambient conditions. The model estimated the time constants for moisture diffusion through plastic walls and openings [7]. This way, one can estimate the average moisture content inside the enclosure. How ever, the model is difficult to apply when the geometry is complex and also when several materials are employed in the body of the enclosure [8]. In another study, Tencer and Moss [9] discussed the absolute humidity control method that relies on minimization of water ingress through a careful selection of appropriate materials and design, and at the same time uses a desiccant to remove the water which makes its way into the enclosure, theoretically [9]. Dahan et al. [6] used an electrical analogy to adapt the QSS model to the moisture ingress into a package containing walls or elements of different thicknesses or properties. It is worth while mentioning that in the electrical analogy only the volume of the enclosure is considered in the calculations, regardless of its geometrical shape [6]. On the other hand, computational fluid dynamics (CFD) modeling allows the analysis of complex geometries and provides detailed information on temperature and humidity distributions [10]. Using CFD air and moisture transport in an enclosure can be simulated taking all possible boundary conditions into account. Furthermore, CFD modeling is a strong supplement to expensive and tedious experiments [11].

When a system is potentially affected by several factors, a screening statistical method can be used in order to estimate the main effects of active factors and possible interactions that involve the active factors. A two-level factorial design (FD) provides suitable designs for screening the influential factors, assuming the linear behavior model [12,13]. In a 2^k factorial design, the model for analyzing responses (observations) is given by Montgomery [14]:

$$y = \beta_0 + \sum_{j=1}^{k} \beta_j x_j + \sum_{i<j} \sum \beta_{ij} x_i x_j + \in, \tag{1}$$

where y is the response, the β's are parameters whose values are to be determined, x's are variables that represent the factors and $\in$ is a random error term. In this approach, higher-order interaction effects are initially neglected. However, the presence of such effects are checked and in case, they can be considered using a suitable design [14]. CFD can be combined with the FD method in order to optimize the effects of different factors [12,15–17].

In this work, first CFD modeling with an isothermal condition is used to study the moisture distribution as well as the transfer time into a typical electronic enclosure with an opening. Then the results are compared with the well-known RC modeling approach. The CFD simulation results are integrated with FD. to provide a design space of the investigated factors so that the level of significance of each factor can be clarified at the whole range. The aim of this part of the study is to replace the CFD calculations with a simple equation derived from analysis of variance (ANOVA) of the FD points. Furthermore, this study provides useful data enabling the design of a breathable enclosure that allows the moisture and dusts to escape or let the electronics inside the enclosure to dry out on hot, sunny days or similar occasions. The effects of a heat producing electronic device inside the enclosure is also simulated numerically in a non-isothermal study. Moreover, the local climate inside the enclosure exposed to harsh cyclic ambient conditions is investigated.

The paper is divided into three sections: in Section 2, the model set-up as well as the mathematical model for the isothermal case are presented. This is followed by an explanation of the factorial design and the influential parameters used for the ANOVA. Then the model set-up and the numerical model for the non-isothermal case are introduced. All numerical modeling are conducted in the COMSOL Multiphysics™ version 5.1 software package. The results of the study are presented in Section 3, which come into parts as follows:

- Isothermal studies
  - 3D numerical simulation of transient moisture transfer into the enclosure.
  - Statistical analysis of the influential factors on the moisture diffusion time.
- Non-isothermal studies
  - Cyclic internal temperature changes.
  - Cyclic ambient temperature and relative humidity changes.

And finally the main findings are summarized in Section 4.

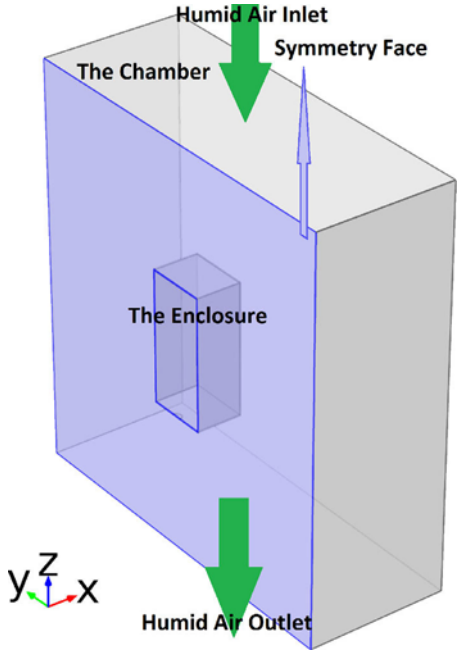

Fig. 1. A scheme of the geometry of the electronic enclosure located in the controlled chamber.

Table 1
Dimensions of the investigated geometries.

Enclosure	Inner dimensions (W × D × L) [mm]	188× 128 × 276
	Outer dimensions (W × D × L) [mm]	190× 130 × 280
Chamber	Inner dimensions (W × D× L) [mm]	600× 800 × 850
Opening	Diameter [mm]	2

2. Methods

2.1. Isothermal studies

A three-dimensional (3D) model is developed for investigating the moisture transfer into a typical electronic enclosure. The model consists of the conservation equations for mass and momentum. As the whole study is assumed to be isothermal, there is no need for solving the energy equations. The geometry which the model is developed for is shown in Fig. 1. As seen in Fig. 1, the case is assumed to be symmetric around the mid-plane. Table 1 summarizes the dimensions used in this study corresponding to the work carried out by Conseil et al. [18], which the isothermal moisture transfer into electronic enclosures is investigated experimentally.

In the climatic chamber, humid air enters from the top face and exits at the bottom face; so that a constant and consistent humidity is provided all over the chamber, which is the surrounding of the enclosure. Mass conservation equations are solved for both the surrounding and inside the enclosure; noting that the transfer mechanisms in the two domains are not exactly the same. Since there is no air flow inside the enclosure, moisture is transferred only by diffusion through the opening as well as the diffusion inside the enclosure itself. On the other hand for the surrounding, both convection and diffusion are responsible for the moisture transfer because of the air flow.

Eq. (2) describes species transport through diffusion and convection based on the following mass balance equation:

$$\frac{\partial c}{\partial t} + \mathbf{u} \cdot \nabla c = D \nabla \cdot (\nabla c), \tag{2}$$

where

- c is the concentration of the species [mole/m^3].
- D denotes the diffusion coefficient (assumed to be independent of c [m^2/s].
- $\mathbf{u}$ is the velocity vector [m/s].

The first term on the left-hand side corresponds to the accumulation of the species (moisture in this study). The second term accounts for the convective transport due to a velocity field u. On the right-hand side of the mass balance equation, the term describes the diffusion transport, accounting for interaction between the species and the medium. This equation

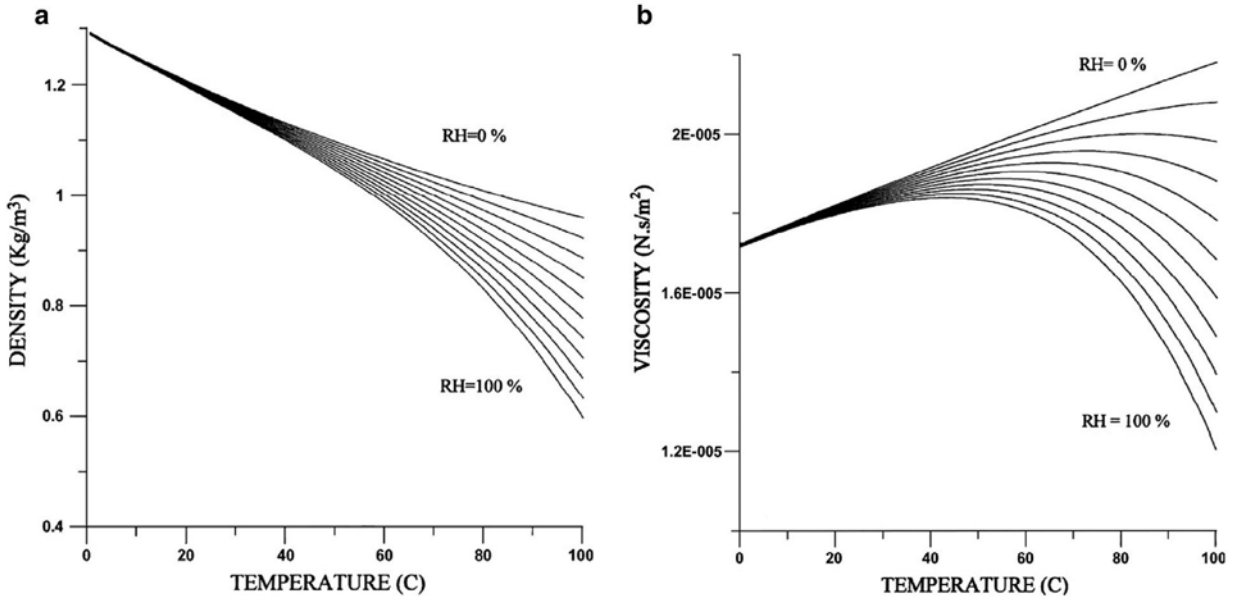

Fig. 2. (a) Density changes for humid air as a function of temperature at different RH values, and (b) Viscosity changes for humid air as a function of temperature at different RH values [23].

is fully solved for the climatic chamber where both mass diffusion and convection happens. However, for the region inside the enclosure the convective term is neglected, and Eq. (2) reduces to the following equation (Fick's second law):

$$\frac{\partial c}{\partial t} = D \cdot \nabla^2 c. \tag{3}$$

It should be noticed that the moisture diffusion coefficient into the air (D) is a function of temperature which can be obtained by the regression curve fit to data from Bolz and Tuve [19–22].

$$D = -2.775 \times 10^{-6} + (4.479 \times 10^{-8})T + (1.656 \times 10^{-10})T^2. \tag{4}$$

The velocity distribution in the climatic chamber is obtained by solving the momentum and the continuity equations. In this study, all the simulations were done under the isothermal (at 25 °C) assumption. It should be noticed that ρ and μ for humid air are a function of humidity (See Fig. 2a and b). According to Fig. 2a, at 25 °C the density changes versus humidity are negligible. Moreover at 25 °C, humidity changes, do not violate the assumption of constant viscosity, neither (see Fig. 2b).

For the constant ρ and μ, the momentum equation is similar to that used in Jabbari et al. [24]:

$$\rho \frac{\partial \mathbf{u}}{\partial t} + \rho(\mathbf{u} \cdot \nabla)\mathbf{u} = \nabla \cdot \left[-p\mathbf{I} + \mu\left(\nabla \mathbf{u} + \left(\nabla \mathbf{u}^{\top}\right)\right)\right] + \mathbf{F}. \tag{5}$$

Where

- ρ is the density [kg/m^3].
- p is pressure [Pa].
- μ is the viscosity [kg/(m^{2}s)].
- $\mathbf{I}$ is the unit tensor.
- $\mathbf{F}$ is the volume force vector [N].

Regarding the constant ρ assumption, the continuity equation reduces to [24]:

$$\nabla \cdot \mathbf{u} = 0. \tag{6}$$

The transient calculation starts from a point that the initial relative humidity is the same for both the chamber and the enclosure. Furthermore, the velocity is set to be zero at the $t = 0s$ for the whole domain. It is assumed that the humid air enters the chamber through the top face (see Fig. 1) with a constant velocity and a constant relative humidity. The pressure drop and gravity effects are neglected.

2.2. Factorial design

A two level full factorial design is applied on four parameters (2^4) based on the obtained CFD simulation results in order to check the significance of their influence on the diffusion time of moisture into the enclosure at constant ambient

Table 2
The studied ranges of the parameters in the factorial design.

Factor	Notification	Coded symbol	Low level	High level	Unit
Length of the opening (or tube)	L	A	2.00	50.00	[mm]
Radius of the opening	R	B	0.5	5.00	[mm]
Temperature	T	C	273.15	333.15	[K]
Initial RH	RH	D	40.00	80.00	[%]

temperature and relative humidity. In order to check for the presence of probable curvatures a center-point is also added to the design. Therefore, there are 17 cases to be investigated ($2^4 + 1 = 17$). These four parameters and their range of study are summarized in Table 2.

It should be noticed that in order to study the effect of the size of the opening, the length of the cylindrical shape opening is in the range of 2–50 mm (see Table 2); as the thickness of the wall is 2 mm, higher values of the length describe the case of a tube connected to the enclosure at the opening position.

2.3. Non-isothermal studies

For the non-isothermal case, the PC box is exposed to cyclic climatic conditions. The momentum, continuity and energy equations are fully coupled in order to obtain the velocity field and the temperature distribution. These values are used in the mass balance equation (Eq. (2)) to calculate the concentrations. It should be noted that in the non-isothermal studies, the density changes are regarded in the momentum and continuity equations Eqs. (7) and (8)). Volume forces caused by density changes with temperature are also considered. Thus, the term **F** in the momentum equation (Eq. (7)) is defined as below [25]:

$$\rho\frac{\partial \mathbf{u}}{\partial t} + \rho(\mathbf{u}\cdot\nabla)\mathbf{u} = \nabla\cdot\left[-p\mathbf{I} + \mu\left(\nabla\mathbf{u} + \left(\nabla\mathbf{u}^{\top}\right)\right) - \frac{2}{3}\mu(\nabla\cdot\mathbf{u})\mathbf{I}\right] + \mathbf{F}, \tag{7}$$

$$\frac{\partial \rho}{\partial t} + \nabla\cdot(\rho\mathbf{u}) = 0, \tag{8}$$

$$F_x = F_y = 0;\ \ F_z = -\rho\times g_z. \tag{9}$$

The value of the diffusion coefficient of moisture into air is updated with temperature using Eq. (4), and the temperature field is solved using

$$\rho C_p\frac{\partial T}{\partial t} + \rho C_p\mathbf{u}\cdot\nabla T = \nabla\cdot(k\nabla T) + \mathbf{Q}. \tag{10}$$

Having the temperature and moisture concentration, RH is estimated all over the enclosure using Eqs. (11), (12) and (13) [26].

$$p_{sat} = 6140.7\times 10^{\frac{7.5\times(T-273.15)}{T-35.85}}, \tag{11}$$

$$c_{sat} = \frac{p_{sat}}{R_{const}\times T}, \tag{12}$$

$$RH = \frac{c\times 100}{c_{sat}}. \tag{13}$$

Fig. 3 shows the geometry of the PC box and the investigated points inside.

3. Results and discussion

3.1. Isothermal studies

3.1.1. 3D numerical simulation of transient moisture transfer into the enclosure

Fig. 4 displays the average moisture concentration in the enclosure vs. time in the case that the humid air enters the climatic chamber with the velocity and relative humidity of 0.02 m/s and 98%, respectively. Besides that, the estimated curve by the RC approach developed by Tencer [7] for the same conditions is displayed. The initial relative humidity was 40% at 25 °C. As it is shown in Fig. 4, it takes about 20 days for the air inside the enclosure to reach the ambient RH of 98%. However, after about 7 days the RH is more than 90%. Not surprisingly, as the mass transfer driving force (the concentration difference between the climatic chamber and the enclosure within the chamber) decreases with time, the moisture transfer rate also decreases. The time constant in the RC approach and the mean moisture concentration inside the enclosure is

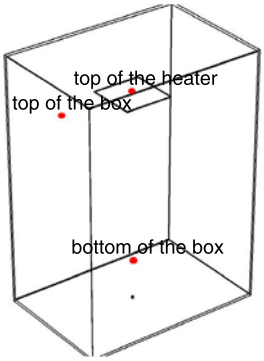

Fig. 3. The geometry of the PC enclosure and positions of the investigated points in the non-isothermal studies.

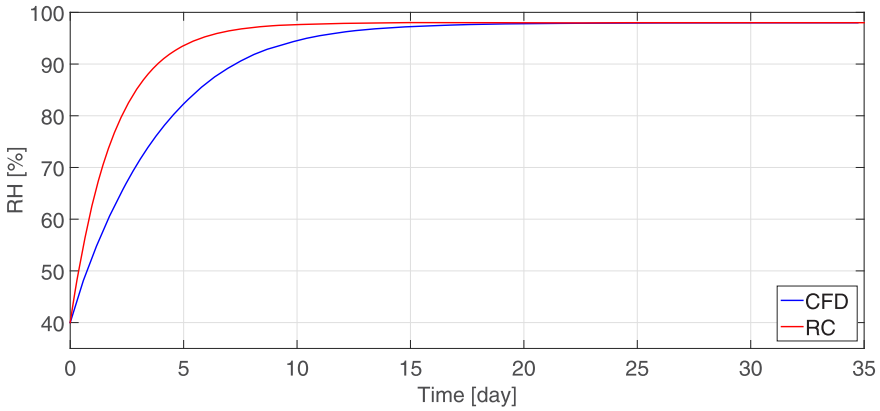

Fig. 4. The average moisture content in the enclosure (RH [%] vs. time [day]).

calculated using Eqs. (14) and (15), respectively [7].

$$\tau = \frac{V \times L}{A \times D}. \tag{14}$$

- V is the volume of the enclosure [m^3].
- L is the length of the opening [m].
- A is the surface area of the opening [m^2].
- D denotes the diffusion coefficient [m^2/s].

$$c = c_{ambient} - (c_{ambient} - c_{initial})exp\left(\frac{-t}{\tau}\right). \tag{15}$$

The RC approach generally shows the same behavior as the CFD simulation; however, the pace of the RH increase is faster in the RC method (the time constants for the RC and the CFD in this case is 1.95 and 3.87 days, respectively). There are some simplifying assumptions in the RC method that can explain this deviation. In the RC approach, the resistance against the mass transfer inside the volume of the enclosure is completely neglected; in other words, the concentration is assumed to be homogeneous all over the volume inside the enclosure over time. Fig. 5 depicts the concentration profile at the centreline, in the symmetry face of the enclosure. According to this figure, there is a concentration gradient inside the enclosure which does not seem to be negligible, especially at the initial days. The concentration gradient decreases over time, though. This gradient reveals the presence of the resistance inside the volume; which delays the mass transfer into the enclosure; although it is less significant compared to the delay that the opening causes.

Furthermore, the RC approach only considers the size of the volume not the geometrical shape or other details such as the position of the opening; on the other hand, in the 3D CFD simulations all the details of the enclosure are taken into account. Fig. 6 demonstrates the effect of the position of the opening in the enclosure, comparing three different cases. In position 1, the opening is located in the center of the bottom face of the enclosure (standard case); in position 2 it is located at the corner of the bottom face, and finally in position 3 it is located in the center of a side face (see sub-Fig. 6). According to the simulation results presented in Fig. 6, the RH inside the enclosure follows the same trend for the positions 1 and 3 (time constant = 3.8 days). Nevertheless, for position 2 the trend is slightly different; in this case, the moisture passes longer distance to reach the corners of the enclosure (time constant = 4.6 days).

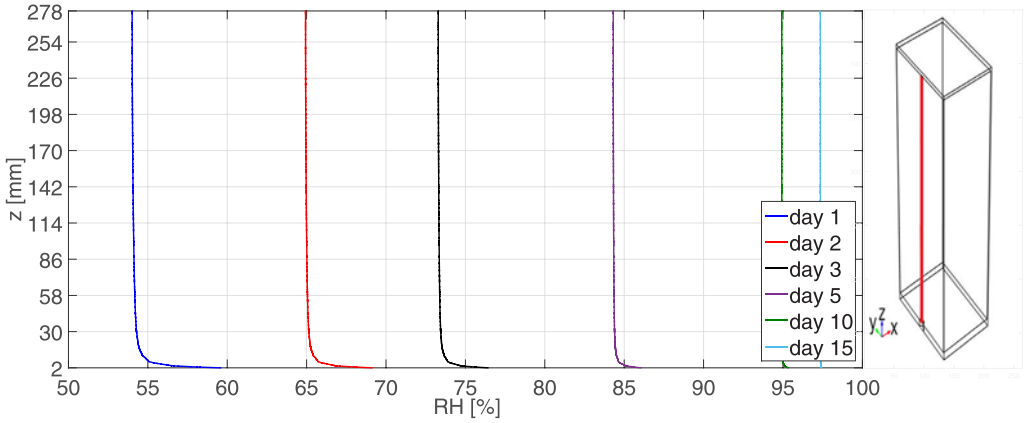

Fig. 5. The concentration profile at the center of the symmetry face at different times.

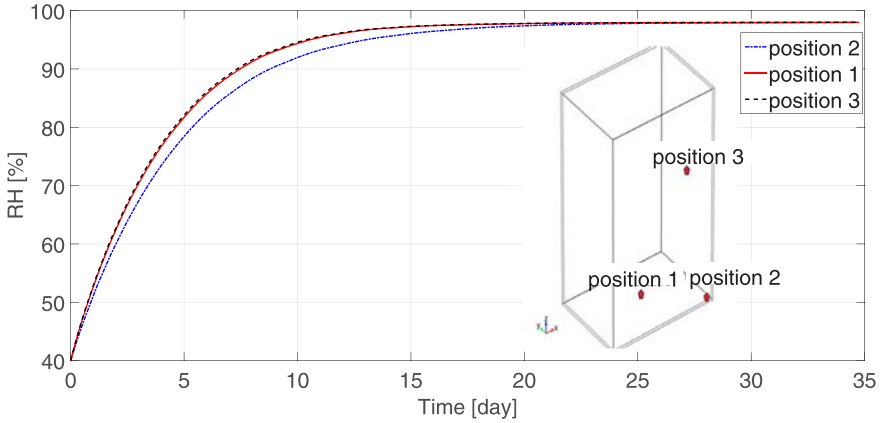

Fig. 6. The average RH inside the enclosure for different positions of the opening at 25 °C. The sub-figure shows the position of the opening in the three investigated cases.

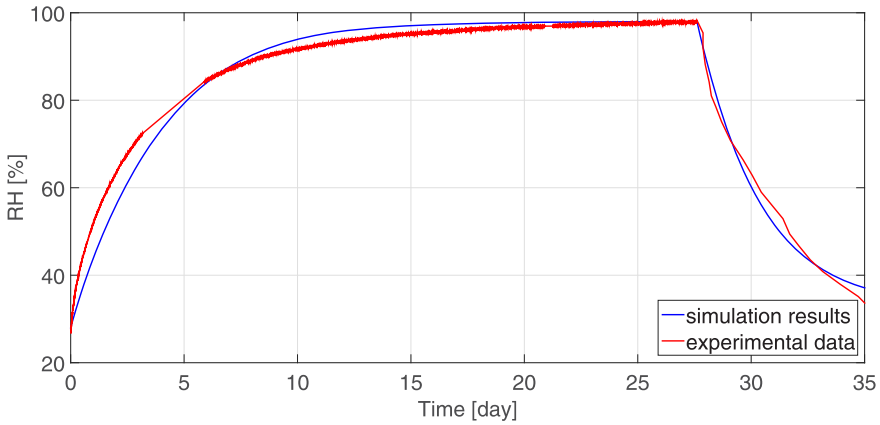

Fig. 7. Comparison between the CFD simulation result (position 1) and the experimental data from Conseil et al. [18].

The CFD model is validated by comparing the simulation results with experimental data from the study carried out by Conseil et al. [18]; in which a climatic chamber was used to set specific predefined values for the ambient temperature and RH in the surrounding of the enclosure. First, the enclosure was exposed to the temperature of 25 °C and RH of 98%; then, the ambient condition was set to a RH of 33%. The temperature was kept at 25 °C. The initial RH in the enclosure was 28%. According to Fig. 7, the CFD simulation results are in a good agreement with the experimental data, visually. The time constants derived from the experimental data and the simulations for the 3.13 and 3.82 days are moisture ingress part,

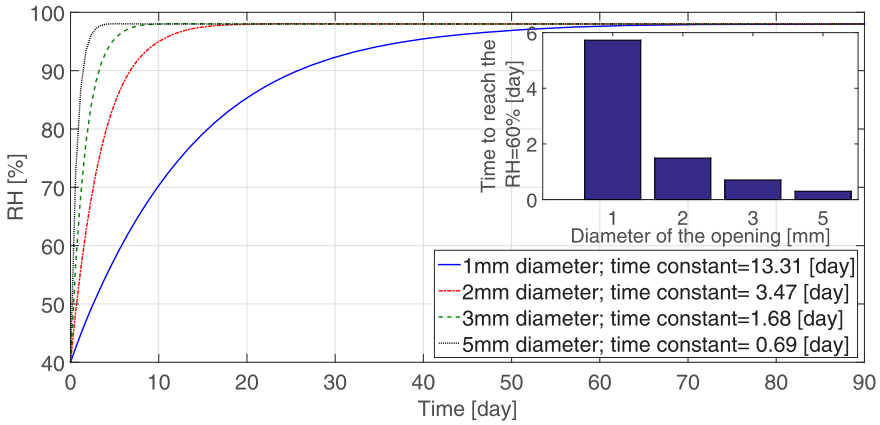

Fig. 8. The effect of the opening radius size at 25 °C (The sub-figure shows the estimated diffusion time to reach RH = 60% for the different opening sizes.).

Table 3
Resistance values against the mass transfer.

		$R_{opening}[s/m^3]$		$R_{enclosure}[s/m^3]$
$R = 0.5$[mm]	$R = 1$[mm]	$R = 1.5$[mm]	$R = 2.5$[mm]	
1.0186×10^8	2.5465×10^7	1.1318×10^7	4.0744×10^6	4.5878×10^5

Table 4
The factorial design table for the factors and the responses.

Case #	A [mm]	B [mm]	C [K]	D [%]	Response (diffusion time) [s]
1	2.00	0.50	273.15	40.00	8,500,000
2	50.00	0.50	273.15	40.00	208,000,000
3	2.00	5.00	273.15	40.00	143,000
4	50.00	5.00	273.15	40.00	1,474,000
5	2.00	0.50	333.15	40.00	6,210,000
6	50.00	0.50	333.15	40.00	149,450,000
7	2.00	5.00	333.15	40.00	464,000
8	50.00	5.00	333.15	40.00	1,544,000
9	2.00	0.50	273.15	80.00	4,892,000
10	50.00	0.50	273.15	80.00	166,460,000
11	2.00	5.00	273.15	80.00	108,000
12	50.00	5.00	273.15	80.00	1,095,000
13	2.00	0.50	333.15	80.00	3,815,000
14	50.00	0.50	333.15	80.00	28,500,000
15	2.00	5.00	333.15	80.00	72,000
16	50.00	5.00	333.15	80.00	880,000
17	26.00	2.75	303.15	60.00	18,318,000

respectively. The values are 30.8 and 30.2 days for the second part of the graph, respectively, where the RH is decreasing inside the enclosure.

As the opening seems to be the significant resistance against the mass transfer, the moisture transfer into the enclosure with different opening sizes is compared (see Fig. 8). It is important to maintain a RH below the threshold value of 60%; the damaging level could be when the RH inside the enclosure exceeds this critical level (in the range of 60–90% depending on the electronics design and cleanliness) [3,9,27]. According to Fig. 8, it takes about four times longer for the enclosure with the 1 mm diameter opening to reach the critical values of 60% relative compared to the one with the 2 mm diameter opening. On the other hand, for the enclosure with the 3 mm diameter opening it is about 9 times faster. This demonstrates the non-linear nature of the diffusion time as a function of the opening si ze (Table 3).

3.2. Analysis of variance

3.2.1. Model fitting and statistical analysis

Table 4 shows the factorial design matrix and the CFD simulation results (moisture diffusion time into the enclosure) for each of the 17 cases. It should be noticed that regarding the distribution of the results, a data transformation is recommended based on the Box–Cox method. Constancy of the error variance and normality of distribution are two essential

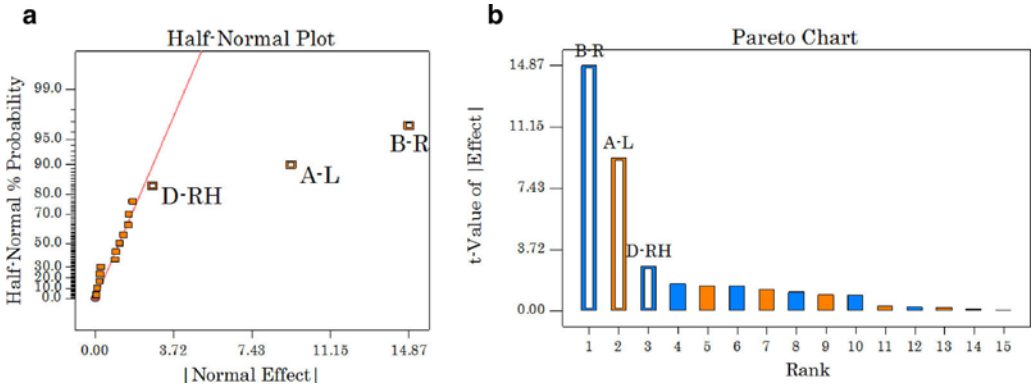

Fig. 9. (a) Half normal probability plot of the effects, and (b) the Pareto chart.

Table 5
The factorial design table for the factors and the responses.

Source	Sum of squares	Degree of freedom	Mean square	*F* Value	*p*-value (Prob > *F*)	
Model	17.70	3	5.90	104.85	> 0.0001	Significant
A	4.84	1	4.84	86.09	> 0.0001	Significant
B	12.44	1	12.44	221.11	> 0.0001	Significant
D	0.41	1	0.41	7.35	0.0189	Significant
Curvature	0.53	1	0.53	9.39	0.0098	Significant
Residual	0.68	12	0.056			
Total	18.90	16				

assumptions in the ANOVA [28]. Based on the Box–Cox method, if a logarithmical transformation is applied on CFD simulation results of the 17 cases, the two assumptions are more satisfied.

The half-normal probability plot of the effects is displayed in the Fig. 9a, together with the rank of the effects by the Pareto chart in Fig. 9b. According to the half-normal probability plot, radius and length of the opening as well as the initial relative humidity are the significant factors affecting the moisture transfer time into the enclosure. The rank of their significance is as below:

$$B > A \gg D. \tag{16}$$

Thus, a regression model consisting of the significant factors is proposed:

$$\begin{aligned}\log(\text{Response}[s]) &= 7.52153 \\ &+ 0.022926 \times L[\text{mm}] \\ &- 0.39190 \times R[\text{mm}] \\ &- 8.03837 \times 10^{-3} \times \text{RH}[\%].\end{aligned} \tag{17}$$

The statistical ANOVA of the results obtained with a confidence level of 95% (*p*-value equals to 0.05) is summarized in Table 5. The *p*-values provide a cut-off beyond which assert that the findings are statistically significant [17].

According to the Table 5, the *F*-test yields a very low probability value (*P*-value < 0.0001) which indicates that the model is highly significant; however, the curvature is significant, too. Thus, the regression model is not suitable enough for predicting the center-point and consequently other internal points of the investigated space. In fact, it can only predict the factorial points successfully. It is worth to mention that, this regression model can be used to find the critical parts of the design space for further investigations and it is the initial step for finding an accurate model that can describe the behavior of the response in the whole space.

3.2.2. Model adequacy checking

The coefficient of determination (R^2) measures the proportion of total variability explained by the model. For an acceptable fit model, R^2 should be higher than 0.80 [29]; hence, the closer R^2 is to unit, the better. The R^2 always gets closer to 1 as more terms are added to the regression model; thus, it is recommended to use an adjusted-R^2 to evaluate the model adequacy since it is adjusted for the number of terms in the model. For a well fitted regression model, the adjusted-R^2 should be higher than 0.90 [14,29]. In this work, the R^2 and adjusted-R^2 for the regression model are 0.9363 and 0.9216, respectively. These numbers indicate that the model Eq. (17) describes the process well.

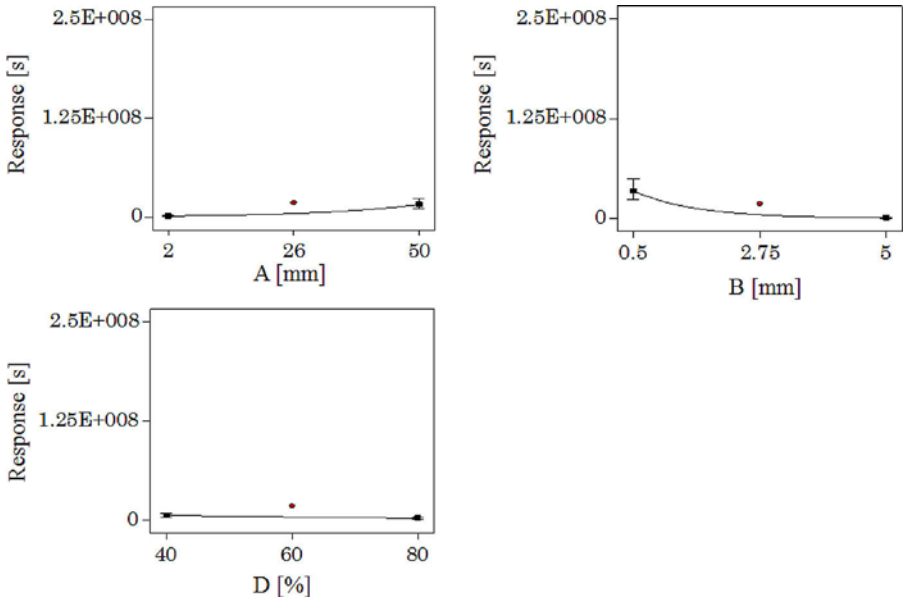

Fig. 10. The main effect plots.

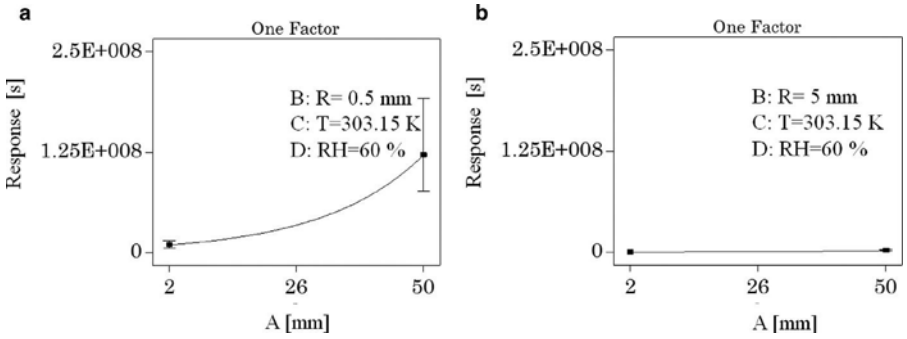

Fig. 11. The effect of the length of the opening at (a) the low and (b) high level of the radius.

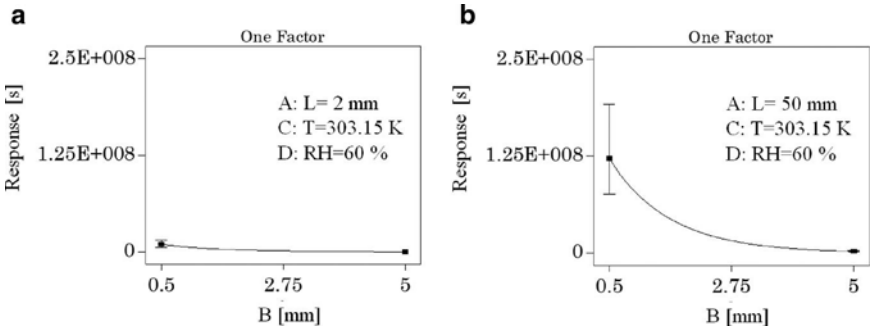

Fig. 12. The effect of the radius of the opening at (a) the low and (b) high level of the length.

3.2.3. Main and interaction effects

The effects of the main factors on the response are shown in Fig. 10. As seen from Fig. 10, the length of the opening has a positive effect; however, the radius of the opening and the relative humidity affects the response negatively. Considering the diffusion resistance of the opening against the mass transfer rate, the resistance and consequently the moisture diffusion time increases as the length of the opening increases or the radius decreases, which is in agreement with the results from the RC approach [7] .

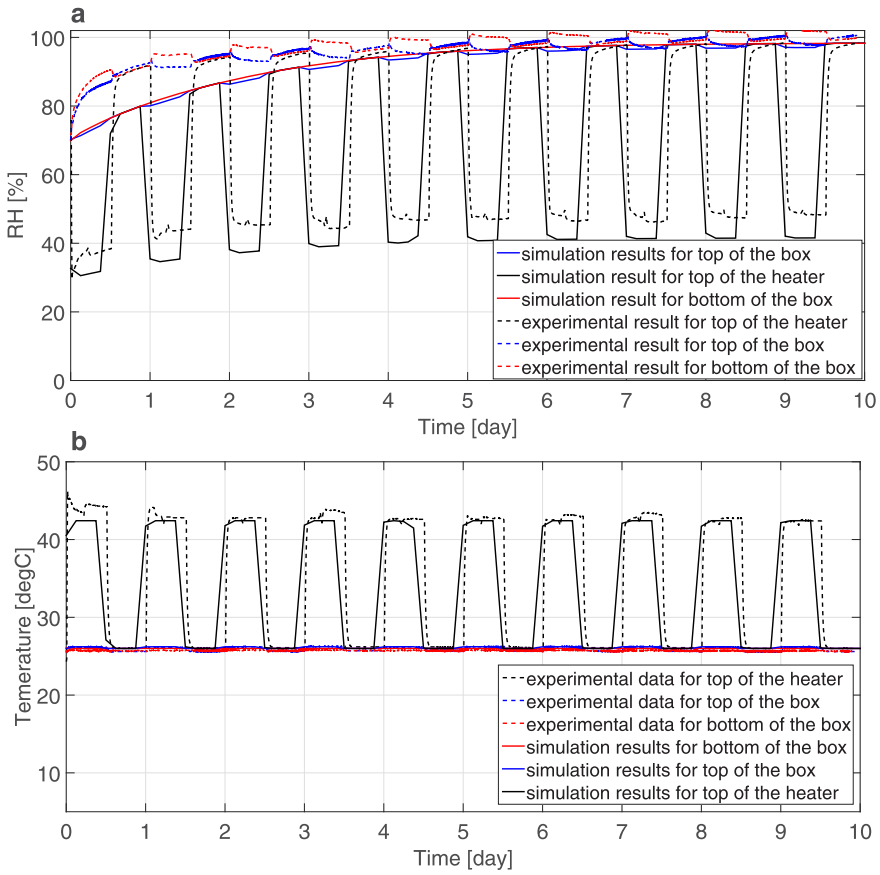

Fig. 13. (a) The the local climate, RH, and (b) temperature inside the enclosure for case (i).

The significance of these effects is shown in Figs. 11 and 12. In case that radius is 5 mm (Fig. 11b), the length changes do not influence the response seriously; on the other hand, in case that radius is only 0.5 mm, the length of the opening plays a key role (see Fig. 11a). Similarly, when the length is 2 mm (Fig. 12a), the response changes are not that significant; however, in the case of 50 mm length, the response changes are noticeable (see Fig. 12b).

3.3. Non-isothermal studies

3.3.1. Cyclic internal temperature changes

A heating plate with the size of 50 mm × 50 mm × 1 mm is considered at the top of the enclosure, in the center. The plate is switched on and heats up to 42.5 °C for 12 h and then is switched off for another 12 h so that its temperature reaches and stays at 26 °C. This cycle is repeated for more than eight days. The local climate inside the enclosure is studied in two cases:

(i) Exposure to an ambient temperature and RH of 25 °C and 98%, respectively.
(ii) Exposure to an ambient temperature and RH of 25 °C and 40%, respectively.

In case (i), the initial RH and temperature are 70% and 25 °C and in case (ii) these values are 100% and 25 °C, respectively. It should be noted that all the operation conditions are based on the experimental study conducted by Conseil et al. [18]. Fig. 13 shows the simulation results and compares them with the experimental data for case (i). The simulation results just as the experimental data show a gradual increase of RH inside the enclosure; however, the trend is slower in the simulations for the first couple of days. After about 4 days, the simulation results and the experimental measurements get much closer, visually.

The point at the top of the heater, experiences large RH changes consistent with the temperature changes. On the other hand, the two other investigated points do not see severe RH changes with the 12 h on/off scenario. This is due to the buoyancy effect that drives the natural convection inside the enclosure. As the warm air tends to stay at the top (because of lower density) and cold air at the bottom; the heat is not much distributed in the enclosure. Fig. 13b displays the small changes of temperature over the on/off cycles for these points; however, the point on top of the enclosure is just

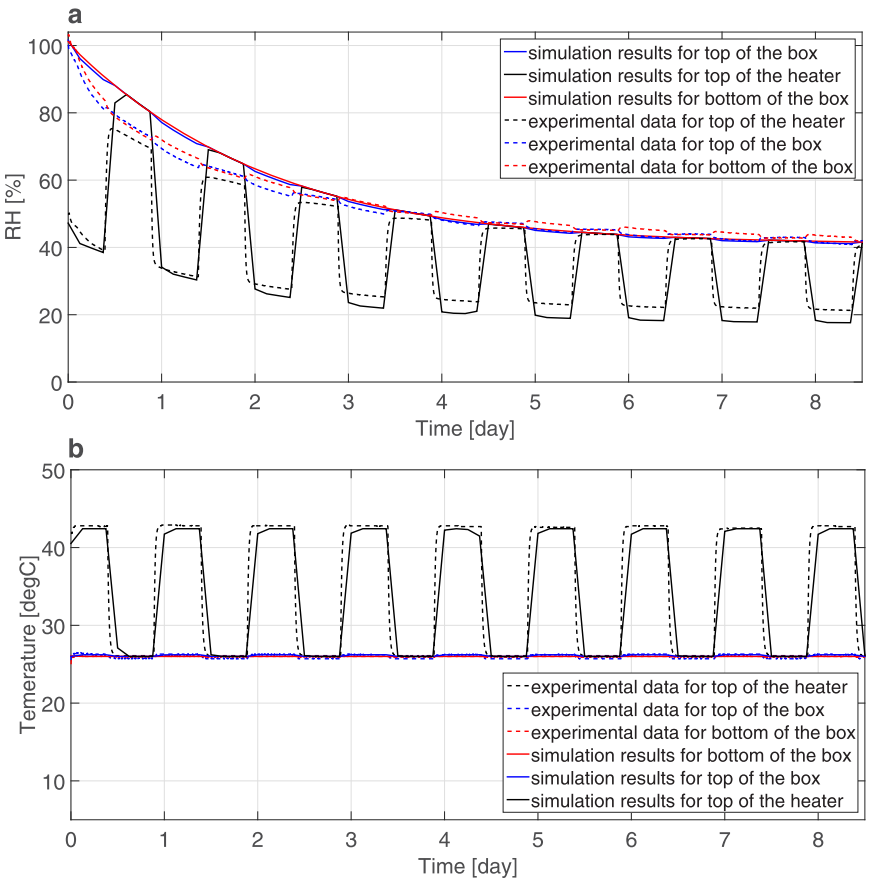

Fig. 14. (a) The the local climate, RH, and (b) temperature inside the enclosure for case (ii).

following the cycles. It should be noted that in the experimental measurements, some deviations from the higher set point value (42.5 °C) are observed; especially at the beginnings, where even values of about 46 have been recorded. In the CFD simulations these deviations have not been regarded and it is considered that the high and low temperature is exactly 42.5 and 26 °C every 12 h, respectively.

Generally, the RH changes are more affected by temperature rather than the moisture concentration. As presented previously in the isothermal section, even in the case that the mass transfer is just driven by diffusion, there is not a big diversity in the distribution of moisture concentration inside the enclosure. In the non-isothermal cases there are some air movements driven by the volumetric forces that increase the rate of mass transfer. It is seen that when the heater is on, the RH at the top of the heater is at least 40% lower than the two other points during the 10 days.

Fig. 14 shows the local climate inside the enclosure for case (ii). Gradually the RH inside the enclosure decreases from 100% to the ambient value (40%). This takes about 8 days and a half. The same as in case (i), in the initial days, the predicted mass transfer rate by the CFD simulations is lower than what the experimental measurements show. However, after three days the estimated and the measured values get much closer. The lower-estimation of the mass transfer rate could be due to the fact that in the non-isothermal studies the air flow outside the enclosure is not considered in the CFD simulations—the air flow might help the moisture ingress through the 2 mm diameter hole.

3.3.2. Cyclic ambient temperature and RH changes

In this part, the enclosure is exposed to cyclic conditions defined in the STANAG (standard agreement) 2895, category of B2; which specifies the temperature, RH and solar radiation for 24 h [30]. Category B2 applies to those areas which experience moderately high temperatures accompanied by high humidity [30]. Fig. 15a–c show the STANAG-B2 conditions as well as the estimated temperature and RH inside the enclosure.

According to Fig. 15c, the estimated temperature inside the enclosure follows the same trend as the experiments. It should be noted that the experimental measurements show values of higher than 35 °C. However, according to the STANAG 2895, category of B2, the highest ambient temperature is 35 °C, and thus the temperature inside the enclosure should always be lower than this value. Seen from Fig. 15b the RH inside the enclosure is lower estimated by the CFD simulations compared to the experimental data; however, it still shows the same trend. As the temperature prediction is not far away

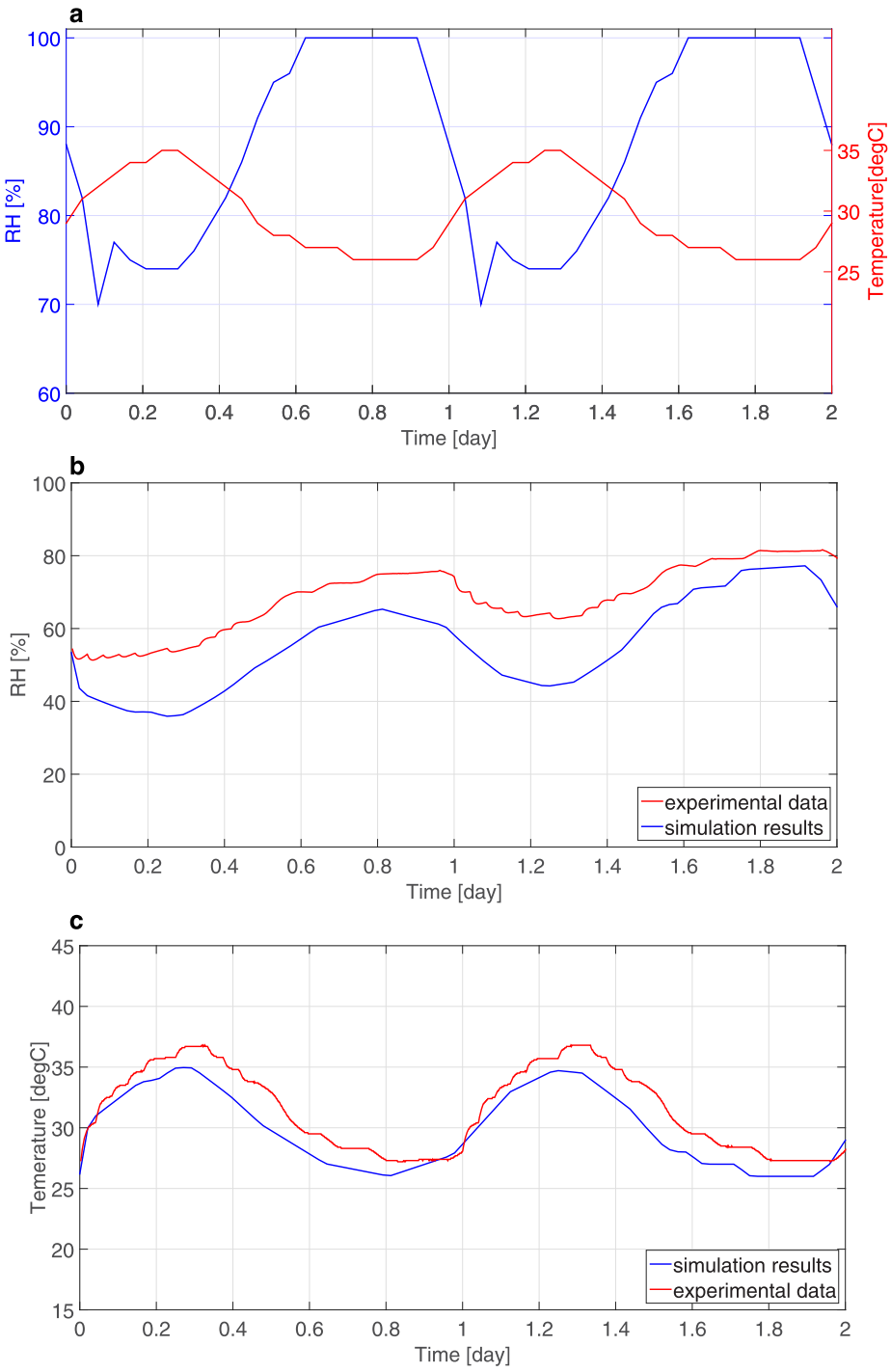

Fig. 15. The local climate inside the PC enclosure exposed to the STANAG 2895, catefory of B2 conditions.

from the measured values; the gap in the RH comparison is most probably due mass transfer calculations. As previously explained, this could be due to disregarding the air flow outside the enclosure in the CFD simulations. Furthermore, moisture uptake by the PC might influence the local climate in the first couple of cycles, Based on the initial moisture concentration in the PC walls of the enclosure, after few cycles it will also get consistent with the cyclic changes.

The maximum ambient temperature seen in the STANAG 2895 is 35 °C which happens after 7 h (0.3[day]) for the first time. According to the CFD results this value is recorded inside the enclosure also after 7 h (0.3[day]). In fact, at the experiments the maximum temperature happens at this time, first. This observation demonstrate the fast rate of heat transfer

into the PC enclosure. In other words, the temperature inside the enclosure responds to the ambient temperature changes relatively fast (compared to RH). For the RH, despite the fact that the ambient value is at 100% for 8 days, the inner RH for the PC enclosure does not reach higher values than 67 and 76% at the first day, according to the CFD simulations and the experimental data, respectively. This is due to the fact that heat is transferred through the outer walls and also the small opening; on the other hand, moisture can only get into the enclosure through the small opening.

4. Conclusions

A 3D CFD model is developed for investigating the moisture transfer into a typical electronic enclosure both for isothermal and non-isothermal conditions. The numerical simulation results for both conditions are compared with corresponding experimental results from the literature, and a good agreement is found.

The results from the isothermal condition are also compared with the well-known RC circuit modeling, which shows that the RC method under-estimates the time constant for the moisture ingress into the enclosure. The verified model in the isothermal condition is then used for further investigation of influential parameters and statistical ANOVA. The results show that for a typical electronic enclosure, the position of the opening does not make a huge change in the moisture diffusion time into the enclosure. It is, moreover, found that there is a non-linear relationship between the radius of the opening and the diffusion time. Based on the ANOVA, it is concluded that a linear regression model is not suitable enough for predicting all the points in the design space; in fact, the proposed regression model can estimate the response only at the factorial points. However, it should be highlighted that the 2^k design is particularly useful at the initial steps of a study, as it provides the smallest number of runs with which k factors can be studied in a complete factorial design.It should be emphasized that the findings from the ANOVA match well with what that could have been found from a corresponding RC analysis. However, the present CFD analysis is of much more general nature and can be used on any case of geometrical complexity. Moreover, based on the results of this analysis, the critical parts of the design space for more investigations are recognized.

According to the non-isothermal studies, the heater only affects the temperature locally and areas away from the heater do not experience severe changes. As the heater is located on the top, it does not cause a sensible air flow so that the heat can be transferred to all parts of the enclosure. It is interesting to compare this case to the case where the heater is located at the bottom of the enclosure where volumetric forces are stronger. In case of the exposure to the cyclic ambient RH and temperature changes, the PC enclosure responds faster to the temperature changes compared to the RH changes. The trends predicted by the CFD simulations can be used to decide on when and where to put some adsorbent and/or heat mass inside the enclosure to control the local climate.

The effect of the presence of some commercial adsorbent inside the enclosure and the delay time caused by them are interesting issues to be studied in future work. Furthermore, the buffer effect of the enclosure material as well as the electronics might also be an attractive matter to be interesting to investigate in the future.

Acknowledgment

The current research has been conducted as part of the ICCI project from the Danish council for Independent Research, Technology and Production (FTP) and the IN SPE project from the Danish Innovations Fonden which are highly acknowledged. Moreover, the authors would like to acknowledge the commitment and help of the industrial partners in this project.

References

[1] E. Parsa, H. Huang, A. Dasgupta, Multi-physics simulations for combined temperature/humidity loading of potted electronic assemblies, Microelectron. Reliab. 54 (2014) 1182–1191.
[2] V. Mei, X. Yao, A numerical method on thermal-humidity behavior of electronic packaging, in: Proceedings of the ICEPT-HDP-2011, IEEE, Shanghai, China, 2011, pp. 1044–1048.
[3] J.B. Jacobsen, J.P. Krog, A.H. Holm, L.Rimestad, A. Riis, Climate-protective packaging: using basic physics to solve climatic challenges for electronics in demanding applications, IEEE Ind. Electron. Mag. (2014) 51–59.
[4] M.R. Keenan, Moisture Control in Sealed Electronic Packages, Technical Report, Sandia National Laboratories, 1990.
[5] T. Ferguson, J. Qu, Moisture absorption analysis of interfacial fracture test specimens composed of no-flow underfill materials, ASME. J. Electron. Packag. 125 (2003) 24–30.
[6] N. Dahan, A. Vanhoestenberghe, N. Donaldson, Moisture ingress into packages with walls of varying thickness and/or properties: a simple calculation method, IEEE Transactions on components, packaging and manufacturing technology, 2 (11) (2012) 1796–1801.
[7] M. Tencer, Moisture ingress into nonhermetic enclosures and packages: a quasi-steady state model for diffusion and attenuation of ambient humidity variations, in: Proceedings of the 44th Electronic Components and Technology Conference, 1994, pp. 196–209.
[8] J. Punch, R. Grimes, G. Heaslip, T. Galkin, K. Vakevainen, V. Kyyhkynen, E. Elonen, Transient hygrothermal behaviour of portable electronics, in: Proceedings of the 6th International Conference on Thermal, Mechanical and Multi-Physics Simulation and Experiments in Micro-Electronics and Micro-Systems, 2005. EuroSimE 2005, 2005, pp. 398–405.
[9] M. Tencer, J. Moss, Humidity management of outdoor electronic equipment: methods, pitfalls, and recommendations, EEE Trans. Compon. Packag. Technol. 25 (1) (2002) 66–72.
[10] M.V. Belleghem, H.J. Steeman, M.S.A. Janssens, M.D. Paepe, Sensitivity analysis of CFD coupled non-isothermal heat and moisture modelling, Build. Environ. 45 (2010) 2485–2496.
[11] M. Delele, A. Schenk, E. Tijskens, H. Ramon, B. Nicola, P. Verboven, Sensitivity analysis of CFD coupled non-isothermal heat and moisture modelling, J. Food Eng. 91 (2009) 228–239.
[12] S.J. Cheng, J.M. Miao, S.J. Wu, Investigating the effects of operational factors on PEMFC performance based on CFD simulations using a three-level full-factorial design, Renew. Energ. 39 (2012) 250–260.

[13] T. Katsaounis, M. Aggarwal, Two-level screening designs derived from binary nonlinear codes, J. Korean Stat. Soc. 45 (2015) 210–220, doi:10.1016/j.jkss.2015.10.001.
[14] D. Montgomery, Design and Analysis of Experiments, John Wiley & Sons, Inc., Hoboken, 2013.
[15] Y. Yang, Y. Wang, P. Tseng, Numerical optimization of heat transfer enhancement in a wavy channel using nanofluids, Int. J. Heat Mass Transf. 51 (2014) 9–17.
[16] N.H. Wong, S. Heryanto, The study of active stack effect to enhance natural ventilation using wind tunnel and computational fluid dynamics (CFD) simulations, Energy Build. 36 (2004) 668–678.
[17] W. Rukthong, W. Weerapakkaroon, U. Wongsiriwan, P. Piumsomboon, B. Chalermsinsuwan, Integration of computational fluid dynamics simulation and statistical factorial experimental design of thick-wall crude oil pipeline with heat loss, Adv. Eng. Softw. 86 (2015) 49–54.
[18] H. Conseil, M.S. Jellesen, R. Ambat, Experimental study of water absorption of electronic components and internal local temperature and humidity into electronic enclosure, in: Proceedings of the 2014 IEEE 16th Electronics Packaging Technology Conference (EPTC), 2014.
[19] A. Fabbr, C. Cevoli, 2D water transfer finite elements model of salami drying, based on real slice image and simplified geometry, J. Food Eng. 158 (2015) 73–79.
[20] M. Bakhshi, B. Mobasher, C. Soranakom, Moisture loss characteristics of cement-based materials under early-age drying and shrinkage conditions, Constr. Build. Mater. 30 (2012) 413–425.
[21] P. Eliaers, J. Pati, S. Dutta, J.D. Wilde, Modeling and simulation of biomass drying in vortex chambers, Chem. Eng. Sci. 123 (2015) 648–664.
[22] J. Songok, P.S.M. Toivakka, Temperature effects on dynamic water absorption into paper, J. Colloid Interface Sci. 418 (2014) 373–377.
[23] P. Tsilingiris, Thermophysical and transport properties of humid air at temperature range between 0 and 100 °C, Energ. Convers. Manag. 49 (2008) 1098–1110.
[24] M. Jabbari, R. Bulatova, J. Hattel, C. Bahl, An evaluation of interface capturing methods in a VOF based model for multiphase flow of a non-Newtonian ceramic in tape casting, Appl. Math. Model. 38 (13) (2014) 3222–3232.
[25] P.S. Nasirabadi, M. Jabbari, J.H. Hattel, Numerical simulation of transient moisture and temperature distribution in polycarbonate and aluminum electronic enclosures, in: Proceedings of the 2016 17th International Conference on Thermal, Mechanical and Multi-Physics Simulation and Experiments in Microelectronics and Microsystems (EuroSimE), 2016, pp. 1–6.
[26] COMSOL 5.1 User Guide, 2015.
[27] R. Ciprian, B. Lehman, Modeling effects of relative humidity, moisture, and extreme environmental conditions on power electronic performance, in: Proceedings of the Energy conversion congress and exposition, 2009, pp. 20–24.
[28] G.E.P. Box, D.R. Cox, An analysis of transformations, J. R. Stat. Soc. Series B Stat. Methodol. 26 (1964) 211–252.
[29] S.M.S. Shahabadi, A. Reyhani, Optimization of operating conditions in ultrafiltration process for produced water treatment via the full factorial design methodology, Sep. Purif. Technol. 132 (2014) 50–61.
[30] The climatic and environmental conditions. URL http://standards.globalspec.com/standards, 1986, (accessed 15.07.16).

Appendix B
Paper II (submitted to the Microelectronics Reliability journal)

Elsevier Editorial System(tm) for Microelectronics Reliability

Manuscript Draft

Manuscript Number:

Title: A 3D Numerical study of humidity evolution and condensation risk on a Printed Circuit Board (PCB) exposed to harsh ambient conditions

Article Type: Research Paper

Keywords: Multiphysics; CFD; Local climate; Electronics enclosure; Condensation risk; Humidity management

Corresponding Author: Ms. Parizad Shojaee Nasirabadi, M. Sc.

Corresponding Author's Institution: Danmarks Tekniske Universitet

First Author: Parizad Shojaee Nasirabadi, M. Sc.

Order of Authors: Parizad Shojaee Nasirabadi, M. Sc.; Jesper H Hattel, Professor

Abstract: In many applications, electronics enclosures are exposed to harsh environmental conditions. For a reliable design, it is crucially important to understand the effects of such conditions on the local climate inside the enclosures. In this study, the relative humidity (RH) and temperature inside an electronics enclosure exposed to harsh ambient conditions (relative humidity of 100% and cyclic temperature changes from 10 to 50 [°C]) are studied by developing a full 3D finite element based CFD model. The RH evolution is studied in three stages: first, in an empty enclosure, then in an enclosure with a PCB, heatsink and a heater, and finally in the case of an internal cyclic heat load. In all three parts, the effect of the opening size of the enclosure is also studied. The numerical simulation results are compared with corresponding experimental results from the literature, and a good agreement is found. The presence of components inside the enclosure damps the response of the internal climate to the ambient changes and this is especially the case for the aluminum heatsink. In case of exposure to RH of 100 [%], controlling the moisture concentration appears to be more effective than controlling temperature with the aim of reducing the condensation risk on the PCB.

A 3D Numerical study of humidity evolution and condensation risk on a Printed Circuit Board (PCB) exposed to harsh ambient conditions

Parizad Shojaee Nasirabadi[1, 2], Jesper Henri Hattel[1]
[1]Process Modelling Group, Department of Mechanical Engineering, Technical University of Denmark, Nils Koppels Allé, 2800 Kgs. Lyngby, Denmark
[2] The George W. Woodruff School of Mechanical Engineering, Georgia Institute of Technology, Atlanta, GA 30332, USA

ABSTRACT

In many applications, electronics enclosures are exposed to harsh environmental conditions. For a reliable design, it is crucially important to understand the effects of such conditions on the local climate inside the enclosures. In this study, the relative humidity (RH) and temperature inside an electronics enclosure exposed to harsh ambient conditions (relative humidity of 100% and cyclic temperature changes from 10 to 50 [°C]) are studied by developing a full 3D finite element based CFD model. The RH evolution is studied in three stages: first, in an empty enclosure, then in an enclosure with a PCB, heatsink and a heater, and finally in the case of an internal cyclic heat load. In all three parts, the effect of the opening size of the enclosure is also studied. The numerical simulation results are compared with corresponding experimental results from the literature, and a good agreement is found.

The presence of components inside the enclosure damps the response of the internal climate to the ambient changes and this is especially the case for the aluminum heatsink. In case of exposure to RH of 100 [%], controlling the moisture concentration appears to be more effective than controlling temperature with the aim of reducing the condensation risk on the PCB.

KEY WORDS: Multiphysics; CFD; Local climate; Electronics enclosure; Condensation risk; Humidity management

NOMENCLATURE

C_p specific heat of the fluid at constant pressure [J/kg.K]

c concentration of the species [mole/m^3]

D moisture diffusion coefficient [m/s]

F volume force vector [N]

g acceleration due to gravity [m/s^2]

I unit tensor

p pressure [pa]

T temperature [K]

t time [s]

u velocity vector [m/s]

Greek symbols

μ dynamic viscosity [Pa.s]

ρ mass density [kg/m^3]

Subscripts

x, y, z direction coordinates

INTRODUCTION

Thermal performance is identified as one of the primary goals in electronics system design. In fact, the prediction of thermal performance of electronic equipment is a necessity in order to reduce the time to bring products to the market [1]–[3]. Beside thermal management, humidity management and condensation risk are major concerns. Exposure to high relative humidity (RH) leads to condensation of water on the printed circuit boards (PCBs). The concentration of water molecules rises as the RH increases. The thickness of the molecular layers of water eventually permits ionic conduction which can lead to changes in electrical resistance and even short circuits. This phenomenon accelerates the rate of corrosion. Hence, in order to protect electronic devices from the effects of water vapor, it is essential that the RH inside the enclosure does not reach a level that threatens the electronics functionality within the required lifetime [4]–[8]. Depending on the electronics design and its cleanliness, the critical range of RH for corrosion failure varies from 60 [%] to 90 [%] [3], [9], [10].

Generally, moisture can get into electronics enclosures in two ways: firstly, the moisture is sealed into the package during manufacturing. This quantity of water is fixed at the assembly time and the moisture may reside in the trapped air, be adsorbed to free surfaces or dissolved in component materials. It should be noted that even for hermetically sealed enclosures, this moisture must be considered. The second source of moisture ingress is leakage or permeation into the package from the external environment. The magnitude of this contribution changes with storage time and depends on

the details of the seal design as well as the storage conditions [9]. Considering the fact that, moisture related failures are related to the RH rather than the absolute humidity, thermal and humidity management are strongly interconnected [10]. By definition, relative humidity is the ratio of the absolute humidity to the maximum possible (saturated) absolute humidity at a specific temperature.

Thus, *RH* can be maintained below the threshold value either by maximizing the saturation limit (thermal control) or by minimizing the absolute humidity (moisture control) [11].

Belov et al [8] employed a heater on the critical places for condensation, in order to keep the temperature of these critical places for condensation higher than the dewpoint (maximizing saturation limit). In their work, beside the experiments, the simplifying Boussinesq approximation was used to develop a 3D computational fluid dynamics (CFD) model for a parametric study. In another study, Hygum and Popok [12] also utilized the Boussinesq approximation to numerically study the humidity evolution on the electronics inside an enclosure with an opening using a 2D model (minimizing the absolute humidity). Bayerer et al. [13], Tencer and Moss [11], [14] and Dahan et al. [15] applied quasi-steady-state (QSS) models to study moisture transfer into electronics enclosures. These models apply resistance-capacitor circuits based on the hygro/thermal -electrical analogy [11], [13]–[15]. Despite the significance of the effect of humidity management on the lifetime of the electronics, there are only a few papers which have focused on this issue.

Numerous parameters affect the local climate inside electronics enclosures, such as material properties, dimensions of the enclosure and the electronics, components and their configurations and finally environmental conditions. Ambient condition changes are significantly affecting the local climate inside electronics enclosures. In applications such as military, industrial, commercial or consumer electronics, certain equipment may contain devices highly sensitive to environmental conditions. Understanding the effects of these conditions on the local climate inside the electronics enclosures and applying this knowledge during the design improves the reliability of the equipment and consequently reduces failures and maintenance costs [6], [16], [17]. In the above mentioned studies, simplified models have been used to describe the heat and mass transfer. However, nowadays, the power of computers allow us to handle larger models.

In order to precisely predict the local climate inside electronics enclosures, one has to perform coupled momentum, heat and mass transfer analysis on the system composed of several components of various sizes (such as PCBAs, heatsinks …) in a tight space. The method of choice for making such predictions

is mostly CFD [14], [18], [19]. Application of CFD analysis for the thermal design of electronics systems has the potential to provide accurate solutions and to assess them in different cases [19].

The aim of the present study is to investigate the effect of ambient conditions on the RH evolution on a PCB placed in an electronics enclosure. To achieve this purpose, a full 3D CFD model is developed for a typical aluminum enclosure with a PCB, heatsink and a heater inside, with an opening.

In order to look into the effect of both maximizing the saturation limit and minimizing the absolute humidity, four different cases are defined. In the first two cases, an empty enclosure is exposed to cyclic ambient temperature and high RH with two different opening sizes. In the other two cases, the PCB, heatsink and heater are located inside the enclosure exposed to the same ambient conditions with two different opening sizes, as before. The effect of an internal cyclic heat load to the PCB is also studied.

The commercial software package COMSOL Multiphysics^{TM} version 5.1 is used for running all the CFD simulations. The simulation results for temperature are compared with experimental data from a similar work in the literature.

THEORY AND METHODS

Geometries and Governing Equations

Figure 1 presents the studied symmetry geometries in case of a) an empty enclosure and b) an enclosure with the components (PCB, heatsink and heater) inside. Table 1 shows the dimensions of each of these components. These parameters are typical of outdoors electronics enclosures [16].

In this work, to estimate the velocity profile caused by volumetric forces, the energy equation is fully coupled with the momentum and continuity equations. Figure 2 demonstrates the way that these equations are coupled. The continuity equation or equation for the overall mass balance is:

$$\frac{\partial \rho}{\partial t} + \nabla.(\rho \mathbf{u}) = 0 \qquad (1)$$

The equation for the momentum transport is:

$$\rho \frac{\partial \mathbf{u}}{\partial t} + \rho(\mathbf{u}.\nabla)\mathbf{u} = \nabla.\left[-p\mathbf{I} + \mu(\nabla \mathbf{u} + (\nabla \mathbf{u}^T)) - \frac{2}{3}\mu(\nabla.\mathbf{u})\mathbf{I}\right] + \mathbf{F} \qquad (2)$$

, in order to consider the buoyant flow, the volume force is considered as given below:

$$F_x = F_y = 0; \quad F_z = -\rho \times g_z \qquad (3)$$

The energy equation reads:

$$\rho C_p \frac{\partial T}{\partial t} + \rho C_p \mathbf{u}.\nabla T = \nabla.(k\nabla T) + Q \qquad (4)$$

Having obtained the velocity and temperature profiles, the moisture transfer into the enclosure is calculated by solving the following diffusion-convection equation:

$$\frac{\partial c}{\partial t} + \mathbf{u}.\nabla c = D\nabla.(\nabla c) \qquad (5)$$

Generally, natural convection problems are challenging because the resulting velocity is part of the nonlinear solution. For such a problem, it is very important to use a proper solver to achieve convergence. The solver settings are chosen as explained in a previous work [19].

Table 1 The Dimensions of the Geometries

Item	**Dimensions [mm]**	**Material**
Enclosure	Inner: 188×128×276 Outer: 190×130×280	Aluminum
Heater	50×1×50	Silicon
heatsink	80×10×100	Aluminum
PCB	30×1.6×130	Compact FR-4 and copper layers

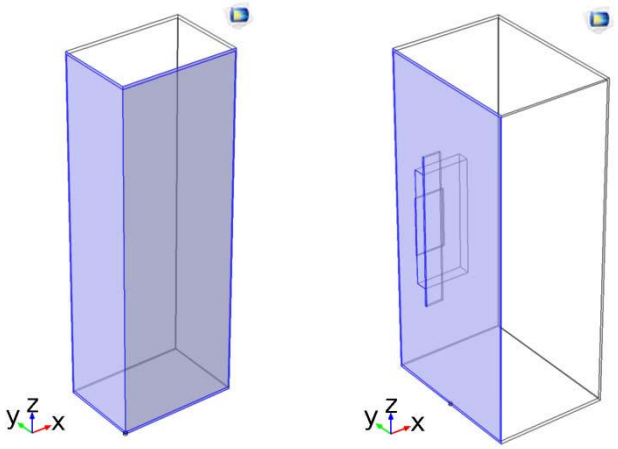

(a) (b)

Figure 1 Illustration of the investigated geometries; (a) empty enclosure, (b) enclosure with components inside (Symmetry faces are shown in blue).

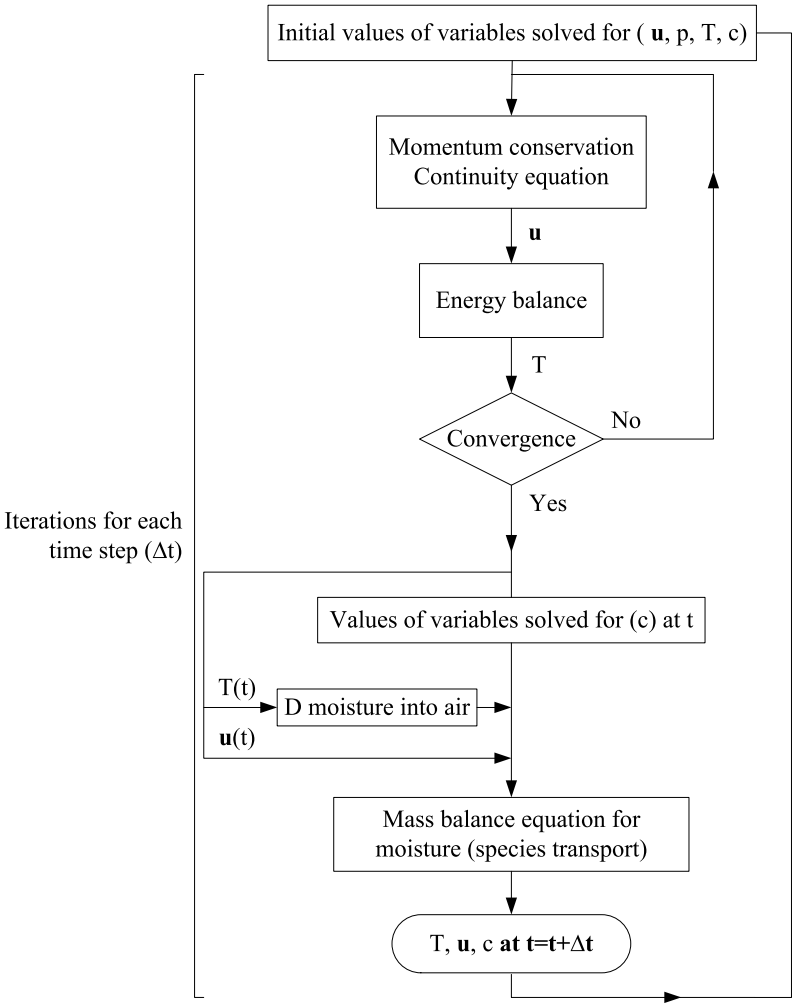

Figure 2 Flowchart of the solving method

Material properties

The thermodynamic properties such as density and specific heat capacity of air are automatically updated with temperature according to the software data base. The moisture diffusion coefficient into the air is also a function of temperature. Marrero and Mason suggested the following equation for estimation the diffusion coefficient [20]:

$$D_{air} = 1.87 \times 10^{-10} \times T^{2.072} \qquad (6)$$

The moisture diffusion coefficient into air can also be obtained by a regression curve fit to data from Bolz and Tuve [21]–[24]:

$$D_{air} = -2.775 \times 10^{-6} + (4.479 \times 10^{-8})T + (1.656 \times 10^{-10})T^2 \qquad (7)$$

Figure 3 compares the two correlations. It is seen that the estimated values are very close within the temperature range of 0 to 100 [°C]. In this work, the correlation developed by Boltz and Tuve is used.

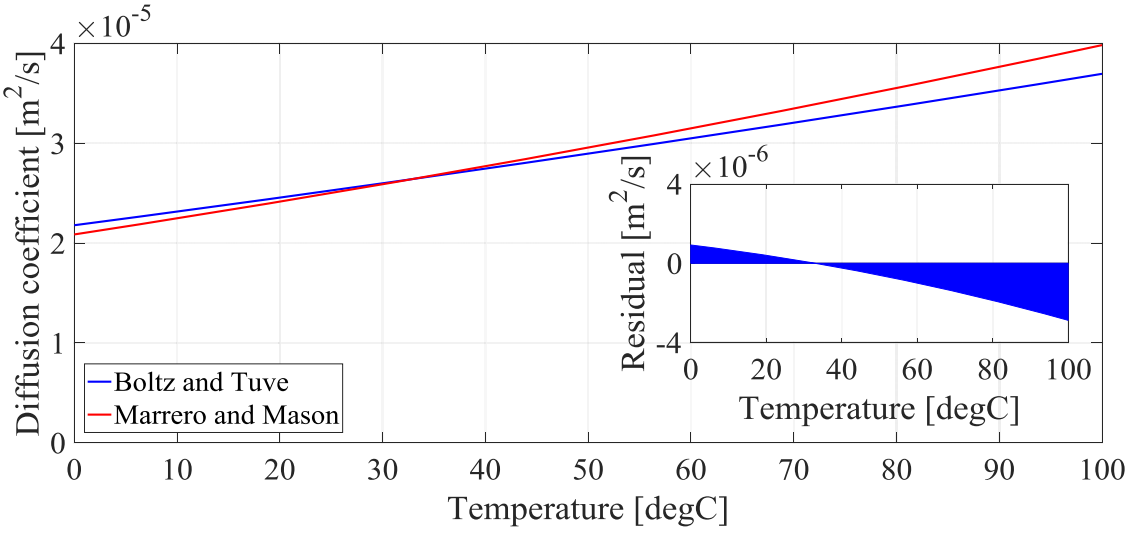

Figure 3 Moisture diffusion coefficients into air

A PCB is typically a layered composite consisting of copper foils and a glass-reinforced polymer (FR-4). A cross-sectional view of such a laminated structure is illustrated in Figure 4. The figure displays the numbering system that will be used for indicating the different layers, numbered 1 to *n*. In many thermal calculations, it is convenient to treat such a layered structure as a homogeneous material with two different effective thermal conductivities: one describing heat flow within the plane ($k_{\text{in plane}}$) and another for heat flow through the thickness of the plane (k_{through}) [25].

$$k_{in\,plane} = \frac{\sum_{i=1}^{n}(k_i \times thickness_i)}{\sum_{i=1}^{n} thickness_i} \qquad (8)$$

$$k_{through} = \frac{\sum_{i=1}^{n} thickness_i}{\sum_{i=1}^{n}(thickness_i / k_i)} \qquad (9)$$

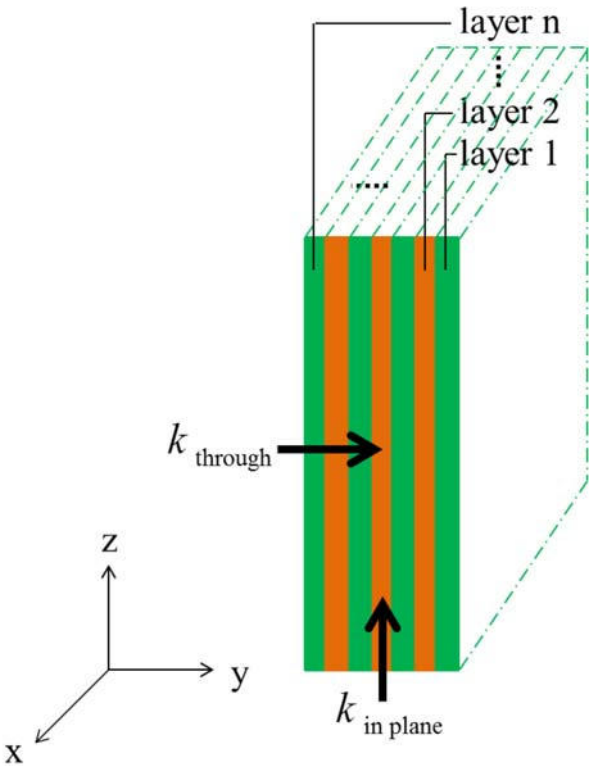

Figure 4 A schematic cross-sectional view of a PCB

Now, the anisotropic heat conductivity of the PCB is taken into the calculations by the following diagonal matrix:

$$k_{PCB} = \begin{bmatrix} k_{in\,plane} & 0 & 0 \\ 0 & k_{through} & 0 \\ 0 & 0 & k_{in\,plane} \end{bmatrix} \qquad (10)$$

Initial and Boundary Conditions

The initial relative humidity, temperature, pressure and velocity are 30 [%], 24 [°C], 0 [Pa] and 0 [m/s], respectively. The ambient RH is set at 100 [%] at the opening. The temperature of the outer walls of the enclosure is cycling as shown in Figure. 5. The opening is considered as an open boundary with no viscous stress.

$$\left[\mu(\nabla \mathbf{u} + (\nabla \mathbf{u}^T)) - \frac{2}{3}\mu(\nabla . \mathbf{u})\mathbf{I}\right]\mathbf{n} = 0 \qquad (11)$$

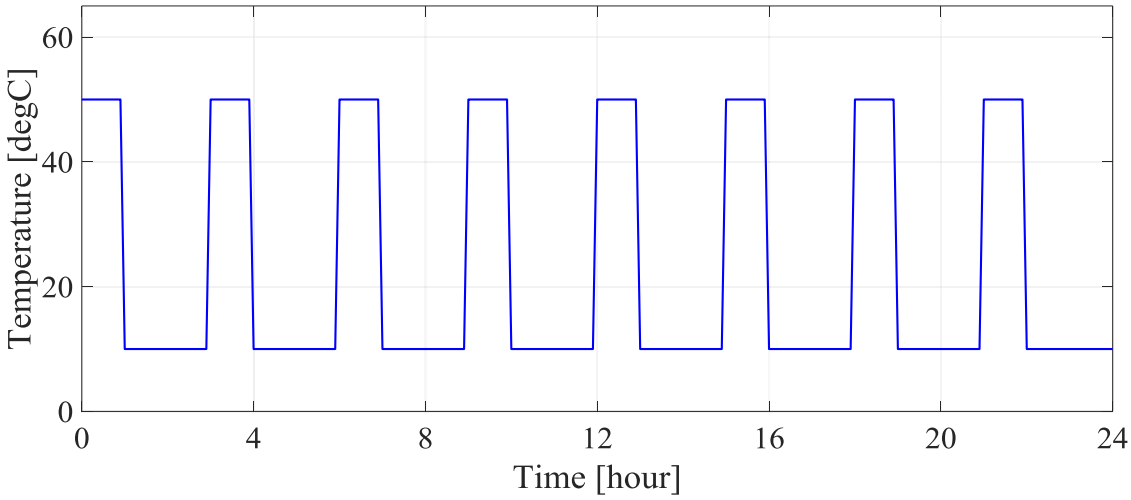

Figure 5 The cyclic ambient temperature boundary condition.

In order to study the effect of ambient condition changes, opening size, presence of electronics and internal heat load cycles of the electronics on the local climate (temperature and RH) inside the enclosure, four cases are considered as explained in Table 2. In all four cases, the enclosure is exposed to the same ambient conditions. In the first part of the study, the responses of empty enclosures with two different opening sizes are studied. Next the RH and temperature of the PCB is estimated in cases 3 and 4. Finally, the local climate on the PCB is studied when a cyclic heat load is imposed to the PCB by the heater, as displayed in Figure 6.

Table 2 The four investigated cases

Case #	**Opening size (diameter)**	**Content of the enclosure**
1	1 [mm]	empty
2	3 [mm]	empty
3	1 [mm]	PCB, heater, heatsink
4	3 [mm]	PCB, heater, heatsink

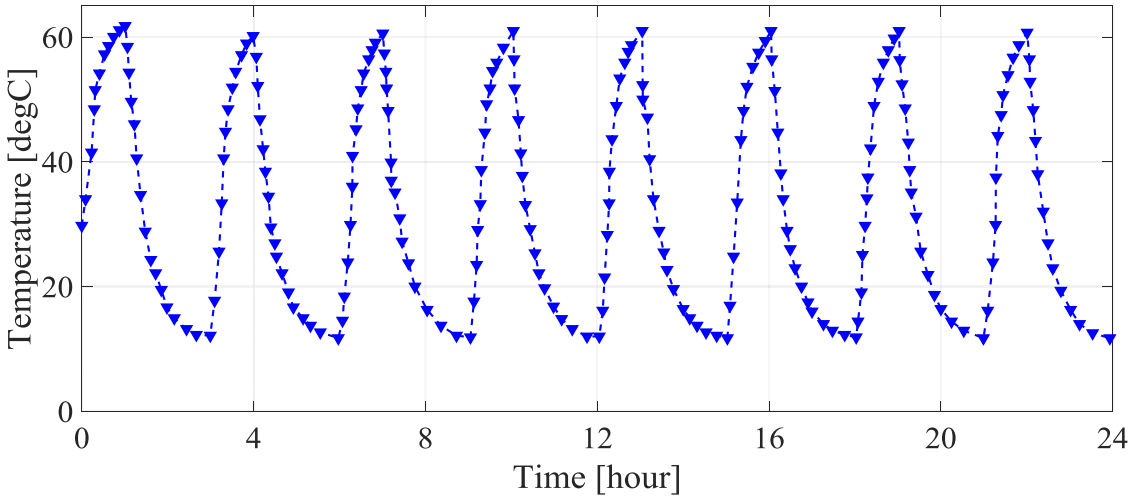

Figure 6 The measured transient temperature of the silicon heater [16].

The temperature of the heater is prescribed according to the experimental work conducted by Conseil et al [16], so that the CFD simulation results can be compared with the results from their study.

RESULTS AND DISCUSSION

Figure 7 shows the temperature at the center of the aluminum enclosure. The temperature has a fast response to the ambient changes in both cases of opening sizes of 1 and 3 [mm] diameter. The outer walls being exposed to the ambient changes are mainly responsible for the internal temperature and the opening size cannot make a severe change. Not surprisingly, the air flow through the opening is negligible due to its small size; thus, the air flow does not cause sensible convection to accelerate the heat transfer and consequently the temperature response. Hence, the estimated temperatures are not noticeably different for the cases 1 and 2.

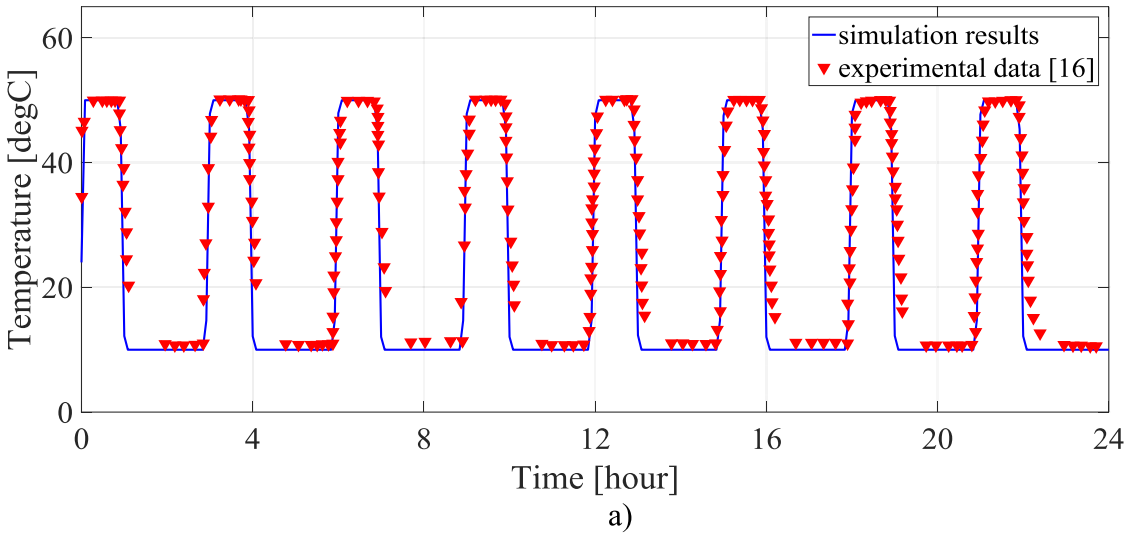

a)

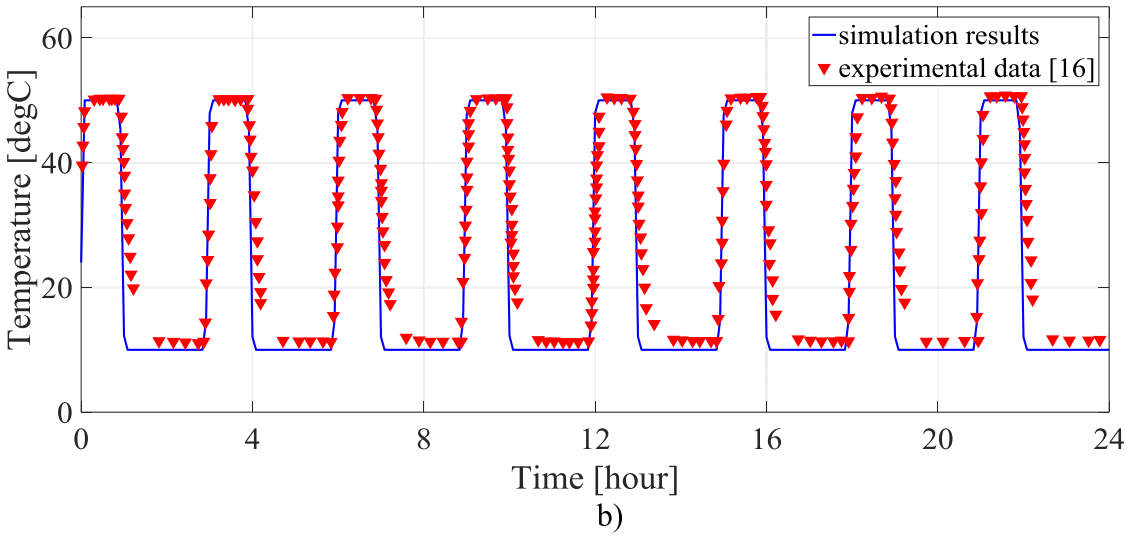

b)

Figure 7 The temperature at the center of the Al enclosure for a) case 1 and b) case 2

Figure 8 shows the RH changes at the center of the enclosure versus time. In case 2, the moisture transfer through the opening is so fast that in the first cycle (about 1 hour) the internal RH has reached the maximum value (100 [%]); on the other hand, in case 1, the RH has reached the 100 [%] value after 3 temperature cycles (9 hours). Similarly, the minimum RH value for every cycle increases over time more rapidly for case 2 as compared to case 1. This is due to the fact that the moisture ingress through the 3 [mm] diameter opening is about a factor of 9 ($3^2/1^2$) faster than the 1 [mm] diameter one (the moisture transfer time constant has been extensively studied in a previous works [6]). Hence, in case 2

both moisture concentration and temperature changes are actively affecting the RH. However, in case 1, after 3 cycles when the moisture concentration in the enclosure has reached the saturation value at 10 [°C], the RH cycling behavior is not changing, demonstrating the small rate of moisture transfer through the 1 [mm] diameter opening.

According to figure 8, in case of constantly high ambient RH, minimizing the absolute humidity is a more effective solution compared to maximizing the saturation limit.

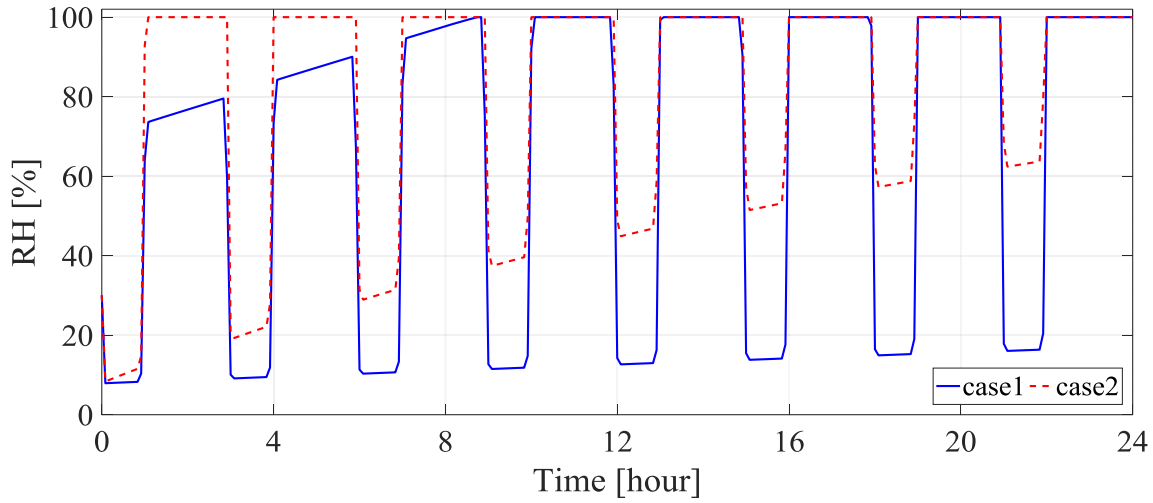

Figure 8 The RH at the center of the Al enclosure.

For cases 3 and 4, the temperature and RH on top of the PCB are displayed in Figure 9 and Figure 10, respectively. The presence of the components, especially the heatsink, reduces the internal temperature changes compared to the case in which the enclosure was empty. In fact, the amplitude of the temperature changes is reduced in the presence of the thermal mass which causes a delay in the temperature response, and in this case, temperature cycles are not long enough to heat and cool the components to the highest and lowest ambient values (50 and 10 [°C]); thus, if the thermal mass was small enough or the time period of the maximum and minimum temperatures were long enough, the temperature of the thermal mass could reach the ambient maximum and minimum values.

According to Figure 10, the presence of the components, especially the heatsink, decreases the risk of condensation in the enclosure; however, it does not prevent it. For case 3 the RH reaches the 100 [%] after 6 cycles. For case 4, the period that the RH is at 100 [%] is shorter compared with the empty enclosure.

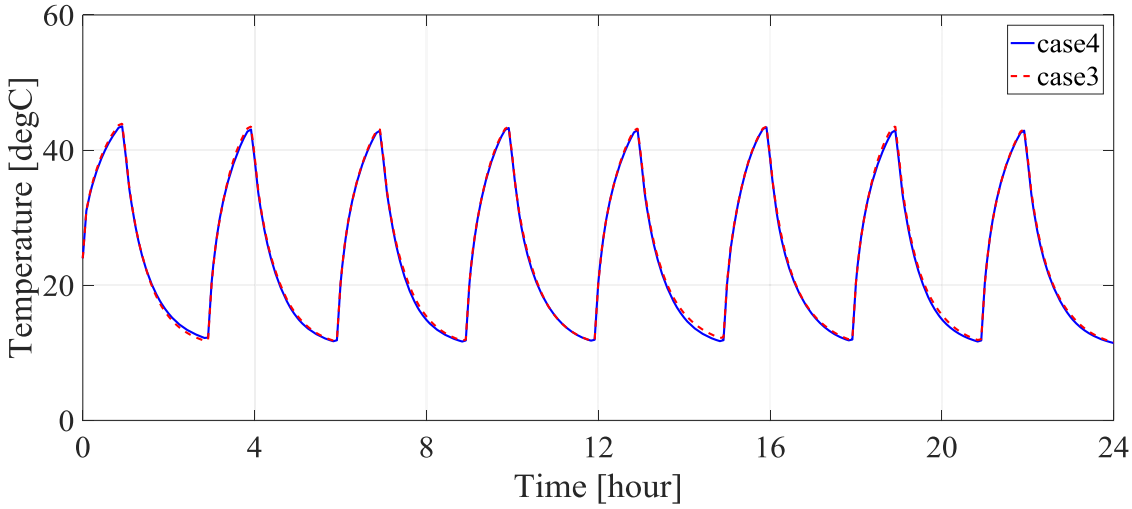

Figure 9 The temperature at the center of the Al enclosure.

Figure 11 displays the temperature and velocity profiles at different time sections of the cycling period. After 0.5 [hr], the devices inside the enclosure are heating up from the initial temperature (25 [°C]) to the ambient value (50 [°C]). It is shown that the devices are colder than the trapped air. Thus, the air close to the devices flows downwards. After 1 [hr], the ambient is getting cold; thus, the air and the electronics inside start getting influenced by the new conditions. In Figure 11 (b), it is shown that in spite of the fact that the temperature of the trapped air is influenced rapidly by the new condition, the devices inside are still about 50 [°C]. In this case, as the devices inside are warmer, the air close to them flows upwards. It should be noticed that the velocity magnitudes for Figure 11 (b) are higher than Figure 11 (a). This is due to the higher temperature gradient inside the enclosure. In Figure 11 (c), the ambient temperature has heated up to 50 [°C]; however, the devices inside are much colder and it takes much more time for them to reach the ambient temperature and considering this, the air close to them flows downwards. On the other hand, the air close to the vertical walls of the enclosure moves upwards, since they are warmer. It is seen that the ambient changes have caused some considerable buoyant flow inside the enclosure with a maximum air velocity of about 0.25 [m/s].

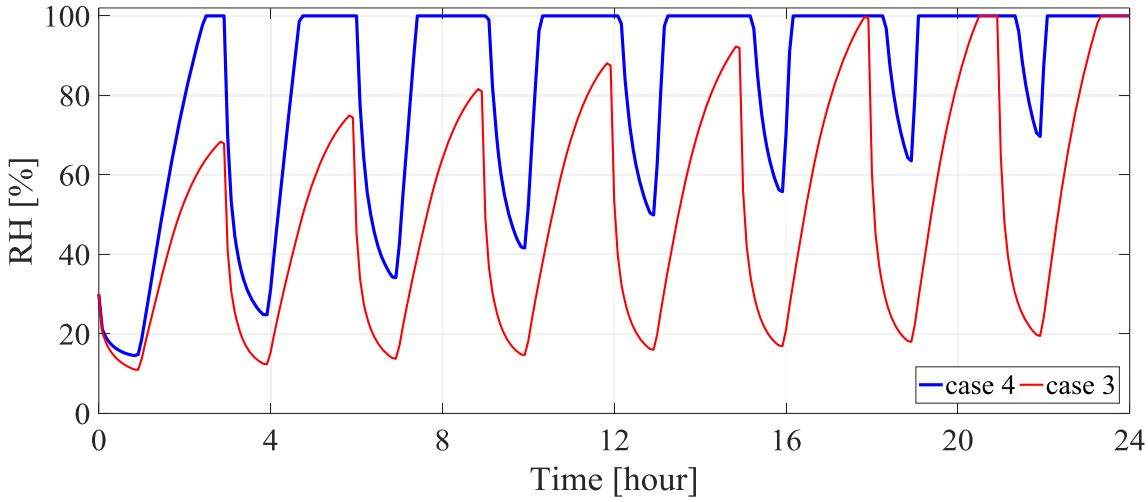

Figure 10 The RH on the PCB.

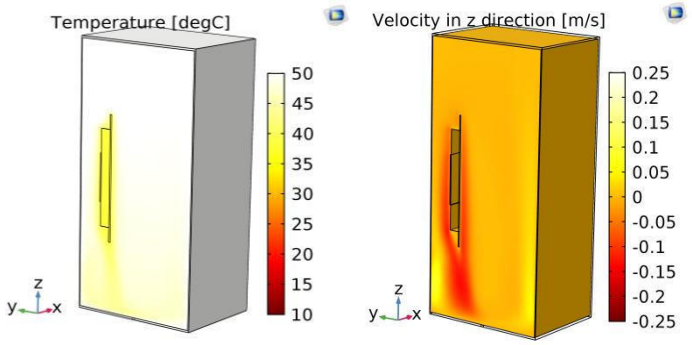

a) t=0.5 hr

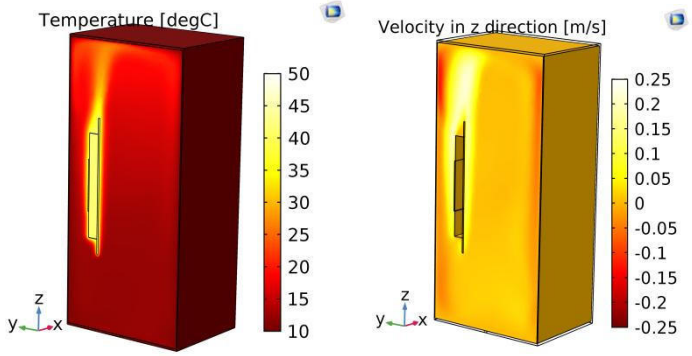

b) t=1 hr

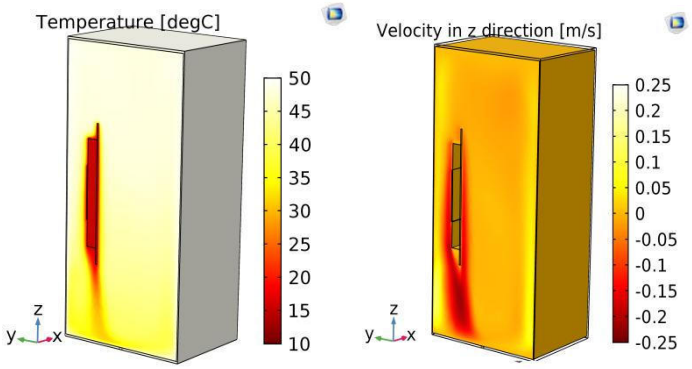

c) t=3 hr

Figure 11 The temperature and velocity profile inside the enclosure at different times.

Figure 12 compares the numerical simulation results with the experimental data from the literature, when a cyclic heat load is imposed to the PCB by the silicon heater. As demonstrated, there is an acceptable agreement between the numerical and the experimental work; however, it is noted that the maximum temperature peak is underestimated up to 3 [°C] by the CFD results. It is worth to mention that there is an inevitable error in the data reading from the literature at the peaks where the changes are sharp and consequently the gradients are high. Besides, performing the experiments also involves errors, especially at these peaks when sudden changes happen to the both internal and external conditions.

The RH value on the PCB, during the heat loading cycles is shown in Figure 13. Despite the fact that the average RH value over the day for both case 3 and 4 is less than in the situation where there is no internal heating, the condensation risk is not much decreased.

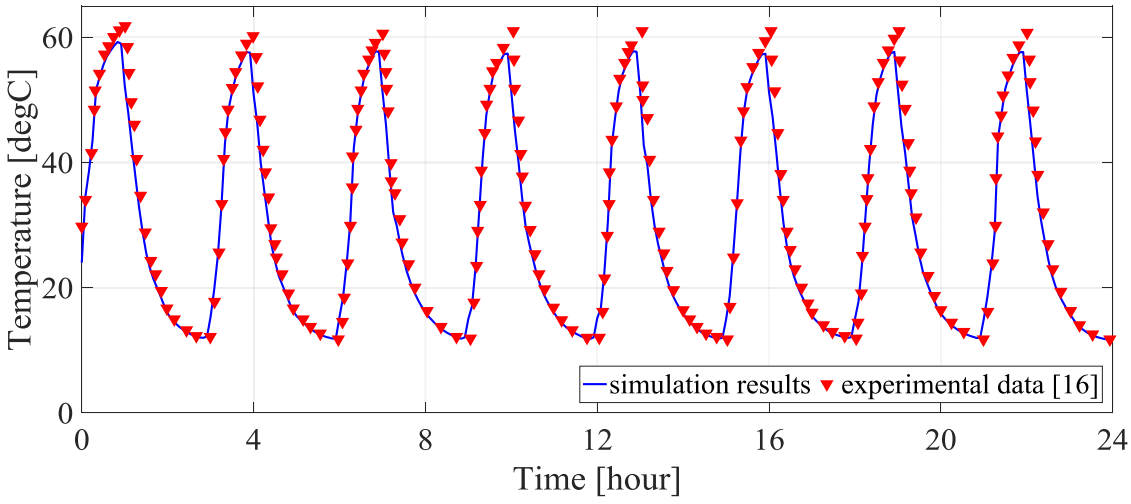

a)

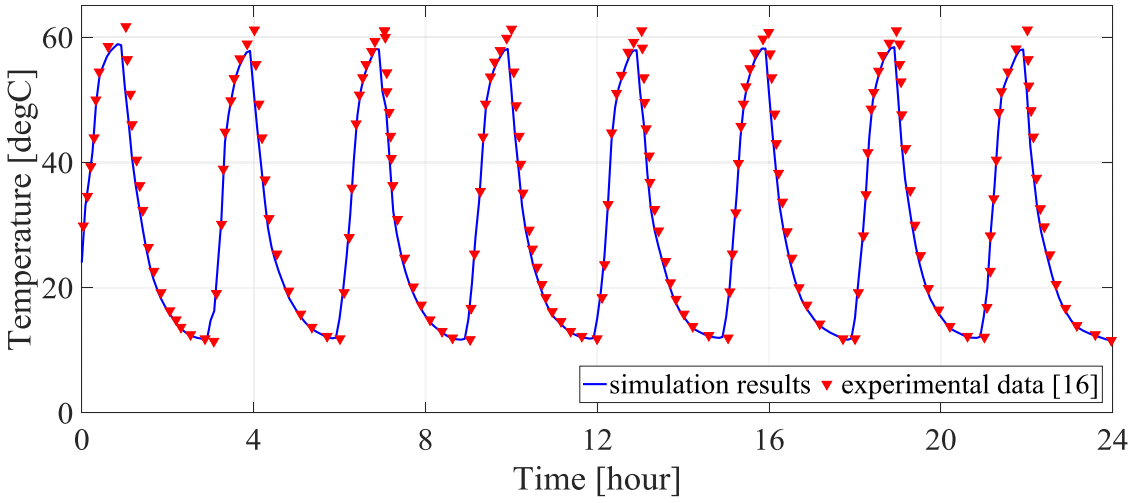

b)

Figure 12 The temperature on the PCB for a) case 3 and b) case 4, during the heat loading cycles.

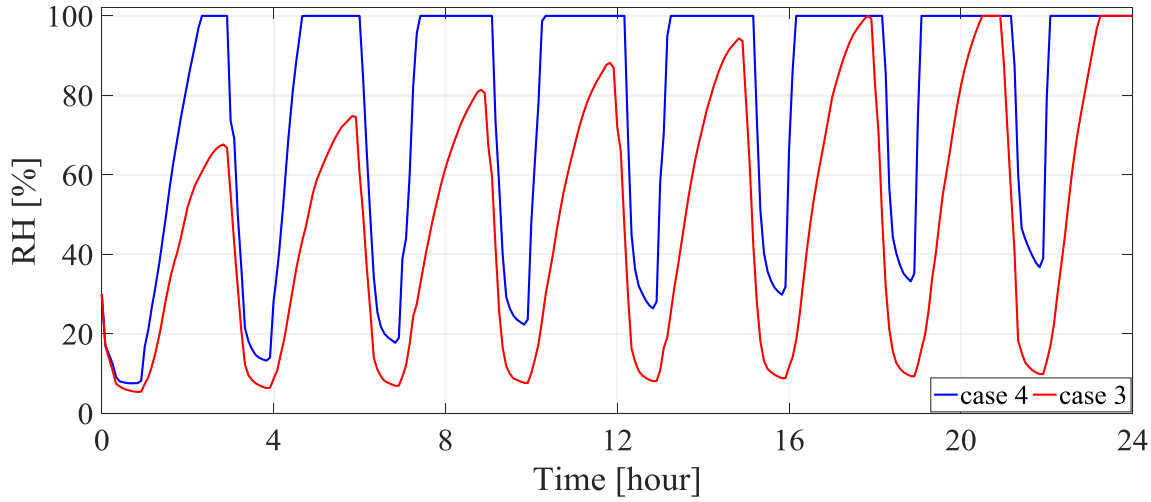

Figure 13 The RH on the PCB during the heat loading cycles.

CONCLUSIONS

A 3D finite element based CFD model is developed for investigating the RH evolution on a PCB inside an electronics enclosure. The local climate inside the enclosure is investigated in three stages: first, the response of an empty enclosure to the ambient conditions is investigated, then an enclosure with some components inside is considered and finally the effect of simultaneous internal and external temperature changes is studied. In all the three parts, the effect of the opening size of the enclosure is also studied. The numerical simulation results are compared with corresponding experimental results from the literature, and a good agreement is found.

The presence of the components inside the enclosure especially the aluminum heatsink causes a delay to the ambient thermal cycles and also shortens the amplitude of the cyclic changes. Thus it helps to reduce RH on the PCB. On the other hand, the moisture transfer happens through the bottom hole of the enclosure. Despite the fact that a temperature increase accelerates the diffusion, the mass transfer resistance which is affected by the geometrical sizes beside the diffusion coefficient is not significantly affected. Thus, the moisture transfer is mostly controlled by the opening size rather than the temperature. Controlling the moisture concentration inside the enclosure is more effective compared to the temperature cycles in reducing the condensation risk on the PCB.

It should be noted that the buoyant flow inside the enclosure reduces the mass transfer resistance inside the enclosure. The cyclic internal heat load also helps this effect.

The simulation results demonstrate that the temperature profile and consequently the RH profile are mainly controlled by the buoyant air flow (natural convection) rather than heat conduction inside the enclosure.

ACKNOWLEDGMENTS

The current research has been conducted as part of the ICCI project from the Danish council for Independent Research, Technology and Production (FTP) and the IN SPE project from the Danish Innovations Fonden which are highly acknowledged. Moreover, the authors would like to acknowledge the commitment and help of the industrial partners in this project.

REFERENCES

[1] F. Song, B. Zhao, X. Yang, Y. Jiang, V. Gopal, G. Dobbs, and M. Sahm, "A new approach on zonal modeling of indoor environment with mechanical ventilation," *Build. Environ.*, vol. 43, no. 3, pp. 278–286, 2008.

[2] C. Sapia and G. Sozio, "CFD transient model of the natural convection heat transfer for an heat sink effects of increasing surface and fins spacing," in *International Workshop onThermal Investigations of ICs and Systems, THERMINIC*, 2011, pp. 1–6.

[3] C. E. Triplett and B. Joiner, "An experimental thermal characterization of a 272 PBGA within an automotive engine controller module," in *Semiconductor Thermal Measurement and Management Symposium, 1998. SEMI-THERM Proceedings 1998., Fourteenth Annual IEEE*, 1998, pp. 47–54.

[4] P. Shojaee Nasirabadi, M. Jabbari, and J. H. Hattel, "Estimation of water diffusion coefficient into polycarbonate at different temperatures using numerical simulation," *AIP Conf. Proc.*, vol. 1738, no. 1, 2016.

[5] L. Zhu, D. Monthei, G. Lambird, and W. Holgado, "Moisture diffusion modeling and application in a 3D RF module subject to moisture absorption and desorption loads," in *Thermal, Mechanical Multi-Physics Simulation, and Experiments in Microelectronics and Microsystems (EuroSimE), 2010 11th International Conference on*, 2010, pp. 1–6.

[6] P. Shojaee Nasirabadi, M. Jabbari, and J. H. Hattel, "CFD simulation and statistical analysis of moisture transfer into an electronic enclosure," *Appl. Math. Model.*, vol. 44, pp. 246–260, 2017.

[7] D. Leslie, A. Dasgupta, and J. W. C. De Vries, “Quantifying moisture diffusion into three-dimensional axisymmetric sealants,” *2013 14th Int. Conf. Therm. Mech. Multi-Physics Simul. Exp. Microelectron. Microsystems, EuroSimE 2013*, pp. 1–4, 2013.

[8] I. Belov, J. Ryden, J. Lindeblom, Y. Zhang, T. Hansson, F. Bergner, and P. Leisner, “Application of CFD modelling for energy efficient humidity management of an electronics enclosure in storage under severe climatic conditions,” in *International Conference onThermal, Mechanical and Multi-Physics Simulation and Experiments in Microelectronics and Micro-Systems, EuroSimE*, 2008, pp. 1–8.

[9] R. Ciprian and B. Lehman, “Modeling effects of relative humidity, moisture, and extreme environmental conditions on power electronic performance,” in *IEEE Energy Conversion Congress and Exposition*, 2009, pp. 1052–1059.

[10] M.R. Keenan, “Moisture Control in Sealed Electronic Packages,” California, 1990.

[11] M. Tencer and J. S. Moss, “Humidity management of outdoor electronic equipment: Methods, pitfalls, and recommendations,” *IEEE Trans. Components Packag. Technol.*, vol. 25, no. 1, pp. 66–72, 2002.

[12] A. M. Hygum and N. V. Popok, “Humidity evolution (breathing effect) in enclosures with electronics,” in *IMAPS Nordic Annual Conference*, 2015.

[13] R. Bayerer, M. Lassmann, S. Kremp, and I. T. Ag, “Transient hygro-thermal-response of power modules in inverters – mission profiling for climate and power loading,” pp. 25–27, 2014.

[14] M. Tencer, “Moisture ingress into nonhermetic enclosures and packages. A quasi-steady state model for diffusion and attenuation of ambient humidity variations,” *Electron. Components Technol.*, pp. 196–209, 1994.

[15] N. Dahan, A. Vanhoestenberghe, and N. Donaldson, “Moisture ingress into packages with walls of varying thickness and/or properties: A simple calculation method,” *IEEE Trans. Components, Packag. Manuf. Technol.*, vol. 2, no. 11, pp. 1796–1801, 2012.

[16] H. Conseil, V. C. Gudla, M. S. Jellesen, and R. Ambat, “Humidity Build-Up in a Typical Electronic Enclosure Exposed to Cycling Conditions and Effect on Corrosion Reliability,” *IEEE Trans. Components, Packag. Manuf. Technol.*, pp. 1–10, 2016.

[17] J. B. Jacobsen, J. P. Krog, A. H. Holm, and L. Rimestad, “Climate-Protective Packaging,” no. september, pp. 51–59, 2014.

[18] P. Shojaee Nasirabadi, M.Jabbari, and J. H. Hattel, “Numerical simulation of transient moisture transfer into an electronic enclosure,” *AIP Conf. Proc.*, vol. 1738, pp. 1–4, 2016.

[19] P. Shojaee Nasirabadi, M. Jabbari, and J. H. Hattel, “Numerical simulation of transient moisture and temperature distribution in polycarbonate and aluminum electronic enclosures,” in *International Conference on Thermal, Mechanical and Multi-Physics Simulation and Experiments in Microelectronics and Microsystems, EuroSimE*, 2016, pp. 1–6.

[20] T. R. Marrero and E. A. Mason, “Gaseous Diffusion Coefficients,” *J. Phys. Chem. Ref. Data*, vol. 1, no. 1, pp. 3–118, 1972.

[21] A. Fabbri and C. Cevoli, “2D water transfer finite elements model of salami drying, based on real slice image and simplified geometry,” *J. Food Eng.*, vol. 158, pp. 73–79, 2015.

[22] M. Bakhshi, B. Mobasher, and C. Soranakom, “Moisture loss characteristics of cement-based materials under early-age drying and shrinkage conditions,” *Constr. Build. Mater.*, vol. 30, pp. 413–425, 2012.

[23] P. Eliaers, J. Ranjan Pati, S. Dutta, and J. De Wilde, “Modeling and simulation of biomass drying in vortex chambers,” *Chem. Eng. Sci.*, vol. 123, pp. 648–664, 2015.

[24] J. Songok, P. Salminen, and M. Toivakka, “Temperature effects on dynamic water absorption into paper,” *J. Colloid Interface Sci.*, vol. 418, pp. 373–377, 2014.

[25] J. R. Culham and M. M. Yovanovich, “Factors affecting the calculation of effective conductivity in printed circuit boards,” in *InterSociety Conference on Thermal Phenomena*, 1998.

Appendix C
Paper III (submitted to the Applied Thermal Engineering journal)

Manuscript Details

Manuscript number	ATE_2017_5643
Title	Long Term Prediction of Local Climate inside an Electronic Enclosure
Article type	Research Paper

Abstract

Temperature and relative humidity are crucially important for the reliability of electronic devices in outdoor applications. For small enclosures, thermal control by a heatsink that is cooled by natural convection is the most widely used method. In this work, the functionality of a heatsink for partially storing the heat that is generated by the electronics and releasing the stored energy with a time lag for the purpose of enhancing the stability of the local climate inside a typical electronic enclosure is studied using transient 3D CFD simulations. A typical enclosure is assumed to be exposed to Copenhagen outdoor conditions over a two-day time period. In addition to CFD modeling, a Cauer ladder RC model is also developed for fast and long term predictions. A correlation for calculating the Nusselt number representing heat transfer between the trapped air inside the enclosure and the heat sink is derived based on the CFD simulation results. The kinetic energy stored in the gas due to the buoyancy-induced motion of the air is also estimated and is shown to be small in comparison with the stored thermal energy. Compared with CFD simulations, the RC model predicts slightly lower values for temperature, and slightly higher values for RH, in all the investigated cases in cyclic working conditions. The lumped model correctly predicts the trend for temperatures and RH variations, however, suggesting that a properly calibrated RC model can be used for scoping calculations, and more importantly for long-term predictions. The method can be used for any other ambient and working conditions, as long as the temperature difference in the air does not exceed 25 [°C].

Keywords	local climate; electronic enclosure; CFD; RC modelling; heatsink; RH

Corresponding Author	Parizad Shojaee Nasirabadi
Corresponding Author's Institution	Technical University of Denmark (DTU)
Order of Authors	Parizad Shojaee Nasirabadi, Mostafa Ghiaasiaan, Jesper Hattel
Suggested reviewers	Robin Bornoff, Ross Wilcoxon, John Parry

Long Term Prediction of Local Climate inside an Electronics Enclosure

Parizad Shojaee Nasirabadi[1, 2*], S. Mostafa Ghiaasiaan[2], Jesper Henri Hattel[1]

[1] *Process Modelling Group, Department of Mechanical Engineering, Technical University of Denmark, Nils Koppels Allé, Kongens Lyngby 2800, Denmark*

[2] *The George W. Woodruff School of Mechanical Engineering, Georgia Institute of Technology, Atlanta, GA 30332, USA*

[*] *Corresponding author: Tel.: +45 45254754; fax: +45 45251961; E-mail address: parnas@mek.dtu.dk (Parizad Shojaee Nasirabadi).*

Abstract

Temperature and relative humidity are crucially important for the reliability of electronic devices in outdoor applications. For small enclosures, thermal control by a heatsink that is cooled by natural convection is the most widely used method. In this work, the functionality of a heatsink for partially storing the heat that is generated by the electronics and releasing the stored energy with a time lag for the purpose of enhancing the stability of the local climate inside a typical electronics enclosure is studied using transient 3D CFD simulations. A typical enclosure is assumed to be exposed to Copenhagen outdoor conditions over a two-day time period. In addition to CFD modeling, a Cauer ladder RC model is also developed for fast and long term predictions. A correlation for calculating the Nusselt number representing heat transfer between the trapped air inside the enclosure and the heat sink is derived based on the CFD simulation results. The kinetic energy stored in the gas due to the buoyancy-induced motion of the air is also estimated and is shown to be small in comparison with the stored thermal energy.

Compared with CFD simulations, the RC model predicts slightly lower values for temperature, and slightly higher values for RH, in all the investigated cases in cyclic working conditions. The lumped model correctly predicts the trend for temperatures and RH variations, however, suggesting that a properly calibrated RC model can be used for scoping calculations, and more importantly for long-term predictions. The method can be used for any other ambient and working conditions, as long as the temperature difference in the air does not exceed 25 [°C].

Nomenclature

Cp specific heat of the fluid at constant pressure (J/kg.K)
c concentration of the species (mole/m^3)
D moisture diffusion coefficient (m/s)
F volume force vector (N)
g acceleration due to gravity (m/s^2)
I unit tensor
p pressure (pa)
T temperature (K)
t time (s)

u velocity vector (m/s)

Greek symbols

μ dynamic viscosity (Pa.s)

ρ mass density (kg/m^3)

Subscripts

x, y, z direction coordinates

Keywords: local climate, electronics enclosure, CFD, RC modelling, heatsink, RH

1 Introduction

Temperature and relative humidity (RH) management inside electronics enclosures exposed to uncontrolled environmental conditions are critically important for the reliability and durability of electronic components housed in enclosures [1]–[3]. Thus, understanding the effects of environmental conditions, both at component and system levels, and applying this knowledge during the design phase is crucial for reducing the chance of failure and controlling maintenance costs. However, the RH of the operating environment is commonly disregarded during the design of electronics enclosures [2]. Exposure to high RH and the consequent condensation is a severe concern because it accelerates corrosion and migration mechanisms [3]. Cyclic external conditions can cause condensation when high RH levels are reached during daytime and are followed by a drop in the temperature at night, as a result of which the vapor stored in the trapped air inside the enclosure can exceed the saturation level [4].

Despite the significance of the effect of the local climate inside the enclosures on the reliability of electronics, only a few relevant investigations have been reported in the past. Tencer [5] developed a simple quasi-steady-state (QSS) model to estimate the time constants for moisture diffusion through plastic walls and openings into a typical electronics enclosure. The model is fast; however, it is difficult to apply in case of a complex geometry, or when the body of the enclosure consists of several materials [6]. Tencer et al. [7] also introduced a method for controlling RH inside an enclosure. The method uses dissipated heat from electronics to maintain a proper temperature difference between the ambient and the critical surfaces in order to reduce the RH, and simultaneously through the use of diffusion plugs which provides for relatively fast humidity equilibrium between the trapped air inside the enclosure and the ambient in order to minimize condensation risk. The critical range of humidity for corrosion failure is 60–90% depending on the electronics design and cleanliness [6]. Using an electrical analogy, Dahan et al. [8] applied a QSS model to the moisture ingress into a package containing walls or elements of different thicknesses or properties. Punch et al. [3] developed a first-order coupled hygrothermal model to represent the response of an electronics enclosure to variations in ambient temperature and RH and showed that moving from one environment to another can cause condensation. A CFD modelling tool was developed by Belov et al. [1] for investigation of moisture transfer into a non-hermetic electronics enclosure with a number of printed circuit boards inside. Using CFD simulations, Shojaee et al. [9], [10] studied moisture ingress into a standard polycarbonate electronics enclosure exposed to harsh ambient conditions. Furthermore, they integrated a CFD model with a two level factorial design to

identify the significant geometric and operational factors as well as the potential interactions among them [10].

Kremp and Schilling [11] experimentally investigated the influence of different cycling profiles on condensation risk inside an enclosure. Furthermore, they studied the condensation risk in case of long term humidity build-up inside an electronics enclosure. Conseil et al. [12] also conducted experiments in order to study the temperature changes and moisture built-up inside polycarbonate and aluminum electronics enclosures exposed to day/night RH and temperature cycles.

Experiments for monitoring the local climate inside enclosures are often long and tedious, and are typically lasting for a couple of days. Thus, there is a need for a reliable predictive model which is computationally fast and therefore capable of long term predictions, such as seasonal or annual, predictions, using realistic ambient conditions. CFD simulations can provide detailed information about transient temperature and RH distributions by considering all the geometric complexities of an electronics enclosure and the components inside [13], [14]. For that reason CFD simulation is a widely used method in the design of electronics enclosures. However, such CFD simulations are often time consuming and CPU-intensive, and are therefore unsuitable for true long term analyses. On the other hand, lumped models based on the fundamental similarity between heat and mass transfer on one hand and the transfer of electric charge in an electrical circuit on the other, are capable of fast and easy predictions [15]; nevertheless, because of their underlying simplifying assumptions as well as their implemention constraints they lack accuracy. For instance, implementing natural convection in a RC model is challenging because quantification of capacitance for a convective system is not straight forward. A complicating factor with respect to implementing natural convection in a RC model is that the natural convection heat transfer coefficient is a function of the temperature difference between the fluid and the cooled surface. Since this temperature difference is part of the solution itself, an iteration loop is needed for the temperature calculations. Khane and Usman [16] attempted to estimate the capacitance for the energy stored in a fluid during natural convection. They conducted CFD simulations for a Rayleigh–Benard convection system using FLUENT commercial software. They applied a constant heat flux on the heat source side of their simulated system, and monitored the sink side heat flux. By analyzing the variation of the heat flux of the heat-sink side with time, they estimated the total energy stored in the fluid. Thereafter, by comparing the conduction vs. convection system, they determined the capacitance [16].

Heatsinks cooled by natural convection have been used for the thermal management of low-power-density devices for a long time. This is due to several appealing features, including high system reliability, simplicity, robustness, maintenance-free operation, and zero power consumption [17], [18]. Typically, a heat sink is a thermal heat transfer device, employed to dissipate heat from a high temperature heat source to a lower temperature surrounding [19]. In electronics enclosure applications the heatsink is often attached to the walls of the enclosure to facilitate the transfer of the heat that is extracted from the devices to the ambient. A major problem with this arrangement is that the electronics can be directly influenced by the ambient temperature. Thus, during night or early morning

when the device may not be working, its temperature falls down as the ambient temperature does. The RH in the enclosure then increases and there is a risk of condensation.

In this work, we model a heatsink that is placed inside an enclosure without contacting the enclosure walls. With this arrangement the heat sink can store the heat generated by the electronics to be used for lowering the RH later when the electronics are not working. We thus utilize the time delay that heat sinks can provide for heat transfer because of their high thermal capacity, in order to mitigate the adverse effects of surface-humidity interactions. First, a typical aluminum electronics enclosure containing a PCB with a silicone heater and a heatsink, which is exposed to Copenhagen outdoor conditions, is extensively studied using transient 3D CFD simulations. An equivalent Cauer ladder RC model is then developed for the heat and moisture transfer in the system. The natural convection capacitance and resistance are estimated by analysis of the CFD simulation results. Thereafter, CFD results are compared with RC calculations. The RC model is then used for further parametric calculations.

2 Methodology

2.1 Case description

Fig. 1 presents a schematic diagram of the electronics enclosure investigated in this work. It contains a PCB, a heat producing component and a thermal mass (heatsink). Table 1 shows the material and dimensions of each of these components. These parameters are typical of outdoors electronics enclosures.

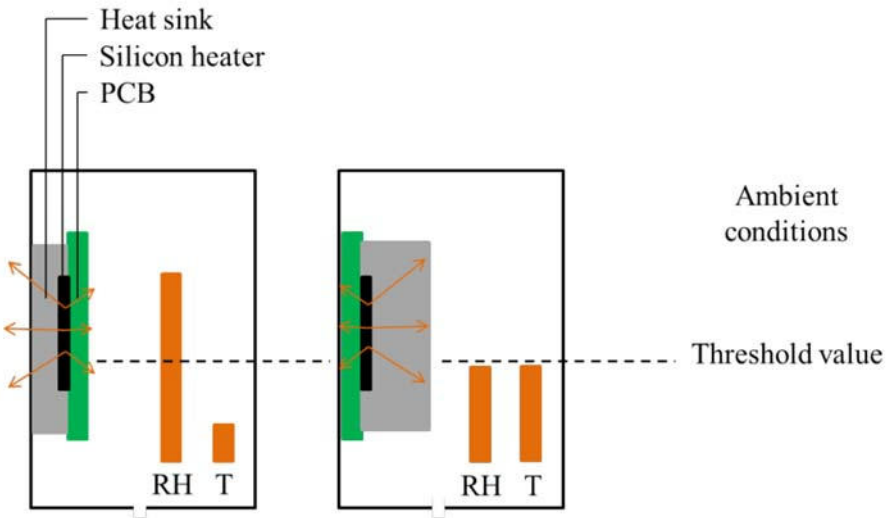

Fig. 1 The schematic diagram of the electronics enclosure and the components inside.

Table 1 Material and dimensions of the electronics enclosure and the components inside

	Material	Dimensions *[mm]*
enclosure	Aluminum	Inner 188×128×276 Outer 190×130×280
PCB	FR4 (epoxy circuit board material)	30×1.6×130

Heat producing component	Silicon	30×1.6×50
Thermal mass	Copper	80×10-70×100

To examine parametric dependencies, four cases, representing 4 different sizes for the thermal mass, are modeled (the width and the length of the thermal mass are constant for all the cases). Table 2 summarizes the thermal masses for the studied cases.

Table 2 The four studied cases.

Case number	Thermal mass size $[m^3]$
1	8×10^{-5}
2	2×10^{-4}
3	4×10^{-4}
4	5.6×10^{-4}

2.2 Modeling

2.2.1 CFD Simulation

In this study the air flow is assumed to remain laminar due to relatively low transient temperature gradients which will lead to low free convection-induced flow rates. The working fluid is modeled as a binary mixture (air + water vapor), and is therefore assumed to be Newtonian and compressible. The thermophysical properties (density, specific heat capacity, conductivity and viscosity) of the fluid depend on temperature and RH. However, in the temperature range of interest to this study the effect of RH on the thermophysical properties of air are small and are therefore neglected [20].

For a laminar compressible fluid flow (air, in this study), the mass, momentum and energy conservation equations are:

$$\frac{\partial \rho}{\partial t} + \nabla.(\rho \mathbf{u}) = 0 \qquad (\mathbf{1})$$

$$\rho\left(\frac{\partial \mathbf{u}}{\partial t} + \mathbf{u}.\nabla\mathbf{u}\right) = -\nabla p + \nabla.(\mu\left(\nabla\mathbf{u} + (\nabla\mathbf{u})^T\right) - \frac{2}{3}\mu(\nabla.\mathbf{u})\mathbf{I} + \mathbf{F} \qquad (\mathbf{2})$$

$$\rho c_p \frac{\partial T}{\partial t} + \rho c_p \mathbf{u}.\nabla T = \nabla.k(\nabla T) + Q \qquad (\mathbf{3})$$

where

$$F_z = -\rho g;\ F_x = F_y = 0 \qquad (\mathbf{4})$$

The species mass conservation equation is:

$$\frac{\partial c}{\partial t} + \mathbf{u}.\nabla c = D\nabla^2 \mathrm{c} \qquad (\mathbf{5})$$

In this work, first, the transient temperature and velocity profile are calculated by solving the coupled continuity, momentum and energy conservation equations. The calculated transient velocity and temperature distributions are then used for solving the mass species equation in order to derive the

moisture distributions (see Fig. 2). The water vapor-air binary diffusion coefficient is calculated from the following curve fit to the data of Bolz and Tuve [10]:

$$D = -2.775 \times 10^{-6} + \left(4.479 \times 10^{-8}\right)T + \times 10^{-6}(1.656 \times 10^{-10})T^2 \qquad (\mathbf{6})$$

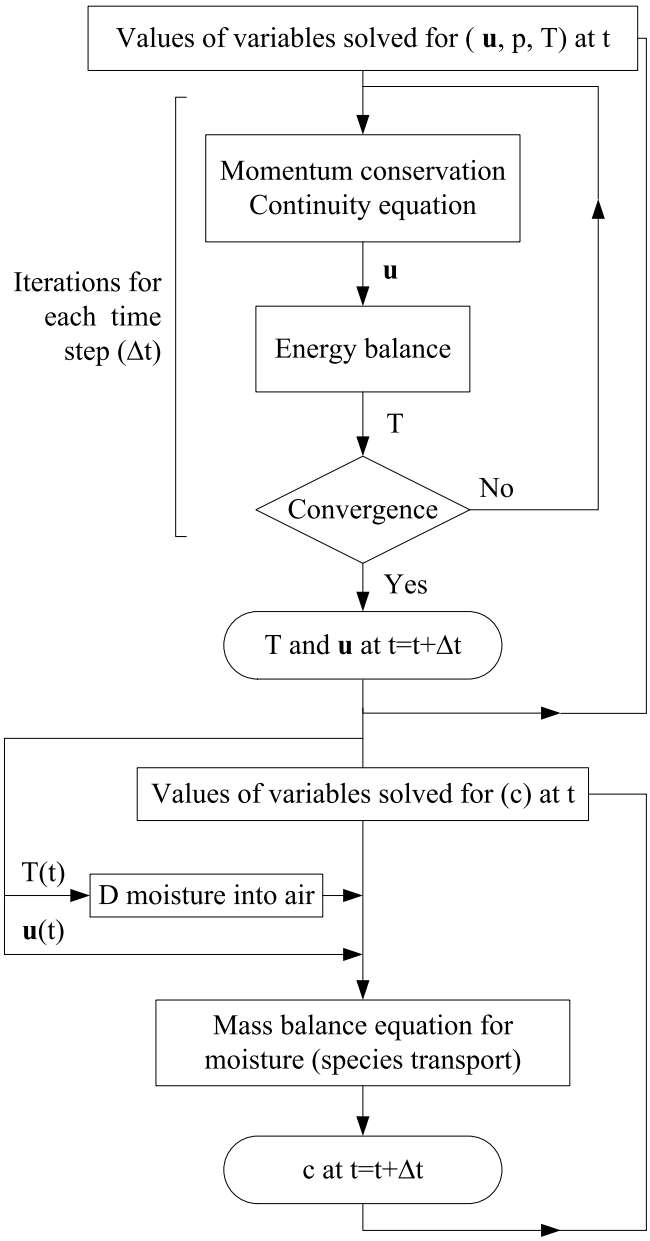

Fig. 2 Flowchart of the solution method.

The CFD simulations are conducted using the commercial finite element code COMSOL Multiphysics^{TM} version 5.2. In COMSOL Multiphysics^{TM}, the solvers split each problem–whether

linear or nonlinear– into one or more linear systems of equations by approximating the given problem with a linearized problem. In this work, velocity is part of the nonlinear solution of coupled energy and momentum transfer equations. The parallel direct solver (PARDISO) is utilized as the linear system solver. This memory efficient solver works on general sparse linear systems of the form Ax = b and use LU factorization on the matrix A to compute the solution x [21]. The time-dependent solver is based on the backward differentiation formula (BDF) method, with the maximum order set to two.
Due to the complicated structure of the modeled system, an unstructured mesh composed of tetrahedral elements is applied on the computational domain in all the simulations. The adaptive mesh refinement method is used to improve the mesh quality. Mesh convergence was examined to ensure the accuracy of the numerical results.

2.2.2 Lumped modeling

For the purpose of fast calculation of temperature of the electronics and moisture content of the air, an RC model is developed based on the CFD simulation results. Fig. 3 demonstrates the Cauer ladder circuit for the investigated system. The equivalent electrical circuit for steady state is only composed of resistances, the values of which can be obtained using well-known equations. For transient analysis, electrical capacitors are needed to represent the accumulation of energy in the materials. For conduction heat transfer the capacity can be easily calculated (see Table. 3); however, for convection, specifically natural convection, in addition to the fluid internal energy, energy is also stored in the form of kinetic energy of the fluid [16].

Table 3. Resistance and capacity values for equivalent electrical circuit analogy

	Resistance	**Capacitor**
Conduction	$\frac{L}{k \times A}$	$\rho \times V \times C_p$
Convection	$\frac{1}{h \times A}$	$studied\ in\ this\ work$

Generally, for natural convection, the heat transfer coefficient (h) is found from correlations of the following form [22]–[24]:

$$Nu = \frac{[q_s^{"}/(\Delta T)]L}{k} = \frac{hL}{k} = c(Gr \times Pr)^m = c(Ra)^m \qquad (7)$$

$$Gr_L = \frac{g\beta\,(\Delta T)L^3}{\nu^2} \qquad (8)$$

$$Pr = \frac{C_p \mu}{k} \qquad (9)$$

where Nu, Gr and Pr represent Nusselt, Grashof, and Prandtl numbers. The values of the constants c and m depend on geometry, configuration (orientation), and whether the natural convection boundary

layer is laminar or turbulent. Disregarding the material thermophysical property changes with temperature, the heat transfer coefficient (h) is evidently a function of temperature difference (ΔT). Furthermore, the capacity of the capacitor responsible for the natural convection also depends on temperature because the temperature gradient is the sole cause of the buoyant flow in the bulk of the fluid. In this work, the ΔT dependency of the convective resistance and capacity value is derived from the CFD simulations.

Thermal resistances of the medium are not the only resistances against heat transfer. When heat leaves a heat source of finite dimensions and enters a larger region, there is a spreading resistance. Generally, expressions that can be used for the calculation of this resistance depend on dimensionless geometric and thermal parameters [25]. Here, the spreading resistance is calculated using the following equation [23]:

$$R_{spreading} = \frac{1 - 1.410A_r + 0.344A_r^{\,3} + 0.043A_r^{\,5} + 0.034A_r^{\,7}}{4k_{sub}A_h^{\,1/2}} \qquad (\mathbf{10})$$

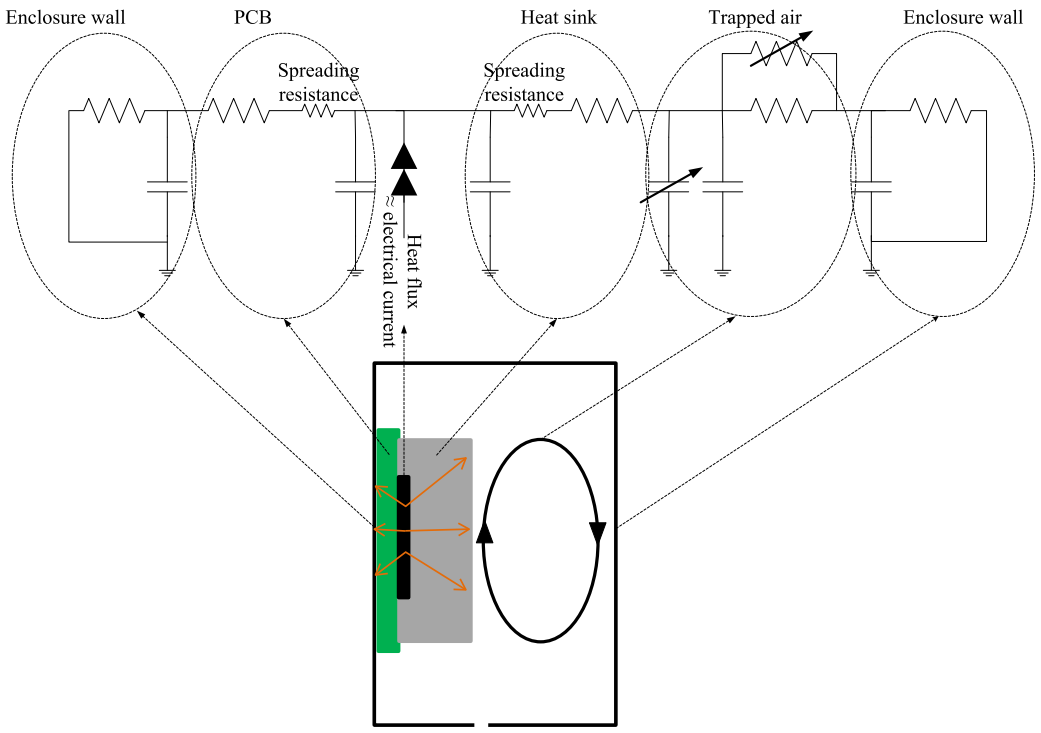

Fig. 3 The equivalent electrical Cauer ladder circuit for the heat transfer inside the enclosure.

The equivalent electrical circuit for moisture transfer is shown in Fig. 4. For mass transfer, the only resistance considered is associated with the small opening at the bottom of the enclosure, and the capacitance represents the volume of the cavity inside the enclosure [5]. This is justified because

saturated air-vapor condensations were not approached anywhere in the system in any of the simulations and therefor no condensation could have occurred in any of the simulations.
The equivalent circuits are implemented in the *Matlab/Simulink* version 2016b. *SimRF* and *Simscape* modules are used to represent and analyze the electrical circuit. The constant and variable resistances and capacitors are obtained from the SimRF module and the voltage and current sources are obtained from the Simscape module [26].

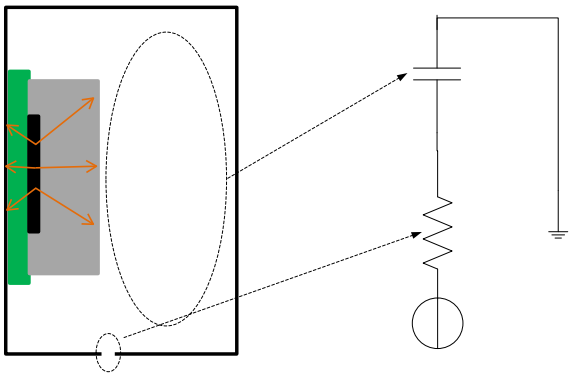

Fig. 4 The equivalent electrical Cauer ladder circuit for the moisture transfer.

2.2.3 Boundary and Operating Conditions

The ambient temperatures and vapor concentrations represent Copenhagen's conditions on typical summer days (July 1st and 2nd). The data have been derived from COMSOL database. Fig. 5 shows the ambient temperatures and moisture concentrations during the aforementioned two days. The water saturation vapor pressure is found from [27],

$$p_{sat} = 6140.7 \times 10^{\frac{7.5 \times (T - 273.15)}{T - 35.85}} \qquad (11)$$

The humidity ratio is defined as

$$RH = \frac{c}{c_{sat}} \qquad (12)$$

The concentration of water vapor in saturated air-water vapor mixtures can be found from steam property tables. For simplicity of computations, however, one may use

$$c_{sat} = \frac{p_{sat}}{R_{const} \times T} \qquad (13)$$

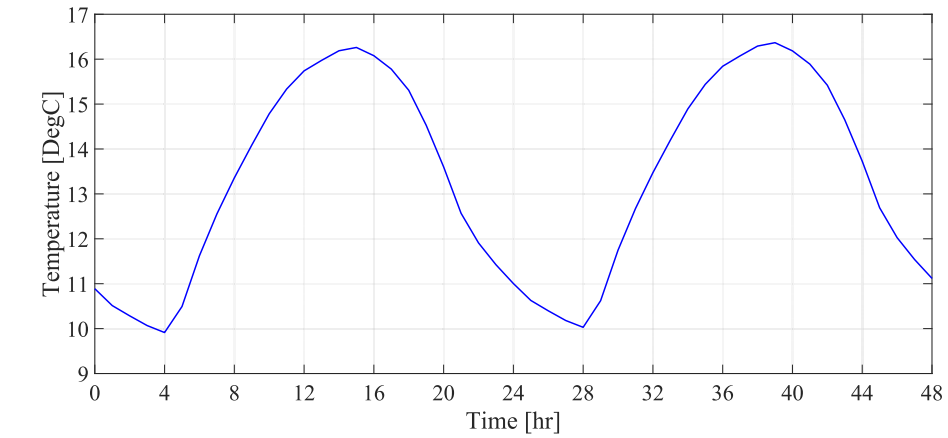

a

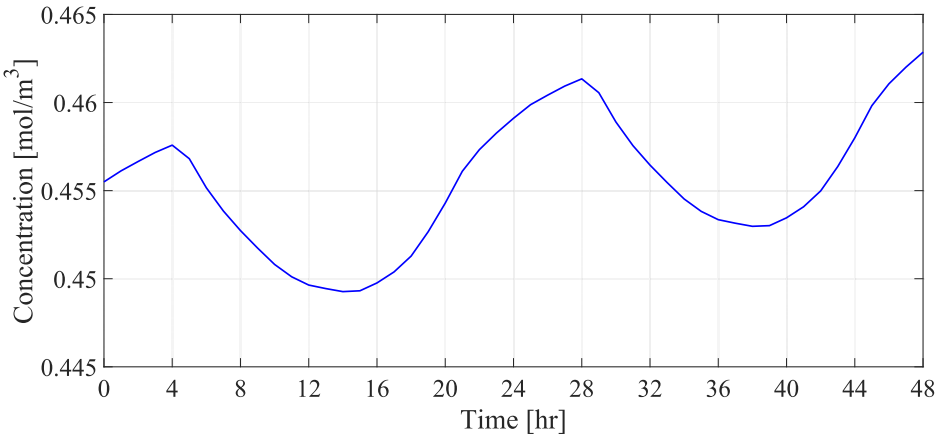

b

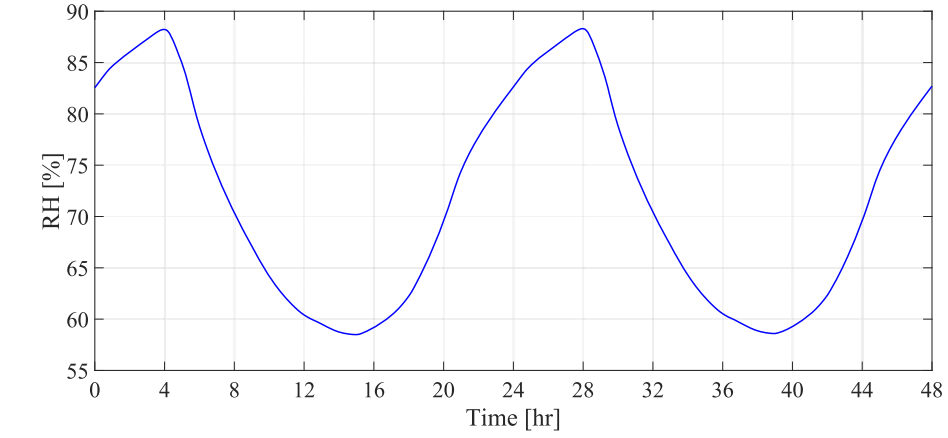

c

Figure 5 The a) temperature, b) moisture concentration and c) RH transient changes on July 1st and 2nd 2016 in Copenhagen.

In the simulated electronics enclosures the heater works on ON/OFF cycles in the first 24 hours but works continuously afterwards. Fig. 6 shows the heat flux of the heater versus time. For the CFD simulations, the dynamic boundary conditions are directly imported to and read by COMSOL Multiphysics^{TM}. However, for the RC simulations in Simulink/ Matlab, the scattered data are converted into mathematical functions using the MATLAB curve fitting toolbox version 2016b; so that the convergence is achieved easier.

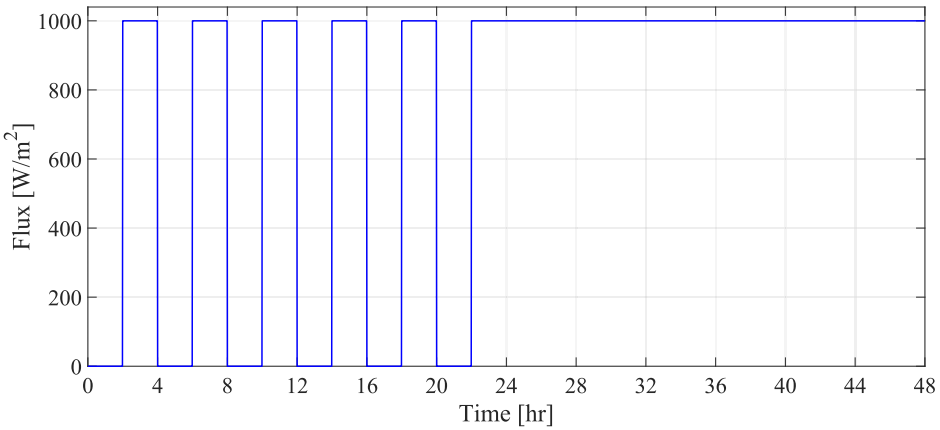

Figure 6 The heat flux emitted from the heater versus time.

3 Results and Discussion

3.1 CFD results

The parametric effect of different sizes of copper thermal mass on the temperature of the PCB is shown in Fig. 7. The temperature of the PCB is affected by the size of the thermal mass as well as natural convection in the air trapped inside the enclosure. All other parameters are kept unchanged in the depicted four cases. During the ON/OFF cycle, the amplitudes of the temperature changes are damped as the thickness of the thermal mass is increased. Furthermore, when the heater is working continuously, a larger thermal mass cools down the PCB more than a smaller one. As expected, with a bigger thermal mass, the temperature of the thermal mass will be lower during the time that the heater is on. Lower temperature difference in the trapped air leads to a lower Gr and therefore a lower Nu and a weaker natural convection heat transfer coefficient. Thus, on one hand increasing the size of the thermal mass enhances conduction which tends to help the cooling down of the PCB. On the other hand, increasing the size of the thermal mass slows down free convection which has an opposite effect on the cooling of the PCB. It should be emphasized, however, that this cooling process is dynamic. The thermal behavior of the system is influenced by the cycle period and the heat flux as well.

Fig. 8 shows the variation of the average RH in the enclosure with time for the aforementioned four cases. The moisture concentration in the ambient air remained almost unchanged during the two days. As a result, the moisture concentration difference between the ambient air and the air trapped inside the enclosure (the driving force for moisture transfer) was small and consequently the vapor mass transfer

through the opening was insignificant. Thus, the RH inside the enclosure was mostly affected by temperature rather than moisture concentration.

In general, there is a risk of condensations when the electronics are in OFF mode, especially during early hours of the day when the ambient temperature is low (see Fig. 5a). Increasing the thickness of the thermal mass from 10 *mm* to any of the other three values reduces the RH at the vicinity of the PCB. However, the largest thermal mass does not necessarily provide the most desirable local climate for the PCB, and this is due to the dynamic nature of the heat transfer in this system. For instance, in the second, third and fourth cycles the 25 mm and 50 mm thickness thermal masses provide the surface of the PCB with a lower RH than the 70 mm-thick thermal mass-one. Therefore, the size of the thermal mass should be optimized based on several parameters including the working cycle of the electronics, the rate of heat generation, and the ambient conditions.

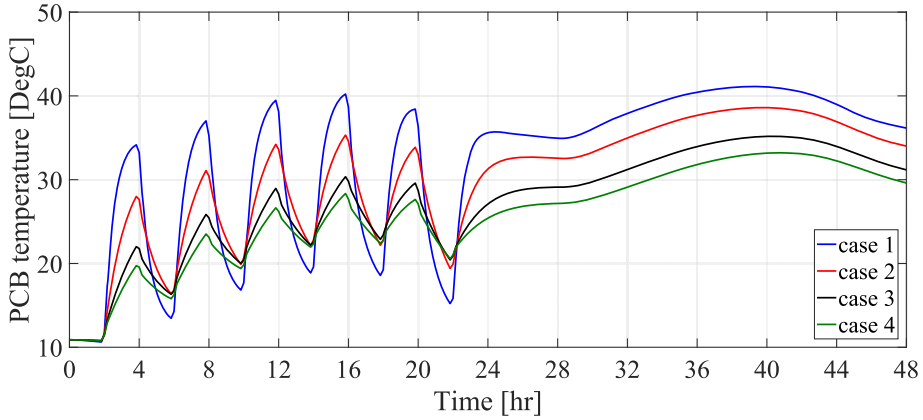

Figure 7 The average PCB temperature for the four case studies versus time.

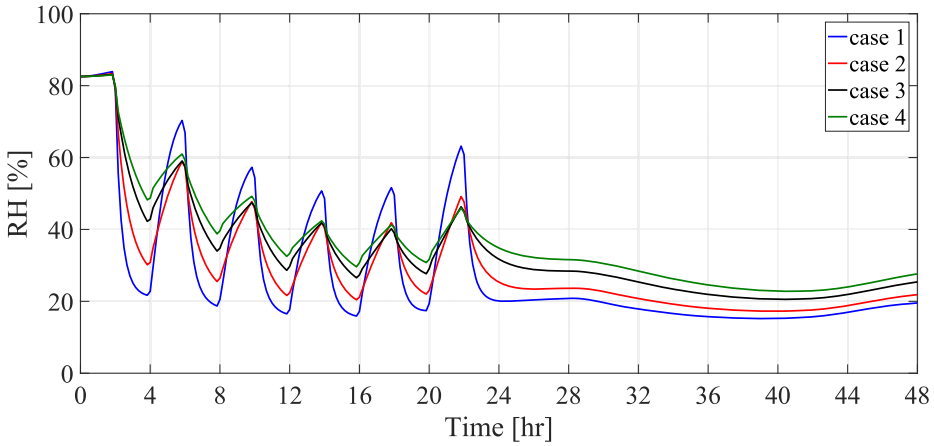

Figure 8 The average RH on the PCB for the four case studies versus time.

The dependence of Nu on ΔT and Ra for the natural convection is displayed in Fig.9 for the four cases. In comparison with the case with the largest thermal mass, the air trapped inside the enclosure with the

smaller thermal mass experiences higher temperature gradients and therefore experiences a slightly larger range of variation in Ra. The profiles of Nu versus Ra and ΔT are approximately the same for all four cases, in terms of trend as well as magnitude both, however. The variations of Nu as a function of Ra and ΔT are monotonic and appear to follow a power function, while the relation between Ra and ΔT is approximately linear. These functional dependencies are of course the result of the complex dependence of Nu and Ra on fluid properties as well as geometry. However, given that in practice the fluid properties (i.e., properties of air that is partially saturated with water vapor) vary only over small ranges, similar functional dependencies should be expected. For a specific geometry it should therefore be possible to derive simple empirical correlations for the calculation of the Nu and Ra using the ΔT . Equation (14) demonstrates Nu versus Ra and the ΔT for the system studied here (see Fig. 9)

$$Nu = 9.968(\Delta T)^{0.2353} = 0.5096(Ra)^{0.2536} \qquad (14)$$

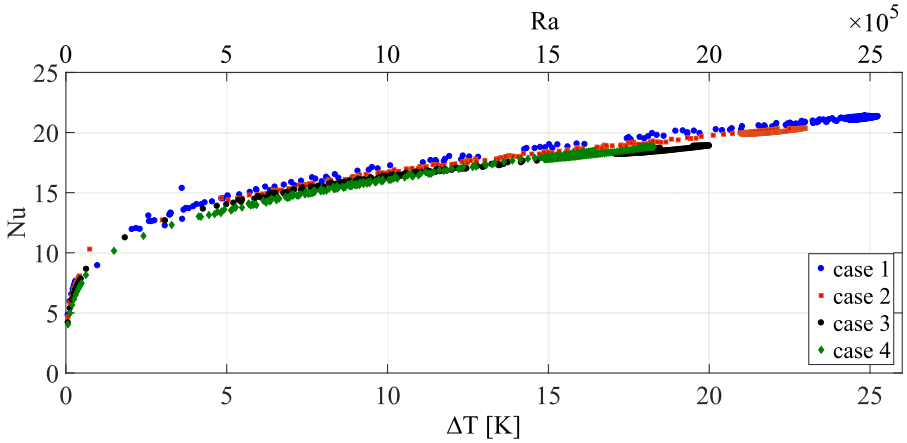

Figure 9 The Nu correlation with Ra and the temperature difference

In transient convection problems the change in the kinetic energy of the fluid must be considered in the energy balance. The relative significance of stored kinetic energy in electronics enclosures will now be discussed. The contribution of fluid kinetic energy in natural convection electronics cooling was discussed by Khane et al. [16] in 2010. Khane et al. performed a set of numerical simulations representing the Rayleigh–Bénard convection in an experimental apparatus. The portion of the kinetic energy stored in the fluid was determined by monitoring the heat flux from the heat sink while a constant flux was imposed by the heat source. The difference between the two fluxes represented the total rate of energy gain by the fluid (internal energy + the energy associated with the motion). The rate of accumulation of kinetic energy was then determined by subtracting the rate of accumulation of internal energy from the total rate of energy accumulation in the fluid [16]. In this work, the kinetic energy of the trapped air is directly estimated by the forthcoming integration over the fluid volume:

$$E_K = \frac{1}{2}\int_V \rho(|\vec{U}|)dV \qquad (15)$$

where the ρ and $\vec{U}$ are calculated by the full 3D CFD simulations. Fig. 10 shows the kinetic energy changes inside the system versus the temperature difference that the trapped air experiences. For design and analysis convenience, the correlation between the kinetic energy and the temperature of the air should be derived. We define the design energy capacity according to

$$C_{KE} = \frac{\Delta E_{KE}}{\Delta T} \qquad (16)$$

However, a comparison between the thermal capacity and the kinetic energy capacity of the fluid in the systems considered revealed that the stored kinetic energy is smaller than the stored thermal energy, typically by 9 orders of magnitude, and could be neglected, as expected.

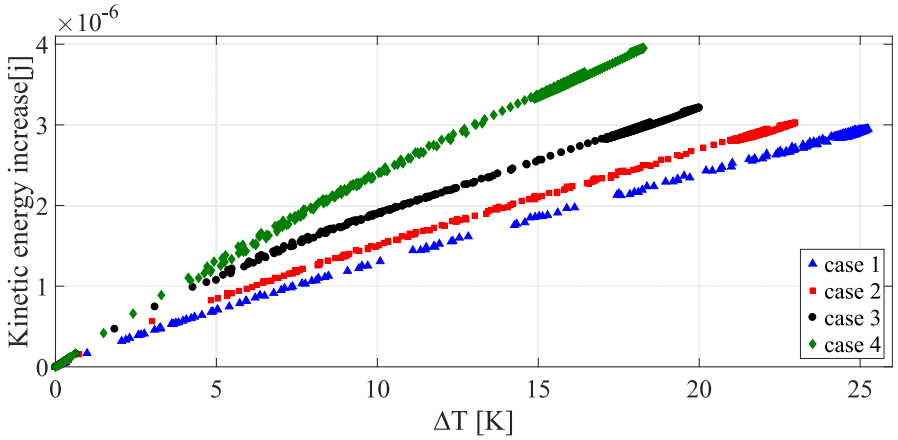

Figure 10 The Kinetic energy changes for the trapped air inside the enclosure.

4.2 RC results

Using the derived resistance and capacity values from the CFD simulations for the air trapped inside the enclosure, an RC-based modeling is now conducted for the aforementioned four cases that are summarized in Table 1.

Fig. 11 compares the results from the RC method with the CFD simulations. For all the four cases the RC model is underestimating the temperature during the two days, except for about 10 hours in the second day for case 4 where the difference between the RC and CFD results is less than 1°C. Despite this, the lumped analysis is presenting the same trend during both ON/OFF cycles, as well as during the time when the heating is continuously on. There are several assumptions in the RC analysis that cause the differences with the CFD calculations, such as the 1D heat transfer assumption, uniformity of the temperature in each of the thermal bodies as well as the trapped air, and the potential inaccuracies in the correlations for the spreading resistance (see Equation (10)) and Nu (see Equation (14)).

Figure 11 shows that for case 4, where the heatsink is the largest, the CFD result is very close to the RC estimation. On the other hand the discrepancy between the RC model and CFD simulations is the

largest for case 1, where the heatsink inside the enclosure is the smallest and the system is experiencing the largest temperature change. Evidently the discrepancy between the RC model and CFD simulations diminishes as the temperature fluctuations diminish, and is large only when such temperature fluctuations are drastic.

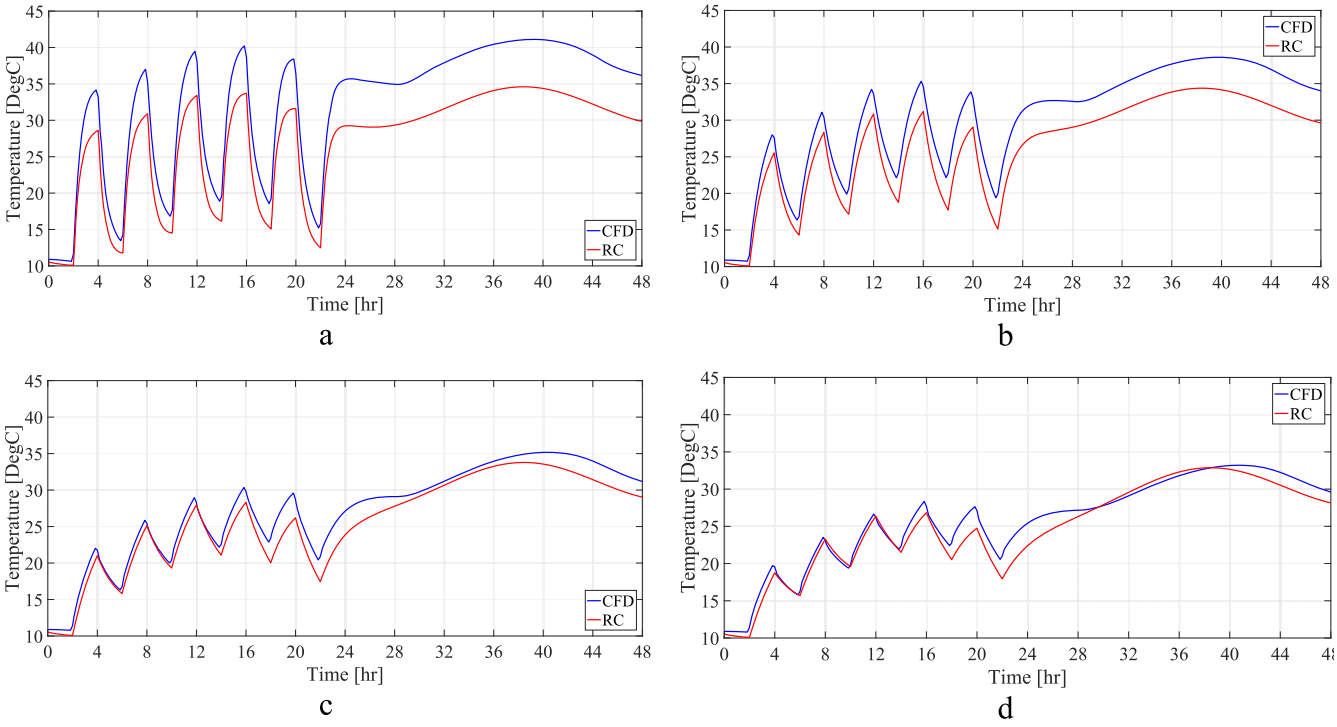

Figure 11 The PCB temperature for a) case1, b) case2, c) case3 and d) case4

In the analysis presented here the vapor concentration is assumed to remain uniform inside the enclosure. This assumption is reasonable, except at very close proximity to cooled surfaces when condensation takes place. The air recirculation caused by natural convection ensures the essentially uniform distribution of vapor concentration in the gas bulk, in particular when condensation does not occur. The vapor concentration varies with time, of course, primarily because of the variation of the vapor concentration in the ambient air. Fig. 12 demonstrate the variation of vapor concentration with time over the two days. As the heatsink size increases, the volume of the air inside the system is decreased and consequently, the response to the ambient changes becomes faster. However, in general, the variation of the ambient moisture concentration is small and smooth. Nevertheless, the RH in the enclosure varies over a significant range, primarily due to the change in temperature.

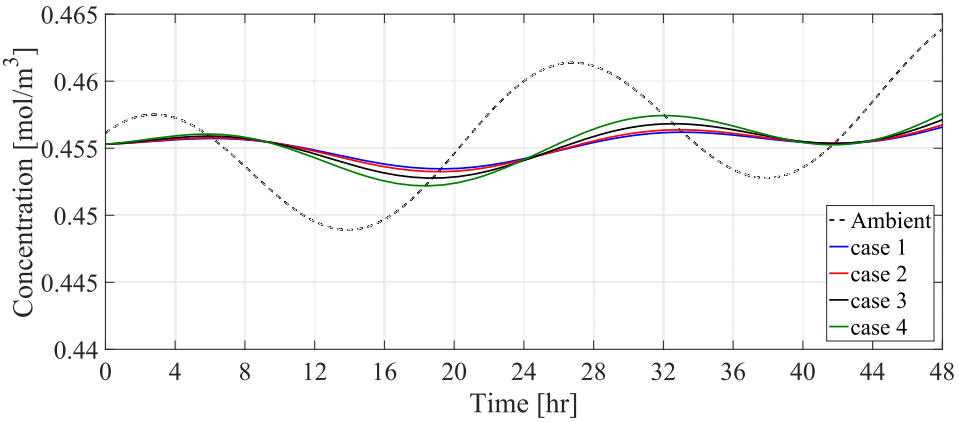

Figure 12 The average moisture concentration inside the enclosure versus time.

It should be emphasized that, in spite of its relatively slight discrepancy with detailed multi-dimensional CFD simulations, the RC method is a useful design tool because it is faster than CFD simulations by orders of magnitude. Thus, for short-term transients a reliable RC model can be used for scoping analysis, making multiple-iteration design procedures feasible. More importantly, RC models can be used for long-term (month or even year-long) simulations. Fig. 13, for example, shows the temperature, moisture concentration and RH histories for the enclosure represented by case 4, in response to the previously described ON/OFF cycles for the months of June, July and August in Copenhagen. For calculating RH for 92 days, these simulations took only 7 minutes on a personal computer with Intel Core i7 (4600M / 2.9 GHz) CPU. On the other hand, a similar calculation using CFD, covering only two days, took about 1460 mins (almost 1 day) on 20 nodes of scientific Linux 6.4 cluster; where each node was configured with Intel Xeon Processor X5550.

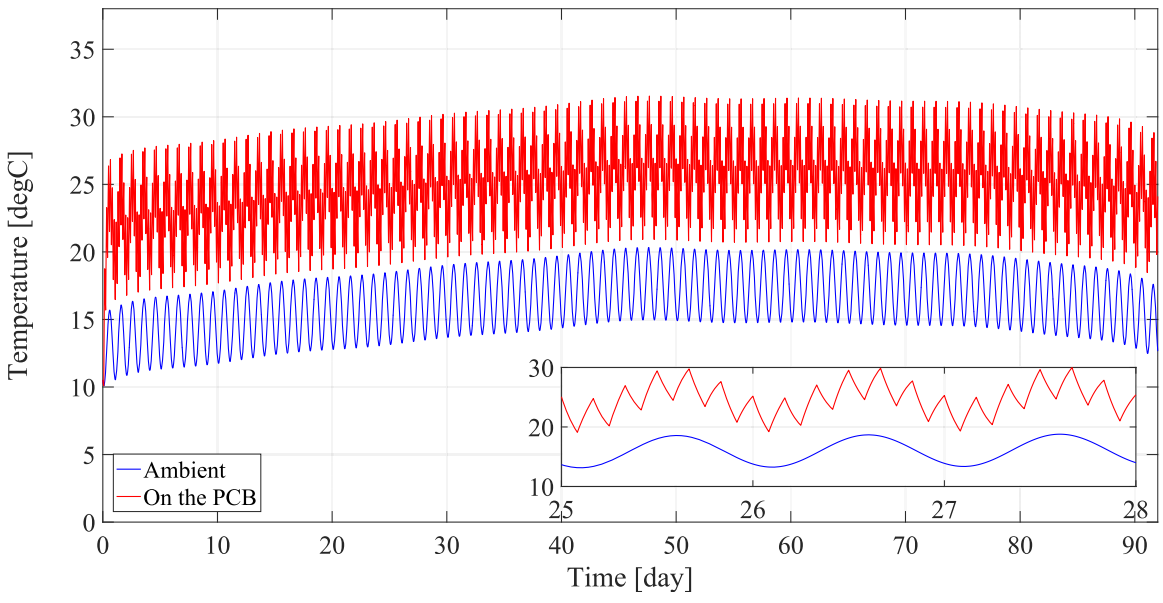

a

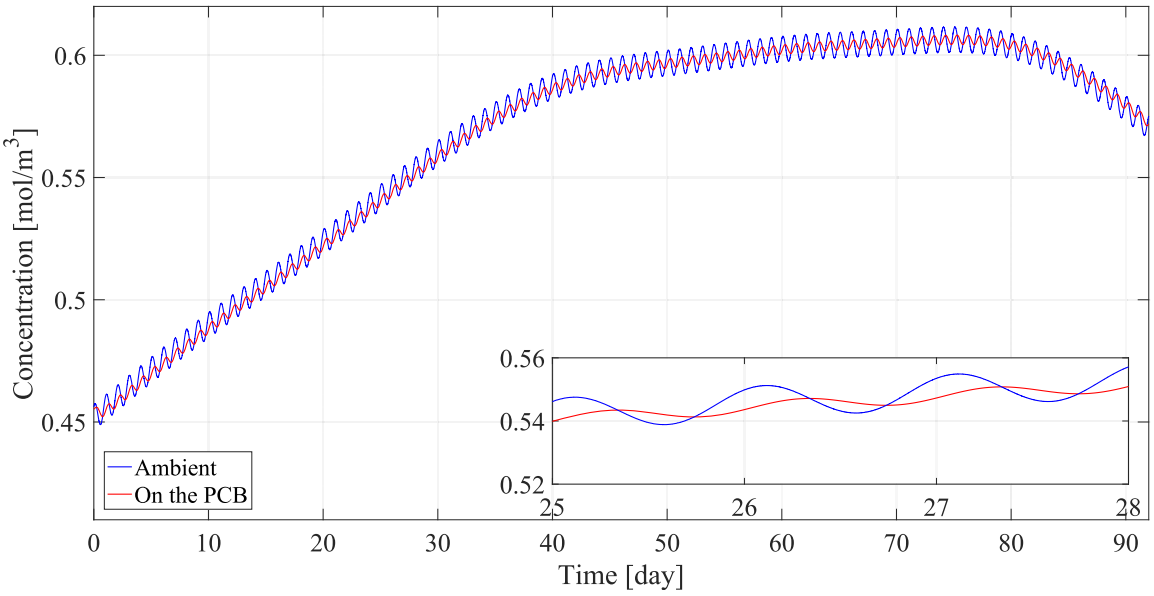

b

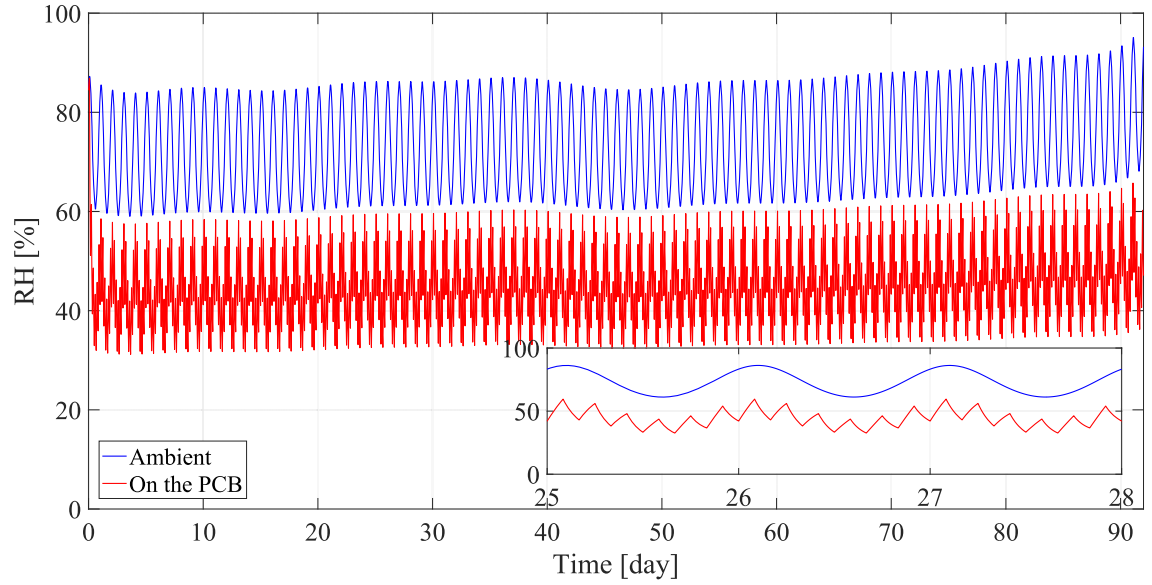

c

Figure 13 The average a) temperature, b) moisture concentration and c) RH on the PCB on June, July and August in Copenhagen.

The analysis presented here also confirms the importance of an optimal design of the thermal mass for electronics enclosures, so that the risk of condensation can be eliminated. The RH typically has its highest value during the early hours of the day; it then decreases for some time before it increases again. The designer should make sure that the thermal mass provides a long enough delay in the heat transfer, so that the stored heat is released when the RH is close to its peak value.

4 Conclusions

In this study, a 3D CFD model was developed to investigate the effect of a thermal mass (typically made of copper), which is installed for storing the heat from the electronics working under cyclic conditions, on the local climate inside a typical electronics enclosure. A Cauer ladder RC model was also developed to predict the RH on the PCB inside the enclosure. The capacitance and resistance values for the natural convection were derived based on the CFD results. Simulations were performed for a typical enclosure containing electronics and exposed to Copenhagen ambience for a period of two days, where four cases with different thermal masses were analyzed. The following concluding remarks can be made:

- The main function of a thermal mass in an electronics enclosure is to maintain the PCB temperature below the threshold value. However, a well-designed thermal mass can also be used for storing the heat generated by the electronics, and releasing the heat with a time delay in order to maintain RH low enough to avoid condensation.
- Due to the dynamic nature of the heat transfer in an electronics enclosure, an excessively large thermal mass does not necessarily provide the most desirable conditions for the PCB. The size of the thermal mass should be optimized based on the enclosure's boundary and operational conditions, including the working cycle of the electronics, the amount of the generated heat, and the ambient conditions.
- In an enclosure with fixed geometry the dependence of Nu representing natural convection on Ra and ΔT inside the enclosure follows a simple power function; furthermore, a linear relation is observed between Ra and ΔT. These simple correlations can be utilized for fast scoping analyses.
- A comparison between the magnitudes of the thermal energy and kinetic energy that are stored in the air inside a typical enclosure reveals that the kinetic energy is small and can be neglected.
- The Cauer ladder RC model slightly underestimated the temperature during the two days in all the four cases. The typical discrepancy was about 1 to 7 [°C]. However, the lumped RC model successfully predicted the trends of temperature and RH changes inside the enclosure. The technique can be useful for scoping analysis for short transients, and more importantly for long-term transients.
- Spreading resistances are important for both the heatsink and PCB and should be considered in the analysis of electronics enclosures.
- Even when the daily ambient moisture concentration changes are small and smooth, the RH undergoes drastic variations primarily because of the variation of ambient temperature.

Acknowledgement

The current research has been conducted as part of the ICCI project from the Danish Council for Independent Research, Technology and Production (FTP) and the IN SPE project from the Danish Innovations Fonden which are highly acknowledged. Moreover, the authors would like to acknowledge the commitment and help of the industrial partners in this project.

References

[1] I. Belov, J. Ryden, J. Lindeblom, Y. Zhang, T. Hansson, F. Bergner, and P. Leisner, "Application of CFD modelling for energy efficient humidity management of an electronics enclosure in storage under severe climatic conditions," in *International Conference onThermal, Mechanical and Multi-Physics Simulation and Experiments in Microelectronics and Micro-Systems, EuroSimE*, 2008, pp. 1–8.

[2] R. Ciprian and B. Lehman, "Modeling effects of relative humidity, moisture, and extreme environmental conditions on power electronic performance," in *IEEE Energy Conversion Congress and Exposition*, 2009, pp. 1052–1059.

[3] J. Punch; R. Grimes; G. Heaslip ;T. Galkin;K. Viikevainen; V. Kyyhkynen and E. Elonen, "Transient hygrothermal behaviour of portable electronics," in *International Conference on Thermal Mechunical and Multiphysics Simularion and Experiments in Micro-Electronics and Micro-Sysrem*, 2005, pp. 398–405.

[4] S. Kremp, O. Schilling, and V. Müller, "Empirical study on humidity conditions inside of power modules under varying external conditions," in *International Conference on Integrated Power Electronics Systems*, 2016, pp. 1–6.

[5] M. Tencer, "Moisture ingress into nonhermetic enclosures and packages. A quasi-steady state model for diffusion and attenuation of ambient humidity variations," *Electron. Components Technol.*, pp. 196–209, 1994.

[6] P. Shojaee Nasirabadi, H. Conseil-gudla, S. Mohanty, M. Jabbari, R. Ambat, and H. Jesper, "Semi-Empirical Prediction of Moisture Build-up in an Electronic Enclosure Using Analysis of Variance (ANOVA)," in *IEEE Electronics Packaging Technology Conference, EPTC*, 2016, pp. 785–790.

[7] M. Tencer and J. S. Moss, "Humidity management of outdoor electronic equipment: Methods, pitfalls, and recommendations," *IEEE Trans. Components Packag. Technol.*, vol. 25, no. 1, pp. 66–72, 2002.

[8] N. Dahan, A. Vanhoestenberghe, and N. Donaldson, "Moisture ingress into packages with walls of varying thickness and/or properties: A simple calculation method," *IEEE Trans. Components, Packag. Manuf. Technol.*, vol. 2, no. 11, pp. 1796–1801, 2012.

[9] P. Shojaee Nasirabadi, M. Jabbari, and J. H. Hattel, "Numerical simulation of transient moisture and temperature distribution in polycarbonate and aluminum electronic enclosures," in *International Conference on Thermal, Mechanical and Multi-Physics Simulation and Experiments in Microelectronics and Microsystems, EuroSimE*, 2016, pp. 1–6.

[10] P. Shojaee Nasirabadi, M. Jabbari, and J. H. Hattel, "CFD simulation and statistical analysis of moisture transfer into an electronic enclosure," *Appl. Math. Model.*, vol. 44, pp. 246–260, 2017.

[11] S. Kremp and O. Schilling, "Realistic climatic profiles and their effect on condensation in encapsulated test structures representing power modules," *Microelectron. Reliab.*, vol. in press, 2017.

[12] H. Conseil, V. C. Gudla, M. S. Jellesen, and R. Ambat, "Humidity Build-Up in a Typical

Electronic Enclosure Exposed to Cycling Conditions and Effect on Corrosion Reliability," *IEEE Trans. Components, Packag. Manuf. Technol.*, pp. 1–10, 2016.
[13] C. Sapia and G. Sozio, "CFD transient model of the natural convection heat transfer for an heat sink effects of increasing surface and fins spacing," in *International Workshop onThermal Investigations of ICs and Systems, THERMINIC*, 2011, pp. 1–6.
[14] V. Eveloy, J. Lohan, and P. Rodgers, "A benchmark study of computational fluid dynamics predictive accuracy for component-printed circuit board heat transfer," *IEEE Trans. Components Packag. Technol.*, vol. 23, no. 3, pp. 568–577, Sep. 2000.
[15] D. Chiozzi, M. Bernardoni, N. Delmonte, and P. Cova, "A simple 1-D fi nite elements approach to model the effect of PCB in electronic assemblies," *Microelectron. Reliab.*, vol. 58, pp. 126–132, 2016.
[16] V. Khane and S. Usman, "Further on integrator circuit analogy for natural convection," *Nucl. Eng. Des.*, vol. 240, pp. 609–615, 2010.
[17] R. Huang, W. Sheu, and C. Wang, "Orientation effect on natural convective performance of square pin fin heat sinks," *Int. J. Heat Mass Transf.*, vol. 51, pp. 2368–2376, 2008.
[18] S. S. Anandan and V. Ramalingum, "Thermal Management of Electronics: a Review of Literature," *Therm. Sci.*, vol. 12, no. 2, pp. 5–26, 2008.
[19] K. S. Ong, C. F. Tan, K. C. Lai, and K. H. Tan, "Heat spreading and heat transfer coefficient with fin heat sink," *Appl. Therm. Eng.*, vol. 112, pp. 1638–1647, 2017.
[20] P. T. Tsilingiris, "Thermophysical and transport properties of humid air at temperature range between 0 and 100 °C," *Energy Convers. Manag.*, vol. 49, no. 5, pp. 1098–1110, 2008.
[21] G. A. Reis, I. V. M. Tasso, L. F. Souza, and J. A. Cuminato, "A compact finite differences exact projection method for the Navier – Stokes equations on a staggered grid with fourth-order spatial precision," *Comput. FLUIDS*, vol. 118, pp. 19–31, 2015.
[22] J. P. Holman, *Heat Transfer*, 10th ed. Jefferson City: McGraw-Hill, 2010.
[23] T. L. Bergman, A. S. Lavine, F. P. Incropera, and D. P. Dewitt, *Fundamentals of Heat and Mass Transfer*, 7th ed. Jefferson City: John Wiley & sons, 2011.
[24] S. M. Ghiaasiaan, *Convective Heat and Mass Transfer*. New York: Cambridge University Press, 2011.
[25] M. M. Yovanovich, Y. S. Muzychka, and J. R. Culham, "Spreading Resistance of Isofux Rectangles and Strips on Compound Flux Channels," *J. Thermophys. HEAT Transf.*, vol. 13, no. 4, pp. 495–500, 1999.
[26] "Matlab user's guide," 2012.
[27] "COMSOL Multiphysics 5.1 User Guide," 2015.

Appendix D
Paper IV

Semi-Empirical Prediction of Moisture Build-up in an Electronic Enclosure Using Analysis of Variance (ANOVA)

Parizad Shojaee Nasirabadi[1, *], Hélène Conseil-Gudla[2], Sankhya Mohanty[1], Masoud Jabbari[3], Rajan Ambat[2] and Jesper H. Hattel[1]

[1] Process Modelling Group, Department of Mechanical Engineering, Technical University of Denmark
Nils Koppels Allé, 2800 Kgs. Lyngby, Denmark

[2] Materials and Surface Engineering, Department of Mechanical Engineering, Technical University of Denmark
Nils Koppels Allé, 2800 Kgs. Lyngby, Denmark

[3] Warwick Manufacturing Group (WMG), University of Warwick, Coventry CV4 7AL, UK.

[*] parnas@mek.dtu.dk, +45 45254754

Abstract

Electronic systems are exposed to harsh environmental conditions such as high humidity in many applications. Moisture transfer into electronic enclosures and condensation can cause several problems as material degradation and corrosion. Therefore, it is important to control the moisture content and the relative humidity inside electronic enclosures. In this work, moisture transfer into a typical polycarbonate electronic enclosure with a cylindrical shape opening is studied. The effects of four influential parameters namely, initial relative humidity inside the enclosure, radius and length of the opening and temperature are studied. A set of experiments are done based on a fractional factorial design in order to estimate the time constant for moisture transfer into the enclosure by fitting the experimental data to an analytical quasi-steady-state model.

According to the statistical analysis, temperature and the opening length are found as the most significant factors. Based on analysis of variance of the derived time constants, a semi-empirical regression model is proposed to predict the moisture transfer time constant with an adjusted R^2 of 0.98; which demonstrated that the model can be used for estimation with a reasonable accuracy. The results show that the temperature has the highest effect on the moisture transfer time constant. Furthermore, the length of the opening is found to be more influential on the moisture transfer time constant at lower temperatures compare to high temperatures, according to the predictions made through the semi-empirical model.

Introduction

More and more electronics are being used in climatically harsh environments [1]. A significant portion of environment-related reliability problems is either directly or indirectly related to high atmospheric humidity [2]. Exposure to high humidity is responsible for several harmful effects on electronic devices, as they cause corrosion and electrochemical migration, which lead to changes in resistance and short circuits [1], [3], [4]. Moreover, the presence of moisture in a printed circuit board assembly (PCBA) alters its quality, functionality, thermal performance, and thermo-mechanical properties, thereby affecting the overall device performance [5]. It should be noticed that all moisture related failures are related to the relative humidity (RH) rather than the absolute humidity [2]. In order to protect the electronic devices from such failures, it is essential to keep the RH inside the electronic enclosure at a low level [6]. The critical range of humidity for corrosion failure modes is 60–90% depending on the electronics design and cleanliness [2], [4], [7].

There are two sources of moisture ingress into a sealed electronic enclosure. The first is the moisture that is sealed into the package during manufacture. This quantity of water is fixed at assembly time and the moisture may reside in the ambient atmosphere, be adsorbed to free surfaces or dissolved in component materials. Even for hermetically sealed enclosures, this moisture must be considered. The second source of moisture is leakage or permeation into the package from the external environment. The magnitude of this contribution increases with storage time and depends on the details of the seal design as well as the storage conditions [8].

In order to achieve a suitable design for reliability, it is important and crucial to develop a predictive numerical modeling tool that can be used at the early design stage for quick risk assessment of new products subjected to moisture loads [9]. Tencer [10] developed a simple quasi-steady-state (QSS) model with the purpose of understanding the factors governing the kinetics of moisture transfer into enclosures in terms of the properties of the applied materials and the ambient conditions analytically. The model estimates the time constants for moisture diffusion through plastic walls and openings. However, the model is difficult to apply when the geometry is complex and also when several materials are employed in the body of the enclosure [11]. Tencer et al. [2] also discussed a method for the absolute humidity control in another study. The method relies on minimization of water ingress through a careful selection of appropriate materials and design, and at the same time uses a desiccant to remove the water which makes its way into the enclosure, theoretically. Dahan et al. [6] used an electrical analogy to adapt the QSS model to the moisture ingress into a package containing walls or elements of different thicknesses or properties. Belov et al. [12] developed a CFD modelling tool for investigation of moisture transfer into a non-hermetic electronic enclosure containing a number of printed circuit boards. Shojaee et al. [13][14] also investigated moisture ingress into a polycarbonate electronic enclosure using CFD.

In this paper, a semi-empirical regression model is presented for prediction of time constants for humidity build-up in an electronic enclosure. The model is developed by the analysis of variance (ANOVA) of the experimental data in a factorial design frame work. Factorial designs are widely used in experiments involving several factors where it is necessary to study the joint effect of the factors on a certain response. The most important of these designs is that of k factors, each

978-1-5090-4369-9/16/$31.00 ©2016 IEEE

at only two levels. In a 2^k factorial design, it is easy to express the results of the experiment in terms of a regression model. The regression model approach can also be intuitive [15]. In this work, the effects of two geometrical parameters (length and radius of a cylindrical shape opening in the enclosure) as well as two environmental parameters (temperature and initial RH) are investigated using a fractional factorial design. The investigated range of parameter is based on the manufacturing feasibility and the operating conditions proposed by our industrial partners.

Methods

A. Experimental Set-up

The enclosures used for the investigation are made of PC with dimensions of 280 [mm] ×190 [mm] ×130 [mm]. The gasket for the enclosure is made of polyurethane. The IP rating for the enclosure is 66/67, which demonstrates that the enclosures assure a total protection against dust and a protection against strong jets of water or against the effect of immersion in water at a depth of 15 [cm] to 1 [m] [16]. Either a hole with a radius of 0.5, 1 or 1.5 [mm] is drilled on the bottom side of the enclosures, with a corresponding thickness of 2 mm, or a tube with inner radius of 0.5, 1 or 1.5 [mm] and length of 26 and 50 [mm] was mounted on the bottom side of the enclosure. Calibrated sensors are placed in the enclosures for monitoring the temperature and RH (PT1000 and HIH4021, Honeywell), connected to a data logging system (Model 2700 Multimeter, Keithley Instruments). The enclosures are exposed to different climate environments in a climatic chamber (Espec, Escorp PL-3KPH). Fig. 1 shows the experimental set-up.

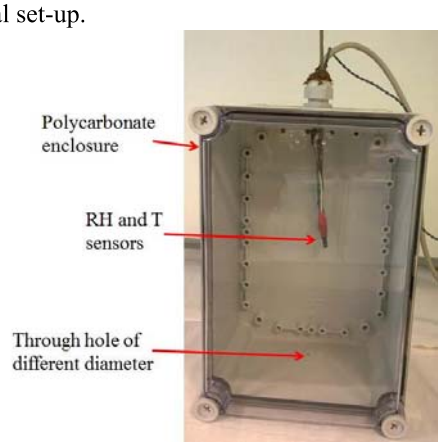

Fig. 1. The experimental set-up.

B. Factorial Design

The effects of four factors on the RH time constants are investigated, namely initial RH inside the enclosure, radius of the opening, length of the opening and operating temperature. Table 1 shows the range of the investigated factors.

Table 1. The investigated parameters and their ranges.

Factor	Notation	Low level -	High level +	Unit
Initial RH	A	40	70	%
Opening radius	B	0.5	1.5	mm
Opening length	C	2	50	mm
Temperature	D	25	60	°C

A full 2^4 factorial design proposes 16 cases of experiments. However, considering the fact that such experiments are very time-consuming it is important to keep the number of the tests as few as possible. Thus a fractional factorial design (2^{4-1}) is used in this work. Moreover, instead of replicating all the experiments, the center point is replicated twice so that the repeatability of the experiments is checked. The presence of center points in two-level factorial designs provides protection against curvature. Furthermore, adding center points to the design allows an independent estimate of error to be obtained [17]. The experiments proposed by the half fractional factorial design are summarized in Table 2.

In a full factorial design, the effects of all the factors are determined individually. On the other hand, in a fractional factorial design the effects are aliased together. In the fractional factorial design used in this study, the defining relation is taken as $I=ABCD$; so that the proposed design has the resolution of IV, which is the highest possible for a 2^{4-1} design. In such designs no main effect is aliased with any other main effect or with any two-factor interaction, but two-factor interactions are aliased with each other [15]. The alias structure of the design in this work is as following:

[A] → A + BCD
[B] → B + ACD
[C] → C + ABD
[D] → D + ABC
[AB] → AB + CD
[AC] → AC + BD
[AD] → AD + BC

Table 2. The proposed experiments by the fractional factorial design.

Case #	A	B	C	D
1	40	0.5	2	25
2	70	0.5	2	60
3	40	1.5	2	60
4	70	1.5	2	25
5	40	0.5	50	60
6	70	0.5	50	25
7	40	1.5	50	25
8	70	1.5	50	60
9	55	1	26	42.5
10	55	1	26	42.5
11	55	1	26	42.5

In a 2^k factorial design (full or fractional), the model for analyzing responses is given by:

$$y=\beta_0+\sum \beta_j x_j+\sum\sum \beta_{ij} x_i x_j+\epsilon \quad (1)$$

, where y is the response, the β's are parameters whose values are to be determined, x's are variables that represent the factors and ϵ is a random error term. In this approach, higher-order interaction effects are initially neglected. However, the presence of such effects is checked and in case, they can be considered using a suitable design [13].

The transient RH build-up is recorded for each test. Then fitting the QSS approach developed by Tencer et al. [10] (equation (2)) to the experimental data in each case, the time constants (τ) are calculated.

$$RH_{enclosure}= RH_{ambient}+(RH_{ambient-} RH_{initial}) \times exp(-time/\tau) \quad (2)$$

It is worth to mention that the QSS model is coming from the solution of the Fick's second law for the general case of an enclosure with a finite volume (V). Considering a cylindrical-shaped opening with the length of L and cross sectional area of A, the time constant is calculated as below:

$$\tau = (V \times L)/(A \times D) \qquad (3)$$

, where D is the moisture diffusion coefficient into the air. It should be noticed that D is a function of temperature which can be obtained by the regression curve fit to data from Bolz and Tuve (see equation (4)) [18],[19][20][21].

$$D = -2.775 \times 10^{-6} + (4.479 \times 10^{-8})T + (1.656 \times 10^{-10})T^2 \quad (4)$$

The ANOVA calculation is done by the Minitab 17 software package. All the calculations are based on a confidence level of 95%.

Results and Discussion

A. Time constant estimation

Fig. 2 demonstrates the experimental results for the RH build-up in the electronic enclosure for each case. Regardless of the operating conditions, it does not take more than 19 days for the internal RH to reach the ambient value of 98 [%].

As shown in Table 2, each case should start at a specific initial RH. However, precise control of the starting values is difficult experimentally; thus there are deviations from these values in each test. Fig. 3 shows the initial RH each case has been started with. This fact imposes some error to the estimations. The fitted QSS model to the experimental data for case 5 is shown in Fig. 4, as an example. The residuals for the fitted curve are shown in the sub-figure. For all the 11 cases, the same procedure is applied to derive the time constant value.

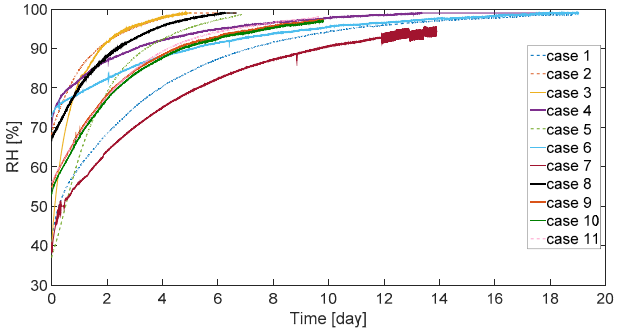

Fig. 2. The RH build-up in the electronic enclosure for the factorial cases.

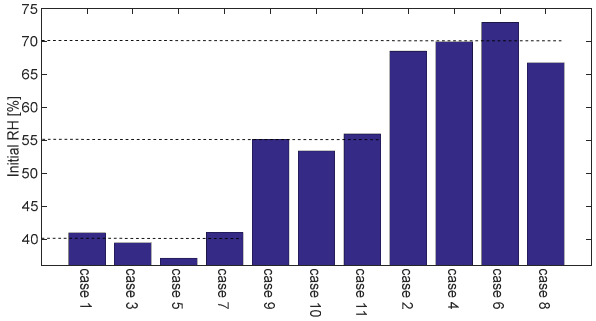

Fig. 3. The initial RH for the factorial cases.

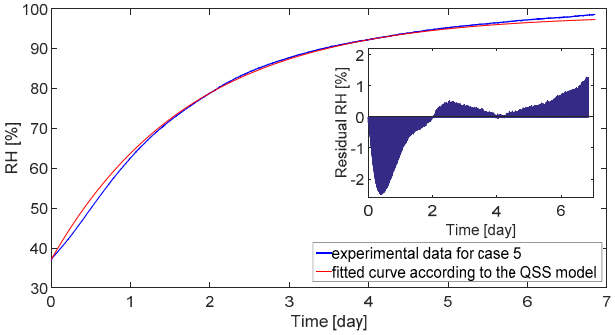

Fig. 4. The fitted QSS model to the experimental data for case 5.

Fig. 5 demonstrates the time constant values and the corresponding adjusted R^2 for each case. For an acceptable fit model, R^2 should be higher than 0.80 [17]; the closer R^2 is to unit, the better. The R^2 typically gets closer to 1 as more terms are added to the model. The QSS model is based on the aforementioned analytical solution to Fick's second law; thus it is not reasonable to modify the function or to add excess terms for making a better fit. Instead it is recommended to use an adjusted R^2 to evaluate the fit adequacy, because it is adjusted for the number of terms in the model. For a well fitted model, the adjusted R^2 should be higher than 0.90 [15], [17]. In this work, for most of the cases (9 out of 11) the adjusted R^2 is well above 0.98; however, there are two cases with an adjusted $R^2 < 0.97$. Regarding the complex nature of such experiments and also the simplifying assumptions of the QSS model, the accuracy of the estimations seems reasonable.

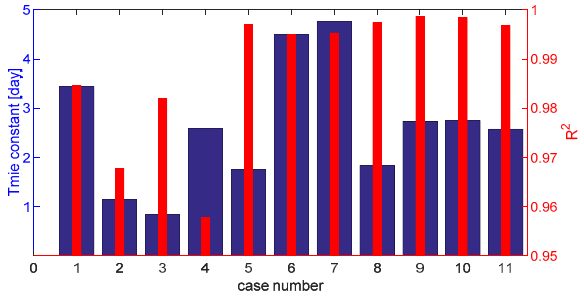

Fig. 5. The time constant values and the adjusted R^2 for the factorial cases.

B. The statistical ANOVA

Generally, in the analysis of data it is often assumed that observations are independently normally distributed with constant variance. The normality of the distribution of the data

can be improved after some suitable transformation of the investigated response [22]. In this study, the normality of the distribution of the response (time constant) is checked. According to the Box-Cox plot, a power transformation (λ=0.51) on the response values is proposed for a more normal distribution (see Fig. 6); then the ANOVA is done on the transformed data.

Table 3 summarizes the ANOVA calculation results. As the statistical ANOVA of the results are obtained with a confidence level of 95%, the p-value to judge the significance of the effect is 0.05. In fact, terms with a p-value lower than 0.05 are statistically significant [13]. According to Table 3, the F-test yields a very low probability value (p-value = 0.005) for the regression model, which indicates that the model is highly significant. For the curvature the p-value is only a bit higher than the considered cut-off; thus, it is not considered as a significant term. Considering a model of higher order can predict the curvature more accurately. Furthermore, the calculated p-values demonstrate that temperature and the opening length are the most significant factors. Fig. 7(a) and (b) displays the normal probability distribution of the effects and rank of the investigated terms, respectively. The *[AD]* term which represents the effect of $A \times D + B \times C$ interactions is also found to be important. Since neither *A* nor *B* are among the influential factors and considering the fact that *B* and *C* are affecting the response in reverse directions, it can be concluded that the significance of *[AD]* is mostly due to the effect of $A \times D$.

Table 3. The ANOVA results for the 2^{4-1} design.

Source	Degree of freedom	Adjusted sum of squares	Adjusted mean square	F-value	P-value
Model	5	1.63978	0.32796	96.75	0.000
A	1	0.00215	0.00215	0.64	0.462
C	1	0.31355	0.31355	92.50	0.000
D	1	1.27625	1.27625	376.50	0.000
AD	1	0.03131	0.03131	9.24	0.029
Curvature	1	0.01652	0.01652	4.87	0.078
Error	5	0.01695	0.00339		
Lack of fit	3	0.01507	0.00502	5.34	0.162
Pure error	2	0.00188	0.00094		
Total	10	1.65673			

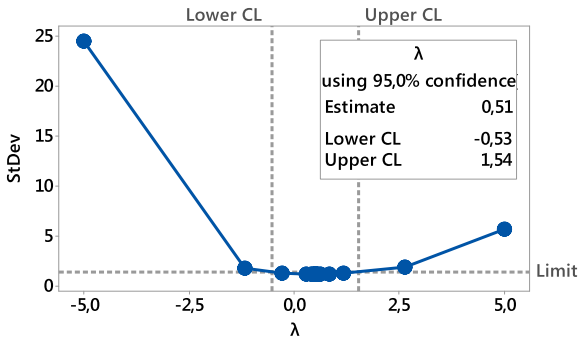

Fig. 6. The Box-Cox plot

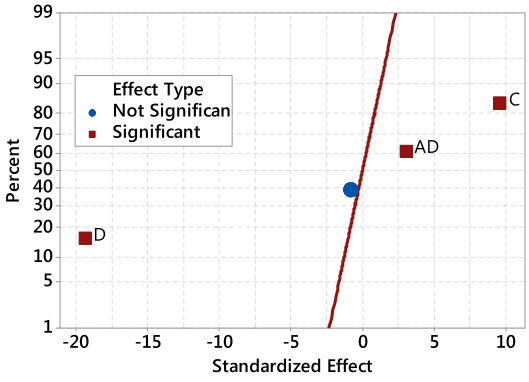

(a)

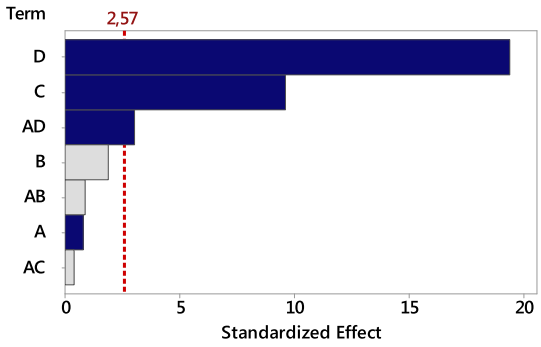

(b)

Fig. 7. The normal probability plot of the effects (a), and the Pareto chart (b)

Based on the ANOVA calculations, a predictive model for the moisture transfer time constant is proposed which can be used in the space of the investigated ranges of the parameters (see equation (5)).

$$\begin{aligned} \textit{Time constant}^{0.51} &= 2.941 - 0.01122 \times \textit{initial RH} \\ &+ 0.008249 \times \textit{Length of the opening} \\ &- 0.03593 \times \textit{Temperature} \\ &+ 0.000238 \times \textit{initial RH} \times \textit{Temperature} \end{aligned} \quad (5)$$

The adjusted R^2 for this regression model is 0.98, which is satisfying. Another important issue to check for the adequacy of a regression model derived from ANOVA, is the distribution of the residuals. The normal probability plot of the residuals in this study does not reveal anything troublesome (see Fig. 8). Thus, the proposed regression model based on the experimental results is suitable for prediction over the studied design space. It is worth to mention that, this regression model can be used to find the critical parts of the design space for further investigations, too.

Fig. 9 shows the time constant changes vs. temperature at different values of length of the opening when the initial RH is 40 [%]. As the temperature increased, the time constants changes less over the length changes; in other words, the length of the opening plays a more effective role at lower temperatures (the time constant variation is 1.8 times bigger at 25 [° C] compared to 60 [° C] vs length changes). The same trend happens when the initial RH is at 70 [%]. The time constant changes vs. the initial RH at different values of length of the opening are displayed in Fig. 9 at the lowest and

highest investigated temperatures. Previously, the ANOVA revealed that the initial RH does not significantly influence the time constant. In Fig. 10 it is seen that the response is changing very slightly with the initial RH at all the values of the length of the opening at both 25 and 60 [° C], despite the fact that the initial RH appears twice in the regression model. In fact, according to the definition of the time constant in the analytical QSS model, the initial RH is not affecting time constant values. Fig. 10 is displayed to emphasize that although RH appears in the semi-empirical model, it does not mean that it is affecting the response significantly.

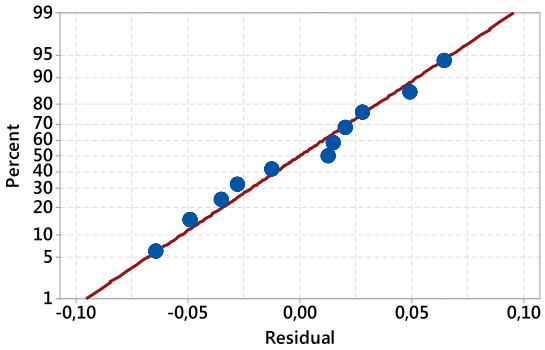

Fig. 8. The normal probability plot of the residuals

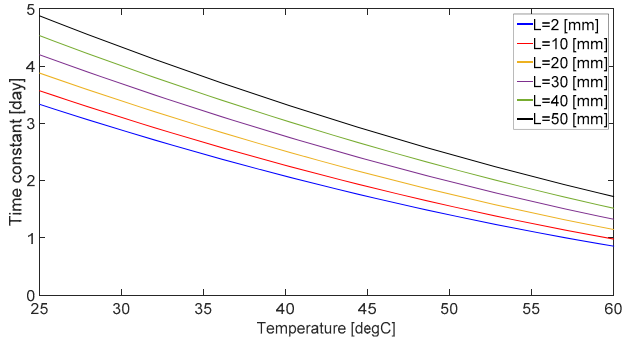

Fig. 9. The time constant vs. temperature at initial RH=40 [%].

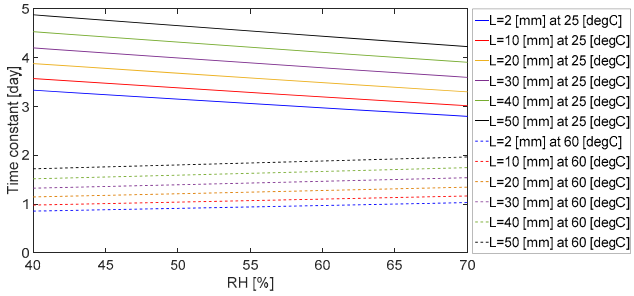

Fig. 10. The time constant vs. RH.

Conclusions

In the present work, the fractional factorial design methodology is used to determine the significant parameters and investigate the interaction among them for the moisture transfer into a typical polycarbonate electronic enclosure with a cylindrical shape opening. Fitting the experimental data to the QSS model for all the cases admits the exponential nature of the RH changes inside the electronic enclosure over time. According to the statistical analysis of the results, the significant factors are ranked as below:

D>C>AD

"A", "C" and "D" denote initial RH inside the enclosure, opening length and temperature, respectively. Based on the ANOVA of the derived time constants, a semi-empirical regression model is proposed to predict the moisture transfer time constant with an adjusted R^2 of 0.98. According to the predicted results, the length of the opening is more influential on the moisture transfer time constant at lower temperatures compare to high temperatures.

The semi-empirical model can be used to find the critical parts of the design space for further investigations with a reasonable accuracy.

Acknowledgments

The current research has been conducted as part of the ICCI project from the Danish council for Independent Research, Technology and Production (FTP) and the IN SPE project from the Danish Innovations Fonden which are highly acknowledged. Moreover, the authors would like to acknowledge the commitment and help of the industrial partners in this project.

References

[1] P. S. Nasirabadi, M. Jabbari, and J. H. Hattel, "Estimation of water diffusion coefficient into polycarbonate at different temperatures using numerical simulation," in *International Conference of Numerical Analysis and Applied Mathematics*, 2016, vol. 30045.

[2] M. Tencer and J. S. Moss, "Humidity management of outdoor electronic equipment: Methods, pitfalls, and recommendations," *IEEE Trans. Components Packag. Technol.*, vol. 25, no. 1, pp. 66–72, 2002.

[3] D. Leslie, A. Dasgupta, and J. W. C. De Vries, "Quantifying moisture diffusion into three-dimensional axisymmetric sealants," *2013 14th Int. Conf. Therm. Mech. Multi-Physics Simul. Exp. Microelectron. Microsystems, EuroSimE 2013*, pp. 1–4, 2013.

[4] R. Ciprian and B. Lehman, "Modeling effects of relative humidity, moisture, and extreme environmental conditions on power electronic performance," *2009 IEEE Energy Convers. Congr. Expo. ECCE 2009*, pp. 1052–1059, 2009.

[5] H. Conseil, M. S. Jellesen, and R. Ambat, "Experimental study of water absorption of electronic components and internal local temperature and humidity into electronic enclosure," *Electron. Packag. Technol. Conf. (EPTC), 2014 IEEE 16th*, pp. 355–359, 2014.

[6] N. Dahan, A. Vanhoestenberghe, and N. Donaldson, "Moisture ingress into packages with walls of varying thickness and/or properties: A simple calculation method," *IEEE Trans. Components, Packag. Manuf. Technol.*, vol. 2, no. 11, pp. 1796–1801, 2012.

[7] J. B. Jacobsen, J. P. Krog, A. H. Holm, and L. Rimestad, "Climate-Protective Packaging," no. september, pp. 51–59, 2014.

[8] M.R. Keenan, “Moisture Control in Sealed Electronic Packages,” California, 1990.

[9] L. Zhu, D. Monthei, G. Lambird, and W. Holgado, “Moisture diffusion modeling and application in a 3D RF module subject to moisture absorption and desorption loads,” in *11th. Int. Conf on Thermal, Mechanical and Multi-Physics Simulation, and Experiments in Microelectronics and Microsystems*, 2010, pp. 1–6.

[10] M. Tencer, “Moisture ingress into nonhermetic enclosures and packages. A quasi-steady state model for diffusion and attenuation of ambient humidity variations,” *Electron. Components Technol.*, pp. 196–209, 1994.

[11] E. E. Jeff Punch, Ronan Grimes, Greg Heaslip, Timo Galkin, Kyosti Viikevainen, Vesa Kyyhkynen, “Transient hygrothermal behaviour of portable electronics,” in *6th Int. Con5 on Thermal Mechunical and Multiphysics Simularion and Experiments in Micro-Electronics and Micro-Sysrem*, 2005, pp. 398–405.

[12] I. Belov, J. Rydén, J. Lindeblom, Y. Zhang, T. Hansson, F. Bergner, and P. Leisner, “Application of CFD modelling for energy efficient humidity management of an electronics enclosure in storage under severe climatic conditions,” in *9th International Conference on Thermal, Mechanical and Multi-Physics Simulation and Experiments in Microelectronics and Micro-Systems*, 2008, pp. 1–8.

[13] P. S. Nasirabadi, M. Jabbari, and J. H. Hattel, “CFD Simulation and Statistical Analysis of Moisture Transfer into an Electronic Enclosure,” *Appl. Math. Model.*, 2016 (*accepted*).

[14] P. S. Nasirabadi, M. Jabbari, and J. H. Hattel, “Numerical simulation of transient moisture transfer into an electronic enclosure,” in *International Conference of Numerical Numerical Analysis and Applied Mathematics*, 2016, vol. 30038.

[15] D. C. Montgomery, *Design and Analysis of Experiments Eighth Edition*. Hoboken: Wiley, 2013.

[16] “Degrees of protection provided by enclosures CENELEC - EN 60529.” [Online]. Available: http://standards.globalspec.com/std/1638833/cenelec-en-60529. [Accessed: 09-Sep-2016].

[17] S. M. Seyed Shahabadi and A. Reyhani, “Optimization of operating conditions in ultrafiltration process for produced water treatment via the full factorial design methodology,” *Sep. Purif. Technol.*, vol. 132, pp. 50–61, 2014.

[18] P. S. Nasirabadi, M. Jabbari, and J. H. Hattel, “Numerical Simulation of Transient Moisture and Temperature Distribution in Polycarbonate and Aluminum Electronic enclosures,” in *17th International Conference on Thermal, Mechanical and Multi-Physics Simulation and Experiments in Microelectronics and Microsystems*, 2016, pp. 1–6.

[19] A. Fabbri and C. Cevoli, “2D water transfer finite elements model of salami drying, based on real slice image and simplified geometry,” *J. Food Eng.*, vol. 158, pp. 73–79, 2015.

[20] J. Songok, P. Salminen, and M. Toivakka, “Temperature effects on dynamic water absorption into paper,” *J. Colloid Interface Sci.*, vol. 418, pp. 373–377, 2014.

[21] M. Bakhshi, B. Mobasher, and C. Soranakom, “Moisture loss characteristics of cement-based materials under early-age drying and shrinkage conditions,” *Constr. Build. Mater.*, vol. 30, pp. 413–425, 2012.

[22] G. E. P. Box and D. R. Cox, “An Analysis of Transformations Revisited, Rebutted,” *J. Am. Stat. Assoc.*, vol. 77, no. 377, p. 209, 1982.

Appendix E
Paper VI

Numerical simulation of transient moisture transfer into an electronic enclosure

P. Shojaee Nasirabadi, M. Jabbari, and J. H. Hattel

Citation: AIP Conference Proceedings **1738**, 030038 (2016); doi: 10.1063/1.4951794
View online: http://dx.doi.org/10.1063/1.4951794
View Table of Contents: http://scitation.aip.org/content/aip/proceeding/aipcp/1738?ver=pdfcov
Published by the AIP Publishing

Numerical Simulation of Transient Moisture Transfer into an Electronic Enclosure

P. Shojaee Nasirabadi, M. Jabbari and J.H. Hattel

Process Modelling Group, Department of Mechanical Engineering, Technical University of Denmark, Nils Koppels Allé, 2800 Kgs. Lyngby, Denmark.

Abstract. Electronic systems are sometimes exposed to harsh environmental conditions of temperature and humidity. Moisture transfer into electronic enclosures and condensation can cause several problems such as corrosion and alteration in thermal stresses. It is therefore essential to study the local climate inside the enclosures to be able to protect the electronic systems. In this work, moisture transfer into a typical electronic enclosure is numerically studied using CFD. In order to reduce the CPU-time and make a way for subsequent factorial design analysis, a simplifying modification is applied in which the real 3D geometry is approximated by a 2D axial symmetry one. The results for 2D and 3D models were compared in order to calibrate the 2D representation. Furthermore, simulation results were compared with experimental data and good agreement was found.

Keywords: moisture, diffusion, CFD, enclosure.
PACS: 80A20

INTRODUCTION

Electronic enclosures serve several packaging functions, such as cooling, touch protection, input–output, IP, and appearance. Unless the enclosure is perfectly sealed and made in truly hermetic materials, moisture may enter it [1]. Moisture can cause corrosion in electronic systems; especially in the presence of ionic contaminants. It can also accelerate electrochemical metal migration mechanisms [2]. In fact, high relative humidity may lead to condensation of water on the metal surfaces. The concentration of molecules of water vapor rises with increasing relative humidity. This molecular thickness of the layers of water may eventually permit ionic conduction that accelerates the rate of corrosion [3]. These degradation mechanisms can lead to changes in electrical resistance and eventually short circuits [2]. Hence, in order to protect electronic devices from the effects of water vapor, it is essential that the relative humidity inside the enclosure does not reach a level that threatens the electronic function within the required lifetime [4].

Modelling tools describing the moisture behavior are very useful to predict and evaluate moisture related problems and in this content computational fluid dynamics (CFD) has been used as a powerful tool for predicting detailed indoor environmental conditions [5] . Using CFD, air and moisture transport into an enclosure can be simulated with perfect control of all boundary conditions. Furthermore, CFD modelling is an alternative to often expensive and tedious experiments [6]. A full blown CFD model does not require transfer coefficients to model the interaction between fluid and solid interface since this is inherently part of the solution itself. Moreover, CFD allows the analysis of complex geometries and provides detailed information on temperature and humidity distributions. One major drawback of CFD though, is the high computational cost [7].

The purpose of this study is to investigate the moisture transfer into a typical electronic enclosure through an opening. To achieve this, transient moisture transfer into a typical electronic enclosure with a bottom hole is studied using CFD. A modified 2D geometry is studied to check whether it is possible to simplify the 3D geometry and reduce calculation time and the results are compared with the real 3D geometry. Furthermore, moisture transfer into a typical electronic enclosure located in a controlled chamber is modelled and the results are validated with experimental data. Thus, this work has two parts as follows: (i) comparison between 3D and modified 2D geometry and (ii) validation of the modeling with experimental data.

International Conference of Numerical Analysis and Applied Mathematics 2015 (ICNAAM 2015)
AIP Conf. Proc. 1738, 030038-1–030038-4; doi: 10.1063/1.4951794
Published by AIP Publishing. 978-0-7354-1392-4/$30.00

MODEL FORMULATION

A scheme of the investigated geometries for the 2D and 3D studies is shown in Figure 1. Dimensions are shown in Table1. Mass conservation equations are solved for both the surrounding (inside the chamber) and inside the enclosure. Regarding the fact there is no air flow inside the enclosure, moisture is transferred only trough diffusion there. On the other hand for the surrounding (inside the climatic chamber), both convection and diffusion are responsible for the moisture transfer because of the air flow. Velocity distribution inside the climatic chamber was provided by solving momentum conservation equations. All simulations are performed with the commercial code *COMSOL Multiphysics*^{TM}. The backward differentiation formula (BDF) method was used for time stepping. The BDF method is an implicit method that uses known solution data determined at several previous time points as well as the unknown solution at the current point. The order of the error term can be easily adjusted by choosing a different number of previous data points. In this work, the minimum and the maximum BDF order is 1 and 2, respectively.

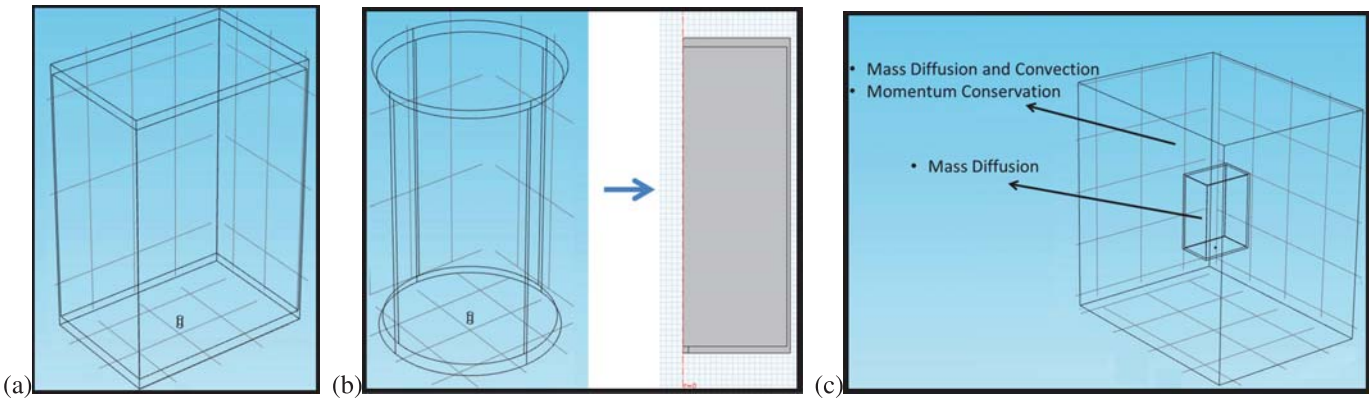

FIGURE 1. (a) schematic of the real 3D geometry (b) schematic of the modified geometry and its 2D axial symmetry form (b) schematic of the 3D geometry of the enclosure located in the controlled climatic chamber and the solved physics.

TABLE 1. Dimensions of the investigated geometries

Enclosure	Inner dimensions(mm) (W × D × L)	188×128×276
	Outer dimensions(mm) (W × D × L)	190×130×280
Chamber	Inner dimensions(mm) (W × D× L)	600×800×850
Hole	Diameter (mm)	2
	Height (mm)	2

Mass conservation equations are solved for both the surrounding (inside the chamber) and inside the enclosure. Regarding the fact there is no air flow inside the enclosure, moisture is transferred only trough diffusion. On the other hand for the surrounding (inside the climatic chamber), both convection and diffusion are responsible for the moisture transfer because of the air flow. Velocity distribution inside the climatic chamber was provided by solving momentum conservation equations (see Figure 2).

MASS BALANCE EQUATION

Equation1 describes chemical species transport through diffusion and convection and implements the mass balance equation:

$$\frac{\partial c}{\partial t} + \mathbf{u} \cdot \nabla c = \nabla \cdot (D \nabla c) \tag{1}$$

Where

- c is the concentration of the species $(mole/m^3)$
- D denotes the diffusion coefficient (m^2/s)
- $\mathbf{u}$ is the velocity vector (m/s)

the first term on the left-hand side corresponds to the accumulation of the species. The second term accounts for the convective transport due to a velocity field u. On the right-hand side of the mass balance equation, the term describes the diffusion transport. This equation is fully solved for the climatic chamber where both mass diffusion and convection happens. For inside the enclosure, since there is no fluid flow, equation (1) reduces to the following equation (Fick's second law):

$$\frac{\partial c}{\partial t} = \nabla \cdot (D \nabla c) \tag{2}$$

Momentum Balance Equation

Momentum Balance Equation is solved for part (ii) where a chamber provides a certain magnitude of relative humidity (RH) by flowing humid air inside. In this study all the simulations were done under the isothermal (25 °C) assumption. It should be noticed that ρ and μ for humid air are function of humidity; however, at 25 °C the changes are negligible and do not violate the assumption of constant viscosity and density [8]. It is worth to mention that D is a weak function of RH; thus, it was also considered to be constant. For constant ρ, the momentum equation is:

$$\rho \frac{\partial \mathbf{u}}{\partial t} + \rho (\mathbf{u} \cdot \nabla) \mathbf{u} = \nabla \cdot \left[-p\mathbf{I} + \mu \left(\nabla \mathbf{u} + \left(\nabla \mathbf{u}^{\top} \right) \right) + \mathbf{F} \right] \tag{3}$$

Where

- ρ is the density
- p is pressure
- μ is the viscosity
- $\mathbf{F}$ is the volume force vector.

To solve the momentum balance equation inside the controlled chamber, the velocity was set to 0.1 m/s at the top face of the chamber and the bottom face of the chamber was considered an outlet with normal flow. Pressure drop and gravity effects were neglected. The momentum transfer is fast for the flowing humid air and the steady state condition is reached in a short period of time; thus, the first term on the left side of Equation 3 can be neglected and velocity distribution can be considered constant during the time. Furthermore, regarding the constant ρ assumption, the continuity equation reduces to:

$$\rho \nabla \mathbf{u} = 0 \tag{4}$$

RESULTS AND DISCUSSION

Simplifying the 3D Geometry to 2D Geometry

Replacing the cubic enclosure with 2D axial symmetry geometry of the same volume and the same height, a modified 2D geometry is proposed (see Figure 1(b)). A constant relative humidity of 98% was applied as boundary condition at the opening for both the 2D and 3D geometries. Figure 2 displays the results.

Comparison of the Numerical Simulation with Experimental Data

An enclosure with a bottom hole located in a controlled chamber is numerically simulated and the results are compared with the experiment in Figure 3. The experimental data are taken from a study done by Conseil et al [9]. RH inside the chamber is kept at 98% at a constant temperature of 25°C. The initial relative humidity inside the enclosure is 28%.

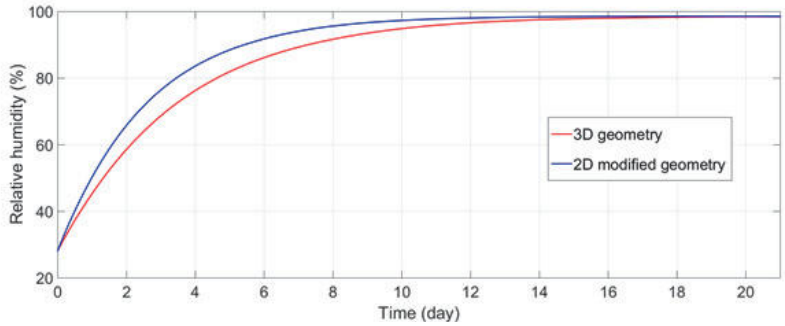

FIGURE 2. Numerical simulation of moisture transfer into an enclosure in case of a 3D and modified 2D geometry

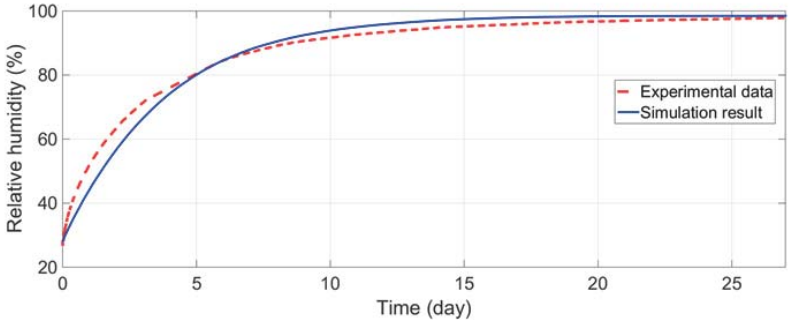

FIGURE 3. Comparison of the numerical simulation with experimental data

CONCLUSIONS

Transient moisture transfer into a typical electronic enclosure was numerically studied using CFD. Fick's second law could successfully predict the local climate of the enclosure exposed to an environment with a high relative humidity (98%). Simulation results also revealed that moisture transfer into an enclosure with a circular base takes less time compared with a rectangular base one of the same volume and height.

In future work, the 2D model will be used as the modelling basis for a 2-level factorial design where influential parameters on the moisture transfer inside the enclosure will be analysed.

REFERENCES

1. J. B. Jacobsen, J. P. Krog, A. H. Holm, L. Rimestad, and A. Riis, *IEEE Ind. Electron. Mag.* **8** (2014).
2. O. Leslie, and A. Oasgupta, "Quantifying Moisture Diffusion into Three-Dimensional Axisymmetric Sealants," in *EuroSimE 14th international Conference on Thermal, Mechanical and Multi-Physics Simulation and Experiments in Microelectronics and Microsystems*, 2013.
3. R. Ciprian, and B. Lehman, "Quantifying Moisture Diffusion into Three-Dimensional Axisymmetric Sealants," in *IEEE Energy Conversion Congress and Exposition(ECCE)*, 2009.
4. N. Dahan, A. Vanhoestenberghe, and N. Donaldson, *IEEE Trans. Compon. Packag. Manuf. Technol.* **2** (2012).
5. F. Song, B. Zhao, X. Yang, Y. Jiang, V. Gopal, G. Dobbs, and M. Sahm, *Build. Environ.* **43** (2008).
6. M. Delele, A. Schenk, E. Tijskens, H. Ramon, B. NicolaÃŕ, and P. Verboven, *J. FOOD ENG.* **91** (2009).
7. M. V. Belleghem, H.Steeman, M. Steeman, A. Janssens, and M. D. Paepe, *Build. Environ.* **45** (2010).
8. P. Tsilingiris, *ENERG. CONVERS. MANAGE.* **49** (2008).
9. H. Conseil, M. S. Jellesen, and R. Ambat, "Experimental Study of Water Absorption of Electronic Components and Internal Local Temperature and Humidity into Electronic Enclosure," in *2014 IEEE 16th Electronics Packaging Technology Conference (EPTC)*, 2014.

Appendix F
Paper VI

A Numerical Investigation of the Effect of Ambient Conditions on Natural Convection Cooling of Electronics

Parizad Shojaee Nasirabadi[1], Jesper H. Hattel[1]

[1] Process Modelling Group, Department of Mechanical Engineering, Technical University of Denmark, Nils Koppels Allé, Kongens Lyngby 2800, Denmark
* Corresponding Author: parnas@mek.dtu.dk, +45 45254754

Abstract

Thermal management is a serious concern in electronic industry. It is important to understand the effects of ambient conditions on cooling of electronics. In this work, the effect of ambient conditions on the thermophysical properties of humid air is estimated in five cities (Copenhagen, Mashhad, Singapore, Las Vegas and Jakarta). Thereafter, the Nu number is calculated for cooling of an isothermal surface in horizontal and vertical orientations. Comparing the results, shows that Pr number is very slightly affected by ambient conditions; however, Gr is following the temperature changes. Among the investigated cities Singapore and Jakarta, the cities with the higher temperature and moisture concentration had the lowest heat transfer coefficients.

1 Introduction

Reliability issue regarding thermal management is a major concern in electronics industry. In many applications electronics are exposed to harsh environmental conditions. For a proper design, it is crucial to study the effect of ambient conditions on thermal management and cooling efficiency [1]–[5].

Natural convection air cooling is recognized as an important and widely used cooling technique. This is mainly due to the appealing features such as accessibility simplicity and robustness, safety operability in harsh environments (contaminated air, vibrations, noise and humidity), high reliability and zero power consumption. All these advantages stimulated considerable research on the development and optimization of heat sinks for natural convection [6]–[8]

Natural convection heat transfer coefficient is a function of temperature difference that the fluid experiences and the material properties namely, density, specific heat capacity, viscosity, expansion coefficient and conductivity [9], [10].

Thermophysical properties of air are influenced by the moisture content; consequently, natural convection heat transfer is also affected. Tsilingiris [11] evaluated the thermophysical properties of moist air as a function of mixture temperature (from 0-100 *[degC]*) and relative humidity (RH), ranging from dry air to saturation conditions. Some of the developed correlations were presented and employed to derive the temperature and RH dependence of the mixture density, viscosity, specific heat capacity and thermal conductivity under the total barometric pressure of 101.3 *[kPa]*. In another study, Melling et al. [12] provided simple analytical correlations for humid air. The correlations were derived from theory and numerical curve fitting for a working pressure of 1 *[bar]* in the temperature range of 100-200 *[degC]*. Zhang et al. [13] also estimated the thermophysical properties of humid air at 101.3 *[kPa]* using the same concepts for the binary mixture of air and water vapour as the two other studies.

In this work, the air cooling by natural convection through heatsinks is investigated in different ambient conditions of several cities, namely Copenhagen, Mashhad, Singapore, Las Vegas and Jakarta for one day. The thermophysical properties of humid air are estimated using the correlations from Tsilingiris' [11] work because of the operating temperatures. The ambient data (moisture concentration and temperature are taken from *COMSOl Multiphysics*^{TM} database. The calculations are done in *MATLAB R2016b*. The Grashof (Gr) and Prandtl (Pr) numbers are calculated transiently with the dynamic ambient changes and finally the Rayleigh numbers (Ra) of the five cases are compared.

2 Theory and methods

Generally, for natural convection, the heat transfer coefficient (h) is derived from the Nu number which is correlated to two other dimensionless numbers namely, Grashof (Gr) and Prandtl (Pr) as below (or Ra). The Nusselt, Prandtl, Grashof, and Rayleigh numbers are defined as equations (1) to (3) [9], [10], [14]. The material properties of air should be estimated at the film temperature defined as the average of air and the surface temperature.

The air temperature dynamically changes over time as it is considered as outdoor temperature of different cities on a summer day (July, 1st 2016). Figure 1-5 displays the moisture content and temperature for Copenhagen, Mashhad, Singapore, Las Vegas and Jakarta. The temperature and hydrodynamic length of the heatsink are considered 60 *[degC]* and 0.1 *[m]*, respectively.

$$Nu = \frac{hL}{k} = f(Gr \times \mathrm{Pr}) = f(Ra) \qquad (1)$$

$$Gr_L = \frac{g\beta(\Delta T)L^3}{\upsilon^2} \qquad (2)$$

$$\mathrm{Pr} = \frac{C_p \mu}{k} \qquad (3)$$

The density of the humid air is calculated by equation *(4)* using the density values for dry air and water vapour:

$$\rho_m = \frac{1}{z_m} \times \frac{P_0}{RT} \times (M_a \frac{P_0 - P_v}{P_0} + M_v \frac{P_v}{P_0}) \qquad (4)$$

, where z_m is the compressibility factor and P_0 and P_v are total air pressure and partial vapour pressure, respectively. M_a and M_v demonstrate molecular weight of air and water, respectively.

Viscosity, thermal conductivity and specific heat capacity are calculated using equations *(5)* to *(9)*:

$$\mu_m = \frac{(1-x_v)\mu_a}{(1-x_v)+x_v\Phi_{av}} + \frac{x_v\mu_v}{(1-x_v)\Phi_{va}+x_v} \qquad (5)$$

$$\Phi_{av} = \frac{\sqrt{2}}{4}(1+\frac{M_a}{M_v})^{\frac{-1}{2}} \times [1+(\frac{\mu_a}{\mu_v})^{\frac{1}{2}}(\frac{M_a}{M_v})^{\frac{-1}{4}}]^2 \qquad (6)$$

$$\Phi_{va} = \frac{\sqrt{2}}{4}(1+\frac{M_a}{M_v})^{\frac{1}{2}} \times [1+(\frac{\mu_a}{\mu_v})^{\frac{-1}{2}}(\frac{M_a}{M_v})^{\frac{1}{4}}]^2 \qquad (7)$$

$$k_m = \frac{(1-x_v)k_a}{(1-x_v)+x_v\Phi_{av}} + \frac{x_v k_v}{(1-x_v)\Phi_{va}+x_v} \qquad (8)$$

$$C_{pm} = \frac{C_{pa}(1-x_v)M_a + x_v M_v C_{pv}}{M_a(1-x_v)+M_v x_v} \qquad (9)$$

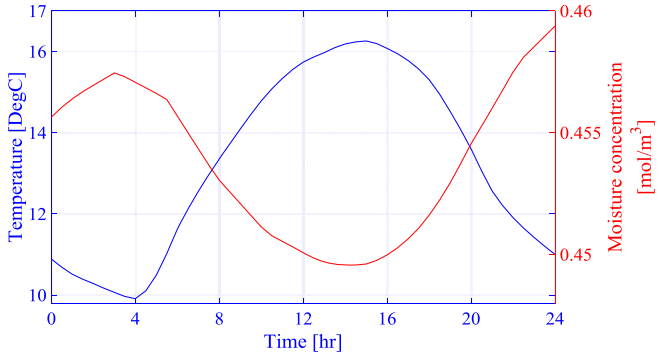

Figure 1: Ambient condition in Copenhagen.

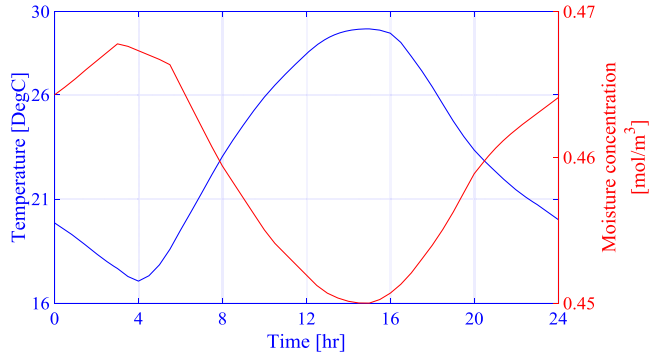

Figure 1: Ambient condition in Mashhad.

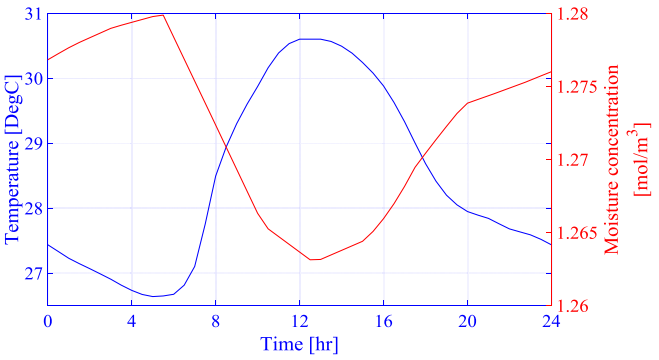

Figure 3: Ambient condition in Singapore.

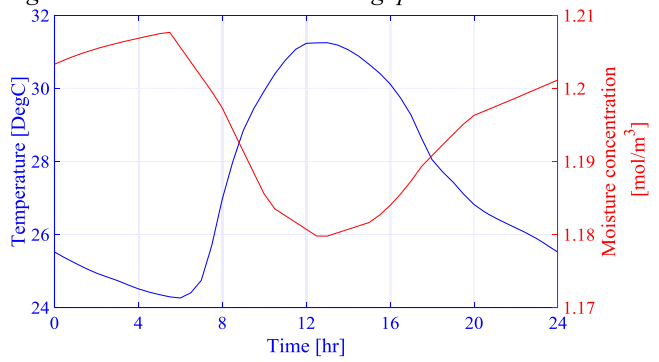

Figure 4: Ambient condition in Jakarta.

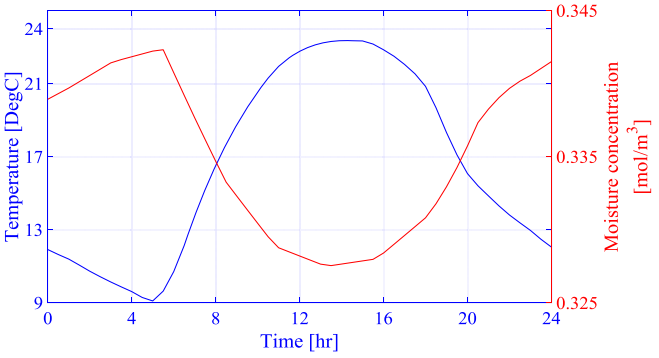

Figure 5: Ambient condition in Las Vegas.

3 Result and discussion

The *Pr* number increases as the specific heat capacity and viscosity increases; on the other hand, it changes reversely with thermal conductivity. The specific heat capacity of dry air is not a strong function of temperature; however, it is monotonously increasing with RH. As the temperature goes higher, the increase percentage enhances. At any constant temperature, the viscosity decreases as RH increases; the trend for temperature is not straightforward, though. Thermal conductivity also presents the same trend with RH and temperature changes as viscosity [11]. Figure 6 shows the Pr changes. In General, the changes are not that significant for the five cities despite the relatively big moisture concentration and temperature differences, demonstrating the negligible effect of *Pr* changes on natural convection heat transfer coefficient changes.

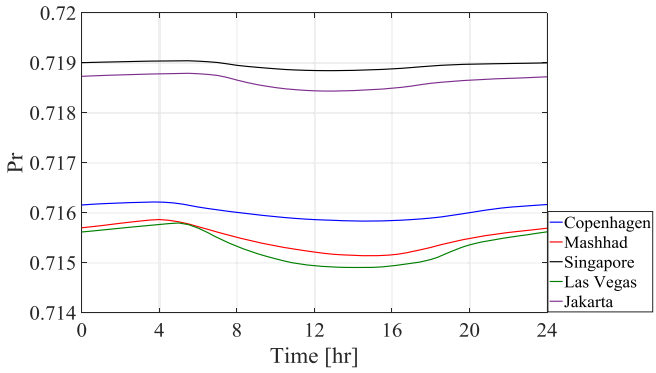

Figure 6: Pr changes in a summer day for the five cities

The trend of *Gr* changes is more complicated than *Pr*; and that is due to the expansion coefficient. The expansion coefficient can be simply defined as equation *(10)* [10].

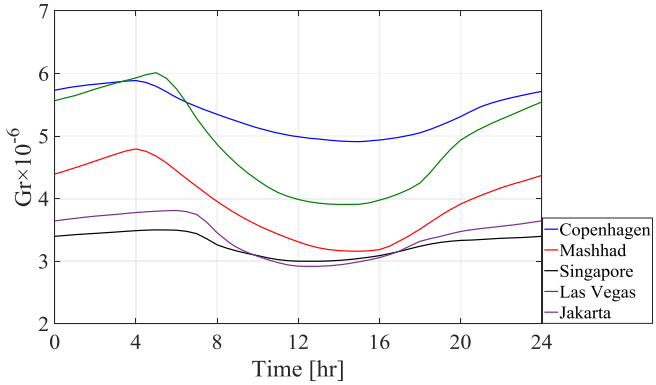

Figure 7: Gr changes in a summer day for the five cities

$$\beta = \frac{1}{T} \qquad (10)$$

Figure 7 displays the Gr changes. The *Gr* shows the same trend as temperature for all of the five cities during the day. The moisture concentration is from around 0.3 *[mol/m^3]* for Las Vegas till around 1.28 *[mol/m^3]* for Singapore. It is observed that the cities with higher moisture concentration have higher *Pr* numbers. This behaviour reveals the dominant effect of temperature compared with moisture concentration. Not surprisingly, *Ra* resembles the *Gr* (see Figure 8).

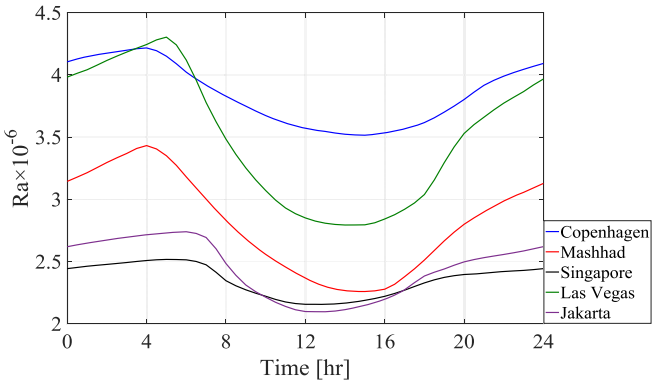

Figure 8: Ra changes in a summer day for the five cities

In order to investigate the heat transfer coefficient for cooling an isothermal surface (at 60 *[degC]*), the mean *Nu* is calculated for horizontal and vertical orientations over the 24 hours. In horizontal case, the mean *Nu* in Copenhagen is 13% higher than Singapore. Singapore and Jakarta having the higher moisture concentration as well as higher daily temperatures are lower in *Nu*. For the vertical orientation the ranking in terms of the mean Nu is the same as horizontal; however it is worth to mention that the mean *Nu* values are higher in horizontal cases compared to vertical cases.

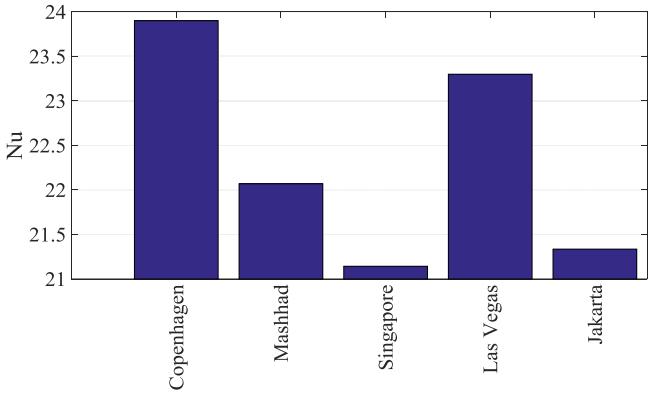

Figure 9: Mean Nu for horizontal position.

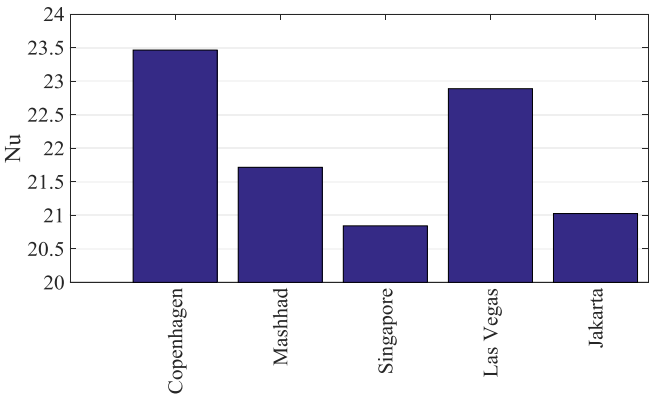

Figure 10: Mean Nu for vertical position.

4 Conclusion

In this study the thermophysical properties of humid air are estimated over temperature and moisture content changes. Furthermore the natural convection heat transfer coefficient is estimated during a summer day of cooling of an isothermal surface in vertical and horizontal orientations in Copenhagen, Mashhad, Singapore, Las Vegas and Jakarta.

The following conclusions are drawn:

- The *Pr* number does not change drastically; despite the very slight changes, it resembles the temperature changes.
- The *Gr* and consequently *Ra* numbers show more sensitivity to the ambient conditions; Singapore and Jakarta having the higher temperatures and moisture concentrations were lower in *Ra* and *Nu* ranking.

Acknowledgements

The current research has been conducted as part of the ICCI project from the Danish council for Independent Research, Technology and Production (FTP) and the IN SPE project from the Danish Innovations Fonden which are highly acknowledged. Moreover, the authors would like to acknowledge the commitment and help of the industrial partners in this project.

References

[1] P. Shojaee Nasirabadi, H. Conseil-gudla, S. Mohanty, M. Jabbari, R. Ambat, and H. Jesper, "Semi-Empirical Prediction of Moisture Build-up in an Electronic Enclosure Using Analysis of Variance (ANOVA)," in *IEEE Electronics Packaging Technology Conference, EPTC*, 2016, pp. 785–790.

[2] P. Shojaee Nasirabadi, M. Jabbari, and J. H. Hattel, "CFD simulation and statistical analysis of moisture transfer into an electronic enclosure," *Appl. Math. Model.*, vol. 44, pp. 246–260, 2017.

[3] R. Ciprian and B. Lehman, "Modeling effects of relative humidity, moisture, and extreme environmental conditions on power electronic performance," *2009 IEEE Energy Convers. Congr. Expo. ECCE 2009*, pp. 1052–1059, 2009.

[4] E. Parsa, H. Huang, and A. Dasgupta, "Multi-physics simulations for combined temperature/humidity loading of potted electronic assemblies," *Microelectron. Reliab.*, vol. 54, no. 6–7, pp. 1182–1191, 2014.

[5] P. Shojaee Nasirabadi, M.Jabbari, and J. H. Hattel, "Numerical simulation of transient moisture transfer into an electronic enclosure," *AIP Conf. Proc.*, vol. 1738, pp. 1–4, 2016.

[6] R. Huang, W. Sheu, and C. Wang, "Orientation effect on natural convective performance of square pin fin heat sinks," *Int. J. Heat Mass Transf.*, vol. 51, pp. 2368–2376, 2008.

[7] Y. Joo and S. Jin, "Comparison of thermal performance between plate-fin and pin-fin heat sinks in natural convection," *Int. J. Heat Mass Transf.*, vol. 83, pp. 345–356, 2015.

[8] G. L. and A. BEJAN, "Heat sinks with sloped plate fins in natural and forced convection," *Int. J. Heat Mass Transf.*, vol. 39, no. 9, pp. 1773–1783, 1996.

[9] J. P. Holman, *Heat Transfer*, 10th ed. Jefferson City: McGraw-Hill, 2010.

[10] T. L. Bergman, A. S. Lavine, F. P. Incropera, and D. P. Dewitt, *Fundamentals of Heat and Mass Transfer*, 7th ed. Jefferson City: John Wiley & sons, 2011.

[11] P. T. Tsilingiris, "Thermophysical and transport properties of humid air at temperature range between 0 and 100 °C," *Energy Convers. Manag.*, vol. 49, no. 5, pp. 1098–1110, 2008.

[12] H. V. Adrian Melling and Stefan Noppenberger and Martin Still, "jpcrd526.pdf," *J. Phys. Chem.*, vol. 26, no. 4, 1997.

[13] J. Zhang, A. Gupta, and J. Baker, "Natural Convection Heat Transfer Coefficients Effect of Relative Humidity on the Prediction of Natural Convection," vol. 7632, no. August, 2007.

[14] S. M. Ghiaasiaan, *Convective Heat and Mass Transfer*. New York: Cambridge University Press, 2011.

Appendix G
Paper VII

Numerical Simulation of Transient Moisture and Temperature Distribution in Polycarbonate and Aluminum Electronic enclosures

Parizad Shojaee Nasirabadi, Masoud Jabbari, Jesper H. Hattel
Process Modelling Group, Department of Mechanical Engineering, Technical University of Denmark
Nils Koppels Allé, 2800 Kgs. Lyngby, Denmark
Email: parnas@mek.dtu.dk, Phone: +45 45254754

Abstract

The challenge of developing a reliable electronic product requires huge amounts of resources and knowledge. Temperature and thermal features directly affect the life of electronic products. Furthermore, moisture can be damaging for electronic components. Nowadays, computational fluid dynamics (CFD) analysis has been proven as a useful tool to exploit the detailed and visualized information about the fluid flows; and hence it can be helpful for predicting local climate inside the electronic enclosures. In this study, the temperature and moisture distributions inside an idealized electronic enclosure with some heat producing components are investigated. It is shown how the enclosure material can influence local climate inside the enclosure using transient numerical simulations. The effect of heat transfer coefficient and wall thickness of the enclosure is also investigated.

The enclosure material and the heat transfer coefficient of the enclosure with the environment are found to be influential on the mean temperature and relative humidity; however, the significance of their effects are not the same at different levels. Natural convection plays a key role in RH and temperature distribution.

1. Introduction

Thermal management of electronic equipment is crucial in order to improve the thermal performance of electronics packaging in the early design stage [1], [2], [3]. To come up with a proper design of a thermal management scheme, one must be able to predict the thermal performance of devices in the environment [4]. The most widely used method of choice for making such predictions is computational fluid dynamics (CFD) [1]. The application of CFD analysis for a reliable design of electronic systems has the potential to generate accurate solutions considering different physics and details of the investigated cases [5].

Natural convection is one of the considered cooling techniques that play an important role in maintaining reliable operation of electronics [6]. Although, forced air cooling has been used to dissipate heat, natural convection cooling is preferable from the viewpoints of miniaturization, lightening, and energy conservation [3]. Furthermore, in some cases the electronics are housed in completely sealed enclosures, hence the cooling of these systems primarily relies on natural convection [7]. In natural convection, fluid motion is due to buoyancy forces within the fluid; buoyancy is due to the combined presence of a fluid density gradient and a body (volume) force that is proportional to density. In practice, the body force is usually gravitational. There are several ways in which a mass density gradient may arise in a fluid; however, the most common situation is due to the presence of a temperature gradient [8], [9]. Generally, natural convection in inclined air-filled enclosures can be described in terms of the full Navier-Stocks equation, the energy equation and the continuity equation. The energy equation and the Navier-Stokes equations are coupled because the temperature dependence of the fluid properties has to be taken into account. This makes the natural convection a complex problem [10].

Besides thermal problems, relative humidity and condensation inside electronic enclosures are major concerns [11]. By definition, relative humidity is a function of temperature; in fact; it is highly controlled by temperature [12]. Considering moisture transfer controlled by temperature distribution and air flow inside an electronic enclosure makes the case more complicated.

In many studies, the effects of configuration of electronic devices inside enclosures and diffusion of moisture into the body of these devices are investigated [3], [13], [14], [15], [16]; however, there are few papers that concern local climate inside the enclosures and also how the enclosure itself or the surrounding can affect it.

In this work, moisture, temperature and velocity distributions are investigated in idealized perfectly sealed enclosures made of aluminum (Al) and polycarbonate (PC). The results are compared to find out the effect of material of the enclosure on the local climate i.e. PC is much less heat conductive compared to Al; on the other hand, it has much higher moisture permeability relative to Al. Based on these properties, the temperature inside the Al box should be less than the PC one; which is in favor of higher RH; on the other hand, moisture can enter the PC box through the walls, this also helps the RH to increase. The contrast between the heat and mass transfer properties of these two materials makes the comparison interesting. In this study, the effect of heat transfer coefficient and wall thickness of an idealized enclosure are discussed. In order to simplify the calculations a cylindrical-shaped enclosure is studied so that the geometry can be presented in an axial

978-1-5090-2106-2/16/$31.00 ©2016 IEEE

2016 17th International Conference on Thermal, Mechanical and Multi-Physics Simulation and Experiments in Microelectronics and Microsystems

symmetry form.

The COMSOL Multiphysics^{TM} version 5.1 is used for running all the CFD simulations.

2. Method

A. Geometry and Model Formulation

A two-dimensional axial symmetry model is developed for investigating the moisture transfer into a cylindrical electronic enclosure. Figure 1 shows the geometry of the enclosure and the three components inside. Table 1 shows the dimensions of the geometry. Component 1 does not produce any heat; however component 2 and 3 are generating heat with a constant flux. There are several physics involved in this model. The air flows inside the sealed enclosure because of the density gradient and buoyancy force caused by the temperature gradient. The temperature and moisture distribution are affected by velocity distribution of the trapped air.

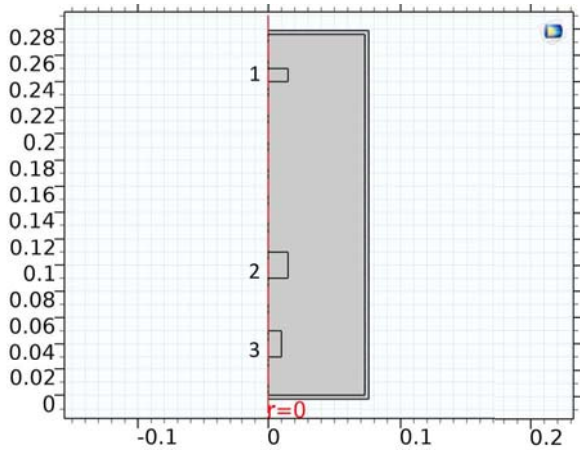

Figure 1. A scheme of the geometry of the cylindrical-shaped electronic enclosure.

The momentum conservation and continuity equations are solved to obtain the velocity distribution. For laminar and incompressible flow, the momentum conservation equation is [17], [18]:

$$\rho\frac{\partial \mathbf{u}}{\partial t}+\rho\left(\mathbf{u}\cdot\nabla\right)\mathbf{u}=\nabla\cdot\left[-p\mathbf{I}+\mu\left(\nabla\mathbf{u}+\left(\nabla\mathbf{u}^{\top}\right)\right)+\mathbf{F}\right] \tag{1}$$

Where

- ρ is the density $[kg/m^3]$
- $\mathbf{u}$ is the velocity vector $[m/s]$
- p is pressure $[Pa]$
- μ is the viscosity $[kg/(m^2 s)]$
- $\mathbf{I}$ is the unit tensor
- $\mathbf{F}$ is the volume force vector $[N]$.

The volume force is considered as below:

$$F_r = 0;\ F_z = -\rho \times g_z \tag{2}$$

For an incompressible flow, the continuity equation reduces to:

$$\nabla\cdot\mathbf{u}=0 \tag{3}$$

The air density values all over the enclosure are calculated based on the temperature value. Thus, these equations are coupled with energy equations. The temperature distribution of the trapped air is obtained by solving the following equations:

$$\rho C_p\frac{\partial T}{\partial t}+\rho C_p\mathbf{u}\cdot\nabla T=\nabla\cdot(k\nabla T)+\mathbf{Q} \tag{4}$$

For the enclosure body, Eq. 4 is also solved to provide the temperature values; regarding the fact that the second term on the left hand side is equal to zero; as the velocity field is zero in the solid body.

The **u**, in the Eq.4 is taken from the simultaneous solution of Eq. 1 and 3; in which the ρ values are updated from Eq.4 based on the temperature values. Coupling all these equations adds complexities to the case. Furthermore, the mass transfer equations are also solved to obtain the concentration and eventually the RH distribution. Equation (5) implements the mass balance equation:

$$\frac{\partial c}{\partial t}+\mathbf{u}\cdot\nabla c=D\nabla\cdot(\nabla c) \tag{5}$$

where

- c is the concentration of the species $[mole/m^3]$
- D denotes the diffusion coefficient (assumed to be independent of c $[m^2/s]$.

This equation is fully solved for the domain inside the enclosure where both mass diffusion and convection happens. In case of PC enclosure in which the moisture permeates into the enclosure through the walls, the convective term (the second term on the left hand side) is neglected, and equation (5) reduces to the following equation (Fick's second law) [19]:

$$\frac{\partial c}{\partial t}=D\cdot\nabla^2 c \tag{6}$$

Moisture diffusion coefficients into the air and PC are functions of temperature. For air, the diffusion coefficient is calculated by the regression curve fit to data from Bolz and Tuve [20], [21], [22], [23].

$$D=-2.775\times10^{-6}+(4.479\times10^{-8})T+(1.656\times10^{-10})T^2 \tag{7}$$

The relation between diffusivity and temperature is described by an Arrhenius equation [24]:

$$D_{PC}=5.4647\times10^{-5}exp(\frac{-5623.45}{T}) \tag{8}$$

For each time step, the equations are solved as described in Figure 2.

Table 1. Dimensions of the studied geometry.

	Enclosure	Component 1	Component 2	Component 3
Radius $[mm]$	73	1.5	1.5	1
Height $[mm]$	276	1	2	2
Thickness $[mm]$	1;3	-	-	-

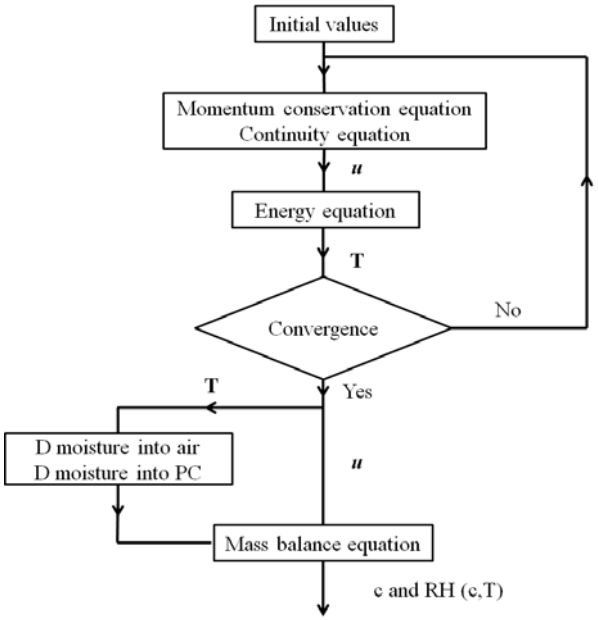

Figure 2. Flowchart of the solved equations.

In this numerical simulation, RH is estimated using the following expression:

$$RH = \frac{x_{vap} p}{p_{sat}(\frac{M_v}{M_a} + x_{vap})} \tag{9}$$

Where

- x_{vap} is the molar fraction of water vapor
- p_{sat} is saturation pressure $[Pa]$
- M_v is the molar mass of water vapor
- M_a is the molar mass of air.

B. Initial and Boundary conditions

All the boundaries of the geometry are set as walls (no slip condition) for solving the Navier-Stokes equations. For energy equation the following boundaries are set:

- Outer walls of the enclosure are exchanging heat with environment with temperature of $T_\infty = 25[^\circ C]$ and heat transfer coefficient of h.
- Component 1 is considered to be thermally insulated.
- Component 2 and 3 are generating heat with the rate of 2 and 1.42 $[W/m^2]$.

Initial conditions for all the studied cases are described in Table 2.

C. Solver System

Natural convection problems are challenging because the resulting velocity is part of the nonlinear solution. Thus, it is important to set a proper solver. In COMSOL Multiphysics^{TM}, the solvers break down each problem– whether linear or nonlinear– into one or several linear systems of equations by approximating the given problem with a linearized problem. The coefficient matrix of the discretized linearized problem is called the Jacobian matrix (or stiffness matrix). In this work, the Jacobian matrix is updated every iteration in order to achieve faster convergence. The PARDISO is used as the linear system solver. This solver works on general sparse linear systems of the form $Ax = b$ and use LU factorization on the matrix A to compute the solution x.

3. Results and discussion

In order to investigate the effect of different factors, four cases are studied for both Al and PC boxes. Table 3 summarizes the conditions of these cases. All the simulations are run for 10 days; however, temperature and velocity values do not significantly change after 10 hours.

A. Temperature and Velocity Distribution

The average temperature of the outer surface of the enclosure and the average temperature inside the enclosure are shown in Table 4 and 5, respectively. Not surprisingly, the outer surface of the Al box is higher than the PC box in all the four cases, representing the fact that the thermal loss through the Al walls are more than PC walls. In the four cases the temperature difference between the PC and Al boxes are not very significant. Comparing case 1 with 3 and case 2 with 4 for PC and Al, it is seen that the thickness is not very influential; however, it should be noticed that in case of $h = 2[W/(m^2K)]$, the average temperature of the outer walls of the Al box is about 0.2 $[^\circ C]$ higher than the PC box; this difference is 0.04 $[^\circ C]$ when h is 12 $[W/(m^2K)]$. This demonstrates that the enclosure material plays a more important role when h is smaller.

As h increases from 2 to 12 $[W/(m^2K)]$, the average temperature inside the enclosures decreases about $2[^\circ C]$ for both Al and PC boxes. The same trend is observed for the average temperature of the outer surfaces of the walls. This fact implies that the heat transfer coefficient between the enclosure and the environment plays more important role relative to the wall thickness.

Despite the fact that the average temperature inside the Al and PC boxes is more or less the same (see Table 5), the

Table 2. Dimensions of the studied geometry.

Solved physics	Initial conditions
Momentum conservation equation	$\mathbf{u} = 0[m/s]$
Continuity equation	$p = 0[Pa]$
Mass balance equation	$c_{ambient} = 1.2516[mole/m^3] \cong RH = 98\% at 25°C$
	$c_{enclosure} = 0.5109[mole/m^3] \cong RH = 40\% at 25°C$

Table 3. Conditions of the four studied cases.

Case number	Wall thickness $[mm]$	Heat transfer coefficient $[W/(m^2K)]$
1	1	2
2	1	12
3	3	2
4	3	12

distribution of the temperature is different. Figure 3 shows the temperature at a horizontal line inside the enclosure for case 3 and 4. For case 3, there are places where the temperature of the PC box is up to $2[°C]$ higher than the Al box. This value is smaller when Al and PC boxes are compared in case 4. This is important when condensation is matter of concern. Average of the velocity magnitude at this line is also calculated. Velocity magnitude is important, since it is controlling the heat transfer resistance inside the enclosure. Generally, in Al boxes the average of the velocity magnitude is higher than PC boxes; however, there is not a straightforward relationship between the average velocity and h or thickness. This fact makes it interesting to use factorial design and analysis of variance to look at the effects of different parameters and their interaction more precisely.

Table 4. Average temperature of the outer surface of the enclosure after 12 hours $[°C]$.

Case number	PC	Al
1	27.210	27.401
2	25.355	25.397
3	27.121	27.301
4	25.342	25.382

Table 5. Average temperature inside the enclosure after 12 hours $[°C]$.

Case number	PC	Al
1	30.048	29.870
2	27.912	27.860
3	29.980	29.765
4	27.946	27.838

Table 6. Average velocity magnitude on after 12 hours [m/s] $[m/s]$.

Case number	PC	Al
1	0.041248	0.045717
2	0.044310	0.045793
3	0.041642	0.046376
4	0.044395	0.046285

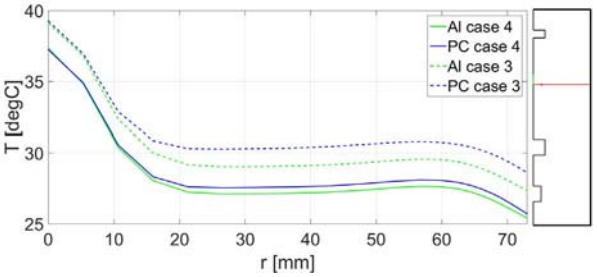

Figure 3. The temperature at a horizontal line inside the enclosure for case 3 and 4.

B. Moisture distribution and RH

Moisture diffusion through walls of the PC enclosures is studied. Figure 4 and 5 display the mean moisture concentration and RH of the trapped air, respectively. Initially, the mean moisture concentration changes of the air are small (see Figure 4); this delay is the time that takes for the moisture concentration of walls to reach a linear distribution. Thereafter, moisture enters the enclosure with a constant rate (the slope of the concentration changes versus time). Apparently, this delay is longer for cases 3 and 4, where the wall thickness is 3 $[mm]$. Furthermore, in these two cases, the moisture transfer rate is smaller compared to cases 1 and 2; which is due to the bigger resistance against mass transfer.

It is also noticeable that the average moisture concentration in cases 1 and 3 is higher compared to cases 2 and 4, respectively; which is attributed to the higher mean temperature and consequently higher diffusion coefficient values.

The RH is a function of temperature as well as the moisture content. In the meanwhile that the concentration changes are small, the temperature increases; thus, the RH experiences a drop. Thereafter, the temperature do not changes with time; on the other hand, moisture concentration increases as explained above. Hence, the RH increases gradually as time goes on and moisture diffuses into the enclosure through the walls.

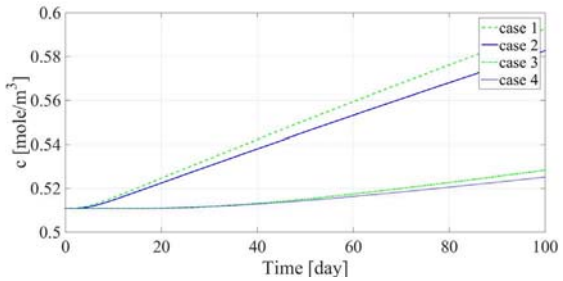

Figure 4. The mean concentration values inside PC box vs. time.

In spite of the fact that in cases 1 and 2, the mean moisture concentrations are close, RH values have a meaningful difference. This is due to the temperature difference in these two cases. The same pattern is for cases 3 and 4.

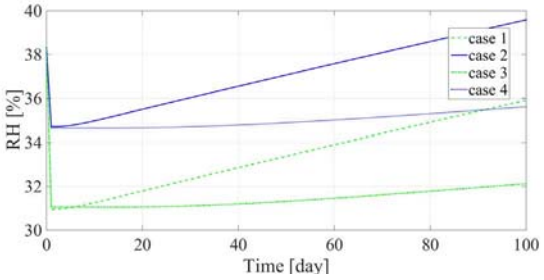

Figure 5. The mean RH values inside PC box vs. time.

4. Conclusions

Transient moisture and temperature transfer into the Al and PC electronic enclosures are investigated. Besides the enclosure material, the effects of wall thickness of the enclosure and heat transfer coefficient with the surrounding environment are studied.

Generally, the mean temperature inside an Al enclosure is less than a PC one; however, the difference is influenced by the wall thickness and heat transfer coefficient; the latter is found to be a more significant factor. Moisture diffusion through the walls of a PC box can increase mean RH of the trapped air, if the box is exposed to high values of RH for a long time.

As the local climate inside the studied electronic enclosures were affected by several factors; it seems interesting to integrate the CFD simulation results with statistical tools such as factorial design and response surface methodology to optimize the influential factors on a desired response, average RH for instance. Furthermore, the study can be extended considering openings in the enclosures.

5. Acknowledgements

The current research has been conducted as part of the ICCI project from the Danish council for Independent Research, Technology and Production (FTP) and the IN SPE project from the Danish Innovations Fonden which are highly acknowledged. Moreover, the authors would like to acknowledge the commitment and help of the industrial partners in this project.

References

[1] C. Sapia and G. Sozio. Cfd transient model of the natural convection heat transfer for an heat sink effects of increasing surface and fins spacing. In *Thermal Investigations of ICs and Systems (THERMINIC), 2011 17th International Workshop on*, pages 1–6, 2011.

[2] H. C. Cheng, I. C. Chung, and W. H. Chen. Thermal chip placement in mcms using a novel hybrid optimization algorithm. *IEEE Transactions on Components Packaging and Manufacturing Technology*, 2:764–774, May 2012.

[3] S. Ogata, E. Sukegawa, and T. Kimura. Performance evaluation of ultra-thin polymer pulsating heat pipes. In *Thermal and Thermomechanical Phenomena in Electronic Systems (ITherm), 2014 IEEE Intersociety Conference on*, pages 519–526, May 2014.

[4] C. Eric Triplett and Bennett Joiner. An experimental thermal characterization of a 272 pbga within an automative engine controller module. In *Fourteenth Annual IEEE Semiconductor Thermal Measurement and Management Symposium*, pages 47–55, 1998.

[5] V. Eveloy, J. Lohan, and P. Rodgers. A benchmark study of computational fluid dynamics predictive accuracy for component-printed circuit board heat transfer. *IEEE Transactions on Components and Packaging Technologies*, 23(3):568–577, Sep 2000.

[6] E. A. M. Elshafei. Natural convection heat transfer from a heat sink with hollow/perforated circular pin fins. In *Thermal Issues in Emerging Technologies Theory and Applications (ThETA), 2010 3rd International Conference on*, pages 185–193, 2010.

[7] M. Ivanova, Y. Avenas, C. Schaeffer, J. B. Dezord, and J. Schulz-Harder. Heat pipe integrated in direct bonded copper (dbc) technology for the cooling of power electronics packaging. In *Power Electronics Specialists Conference, 2005. PESC '05. IEEE 36th*, pages 1750–1755, June 2005.

[8] et al. Incropera, Frank P. *Introduction to heat transfer*. Wiley, 2007.

[9] J.P. Holman. *Heat transfer*. McGraw-Hill, 1997.

[10] W. Schinkel. *Natural convection in inclined air-filled enclosures*. Dutch Efficiency Bureau - Pijnacker, 1980.

[11] P. Shojaee Nasirabadi, M. Jabbari, and J. Hattel. Numerical simulation of transient moisture transfer into an electronic enclosure. 1st International Symposium on Theoretical, Experimental, and Computational Mechanics (TECM-2015), Rodos Palace Hotel, Rhodes, Greece, 23–29 September 2015.

[12] P.T. Tsilingiris. Thermophysical and transport properties of humid air at temperature range between 0 and 100 °C. *Energ. Convers. Manage.*, 49:1098–1110, 2008.

[13] H. B. Fan and M. M. F. Yuen. Multi-scale modeling of moisture transfer in electronic packaging. In *11th International Conference on Electronic Packaging Technology High Density Packaging*, pages 758–761, Aug 2010.

[14] M. Ghassemi, M. Farzaneh, and W. A. Chisholm. A coupled computational fluid dynamics and heat transfer model for accurate estimation of temperature increase of an ice-covered frp live-line tool. *IEEE Transactions on Dielectrics and Electrical Insulation*, 21(6):2628–2633, 2014.

[15] M. Lindgren, I. Belov, A. Johansson, T. Danielsson, N. Gunnarsson, and P. Leisner. Multi-disciplinary approach to design of a power electronics module for harsh environments. In *Thermal, Mechanical and Multi-Physics simulation and Experiments in Microelectronics and Microsystems, 2009. EuroSimE 2009. 10th International Conference on*, pages 1–8, April 2009.

[16] Chunlin Xu, Quan Zhou, Xing Guo, Shannan Zhan, Bo Xiong, Hao Jiang, and Sheng Liu. Analysis of measurement accuracy of air flow sensor influenced by moisture. In *Electronic Packaging Technology (ICEPT), 2015 16th International Conference on*, pages 694–698, Aug 2015.

[17] M. Jabbari and J.H. Hattel. Numerical Modeling of the Side Flow in Tape Casting of a Non-Newtonian Fluid. *J. Am. Ceram. Soc.*, 96(5):1414–1420, 2013.

[18] M. Jabbari, R. Bulatova, J.H. Hattel, and C.R.H. Bahl. An evaluation of interface capturing methods in a VOF based model for multiphase flow of a non-Newtonian ceramic in tape casting. *Appl. Math. Model.*, 38(13):3222–3232, 2014.

[19] M. Jabbari and J. Hattel. Modeling coupled heat and mass transfer during drying in tape casting with a simple ceramics–water system. *Drying Technol.*, 34(2):244–253, 2016.

[20] A. Fabbr and C. Cevoli. 2D water transfer finite elements model of salami drying, based on real slice image and simplified geometry. *J. Food Eng.*, 158:73–79, 2015.

[21] M. Bakhshi, B. Mobasher, and C. Soranakom. Moisture loss characteristics of cement-based materials under early-age drying and shrinkage conditions. *Constr. Build. Mater.*, 30:413–425, 2012.

[22] P. Eliaers, J.R. Pati, S. Dutta, and J. D. Wilde. Modeling and simulation of biomass drying in vortex chambers.

[23] J. Songok and P. Salminenand M. Toivakka. Temperature effects on dynamic water absorption into paper.

[24] Zhangming Mao, X. Luo, J. Yang, and S. Liu. Moisture diffusivity analysis of polycarbonate for led lens. In *11th International Conference on Electronic Packaging Technology High Density Packaging*, pages 1080–1087, 2010.

DTU Mechanical Engineering
Section of Manufacturing Engineering
Technical University of Denmark

Produktionstorvet, Bld. 427A
DK-2800 Kgs. Lyngby
Denmark
Phone (+45) 4525 4763
Fax (+45) 4593 0190
www.mek.dtu.dk
ISBN: 978-87-7475-530-2